SPECTROSCOPIC STUDIES OF COPPER-THIOMOLYBDATE INTERACTIONS

A Thesis Submitted to the College of
Graduate Studies and Research
In Partial Fulfillment of the Requirements
For the Degree of Doctor of Philosophy
In the Department of Chemistry
University of Saskatchewan
Saskatoon

By
Darina Slamova

PERMISSION TO USE

In presenting this thesis in partial fulfillment of the requirements for a Postgraduate degree from the University of Saskatchewan, I agree that the Libraries of this University may make it freely available for inspection. I further agree that permission for copying of this thesis in any manner, in whole or in part for scholarly purposes may be granted by the professor who supervised my thesis work or, in his absence, by the Head of the Department or the Dean of the College in which my thesis work was done. It is understood that any copying or publication or use of this thesis or parts thereof for financial gain shall not be allowed without my written permission. It is also understood that due recognition shall be given to me and to the University of Saskatchewan in any scholarly use which may be made of any material in my thesis.

Request for permission to copy or to make other use of material in this thesis in whole or in part should be addressed to:

Head of the Department of Chemistry

University of Saskatchewan

110 Science Place

Saskatoon, Saskatchewan

S7N 5C9

CANADA

ABSTRACT

Cu is an important trace element in living systems, including animals. It is a part of many enzymes responsible for different processes occurring in the body. However, antagonists can severely decrease the amount of Cu available to the animal, which results in numerous health issues caused by Cu deficiency. The main antagonists of the Cu are thiomolybdates whose effect is especially harsh in ruminants due to their high potential to synthesize these compounds. Thiomolybdates (the ions $MoO_xS_{4-x}^{2-}$, where x = 0-3) are formed in the rumen from molybdate and sulfide (from degradation of sulfate), both of which come from the food and water ingested by the animal.

The first part of the project described in this thesis was to develop reproducible preparative methods of CuTM samples in solution and solids, under conditions as biologically relevant as possible. This crucial information is missing in the literature related to Cu deficiency. The second part studied the structure of the adduct formed between Cu and two of the thiomolybdates: tetrathiomolybdate, TM4 and trithiomolybdate, TM3, as these are the most important in Cu deficiency.

In solution, the appropriate solution medium and the concentration of reactants were chosen to study the stoichiometry of Cu:TM in solution before precipitation occurs.

Conditions for preparation of solid CuTM adducts were chosen to obtain the amount of solid necessary for further studies and to eliminate the formation of unwanted side-products. In the solid phase, the stoichiometry of Cu:TM was investigated by elemental analysis.

EPR spectroscopy of solid CuTM samples revealed the presence of diamagnetic species which were partially identified.

EXAFS studies were performed on both the Mo and Cu K edges. Spectra defined the oxidation states of both main metal atoms, Cu and Mo. Fitting of the measured EXAFS spectra of solid CuTM samples prepared at three different Cu:TM ratios determined the interatomic distances involved in these compounds. This data was used to determine the structure of the CuTM units which polymerize to form the final product. IR spectroscopy was also used to confirm the presence of some of the groups in these adducts.

All the results from the various spectroscopic techniques were then combined to proposed a complete reaction scheme for the two-step formation of the CuTM4 and CuTM3 adduct species.

ACKNOWLEGMENTS

I would like to sincerely thank my supervisor, Dr. Steve Reid, for his constant guidance, support and mentorship throughout this project. Thanks for your commitment and patience.

I would also like to thank my committee members, Dr. Matthew Paige, Dr. David Sanders and Dr. Graham George. Your suggestions and criticisms were both welcomed and appreciated.

Thanks to my lab-mates, to Dr. Rhett Clark, Dr. Joseph Essilfie-Dughan, Dr. Emmanuel Quagraine and Mildred Budu, for both scientific and other help and for creating a friendly working atmosphere.

I would like to thank my Mom and Dad for their life-long support. Thanks to my fiancé, Lubos Kuzma, for his love, help and various sacrifices throughout my study.

Finally, I would like to acknowledge the funding for this project from the Agricultural Development Fund of Saskatchewan and the University of Saskatchewan.

To

My parents and my fiancé Lubos

TABLE OF CONTENTS

LIST OF TABLES

LIST OF FIGURES

LIST OF ABBREVIATIONS

Abs	Absorbance
BN	Boron nitride
BSA	Bovine Serum Albumin
Bu	Butyl
CN	Coordination number
DM	Dry matter
DMF	Dimethylformamide
DMSO	Dimethylsulfoxide
DPPH	2,2-Diphenyl-1-Picrylhydrazyl
EDTA	Ethylenediaamine tetraacetic acid
EPR	Electron paramagnetic resonance
eV	Electronvolt
EXAFS	Extended X-ray Absorption Fine Structure
Exp	Experimental
FT	Fourier Transform
g_e	g-factor of an electron
G	Gauss
GGH	Glycylglycyl-L-histidinate
MHz	Megahertz

His	Histidine
hr	Hour
I	Beam intensity (outgoing)
I_0	Incident beam intensity
IR	Infrared
ISE	Ion selective electrode
Kf	Formation constant
LCA	Linear combination analysis
LMCT	Ligand-to-metal-charge transfer
LMM	Low molecular mass
M	Molarity = moles solute/l solution
min	Minutes
MLCT	Metal-to-ligand charge transfer
mM	Millimolar
MOPS	3-(N-morpholino)propanesulfonic acid
nm	Nanometers
NR	Not reported
PCA	Principal component analysis
pH	Negative log of the hydrogen ion activity
ppt	Precipitate
SOD	Superoxide dismutase
SRF	Simulated rumen fluid
T	Tesla (in EPR)
T	Transmittance (in XAS)

Tbp	Trigonal bipyramidal
TM	Thiomolybdate
TM0	Molybdate: MoO_4^{2-}
TM1	Monothiomolybdate: MoO_3S^{2-}
TM2	Dithiomolybdate: $MoO_2S_2^{2-}$
TM3	Trithiomolybdate: $MoOS_3^{2-}$
TM4	Ttetrathiomolybdate: MoS_4^{2-}
UV	Ultraviolet
VFA	Volatile fatty acids
Vis	Visible
XANES	X-ray Absorption Near Edge Structure
XAS	X-ray Absorption Spectroscopy
λ	Wavelength
ν	Frequency
˚C	Degree Celsius

1. INTRODUCTION

1.1. Copper

1.1.1. Chemistry of Copper

Copper (Cu) is the 29th element in the Periodic Table, belonging to the first transition metals group. It has an average atomic mass of 63.546. The ground state configuration of copper is $1s^2\ 2s^2\ 2p^6\ 3s^2\ 3p^6\ 4s^1\ 3d^{10}$ or [Ar] $3d^{10}\ 4s^1$. Copper can be found mostly as Cu(I) and Cu(II) and less commonly as Cu(III): a few compounds containing Cu(IV) have also been observed.

Cu(I) compounds are mostly colorless, but color (usually red or orange) has also been observed resulting either from anion or charge-transfer bands. The coordination number of Cu(I) compounds can vary from two to five, and therefore various geometries are possible (Table 1.1). The most common geometry for Cu(I) is tetrahedral.

Cu(I) is classified as a soft acid in hard-soft acid-base theory. Therefore it readily reacts with soft bases such as the sulfide ion. Cu-S chemistry includes a large number of compounds. These can be in tetrahedral, octahedral or cubic geometries, and can form large cluster molecules[1].

Coordination number	*Stereochemistry*	*Compounds*
2	Linear	$[CuCl_2]^-$, Cu_2O
3	Trigonal planar	$[Cu(CN)_3]^{2-}$
4	Tetrahedral	$[Cu(py)_4]^+$, CuI
4	Distorted planar	CuL^a
5	sp	$[CuLCO]^a$

Table 1.1 Examples of stereochemistries for d^{10} (Cu^I) compounds[1]. (^aL = a macrocyclic N_4 anionic ligand)

Cu(I) compounds are highly unstable towards water due to their greater lattice and solvation energies and higher formation constants for complexes of the Cu(II) ion, so that ionic Cu(I) derivatives are unstable.[2] Cu(I) compounds are usually readily oxidized to Cu(II) which is very stable. The relative stabilities of Cu (I) and Cu(II) states in normal aqueous solution can be indicated by their redox potentials:

$$Cu^+ + e = Cu \qquad E^0 = 0.52\ V \qquad 1.1$$

$$Cu^{2+} + e = Cu^+ \qquad E^0 = 0.153\ V \qquad 1.2$$

The relative stabilities of Cu(I) and Cu(II) in aqueous solution depend very strongly on the nature of anions or other ligands present and vary considerably with solvent or the nature of neighboring atoms in a crystal.[1]

Cu(II) compounds can also have various coordination numbers and geometries (Table 1.2). However, the most common is tetragonally distorted octahedral geometry, as seen in ($[Cu(H_2O)_6]^{2+}$).

Coordination number	*Stereochemistry*	*Compounds (examples)*
3	Trigonal planar	$Cu_2(\mu\text{-}Br)_2Br_2$
4	Tetrahedral	$Cs_2[CuCl_4]$
4	Square planar	$[EtNH_3]_2[CuCl_4]$
5	Trigonal bipyramidal	$[Cu(bipy)_2I]^+$
5	Square pyramidal	$[\{Cu(dmgH)_2\}_2]$
6	Octahedral	$K_2Pb[Cu(NO_2)_6]$
7	Pentagonal bipyramidal	$[Cu(H_2O)_2(dps)]^{2+}$
8	Dodecahedral (distorted)	$[Cu(O_2CMe)_4]^{2+}$

Table 1.2 Examples of stereochemistry of d^9 (Cu^{II}) compounds[1,3].

In an octahedral environment Cu(II) (d^9) would possess a degenerate ground state. To produce a more stable structure, a geometric distortion will remove this degeneracy in accordance with the Jahn-Teller theorem (Figure 1.1). Therefore, Cu(II) is usually found in a tetragonally distorted octahedral environment with four strongly bound equatorial ligands and one or two weakly bound axial ligands[4]. The reason for the absence of a regular stereochemistry for complexes of the Cu(II) ion originates in the lack of spherical symmetry associated with the d^9 configuration of the Cu(II) ion[5].

Distorted tetrahedral complexes of Cu(II) are also known, as well as intermediates between tetrahedral and square geometry complexes.

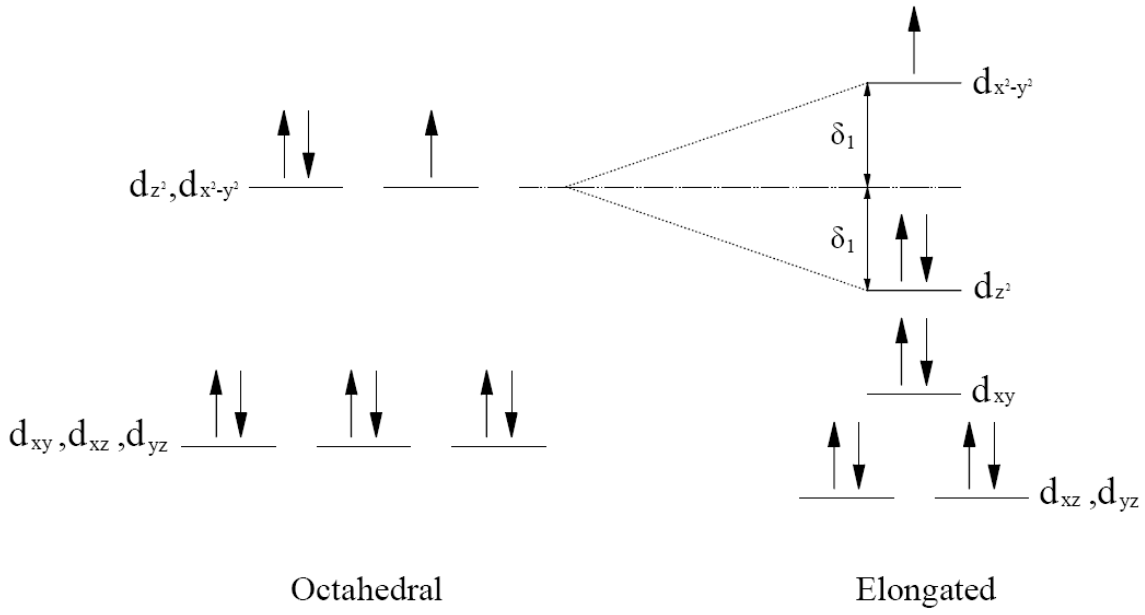

Figure 1.1 d^9 configuration of Cu^{2+} [6].

Due to the relatively low symmetry of the Cu^{2+} characteristic environment, interpretation of the spectra and magnetic properties is complicated. Almost all the complexes of Cu^{2+} are blue or green due to an absorption band in the 600 to 900 nm region of the spectrum[1]. In the solution, the blue color comes the formation of $[Cu(H_2O)_6]^{2+}$ and the Cu(II) salts frequently crystallize as hydrates[3].

EPR spectral properties of Cu(II) compounds are discussed in section 1.4.4.10.

1.1.2. Copper and animals

According to the structural and spectroscopic characteristic of the copper complex at the active site, copper containing enzymes can be divided into following groups:

1. Normal Cu(II) sites where the spectroscopic characteristics are those of the familiar tetragonally coordinated Cu^{2+} ion (sections 1.4.4.10 and 1.4.5.6).

2. “Blue” copper sites, where Cu(II) is in an unusual geometry. The blue color of these sites is caused by very strong absorption in the red part of the visible spectrum assigned for S → Cu LMCT transition. These Cu(II) sites also have anomalous EPR spectra.
3. Coupled two-copper centers, where the antiferromagnetic coupling leads to diamagnetism and an abnormal visible spectra[1].

Many of the Cu proteins are analogs to the iron-containing proteins such as hemocyanin, tyrosinase, amine oxidases, laccase, blue Cu proteins, superoxide dismutase or Cu-containing nitrite reductase.

Not only the animal itself affects the requirement for Cu, but other factors such as the presence of Cu antagonists in the feed are important. Due to the Cu-Mo antagonism, the Cu:Mo ratio should be at least 4:1 to insure adequate Cu availability.[7]

The main source of copper for ruminants is grass. The amount in grasses varies widely for different species, brassicas and cereals being the best source. The concentration of Cu in most studied grass species has been found to be 4.5 - 21.1 mg Cu/kg DM. The amount can change also based on the location and weather conditions[8].

In most animals, Cu is poorly absorbed and this absorption is influenced by its chemical form. In ruminant species, it is only 1 - 3 % of Cu from the diet that is absorbed by the animal. Copper can be absorbed in all segments of the gastro-intestinal tract, but the greatest amount is absorbed in the small intestine. It is absorbed by two mechanisms: saturable (active transport) and unsaturable (simple diffusion).

Intestinal absorption of Cu can be influenced by its chemical form, as well as other dietary factors (Ca, Fe, Zn, Cd, Mo reduce Cu absorption). Absorbed Cu loosely

binds to albumin and amino acids and then is transported through the body.[7] The uptake of the copper by the liver, the most important copper storage organ proceeds in two stages: copper binds to glutathione and then metallothionein before being portioned between biliary secretion, used in the synthesis of ceruloplasmin and stored. Ceruloplasmin receptors in the cell membranes, albumin and amino acids (mainly histidine) facilitate the copper uptake in vitro.[8]

Ionic copper is toxic in the free form, therefore it has to be bound to organic molecules in the body. If there is more Cu present than necessary (more than the available organic molecules), the excess of copper will be bound to high molecular weight molecules and then to low molecular weight molecules.[7] The concentration of copper differs between different organs of ruminants; in the heart it is 3.1 mg/kg, kidneys 3.6 mg/kg and very low in muscle, fat and bones[8]. Primary excretion of unabsorbed Cu is through feces.[7,9]

Copper in the ruminant's body has many functions. These are mostly related to the functioning of the various copper-dependent proteins in the body. Copper is important for the reproduction, bone development, growth, connective-tissue development and pigmentation of the skin appendages. Copper also protects tissues from oxidant stress and is essential in the immune system in ruminants and small animals as it affects the number of cells mediating immunity[8].

1.2. Molybdenum

1.2.1. Chemistry of Molybdenum

Molybdenum (Mo) is the 42nd element in the periodic table. It belongs to the second transition series. It is a rare element found in rocks at a concentration of about

1.2 ppm[3]. The ground state electronic configuration of molybdenum is $1s^2\ 2s^2\ 2p^6\ 3s^2\ 3p^6\ 4s^2\ 3d^{10}\ 4p^6\ 4d^5\ 5s^1$ or [Kr] $4d^5\ 5s^1$. Due to the partially filled 4d orbitals, molybdenum can be found in a variety of oxidation states, from Mo(-II) to Mo(VI). The most common are Mo(IV), Mo(V) and Mo(VI); the others will not be discussed further. The most stable form of molybdenum is the hexavalent molybdate, MoO_4^{2-}. When present in oxidation state lower than +VI, molybdenum aggregation in aqueous solution occurs resulting in the formation of clusters connected by hydroxo or oxo-bridges.[10] In its compounds, molybdenum has a large range of coordination numbers, from 4 to 9 and also a large number of geometries (Table 1.3).

Because of the wide variety of stereochemistries and oxidation states, the chemistry of molybdenum is one of the most complex of the transition elements. Molybdenum can be found in various oxidation states bound to the oxo, thio or sulfide ligands. The Mo/S complexes are characterized by structural diversity and great reactivity. The latter one derives from a close matching of the S 3p and Mo 4d orbital energies which provide low-energy superexchange pathways for intramolecular electron transfer processes. Many molybdenum halides are also well known.

Strong metal-metal bonding is very common for the molybdenum compounds: binuclear species of $Mo_2(O_2CCH_3)_4$ and binuclear halides of Mo have been seen[2].

The molybdenum is usually found in low-spin compounds. Ions with an even number of electrons are often diamagnetic. In cases with an odd number of electrons, there is usually only one unpaired electron[2]. EPR spectral properties are discussed further in section 1.4.4.9.

Oxidation state	*Coordination number*	*Geometry*	*Compounds (examples)*
Mo^{IV}, d^2	4	Tetrahedral	$Mo(NMe_2)_4$
	6	Octahedral	$[Mo(NCS)_6]^{2-}$
	6	Trigonal prism	MoS_2
	8	Dodecahedral or square antiprism	$[Mo(CN)_8]^{4-}$
	8	π-complex	$(\eta^5\text{-}C_5H_5)_2MoCl_2$
Mo^{V}, d^1	5	Tbp	$MoCl_5$ (g)
	6	Octahedral	Mo_2Cl_{10} (s)
	8	Dodecahedral or square antiprism	$[Mo(CN)_8]^{3-}$
Mo^{VI}, d^0	4	Tetrahedral	MoO_4^{2-}
	5	NR	$MoOF_4$
	6	Octahedral	MoO_6
	7	Distorted pentagonal bipyramid	$K_2[MoO(O_2)_2(ox)]$
	8	NR	MoF_8^{2-}

Table 1.3 Examples of different oxidation states and geometries for Mo compounds[1].

1.2.2. Biological significance of Molybdenum

Physiologically relevant Molybdenum is found in oxidation states between +IV and +VI. Molybdenum has been found to be biologically active in more than 30 enzymes, such as xanthine oxidase, nitrate redutase, aldehyde oxidase, sulfite oxidase, arsenite oxidase, formate dehydrogenase and others[10]. It is involved in the catalysis of controlled oxygen transfer, electron substrate, alcohol metabolism, C1 metabolism, etc.

The malfunctioning of the molybdoenzymes can lead to various problems, such as defects in purine metabolism and neurological disorders.[10]

1.2.3. Molybdenum and animals

The molybdenum requirements of animals are very low. For ruminants, the requirements have not been established but are estimated to be less than 2 ppm[11].

Molybdenum is commonly found in soil in concentrations varying from 0.1 – 20 mg/kg DM. The highest amounts are found in marine soils. Its concentration also rises with increasing pH of the soil. The pasture levels vary depending on the soil condition, the average value of Mo was found to be 1.1 mg Mo/kg DM. Its highest levels were found in legumes (0.5 – 2.5 mg Mo/kg DM), lower in grasses (0.33 – 1.44 mg Mo/kg DM) and cereals (0.16 – 0.92 mg Mo/kg DM) (Ref:Underwood). Molybdenum can be easily and rapidly absorbed by livestock, especially in hexavalent forms dissolved in water. [8]

The blood and tissue levels of molybdenum in ruminants are directly proportional to its intake. Molybdenum is not absorbed from the rumen or omasum, but later in the abomasums and small intestine. 90 - 95 % of unabsorbed Mo is excreted in the feces, and the rest by urine.[7] Molybdenum absorbed across intestinal mucosa can be transported in plasma in the free ionic state and stored in the tissues in enzymes such as molybdopterin, or bound to xanthine dehydrogenase, aldehyde oxidase or sulfite oxidase.

Although low intake of molybdenum does not usually result in severe health problems, it can be related to the copper toxicity (section 1.1.2). Molybdenum

deficiency can result into impaired function, retarded growth and anemia development which can be potentially life-threatening.[8,9]

1.3. Thiomolybdates

1.3.1. Introduction to Thiomolybdates

Thiomolybdates are anions with the central atom of Mo surrounded by oxygen and sulfur atoms. The oxidation state of Mo in thiomolybdates is 6+. In this thesis, TM is used as an abbreviation for thiomolybdate. The TM is followed by a number which represents the number of sulfur atoms in the anion (Figure 1.2). TM0, containing no sulfur atom, is also included for completeness.

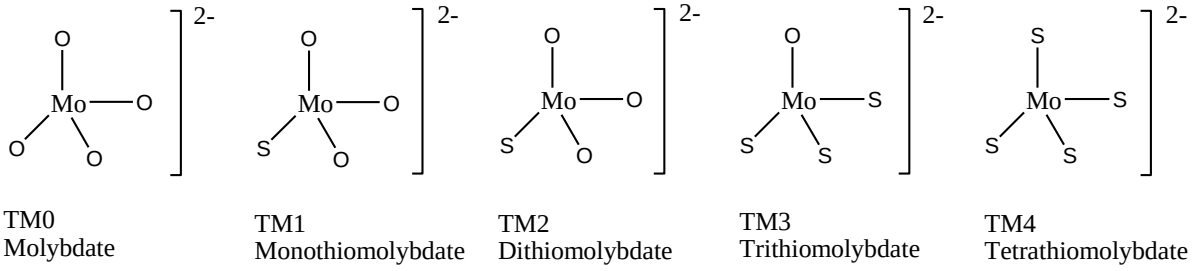

Figure 1.2 Cartoon structures of thiomolybdates.

1.3.2. Laboratory Synthesis of Thiomolybdates

Thiomolybdate synthesis was reported for the first time by Berzelius in 1826[12]. Evaporation of molybdic acid in ammonium sulfide yielded TM4. Although several similar synthetic approaches for TMs were reported later in the 19th and early 20th century, most of them resulted only in the formation of TM4.

Synthesis and spectroscopic characterization of all four thiomolybdates using the reaction between hydrogen sulfide (H_2S) and molybdate ion (MoS_4^{2-}) was first performed by Diemann and Müller[13,14]. Clarke showed that under biologically relevant conditions (temperature 38 - 40 °C and pH = 7), the synthesis of thiomolybdates from molybdate and sulfide proceeds by successive replacement of O by S and ultimately results in the formation of the highest of the thiomolybdates, TM4.[15]

The synthesis of all four thiomolybdates using sodium molybdate and ammonium sulfide by similar methods and their purification was developed by E. Quagraine[16] (section 1.6.3). He prepared TM1 and TM3 as cesium salts ($Cs_2MoO_3S.1/2H_2O$ and Cs_2MoOS_3) and TM2 and TM4 as ammonium salts ($(NH_4)_2MoO_2S_2.2H_2O$ and $(NH_4)_2MoS_4$). He showed that the formation of the higher thiomolybdates is favored by an increased molar ratio of S/Mo, a decrease in pH and increased reaction time. By carefully controlling these conditions any desired thiomolybdate can be prepared and isolated from the solution in reasonable purity (95 % or better).

Syntheses of thiomolybdate salts containing different cations have also been reported in the literature: Cs_2MoS_4[17], $(NH_4)_2MoOS_3$[18], Tl_2MoOS_3[13], $PbMoS_4$[19]. $(NH_4)_2MoOS_3$ was prepared to be used as precursors for the synthesis of larger molecules, Cs_2MoS_4 and Tl_2MoOS_3 were shown to have very low solubility.

Many alkylammoniumthiomolybdates have been prepared by substitution of the ammonium cation by an alkylammonium ion, such as ethylene diammonium[20], tetramethylalkyl, tetrabutylalkylammonium[21], tetraethyldiammonium[18], bis(tetraethylammonium)[22], tetramethylalkylammonium and tetraheptylalkylammonium[23]. These can be used as the precursors for the preparation of larger molecules or can be thermally decomposed to give molybdenum sulfides such as MoS_2 and MoS_3 which are widely used in catalytic reactions.

In these thiomolybdates containing large bulky cations, the Mo atom stays in the same tetrahedral or slightly distorted tetrahedral environment as in the simple thiomolybdates. The interaction between cation and anion can change the stability of the compound: ethylene diammonium TM4 is more stable in air and less soluble than ammonium TM4 due to formation of hydrogen bonds[20] between the TM anion and the ethylenediammonium cation via N-H…S and C-H…S bonds. This results in formation of a three dimensional network.

Most of the examples from the literature report the preparation and study of tetrathiomolybdates and there are very few examples of lower thiomolybdates (TM3, TM2 and TM1), which is most likely due to their instability in air or in solution.

1.3.3. Reactions of Thiomolybdates in Solution

In aqueous solution, thiomolybdates undergo hydrolysis, where S is replaced by O, resulting in the formation of lower thiomolybdates. Their stability varies, the most stable being TM4 (up to one day at pH = 7)[15] and the least stable TM1 (hydrolysis occurs within minutes after its dissolution). Stability in aqueous solution also depends on the environment, mainly pH.[16] In acidic solution TM4 form different polyanions ($(Mo_4S_{15})^{6-}$, $(Mo_2S_7)^{2-}$, $(Mo_4S_{13})^{2-}$) depending on the concentration of H^+, resulting in the formation of MoS_3 as a final step[24].

1.4. Characterization of TMs

1.4.1. UV/Vis Spectroscopy

1.4.1.1. Principles of UV/Vis Spectroscopy

The electronic absorption bands are related to charge-transfer transitions between MOs of the TM species (Table 1.4).

MoS_4^{2-}	$MoOS_3^{2-}$	$MoO_2S_2^{2-}$	MoO_3S^{2-}	MoO_4^{2-}	*Assignment*
467	461				n(S3p) → E(Mo4d)
	395	394	394		π(S3p - Mo4d) → E(Mo4d)
317	311	318			σ_1(S3p - Mo4d) → E(Mo4d)
		288	288		σ_2(S3p - Mo4d) → E(Mo4d)
241	256				n(S3p) → T_2(Mo4d)
	225	219			n(S3p - Mo4d) → T_2(Mo4d)
			224	225	n(O2p) → E(Mo4d)
				208	σ(O2p - Mo4d) → E(Mo4d)

Table 1.4 Electronic absorption spectra of TMs, υ_{max} (nm) and assignments as calculated by Jostes[25].

Thiomolybdates are mostly of characteristic color (deep dark red or purple for TM4, orange or yellow for lower TMS), and their UV/Vis spectra show peaks with maxima characteristic of the charge transfer transition within TM4.

UV/Vis spectroscopy has been widely used to determine the purity of TM samples in solution, because of the characteristic bands (Figure 1.3) of each TM [25,26]. Differences in the spectra caused by O → S substitution are due to changes of the occupied MOs[27].

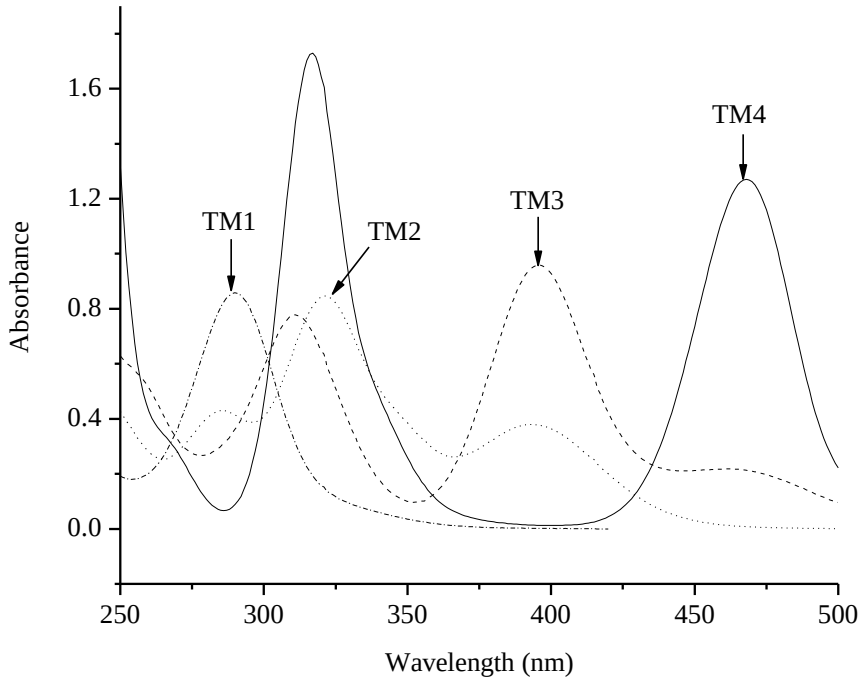

Figure 1.3 Characteristic spectra of TMs[28].

The concentrations needed to collect a UV/Vis spectrum are very low (10^{-4} M) and a spectrum can be obtained in one minute.

Characterization of the thiomolybdates in the solution using UV/Vis spectroscopy is complicated by the overlap of the peaks in the spectra of all four thiomolybdates (Figure 1.3). For this reason the absorption coefficients reported in the literature differ[13-15,18,29]. Recently, improved characterization of the UV/Vis spectra together with the use of computer software for fitting has allowed for more thorough analysis of the species[28]. Due to the sensitivity of spectra to concentration change and the relatively short collection times (compared to other methods), UV/Vis spectroscopy also provides a useful tool in the kinetic study of the formation, hydrolysis and reactions of thiomolybdates.[28,30,31]

1.4.1.2. Job's Method

Using UV/Vis spectrophotometry and Job's method, the ratio of the reactants in a final product can be determined. The simplest scenario is to use a constant total concentration of the reactants B and D. The molar ratio of reactants is changed and therefore also the concentration of the final product (P) changes.

$$bB + dD \overset{K_f}{\leftrightarrows} pP \qquad 1.3$$

where K_f is the formation constant of the product ($K_f = \frac{a_P}{a_B \times a_D}$), a is the activity; b, d and p are stoichiometric coefficient of the B, D and P species, respectively.

If the UV/Vis absorbance of the mixture is monitored at a wavelength where none of the reactants absorb but the product has a strong absorbance, then absorbance of the solution

$$A = \varepsilon_P c_P l \qquad 1.4$$

where ε_P is the molar absorptivity coefficient of the product formed in the solution (in L/mol.cm), c_P is its concentration (in mol/L) and l is the pathlength (in cm). If at a

chosen wavelength the product and also the reactants absorb, then the total absorbance is

$$A = \varepsilon_P c_P l + \varepsilon_B c_B l + \varepsilon_D c_D l \quad (1.5)$$

In the case where the absorbance of the complex is larger than the absorbance of the reactants, when the molar ratio of reactants in the mixture is that of the reaction ratio involved in the formation of the product, the maximum concentration of the product and therefore the maximum absorbance is observed. For reaction

$$B + D \overset{K_f}{\leftrightarrows} P \quad (1.6)$$

the maximum absorbance would be observed at the molar fraction 0.5 for B and 0.5 for D. For the reaction

$$2B + D \overset{K_f}{\leftrightarrows} P \quad (1.7)$$

the maximum absorbance will be observed at the molar fraction $x_B = 2/3$ and $x_D = 1/3$.

For the system with a reaction that proceeds to the complete consumption of at least one the reactants (infinitely high K_f),

$$B + D \overset{K_f}{\leftrightarrows} P \quad (1.8)$$

the maximum absorbance is observed as a sharp peak in the plot of Absorbance of the product vs. molar fraction of reactants (Figure 1.4). At the maximum absorbance point, there are no reactants present in the solution and the concentration of the product can be obtained directly from equation 1.4.

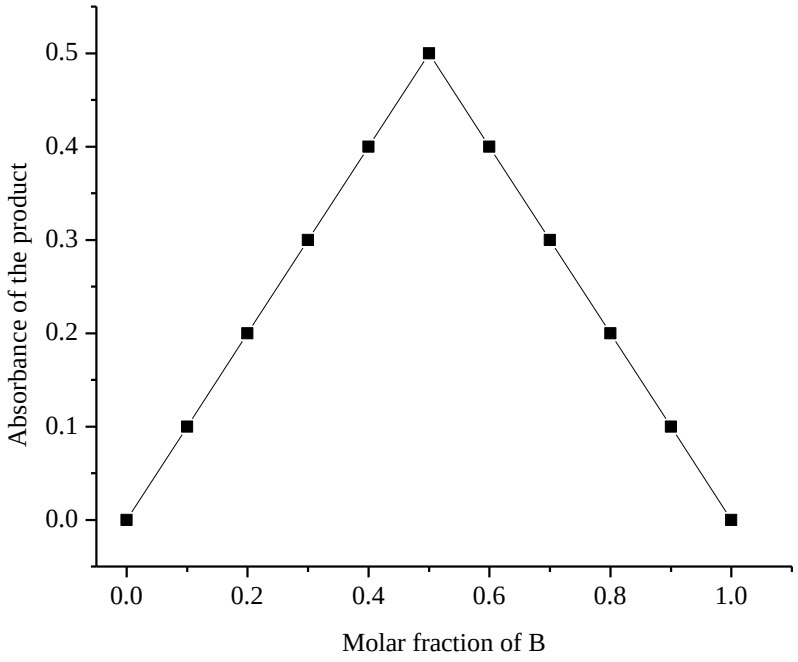

Figure 1.4 Change in absorbance vs. the molar fraction of a reactant for a reaction with 1:1 stoichiometry and very high K_f.

For the system that reaches equilibrium (low K_f),

$$B + D \overset{K_f}{\leftrightarrows} P \qquad 1.9$$

where all components are present, product and reactants, the maximum absorbance is situated on the curved peak of the plot of absorbance of the product vs. molar fraction (Figure 1.5).

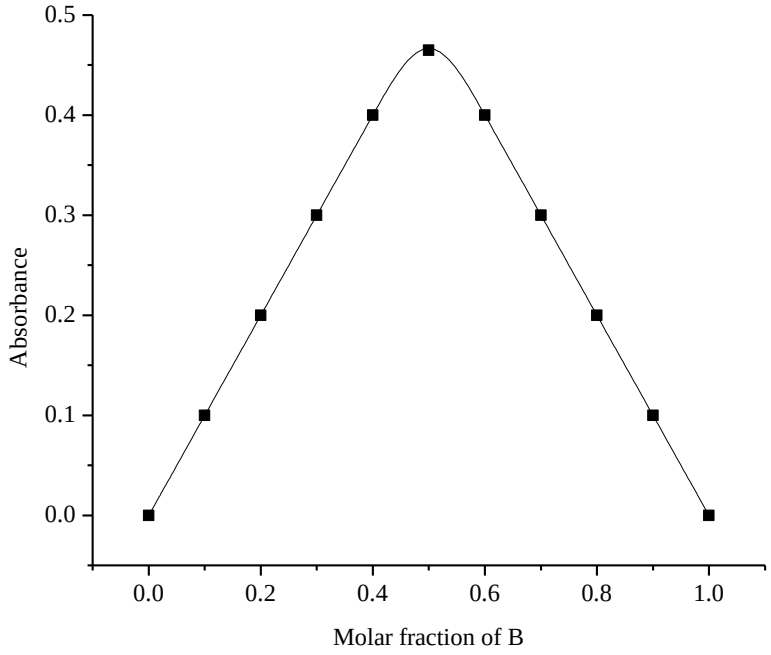

Figure 1.5 Change in absorbance vs. the molar fraction of a reactant for the system with low K_f.

In this case, the stoichiometric product concentration is not reached but can be estimated by extending the lines above the curved portion of the graph. This concentration is then obtained from the intersection of these two lines. The magnitude of the value of K_f can also be estimated from the curvature of the graph.

Another method to determine the ratio of reactants is a titration. Here, the amount of one of the reactants is kept constant, the amount of the other reactants is varied.

In this case, as the ratio of the reactants in the mixture approaches the stoichiometric value, the absorbance of the product is increasing and so therefore is the measured absorbance. When the correct ratio of reactants is reached, the maximum

absorbance is also reached. If more reactant is added into the mixture, the absorbance will not change anymore, except for dilution.

For the system with high K_f, a sharp change in the trend of the graph of measured absorbance vs. amount of the reactant is reached. After this, a plateau is observed (Figure 1.6).

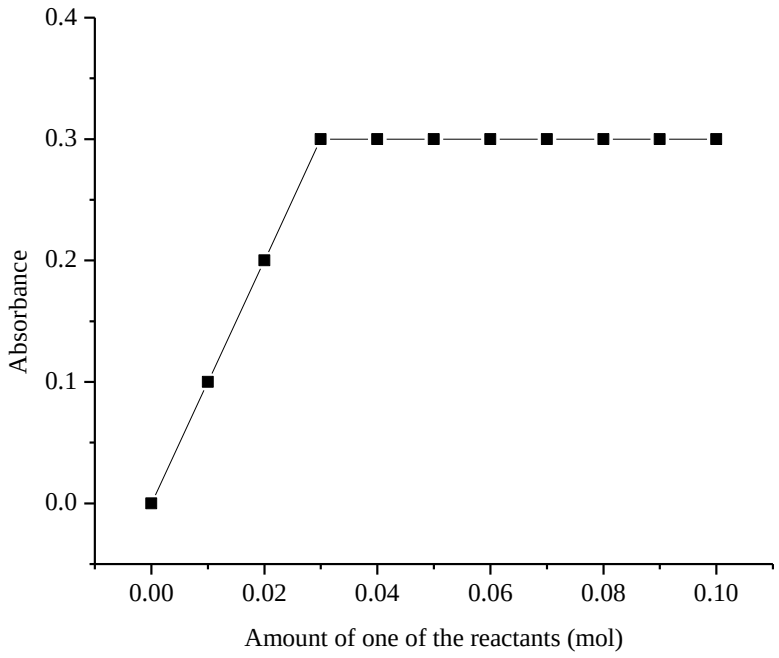

Figure 1.6 Absorbance vs. amount of the reactant for the system with high K_f.

If the K_f is low for the studied system, a curvature (Figure 1.7) is formed as the amount of added reactant is approaching the value of the correct molar ratio. This is because at any point, the maximum concentration is not reached, as all components, product and reactants are present in the system at the same time. The maximum absorbance (and maximum concentration) of the product can be obtained from the

intersection of the two lines. The curvature of the graph can provides estimate of the magnitude of K_f of the system.

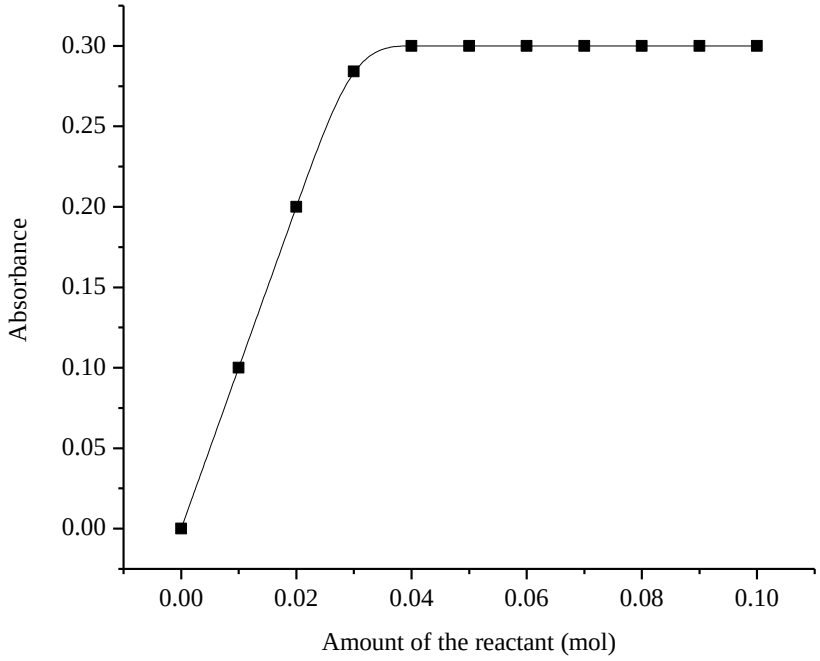

Figure 1.7 Absorbance vs. amount of the reactant for the system with low K_f.

From UV/Vis measurement of the system described above, the estimate of K_f can be obtained.

$$K_f = \frac{[P]^p}{[B]^b[D]^d} \qquad 1.10$$

Total concentration of B species is $c_B = [B] + \frac{b}{p}[P]$ and total concentration of D species is $c_D = [D] + \frac{d}{p}[P]$. Then we can substitute for [B] and [D]:

$$K_f = \frac{[P]^p}{\left(c_B - \frac{b}{p}[P]\right)^b \left(c_D - \frac{d}{p}[P]\right)^d} \qquad 1.11$$

The stoichiometric coefficients can be estimated from the plot at the maximum absorbance of the product, the total concentrations of B and D species are known, as they represent initial concentrations of the reactants put in the mixture. At various wavelengths, the absorbance is calculated from the equation above. The Goal Seek function in Excel (Figure 1.8) can be used to find the K_f value (using a guess for the starting value) by seeking a value for K_f which will minimize the square of differences between measured and calculated absorbances.

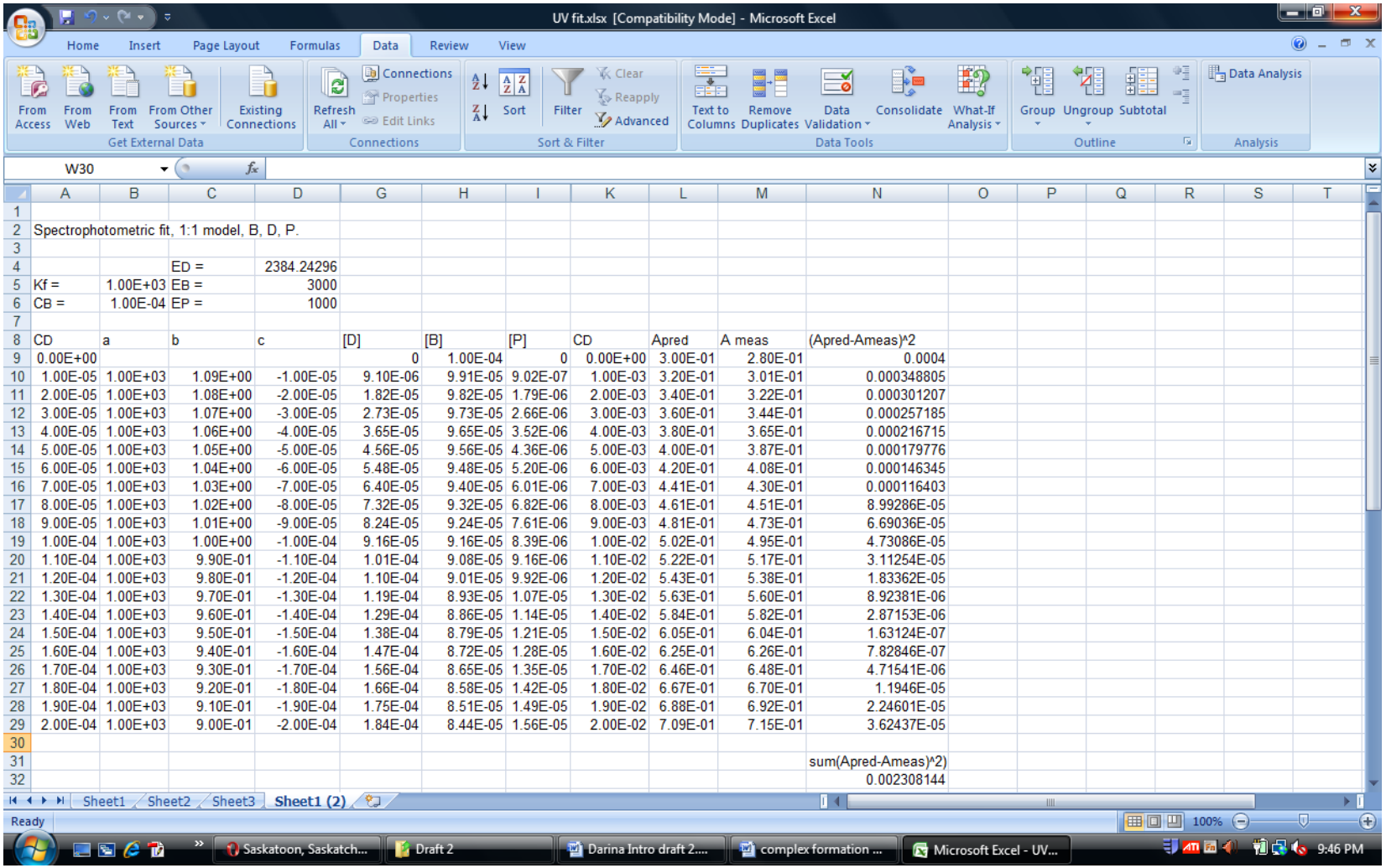

Figure 1.8 Spreadsheet for the calculation of the K_f of the complex formation from the titration data measured by UV/Vis spectroscopy.

1.4.2. ^{95}Mo NMR

NMR of a transition metal nucleus provides direct information about the metal centre in different physical and chemical environments. The chemical shift, δ (in ppm), can give information about the electronic environment about the metal nucleus. The linewidth (width at half height), $\Delta\upsilon_{1/2}$ (in Hz), can provide information about the degree of symmetry of the electric field at the nucleus. The coupling constant, ^{n}J (Hz), can help delineate molecular structure and intramolecular bonding.[32]

Thiomolybdate Mo(VI) complexes have a very large chemical shift range (-2000 - +4000 ppm[32,33]) in ^{95}Mo NMR. The technique has previously been used to determine the approximate purity of thiomolybdates, their equilibrium constants and their inconversion kinetics[34]. In D_2O, Na_2MoO_4 is used as a standard with a shift of 0 ppm. Each replacement of an oxygen by sulfur in the molecule results in the increase of the chemical shift by approximately 500-600 ppm[35,36] and therefore this technique can be used to distinguish between thiomolybdates in solution. Changes in the chemical shift reflect changes in the valence 4d orbitals caused by ligand substitution[37]. The exact chemical shift can also be influenced by the presence of other ligands or different cations in the thiomolybdate: the difference of the ^{95}Mo chemical shift between $(NH_4)_2$TM4 and $(Et_4N)_2$TM4 is a few ppm (Table 1.5). The solvent also plays a role in a chemical shift which shows the interaction of TMs with solvent[38] (Table 1.5).

Despite being a quadrupolar nucleus, ^{95}Mo NMR gives generally sharp peaks with the linewidths reported between 0.3-10 Hz[32]. This is due to the fact that its quadrupole moment is small. The signal width increases with the asymmetry of the molecule; for small and symmetric TMs this linewidth is therefore small.

Compound	*Chemical shift (ppm)*	*Solvent*
$(NH_4)_2[MoS_4]$ [39]	2175	DMSO
$(NH_4)_2[MoS_4]$ [38]	2258	H_2O
$(NH_4)_2[MoS_4]$ [38]	2207	MeCN
$(Et_4N)_2[MoS_4]$ [38]	2252	H_2O
$(Et_4N)_2[MoS_4]$ [38]	2251	D_2O
$[MoO_3S]^{2-}$ [38]	497	H_2O
$[MoO_3S]^{2-}$ [38]	Not observed	MeCN
$(NH_4)_2[MoO_2S_2]$ [38]	1066	H_2O
$(NH_4)_2\ [MoO_2S_2]$ [38]	964	MeCN
$K_3[MoOS_3]Cl$ [38]	1654	H_2O
$K_3[MoOS_3]Cl$ [38]	1587	MeCN

Table 1.5 ^{95}Mo chemical shifts for TMs.

The disadvantage of ^{95}NMR spectroscopy is the need for long collection times due to the low sensitivity of the ^{95}Mo nucleus. Therefore to obtain a signal of reasonable intensity, high concentrations of thiomolybdates in solution and/or long scanning times are needed. The solubility of simple thiomolybdates is relatively low (maximum 0.1 M for TM4, lower for the other TMs). Increased concentration leads to precipitation within minutes most likely due to the polymerization of TMs [14,24,40,41]. At the concentrations used, long scanning times result in the hydrolysis of TMs and consequently to the formation of lower species which contaminate the measured sample[16].

^{95}Mo NMR is not suitable for the unambiguous determination of the Mo oxidation state. The problem is the overlap of ranges (Table 1.6) for molybdenum in

different oxidation states which makes it difficult to distinguish between Mo(VI), Mo(II) and Mo(0) species[32].

Compounds	*^{95}Mo chemical shift range (ppm)*
Polyoxomolybdates (VI)	0 - 300
Mononuclear Mo(VI)	-500 - + 3500
$[Mo_2^{V}O_2X_2]^{2+}$	300 - + 1000
Mo(IV)	-1500 - + 3500
$[Mo_2^{III}]^{6+}$	+ 2500 - + 3500
$[MoNX]^{3+}$	- 300 - + 2500
$[Mo_2^{II}]^{4+}$	+ 3000 - + 4000
Mononuclear Mo(II)	-2000 - + 300
$[Mo_2^{I}]^{2+}$	-1800 - + 300
$[Mo(NO)_2]^{2+}$	-1000 - + 300
Mo(0)	-2000 - -200

Table 1.6 ^{95}Mo NMR chemical shift range[32].

1.4.3. Infrared Spectroscopy (IR)

IR spectra can be used to characterize the presence of certain groups in the thiomolybdates. Mo-S vibrations are normally found in the range 400 – 500 cm^{-1} and the Mo-O vibration very close to 900 cm^{-1}. Laurie et al. measured the IR spectra of all four thiomolybdates[42] (Table 1.7) and the position of the bands agree with results published by different groups[14,43]. Lakshmanan however found that MoS_4^{2-} with Td symmetry has two IR active bands: at 458 and 472 cm^{-1}.[44] The exact position of the

bands for thiomolybdates in the solid state can be slightly influenced by the nature of the cation[18] and its interaction with the anion; tetramethylammonium TM4 has the Mo-S characteristic band at 472 and tetrabutylammonium TM4 at 466 cm^{-1}.[21] The bridging (between MoS_4 units) and terminal S in the Mo-S bonds can also be distinguished based on the frequency of the IR band: Mo-S_t in the range 480 - 510 cm^{-1} and Mo-S_b 430 - 460 cm^{-1}.[45]

Thiomolybdate	*IR band: Mo-S (cm^{-1})*	*IR band: Mo-O (cm^{-1})*
TM4	476	
TM3	470	860
TM2	460	860, 840
TM1	476	880, 860, 840

Table 1.7 Characteristic IR bands for thiomolybdates in aqueous solution[42].

1.4.4. Electron Paramagnetic Resonance (EPR) Spectroscopy

1.4.4.1. Principles of EPR

This is just a brief summary; for a detailed description and explanation of EPR the reader is referred to numerous books available on this subject[46-52]

In the absence of an external magnetic field an electron's magnetic moment is oriented randomly. In an EPR experiments, electron spins will interact with applied electromagnetic radiation in a large, externally applied magnetic field. When this external field is applied, the electrons will align either with or against this field. For resonance to occur, the energy associated with the electromagnetic radiation must be

equal to the energy separation between the levels, according to the Planck equation (Figure 1.9).

$$h\upsilon = \Delta E \qquad 1.12$$

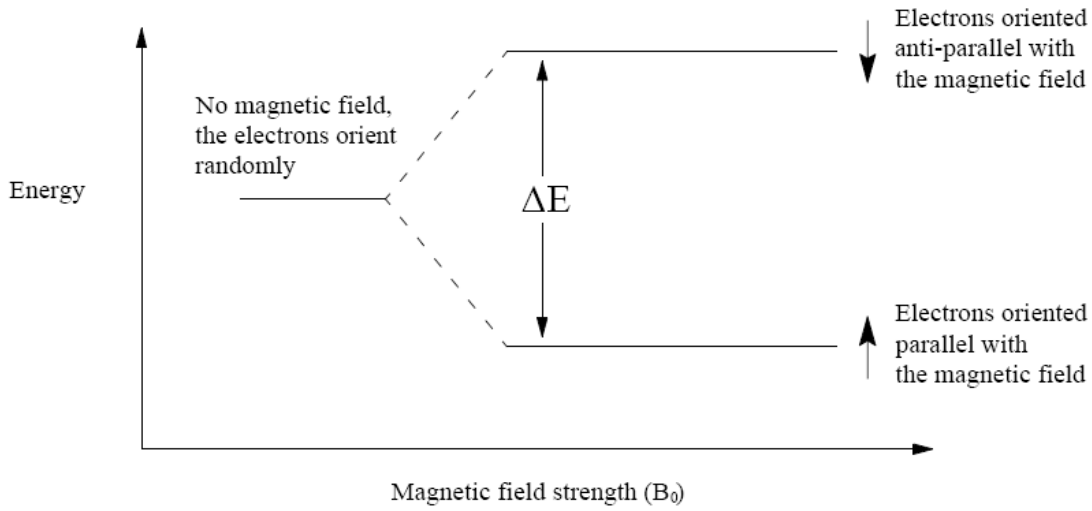

Figure 1.9. The effect of an applied external magnetic field.

In EPR spectroscopy the sample is placed in a magnetic field and a linear field sweep is performed, while simultaneously exposing the sample to a fixed frequency of microwave irradiation. Resonance (EPR absorption) occurs when the irradiation frequency matches the energy level separation created by the magnetic field.

There are many electrons in the studied system that interact with applied magnetic field. During this process some of them will be oriented parallel and some antiparallel to this field. All these electrons contribute to the EPR signal which is a resultant vector and depends on the slightly different electron populations in the two levels, with more being in the equilibrium. This is described by the Boltzmann distribution

$$\frac{N^+}{N^-} = e^{-\left(\frac{\Delta E}{kT}\right)} \qquad 1.13$$

where N^+ and N^- represent the number of electrons oriented parallel and antiparallel to the magnetic field, respectively, k is the Boltzmann constant and T is the temperature. The ratio $\frac{N^-}{N^+}$ can be enhanced by minimizing the temperature and maximizing the energy gap ΔE by maximizing the magnetic field B.

1.4.4.2. The g-factor

The g-factor of an EPR sample determines the position in the magnetic field where an EPR transition will occur. The g-factor helps characterizes the type of EPR sample measured. It can identify a specific metal ion, its oxidation state, spin state or coordination environment. It is defined as

$$g = \frac{h\upsilon}{\mu_B B_0} \qquad 1.14$$

where h is the Plank's constant, ν is the frequency, μ_B is the Bohr magneton and B_0 is the magnetic field value.

The value of g for a free electron is $g_e = 2.0023$. The measured g-factor is usually different from the free spin value. The magnitude of this deviation (Δg) depends upon the magnitude of the spin-orbit coupling, ζ. ζ increases rapidly with increasing atomic number, Δg might be large if there is a significant spin density in p or d orbitals in heavy atoms.[48] Deviation from the free spin value is due to the presence of orbital magnetism that adds or subtract from the spin magnetism. $\Delta g < 0$ when the unpaired electron acquires orbital angular momentum (the magnetic moment associated with orbital angular momentum is 1) and $\Delta g > 0$ if coupling occurs via a filled rather than empty orbital level. [48,53]

Three different types of systems can be studied by EPR spectroscopy: solutions, single crystals and powders (composed of many small randomly oriented crystals). The latter two are solid materials.

In general, g is anisotropic and has three principal values along three orthogonal axes.[48] In this case, there are three different g-values for interaction of a spin with the applied magnetic field along three axes of the crystal (single crystal or small crystal of powder material). The anisotropic g factor varies with the direction (x', y', z') in a single crystal. g-factor forms a symmetric tensor g' with six components g'_{ij} ($g'_{ij} = g'_{ji}$).

$$g = \begin{bmatrix} g'_{x'x'} & g'_{x'y'} & g'_{x'z'} \\ g'_{y'x'} & g'_{y'y'} & g'_{y'z'} \\ g'_{z'x'} & g'_{z'y'} & g'_{z'z'} \end{bmatrix} \qquad 1.15$$

If the g tensor has axial symmetry, then parallel $g_{\parallel} = g_{zz}$ and perpendicular $g_{\perp} = g_{xx} = g_{yy}$ are observed where z is the symmetry axis.[53]

The simplest example is when all the three values of the g-factor are the same, $g_{xx} = g_{yy} = g_{zz} = g$. In this case, the g-factor is isotropic. The resonant field is independent of the orientation of the applied magnetic field with respect to the sample (Figure 1.10). This is characteristic for EPR spectra of solution samples, where the rapid tumbling of molecules results into the observation of only one, average value of the g-factor. In solid samples, an isotropic g-factor is characteristic of symmetry point groups O_h (octahedral) and T_d (tetrahedral).[54]

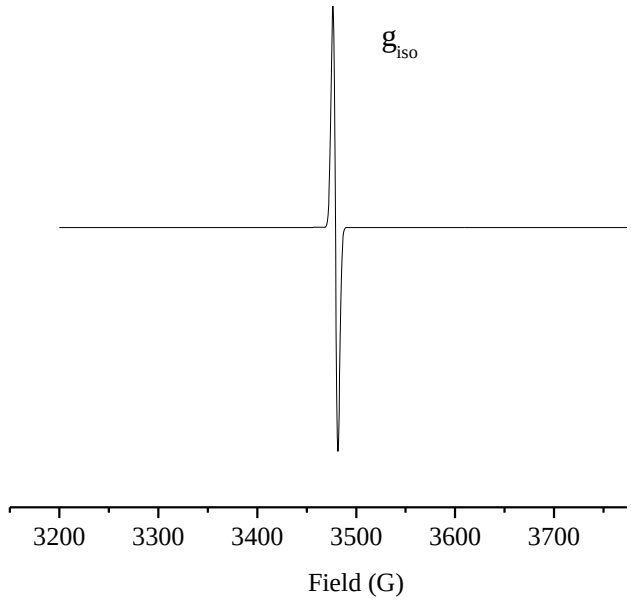

Figure 1.10 EPR spectrum with an isotropic g-factor (no hyperfine structure).

In axial symmetry, parallel, $g_{\parallel}$ and perpendicular, $g_{\perp}$ g-factors with different values are observed (Figure 1.11). These represent the interaction of the magnetic field and the principal axis of the crystal, when they are parallel of perpendicular to each other, respectively. The resulting g-factor is then defined as

$$g^2 = g_{\perp}^2 \sin^2\theta + g_{\parallel} \cos^2\theta \qquad 1.16$$

where θ is the angle between the crystal axes and electromagnetic field orientation. For solids, the axial g-factor can be found in the sample of many symmetry point groups: C_{4v} (square pyramidal), C_{3v} (trigonal pyramidal), D_{2d} (flattened or elongated tetrahedron), D_{4h} (square planar).

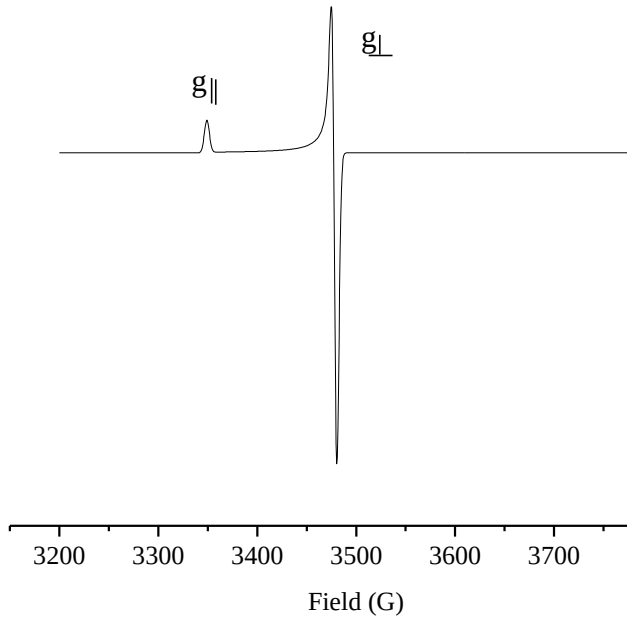

Figure 1.11 EPR spectrum with axially symmetric g-factor.

The rhombic g-factor (Figure 1.12) has three different values of g-factors, g_{xx}, g_{yy} and g_{zz}. This type can be observed in frozen solutions, when the rapid tumbling of the molecules is stopped and EPR behavior of the frozen solution is comparable to the EPR behavior of the solid samples. Rhombic g-factor is also commonly observed for the solid samples, crystals and powders, for symmetry point groups such as C_{2h} (angularly distorted planar), C_{2v} (XMA_2B_2 square pyramid), D_{2h} (MA_2B_2 square planar) C_2, C_s, C_i, C_1.[54]

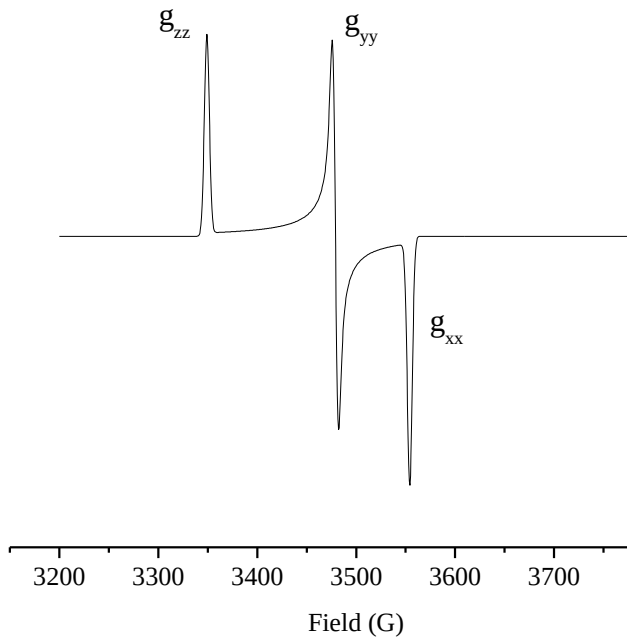

Figure 1.12 EPR spectrum with anisotropic g-factor.

Measuring g factor from polycrystalline or powder samples in the solid phase is more rapid but yields only approximate values. Therefore if it is possible, to get more accurate g factor values, it is advisable to perform single-crystal EPR measurements[55].

1.4.4.3. Hyperfine Interaction

The nucleus possesses a nuclear spin angular momentum. If such a nucleus is in the vicinity of the unpaired electron, it will affect the EPR spectrum. All nuclei with $I \neq 0$ give rise to a local magnetic field which adds to the external magnetic field the electron experiences. The interaction between the unpaired electron and the magnetic nucleus is called hyperfine interaction and leads to the splitting of the EPR lines centered about the g-factor (Figure 1.14). With nucleus I = 0 no hyperfine splitting is observed. For an electron with spin = ½, M_s is either + ½ or – ½ (Figure 1.9). When a

nucleus with I = ½ is present further splitting occurs (Figure 1.13). The resulting number of lines depends on the nuclear spin and can be calculated as 2I+1.[51] Hyperfine interaction is characterized by the hyperfine splitting constant, A, which is usually reported in Gauss (Tesla and cm^{-1} are sometimes used).

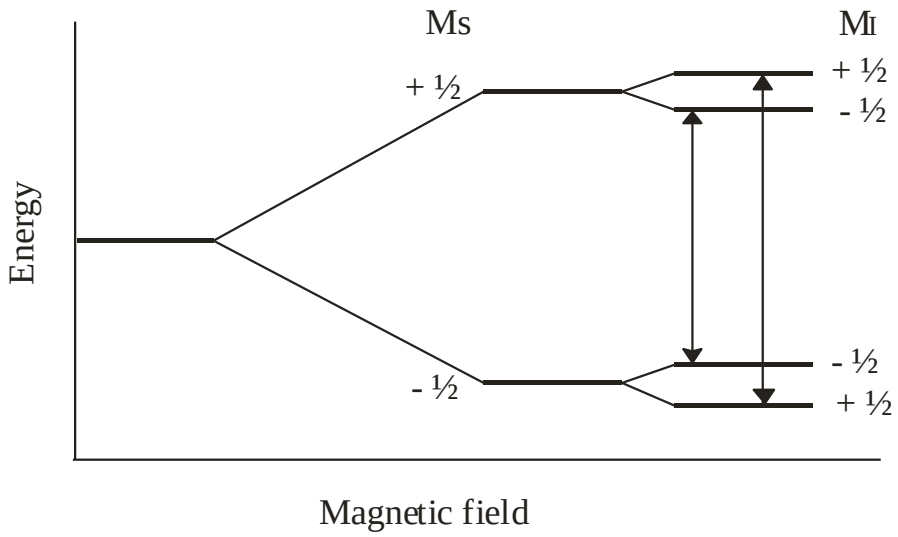

Figure 1.13 Effect of the presence of the nucleus with nuclear spin M_I = ½ on the splitting of an EPR line.

The anisotropy of the hyperfine splitting follows the trend of the anisotropy of the g-factor described above. Isotropic hyperfine interaction is characteristic for the solution when it averages because of the rapid rotation of the molecules[47], the same as mentioned previously in the case of the g-factor. The isotropic EPR spectrum is observed with $g_{xx} = g_{yy} = g_{zz}$ and $A_{xx} = A_{yy} = A_{zz}$[54].

In the axial (tetragonal) symmetry system, two values $A_{\parallel}$ and $A_{\perp}$ are observed for a hyperfine splitting (Figure 1.14). This EPR spectrum is characterized by $g_{xx} \neq g_{yy} = g_{zz}$ and $A_{xx} \neq A_{yy} = A_{zz}$.[54]

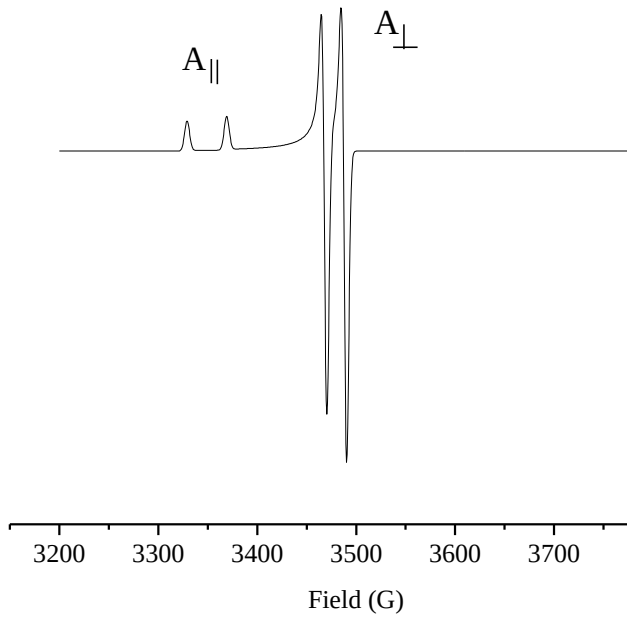

Figure 1.14 Effect of the hyperfine splitting on the EPR spectrum of axial symmetry.

In case of complete anisotropy, three values A_{xx}, A_{yy} and A_{zz} are observed (Figure 1.15). These types of splitting are characteristic for the solid sample and frozen solutions, when the rapid rotation of molecules is frozen. In this case, $g_{xx} \neq g_{yy} \neq g_{zz}$ and $A_{xx} \neq A_{yy} \neq A_{zz}$. This is characteristic of rhombic spectra.[54]

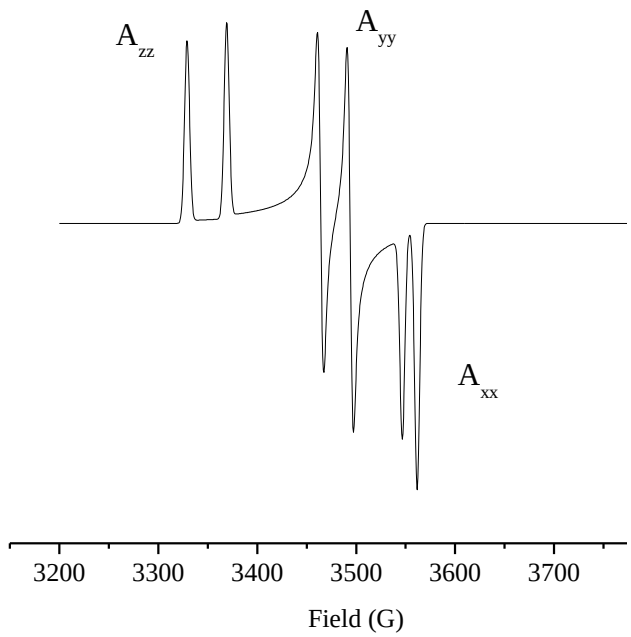

Figure 1.15 Effect of a nucleus with I = ½ on the EPR spectrum, resulting in the hyperfine splitting.

The larger the I value, the more splitting is observed in the spectrum. If several nuclei with a nuclear splitting are present in the same sample, its EPR spectrum gets more complicated and more difficult to analyze. This might be the case when one or more nuclei with nuclear spin larger than zero are ligated to the nucleus already causing the line splitting (section 1.4.4.9), resulting in superhyperfine splitting[56]. On the other hand, this can provide valuable information on the extent of the interaction within the sample.

1.4.4.4. Signal Intensity

There are two factors which have influence on the signal intensity. The first one is the concentration of unpaired electrons in the measured sample: an increased number of unpaired electrons leads to an increased signal intensity. The second one is the

microwave power. The signal intensity increases with the increasing microwave power until saturation is reached. This is determined by the sample's Boltzmann distribution at that power level (equation 1.13).

1.4.4.5. Lineshape of EPR Spectra

The EPR spectrum is recorded as the derivative of the absorption peak to enhance the sensitivity of the instrument. The shape of EPR lines are described by comparison with the Lorentzian (Figure 1.16)

$$y = \frac{a}{1+bx^2} \qquad 1.17$$

and the Gaussian (Figure 1.16) line shapes

$$y = ae^{(-bx^2)} \qquad 1.18$$

where a is the intensity of the signal and b is the linewidth in EPR spectroscopy.

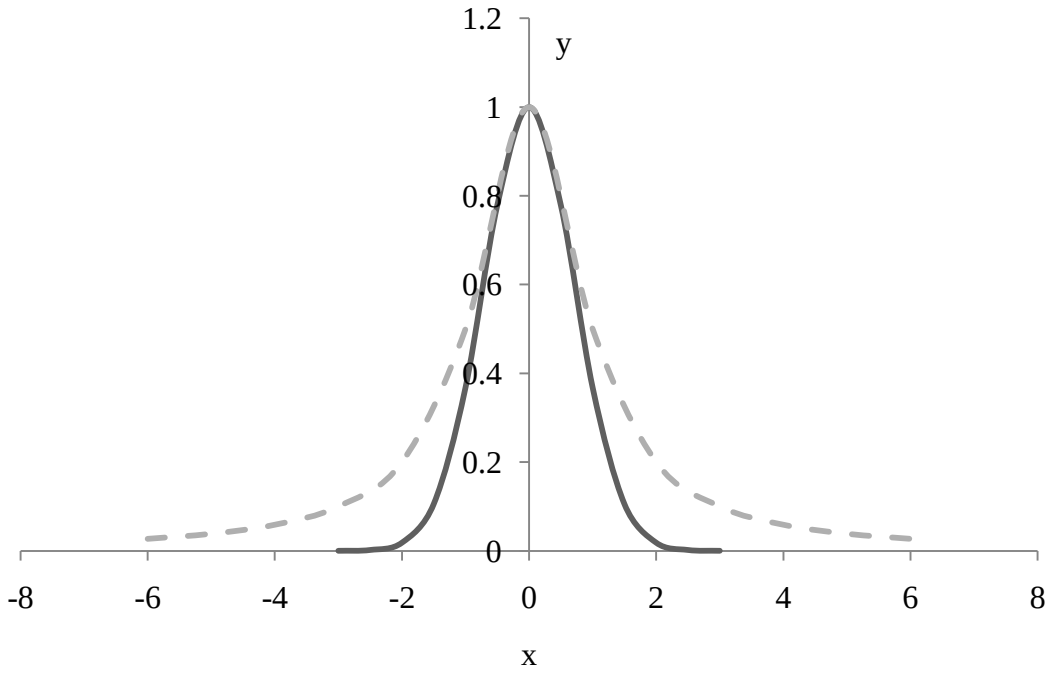

Figure 1.16 Profile of the Lorentzian (broken line) and Gaussian (solid line) functions.

Lorentzian shapes are usually observed for EPR lines of systems in liquid solution if the concentration of paramagnetic centers is low. Lines approach the Gaussian shape if the line is a superposition of many components. Such lines are called inhomogeneously broadened. [51] There are also other factors that lead to broader lines, such as rapidly relaxing electrons (slower relaxation = sharper lines), weak hyperfine interactions and/or anisotropic interactions or a high concentration of unpaired electrons in a sample due to increased "spin-spin" relaxation.

The area under the absorption curve corresponds to the amount of paramagnetic species. Because the integration procedure is complicated due to the asymmetry of the peaks, an approximate integral can be obtained from the derivative curve using peak-to-peak derivative amplitude ($2Y'_{max}$) and peak-to-peak width ΔH_{pp} [51].

$$I \propto Y'_{max}(\Delta H_{pp}) \qquad 1.19$$

1.4.4.6. The EPR Spectrometer

The typical setup of an EPR spectrometer is shown in Figure 1.17 . The microwave bridge has a microwave source which is a klystron, and a detector. The cavity stores microwave energy at its resonant frequency. The signal channel contains necessary electronics which enhances the sensitivity of the spectrometer. The field controller checks and adjusts the magnetic field.[57]

Most commonly used EPR spectrometers use a microwave frequency of 9.5 GHz. But there are EPR spectrometers with different frequency and magnetic field (Table 1.8). The high frequency puts an emphasis on the g-factor which means that g_{xx}, g_{yy} and g_{zz} are better separated on the spectrum. This is in agreement with a resonant condition (equation 1.14) because the value of g-factor depends on applied magnetic field, but the different frequency does not affect the hyperfine splitting.

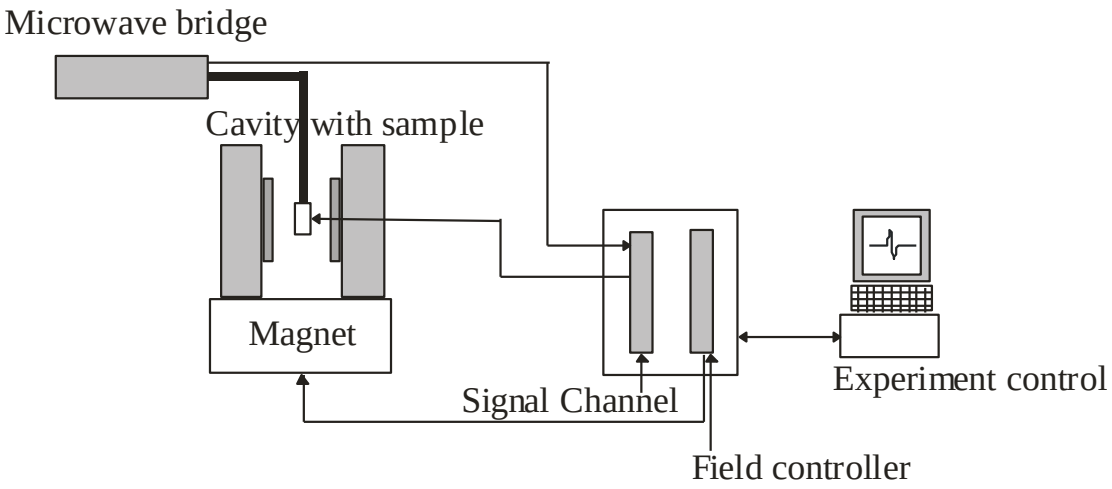

Figure 1.17 Simplified scheme of an EPR spectrometer.[57]

Microwave Band	*Microwave Frequency (GHz)*	B_0 *(for g = 2) Gauss*
L	1.1	392
S	3.0	1070
X	9.5	3389
K	24.0	8560
Q	35.0	12485
W	94.0	33600

Table 1.8 Different types of EPR spectrometers and their working frequencies.

1.4.4.7. Applications of EPR

Systems that can be studied by EPR include:

1. Free radicals: molecules possessing at least one unpaired electron.

2. Biradicals: molecules possessing two unpaired electrons which are far enough from each other that only weak interaction between them exists.
3. Molecules in a triplet state: two atoms, each possessing an unpaired electron, with a strong bond between them. The triplet state can be a ground state or some excited state.
4. Compounds with three or more unpaired electrons.
5. Defects in crystals and solids. One or more electrons can be situated inside or in the close proximity of these defects.
6. Ions with partially occupied electron levels, such as transition metal ions.

This means that EPR can be applied to study a broad range of systems, such as biological systems, chemical systems, conduction electrons, free radicals, gases, irradiated substances, naturally occurring substances, semiconductors, transition elements.[48,53]

1.4.4.8. Computer Simulation

In the case of the EPR spectra of amorphous and glassy materials (powder type), the magnetic spins are oriented randomly. This results in anisotropy of the spectrum and with several EPR active sites, the spectra can get complicated. Therefore, if possible, the spectrum of a single crystal should be measured, which will provide more accurate values of g-factor and hyperfine splitting, if observed. Unfortunately, not all compounds can be crystallized. Therefore to get accurate parameters, computer simulation has to be performed.

The most commonly used for the simulation purpose is the Bruker program Simfonia. WinEPR software is only for simple processing of the spectra when needed

while Simfonia is used for simulation of the measured and processed (when applicable) EPR spectra.

In Simfonia, EPR spectra of both solution and powder samples can be simulated. This has to be chosen before the choice of parameters is made due to the different setup of parameters for the simulation. Prior to the start, the measured spectrum that will be simulated is loaded. The instrumental parameters such as center field, sweep width, modulation amplitude, time constant and conversion time are input.

For powder spectra (Figure 1.18) all the directions for the hyperfine splitting, A, are specified for the nucleus with $I \neq 0$ as well as the number of nuclei of the same type and their nuclear spin. For the electron, the three values of the g-factor are specified. In case of isotropic spectra, all three values are set to be the same. The spin of the electron is set as well as zero-field splittings, D and E, if applicable. The number of theta and phi are the number of steps in the calculation. The higher this number, the more accurate results are obtained.

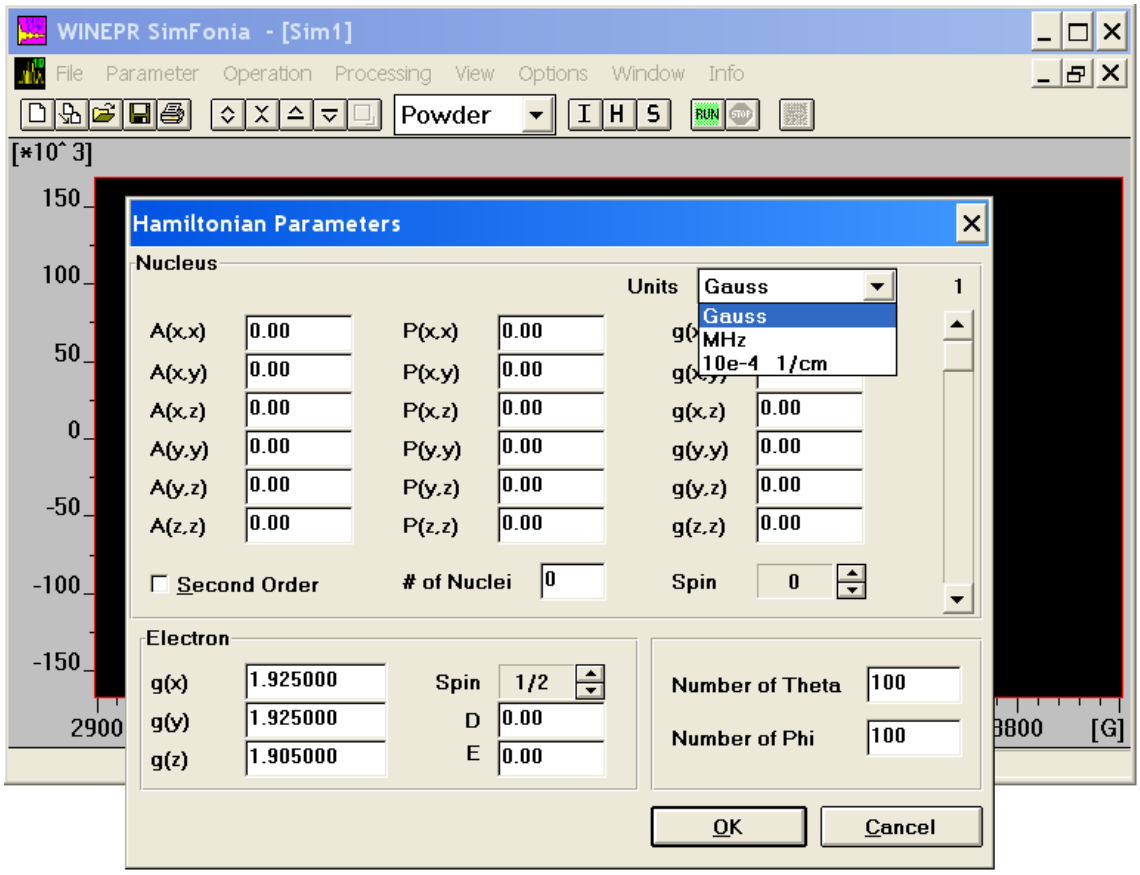

Figure 1.18 The setup of parameters for the simulation of the powder EPR spectrum.

Next, the line width of the spectra in all the directions: x, y and z is specified. The line shape: Gaussian or Lorentzian or their combination can be chosen here.

For solution samples (Figure 1.19), the nucleus is chosen from the built-in periodic table. This also includes properties of the chosen nucleus relevant to the EPR spectra, such as nuclear spin of all the naturally occurring isotopes of the nucleus, their abundances. The hyperfine splitting, A, can be specified in here. The g-factor of the electron is also specified having only one value due to the anisotropy of the spectra.

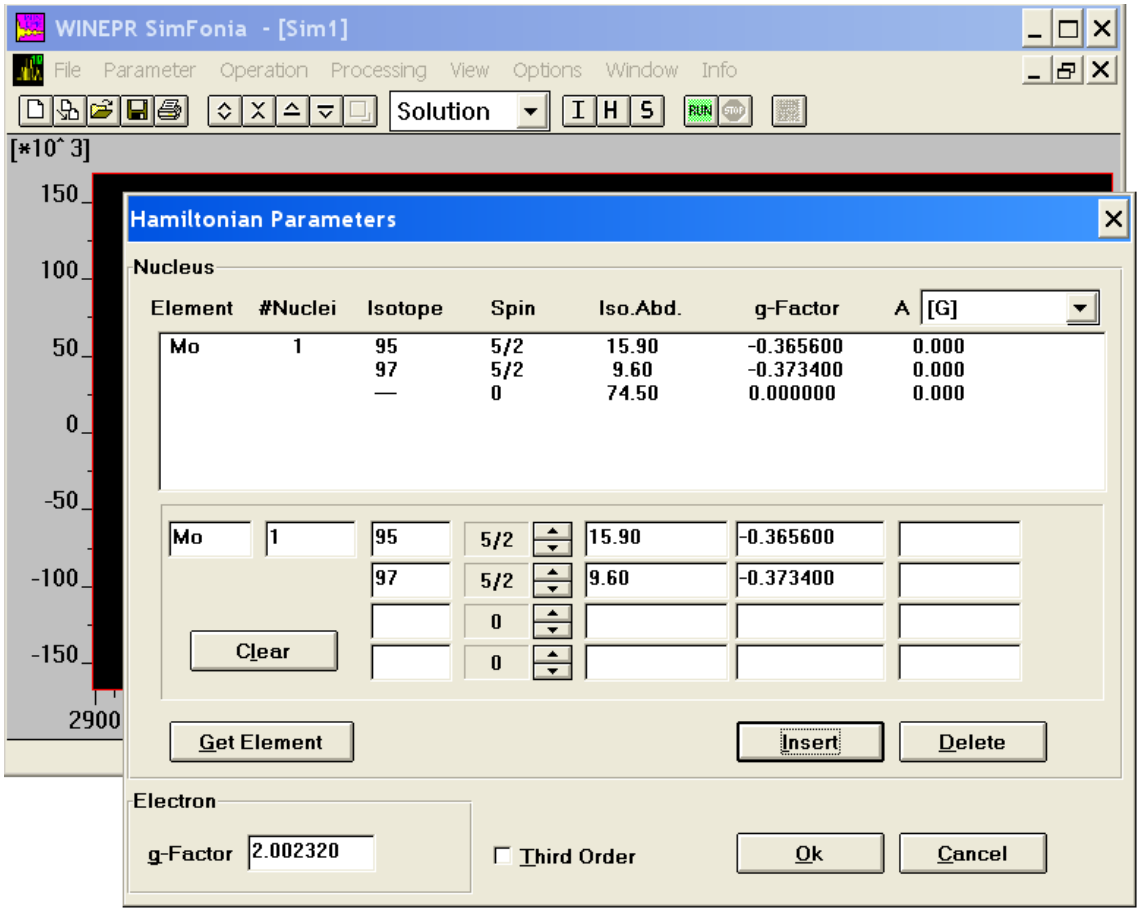

Figure 1.19 The setup of parameters for solution spectra simulation.

After the simulation is complete, both, the experimental and the simulated spectrum are visible in the window. To compare them, they can be overlaid for better comparison. If the difference is observed either visually by comparison of the overlaid spectra or by the third spectrum which is a difference spectrum, then the parameters are adjusted and simulation ran again. When the satisfactory agreement is obtained, the parameters can be obtained from the setup tables.

In case of more complicated spectra, where the spectrum is composed from several signals, each component is simulated separately, and in the end the components are then added together to compose a spectrum.

1.4.4.9. Molybdenum EPR

There are two paramagnetic oxidation states of Mo that can be studied by EPR: Mo^{III} and Mo^{V}. There are only two isotopes of Mo that can have an influence on the spectrum in terms of showing the hyperfine structure (section 1.4.4.3), these are ^{95}Mo and ^{97}Mo, both with I = 5/2. The other isotopes possess nuclear spin I = 0 and do not demonstrate hyperfine splitting in the EPR spectra. The natural abundance of ^{95}Mo and ^{97}Mo is 15.92 % and 9.55 %, respectively. Due to such a low abundance hyperfine splitting might be difficult to observe. Study of molybdenum nitride by Xie[58] and study of ammonium heptamolybdate – citric acid interaction by Andreev[59] are examples of the situation where Mo hyperfine splitting is not visible (Table 1.9, Table 1.10 and Table 1.11).

When hyperfine splitting due to Mo atoms is observed in the EPR spectra, it is in the form of weak satellite signals only. This was observed in the ^{95}Mo enriched sample of $[Mo_3CuS_4]^{4+}$ complexes[60], irradiated frozen solution of MoS_4^{3-} [61], and sulfite-oxidase[62].

The EPR spectra of Mo-containing compounds usually have an anisotropic g-factor and A values related to the symmetry of their compounds (see above: g factor and hyperfine splitting).[52,58-61,63,64] In both the axial and rhombic cases (see Table 1.9 and Table 1.10) anisotropy has been observed in the EPR spectra where the unpaired electron is on Mo. The g-factor of EPR signals due to Mo species usually has values in the range 1.907 - 2.05. The A values can also vary from a few tenths[61] to a few hundreds[60] of a Gauss (Table 1.9, Table 1.10).

	$g_{\parallel}$	$g_{\perp}$	$A_{\parallel}$	$A_{\perp}$
$[MoO(SPh)_4]^-$ [65] $[MoO(SPh)_4]^-$ [66] $[MoO(SPh)_4]^-$ [52]	2.017	1.979	56.3 G	24.6 G 23.8 G [52]
Ammonium heptamolybdate-citric acid powder[59]	1.94	1.92	Not observed	
Molybdenum nitride [58]	1.892	1.935	75 G	
Mo(V) salicyladoxime [64]	1.950	1.935	NR	
$[MoO(SePh)_4]^-$ [52]	2.072	2.005	51.7 G	22.7 G
MoS_4^{3-} [61]	1.953	1.973	54.6 G	32.1 G
Amorphous MoS_3 [67]	1.9013	1.9398	Not observed	

Table 1.9 Characteristic axial g-factors for Mo complexes. (NR = not reported)

	g_{xx}	g_{yy}	g_{zz}	A_{xx}	A_{yy}	A_{zz}
Sulfite oxidase (low pH form)[66]	2.007	1.974	1.968	60.7 G	26.8 G	17.9 G
Sulfite oxidase (high pH form)[66]	1.990	1.966	1.954	58.2 G	22.6 G	12.1 G
Sulfite oxidase (very rapid, xanthine)[66]	2.025	1.955	1.949	47.5 G	19.5 G	20.4 G
(tp)MoVO(bdt)*[66]	2.004	1.972	1.934	53.5 G	12.2 G	53.2 G
Cis, trans—(L-N_2S_2)$Mo^VO(SCH_2Ph)$[66]	2.022	1.963	1.956	62.5 G	25.4 G	23.9 G
Annealed molybdic acid[59]	1.88	1.92	1.93			
LMoO(bdt)[65]	2.004	1.972	1.934	53.5 G	12.2 G	53.2 G
LMoO(edt)[65]	2.018	1.970	1.939	58.5 G	3.5 G	48.7 G
LMoO[$S(CH_2)_3S$][65]	2.017	1.950	1.925	57.0 G	16.4 G	49.7 G
LMoO[$S(CH_2)_4S$][65]	2.022	1.960	1.932	56.5 G	16.6 G	49.7 G
[LMoO(S_2CNEt_2)]$^{+}$[65]	1.980	1.970	1.954	68.8 G	32.1 G	32.1 G
[LMoO{$S_2P(OEt)_2$}]$^{+}$[65]	1.980	1.965	1.953	Not observed		
[MoO$(edt)_2$]$^{-}$[65]	2.052	1.983	1.979	52.9 G	20.0 G	22.2 G

Table 1.10 EPR parameters of rhombic type spectra of Mo compounds.

However, a small number of compounds have isotropic g-factors and A values (Table 1.11).[64,65]

	g	*A*	
Mo(V) salicyladoxime [64]	1.948		
Mo(V) – H_2BPO[64]	2.005	Not resolved parallel and perpendicular	
$[MoO(abt)_3]^-$ [52]	1.990	12.7 G	48.3 G

Table 1.11 Parameters of the isotropic EPR spectra of Mo compounds.

Most commonly studied are complexes of Mo with O or S atoms bound to the central atom. Nikolova observed that EPR signals with g = 1.92 – 1.94 were characteristic for oxo –Mo^{5+} species and g = 1.99 characteristic for Mo^{5+} sites with O, S - surrounding[63] in the study of $MoO_3/\gamma Al_2O_3$ species. Dowerah also assigned an EPR signal with average g-factor = 1.9670 as characteristic of oxo-Mo^{5+} species[68]. However from the Table 1.10 and Table 1.11, it is evident that the g factors larger than g_e = 2.0023 are commonly observed for the species where the unpaired electron is situated on Mo atom. However, a much smaller g-factor value for molybdic acid (1.88) has also been observed (Table 1.10)[59].

The characteristic g-factors are $g_\perp < g_e$ and $g_\parallel > g_e$ [52,59,63,65], however the species having EPR signal due to Mo atoms with both $g_\perp$ and $g_\parallel < g_e$ have also been observed[52,59-61] or both $g_\perp$ and $g_\parallel > g_e$[52] (Table 1.9).

The g-factor of the Mo in the EPR spectra can be influenced by the type of the neighboring atom[63] and the number of these atoms. An increase of the g-factor and a decrease of the A-value (^{95,97}Mo) had been observed as the result of decreasing number

of coordinated S-atoms: compounds with two sulfur ligands have average g-factors = 1.965 - 1.971 and average A values = 35.9 - 38.3. For compounds with four sulfur ligands the average g-factor was found to be 1.990 and average A value 31.5 (Table 1.9)[65].

Values of $g_{xx} > g_e$ are a common feature of compounds containing multiple sulfur donor ligands. The large g values observed in these systems have been attributed to low-energy LMCT [S p → Mo d] charge-transfer bands, sulfur one-electron spin-orbit coupling and metal-ligand covalency.[66]

Even if a Mo-containing compound is EPR active in solid (powder) state, it doesn't have to be in the solution. A case of a solid-state EPR active Mo(V) – benzophenonoxime compound has been reported (but not explained) that doesn't show any signal when dissolved in chloroform.[64]

1.4.4.10. Copper EPR

Copper has one oxidation state, Cu(II) with a d^9 electronic configuration (one unpaired electron), that is EPR active and commonly studied by EPR spectroscopy. Cu(I) and Cu(III) are both diamagnetic and therefore EPR inactive. Furthermore, the two only natural isotopes, ^{63}Cu and ^{65}Cu, both possess nuclear moment I = 3/2 and cause hyperfine splitting observed in the EPR spectra of Cu(II) compounds.

For Cu(II), there is an interaction between magnetic field and the magnetic moment $\mu_L = -\beta_e L$ due to the orbital angular momentum (L) of the electrons. The total interaction is then described by

$$H = -H.(\mu_L + \mu_S) = \beta_e H.(L + 2.0023S)$$ [55] 1.20

where H is the spin Hamiltonian, S is the spin angular momentum and μ_S is the spin momentum.

All three types of spectra (isotropic, axial and rhombic) could be potentially observed in the powder EPR spectra of Cu(II) compounds. There are very few examples of isotropic EPR spectra due to the non-existence of strictly tetrahedral or octahedral geometry of Cu(II) compounds (as these geometries give isotropic spectra). However, isotropic spectra have been observed in $K_2PbCu(NO_2)_6$, $Cu(en)_3SO_4$, $Cu(ompa)_3(ClO_4)_2$ where a dynamic or pseudo-rotational type of Jahn-Teller distortion caused this EPR behavior. Copper(II) complexes containing $Cu(NH_3)_5^{2+}$ with lower than octahedral symmetry and $Cudien_2(NO_3)_2$ with misaligned tetragonal axes also gave rise to isotropic spectra[55].

The axial type of EPR spectrum for the Cu(II) compounds is much more common than isotropic spectra. Such spectra can be divided into two groups, the first one with a lowest value of $g > 2.04$. This is observed for the elongated tetrahedral-octahedral, square-coplanar of square-based pyramidal symmetries ($Cu(NH_3)_4(SCN)_2$, $Na_4Cu(NH_3)_4\{Cu(S_2O_3)_2\}_2.H_2O$, $Cu(1,3pn)_2SO_4H_2O$). This type of spectrum has also been observed for the compounds with rhombic symmetry with misaligned tetragonal axis and rhombic symmetry with aligned axes but with a rhombic component so small that powder measurement is not sensitive enough to resolve[55].

The second type of axial type of Cu(II) EPR spectrum, with lowest value of $g < 2.03$ was observed for tetragonal-octahedral and trigonal-bipyramidal geometries (Ba_2CuF_6, $Cu(NH_3)_2Ag(SCN)_3$.) It is also observed for the rhombic geometry with misaligned axes and rhombic geometry where the rhombic component is too small to be resolved[55].

Axial spectra are most common for the powder EPR spectra of Cu(II) complexes because the most common geometry for Cu(II) is distorted tetrahedral. Axial spectra, exhibit a strong absorption to higher field at $g_{\perp}$ and weak absorption to lower field at $g_{\parallel}$. The hyperfine splitting, $A_{\perp}$, from the nuclear moment of the Cu^{2+} at $g_{\perp}$ is too small to determine. The hyperfine splitting $A_{\parallel}$, arising from the nuclear magnetic moment of the Cu^{2+} at $g_{\parallel}$, is usually much greater, typically in the range of 15 to 25 x 10^{-4} cm^{-1} and four features at $g_{\parallel}$ are often resolved.[56,69]

Ligand field theory predicts that tetragonal Cu(II) will give rise to the EPR signal with $g_{\parallel} > g_{\perp} > 2$ (Table 1.12). The copper nucleus, possessing a spin of 3/2, couples to the unpaired electron and produces a four line hyperfine splitting which is quite evident in the $g_{\parallel}$ region but often unresolved in the $g_{\perp}$ region (Figure 1.20). [4]

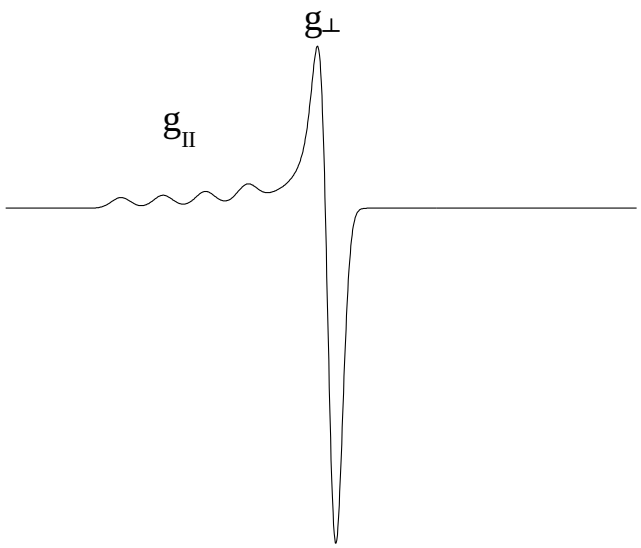

Figure 1.20 X-band tetragonal Cu(II) powder pattern EPR spectrum I = 0; I = 3/2.

	$g_{\parallel}$	$g_{\perp}$	$A_{\parallel}$	$A_{\perp}$
$CuSO_4$[69]	2.413	2.074	15.1 G	
$Cu(NO_3)_2$[69]	2.382	2.068	15.5 G	
Cu-monoethanolamine frozen solution[69]	2.263	2.062	18.3 G	
Cu(II)-acetophenonoxime[64]	2.165	2.053		

Table 1.12 Parameters of the axial EPR powder spectra of Cu compounds. $A_{\perp}$ was not reported as it wasn't resolved in the EPR spectra.

The g-value of the Cu(II) complexes in distorted octahedral coordination is mostly influenced by the four atoms in the plane and very little by the other two atoms, in the elongated axial positions[56] .

Rhombic spectra with the lowest g > 2.04 for Cu(II) compounds are observed for elongated rhombic symmetry: elongated rhombic-tetrahedral, rhombic square-coplanar and distorted square-based pyramidal ($Ba_2Cu(HCO_2)_6.4H_2O$, $Cu(3\text{-Me acac})_2$, $[Cu(1,3pn)_2.H_2O]SO_4$). This type of spectrum was also observed for elongated axial symmetry with misaligned axes[55].

Rhombic spectra (Table 1.13) with the lowest g-factors, < 2.03, are characteristic of compressed rhombic symmetry: compressed rhombic-octahedral, cis-distorted octahedral and distorted trigonal-bipyramidal ($(NH_4)_2Cu(NH_3)_2(CrO_4)_2$, $[Cu(bipy)_2(ONO)]NO_3$, $[Cu(bipy)_2I]I$. This is also observed for compressed axial or rhombic symmetry with misalignment of axes ($Cu(\text{methoxyacetate})_2.2H_2O$ [55].

Hathaway and Billig used a G parameter to distinguish between axial and rhombic symmetry, both of which in certain cases can give rise to and axial type of EPR spectrum. This parameter is defined as

$$G = \frac{g_{\parallel}-2}{g_{\perp}-2} \qquad 1.21$$

G was found to be larger than 4 for axial spectra and smaller than 4 for rhombic EPR spectra[55]. This was later used to determine the symmetry of copper amine complexes by Zhang[69].

The spectra of the tbp copper complexes with N only donor tripodal ligands show a completely different trend from tetragonal complexes: $g_{\perp} > g_{\parallel}$; $A_{\perp} > A_{\parallel}$; resolution of EPR signals in the $g_{\perp}$ region is much better than those of the $g_{\parallel}$ region[70].

	g_{xx}	g_{yy}	g_{zz}	A_{xx}	A_{yy}	A_{zz}
Bis(N-isopropylsalicylaldiminato) Cu(II)[71]	2.188	2.166	2.050	NR		
Bis(N-t-butylsalicylaldiminato) Cu(II)[71]	2.218	2.146	2.051	NR		
Bis(N-n-butylsalicylaldiminato) Cu(II)[71]	2.156	2.072	2.042	NR		
$[Cu(NS_3Me)Br]ClO_4$[70]	2.17	2.04	1.97	109 G	93.9 G	136 G
$Cu(NS_3Me)NCS]ClO_4$[70]	2.35	2.05	2.01	145 G	24.3 G	56.8 G
$[Cu(N_2S_2bz)Cl]PF_6$[70]	2.20	2.18	2.04	109 G	102 G	NR
$[Mo_3CuS_4]^{4+}$	1.923	1.940	1.948	69.6 G	32.1 G	28.6 G

Table 1.13 Parameters of the rhombic powder EPR spectra of Cu compounds. (NR = not reported)

When Cu^{2+} is ligated to another nuclei with $I \neq 0$, such as ^{14}N, ^{15}N and ^{19}F in copper proteins, superhyperfine splitting can be also observed[56]. Chenah observed this splitting from ^{14}N in the EPR spectrum of powder Cu(II)-acetophenonoxime[64].

g-factors of Cu^{2+} can vary depending on the type of ligand attached to the metal and the environment. Lorentzian type lines were observed for Cu^{2+} in the Cu-doped GeS with g = 2.0033.[72]

The physical environment of the EPR active Cu compounds has also been shown to have an influence on the spectra observed. Cu^{2+}-acetophenonoxime has an anisotropic axial spectrum in powder form. In solution, the spectrum is isotropic with a lower g-factor and hyperfine splitting can be observed. However, in a vitrous state, the same compound has an EPR spectrum with such poor hyperfine resolution that Hamiltonian parameters cannot be specified.[64]

As described earlier (sections 1.4.4.2 and 1.4.4.3), in the solution samples of Cu(II) compounds (not including frozen solutions which behave like powders in EPR), only one value of g-factor and hyperfine splitting is observed.

The nature of solvent has a little influence on the g-factor as well as hyperfine splitting values, A. This is most likely related to the interaction between the studied compound and the solvent, as these changes have been very small for salicylaldiminato Cu(II) complexes by Voronkova (Table 1.14)[71].

	g	*A*
Bis(N-isopropylsalicylaldiminato) Cu(II)[71]	Toluene: 2.120 Pyridine: 2.125	Toluene: 71 G Pyridine: 67 G
Bis(N-t-butylsalicylaldiminato) Cu(II)[71]	Toluene: 2.140 Pyridine: 2.141	Toluene: 54 G Pyridine: 52 G
Bis(N-n-butylsalicylaldiminato) Cu(II)[71]	Toluene: 2.113 Pyridine: 2.124	Toluene: 84 G Pyridine: 73 G
Cu(II)-phenonoxime[64]	2.097	90 G

Table 1.14 EPR parameters of the EPR spectra of Cu(II) compound in the solutions.

1.4.4.11. Sulfur EPR

Paramagnetic sulfur has been observed in solid (crystals[73], polycrystalline, amorphous[74] and polymeric state) as well as in solution[75,76].

The amorphous sulfur after UV irradiation provided an anisotropic EPR spectrum, composed from two signals. The EPR parameters of these two signals varied in the value of the g_{zz} factor only and were characterized as the trans and cis configurations of the $-(S)_n$-S* chains[74]. The value of parameters found in this study is comparable to the parameters found in other studies of the S_3^- radical[77] (Table 1.15).

Zdravkova also observed the formation of two signals due to sulfur radicals formed in the UV-irradiated samples of phosphorodithioates. This was assigned to the possibility of partial destruction of the S-S bond, giving rise to the thio radicals (S-S destructed) and dithioradicals (S-S not destructed).

Sample	g_{xx}	g_{yy}	g_{zz}
*Cis –$(S)_n$-S** [74]	2.0016	2.0254	2.0518
*Trans –$(S)_n$-S** [74]	2.0016	2.0238	2.0405
S_3^- in Na_2S_6 [76]	2.0029	2.0235	2.0488
S_3^- in NaCl [77]	2.0014	2.0308	2.0465
S_3^- in KCl [77]	2.0026	2.0319	2.0499
S_3^- in KBr [77]	2.0004	2.0327	2.0508
S_3^- in NaBr [77]	2.0003	2.0348	2.0500
$(MeO)_2P(S)SNH_4$ [78]	1.9877	2.0142	2.0278
$(EtO)_2P(S)SNH_4$ [78]	1.9980	2.0242	2.0405
$[(EtO)_2P(S)S]_2$ [78]	2.0024	2.0259	2.041
$[(PrO)_2P(S)S]_2$ [78]	2.0005	2.0245	2.0395
$[(PrO)_2P(S)S]_2$ [78]	2.0022	2.0251	2.039

Table 1.15 EPR parameters of the sulfur species in powder type of spectra.

In addition to the anisotropic signal of S_3^- observed in the irradiated sample of Na_2S_6 by Gobeltz, another, isotropic signal was observed as well. As its value, g = 2.0280 corresponds to the average value ($g = \frac{g_{xx}+g_{yy}+g_{zz}}{3}$) of the anisotropic signal, it was concluded that the isotropic signal is also due to S_3^- species, but in the liquid phase. Thus powder and solution type of spectra were observed simultaneously in the system[76].

The calculation of the EPR parameters of alkylsulide radicals and ions showed that the monosulfide species has higher values of g_{zz} than the disulfide species but g_{xx} values are same in all the species. Results are summarized in Table 1.16.

Sample	g_{xx}	g_{yy}	g_{zz}
CH_3-S*[79]	2.002	2.017	2.428
CH_3-S*H[79]	2.002	2.018	2.277
CH_3-SS*[79]	2.002	2.028	2.063
CH_3-S*S-CH_3^+ *trans*[79]	2.002	2.017	2.047
CH_3-S*S-CH_3^+ *cis*[79]	2.002	2.020	2.031
CH_3-S*S-CH_3^- *trans*[79]	2.002	2.009	2.028
CH_3-S*S-CH_3^- *trans*[79]	2.002	2.021	2.023

Table 1.16 Calculated g-factors for the sulfur radicals and sulfur ion species.

In solution phase, as expected, an isotropic signal is observed for the sulfur radicals. It is noticeable that S_3^- and S_4^- radicals from Li_2S_n species have very different linewidths (Table 1.17). Levillain assigned this to the differences of the chemical exchange of these radicals with their dimers[75].

Sample	*g*	*linewidth*
S_3^- *in* Na_2S_6 [76]	2.0280	NR
S_3^- *in* Li_2S_n *in DMF*[75]	2.0290	115.8 G
S_4^- *in* Li_2S_n *in DMF*[75]	2.031	15.6 G

Table 1.17 EPR parameters of sulfur radicals in solution.

The hyperfine splitting from the sulfur radicals is difficult to observe because its only isotope with $I \neq 0$ ($I = 3/2$), ^{33}S has a very low natural abundance, 0.76 %.

1.4.5. X-Ray Absorption Spectroscopy (EXAFS)

1.4.5.1. Introduction to EXAFS

An atom contains electrons divided into shells. The number of shells depends on the number of electrons in an atom, which is specific for each element of the Periodic Table. Depending on the position of the electron in a specific shell of an atom, the binding energy of the electron is different. The 1s orbital (first shell, closest to the nucleus of an atom) is by convention called the K shell. The second shell containing 2s and 2p orbitals is called the L shell. The third shell (3s, 3p orbitals) is the M shell, etc.

The x-ray absorption spectrum can be obtained because of the atom's ability to absorb x-rays. For this purpose, the energy of the x-ray used has to be larger than the binding energy of the specific electron in the atom studied. In this case, the electron is ejected from the atom (Figure 1.21). This photoelectron interacts with the electrons of surrounding non-excited atoms (backscatterers). If the energy of the x-ray is scanned from just below to just above the binding energy of the electron in the atom, a rapid rise in the extent of absorption is observed, referred to as an "edge". This part of the spectrum is called the X-Ray Absorption Near-Edge Spectrum (XANES), see Figure 1.22. As the energy of the x-ray used is increased further, the spectrum displays undulations. This is the Extended X-ray Absorption Fine Structure (EXAFS) part of the spectrum; this provides structural information about the molecule studied.

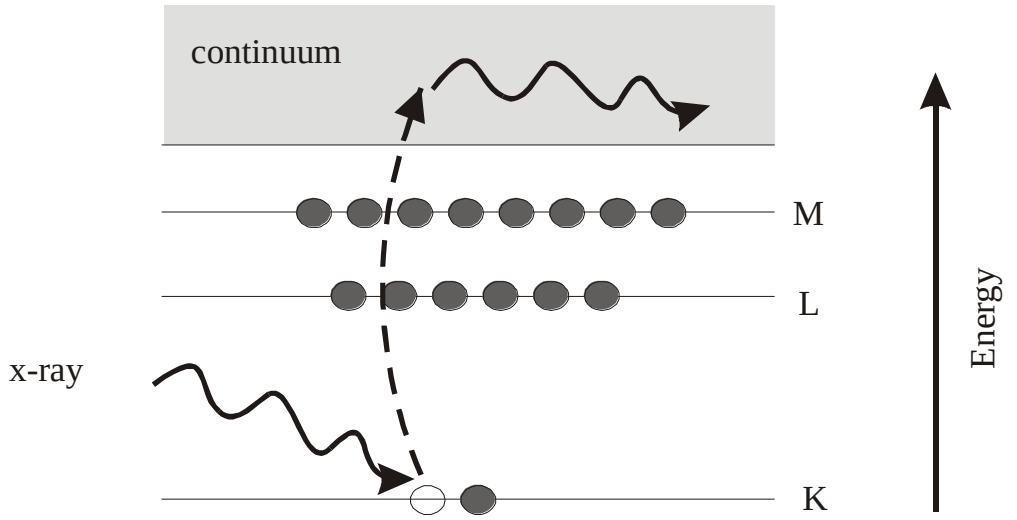

Figure 1.21 Interaction of x-ray and atom.

The XANES part is usually considered to be from 20 eV below to 30 eV above the edge and the EXAFS beyond 30 eV above the edge (Figure 1.22).

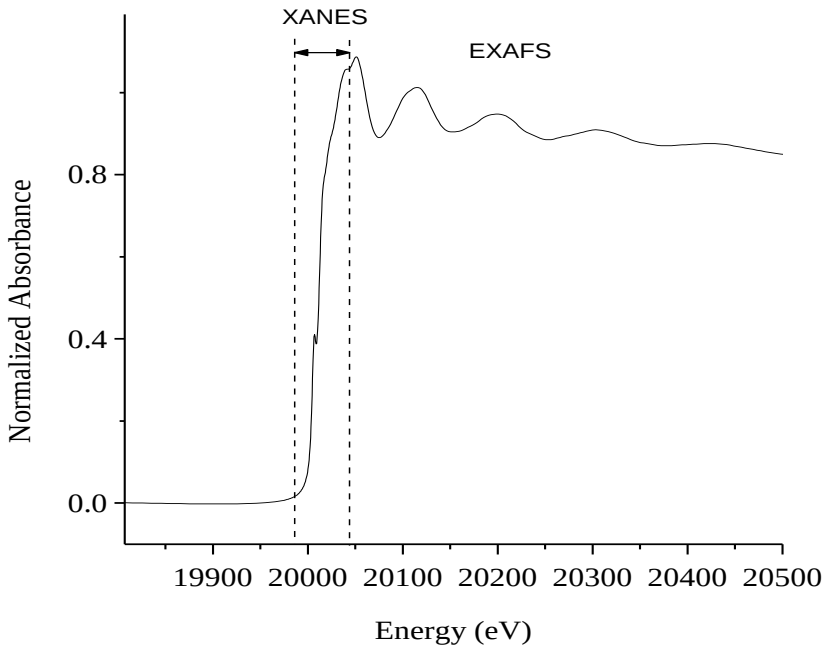

Figure 1.22 Parts of the X-ray absorption spectrum.

The energy (E_0) required to eject the electron from the atom differs for the electrons present in the same atom (largest energy for the core electrons) and also differs for different atoms (increases with increasing atomic mass). This is caused by the variable binding energy of an electron within an atom. The energy of the edge is specific for every element and every orbital in that element. Within the same atom, greater energy will be needed to study an electron in the lower energy level (K edge needs higher energy than L edge) because of its closer proximity and greater attraction to the positive nucleus.

1.4.5.2. Near - edge Spectra and their Analysis

The characteristic position of the edge in the X-ray tables[80] was determined for standard samples which are pure elements. In compounds of the same element, the edge of the spectrum is found at a slightly different energy. This shift is caused mainly by different oxidation states of the element of interest in the sample and is usually in the order of few eV (see sections 1.4.5.6 and 1.4.5.7 for a more detailed discussion).

Sometimes, we can also observe pre-edge features in the near-edge spectra. These bumps that appear on the spectrum before the edge represent the transition of the electron to excited bound states. These features can also help in the determination of the structure around the element of interest. They can be specific for the geometry of the absorbing atom or the type of neighboring atoms (sections 1.4.5.6 and 1.4.5.7).

The near edge and the pre-edge features are also important in the analysis of mixtures. Two techniques have been developed for this purpose. Linear combination analysis (LCA) can be used for analyzing a single spectrum of a mixture. For a mixture under investigation, the library (or set) of the near-edge reference spectra of all the compounds present in this mixture have to be available. During the analysis, the relative proportions of the reference compounds in the mixture are found by fitting them to the

unknown spectrum. LCA gives the best results if the reference spectra (the components of the unknown mixture) are very different. LCA was used to determine the organic sulfur species present in the marine sediments and humic substances[81].

Another method used to analyze near-edge spectra of unknown species is principal component analysis (PCA). PCA can be applied only to extended data sets (a single spectrum is insufficient). The number and the spectral characteristics of the principal components (species) can be determined without an explicit database. Two requirements for PCA are: the number of species present must be smaller than the number of sample spectra, and the species composition of these samples must vary. More details on PCA can be found in Factor Analysis in Chemistry by Malinowski and Howery[82].

PCA and LCA have been used to identify components in complex mixtures where the presence of a large number of compounds is likely. A combination of the two methods has been used in the study of sulfur K XANES spectra of humic acid[83], Cu K XANES spectra of Cu-humate-goethite[84] speciation and Zn speciation in soil[85].

1.4.5.3. Origin of the EXAFS

When the energy of the x-ray is just below the binding energy of the electron, its transition to bound states can be observed as the pre-edge in the EXAFS spectrum. An increase of the x-ray energy to the same value as the binding energy of this electron results in absorption of an x-ray photon by the electron and its transition to the unbound state. This is observed by a strong increase of the absorbance in the EXAFS spectrum, which is called an absorption edge.

When the energy of x-rays increases further it becomes larger than the bonding energy of the electron. The excess of the absorbed energy is used as kinetic energy, where the electron (now called a photoelectron) is ejected from an atom and interacts with other neighboring atoms. The neighboring atom scatters the photoelectron back and therefore is called a backscatterer, as shown in Figure 1.23.

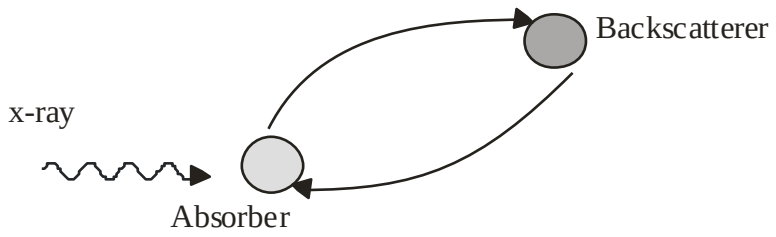

Figure 1.23 Backscattering of an electron from the neighboring atom.

The absorption of an X-ray radiation and the ejection of the electron from an atom give rise to the outgoing wave and the wave which has been backscattered by other atoms. When these two waves are in phase, the absorption shows a maximum called constructive interference. When they are out of phase, the absorption shows a minimum, destructive interference. The interference of these two types of waves gives rise to a sinusoidal variation of μ vs.E (Figure 1.24) which is known as the EXAFS, where μ(E) is the absorption coefficient.[86]

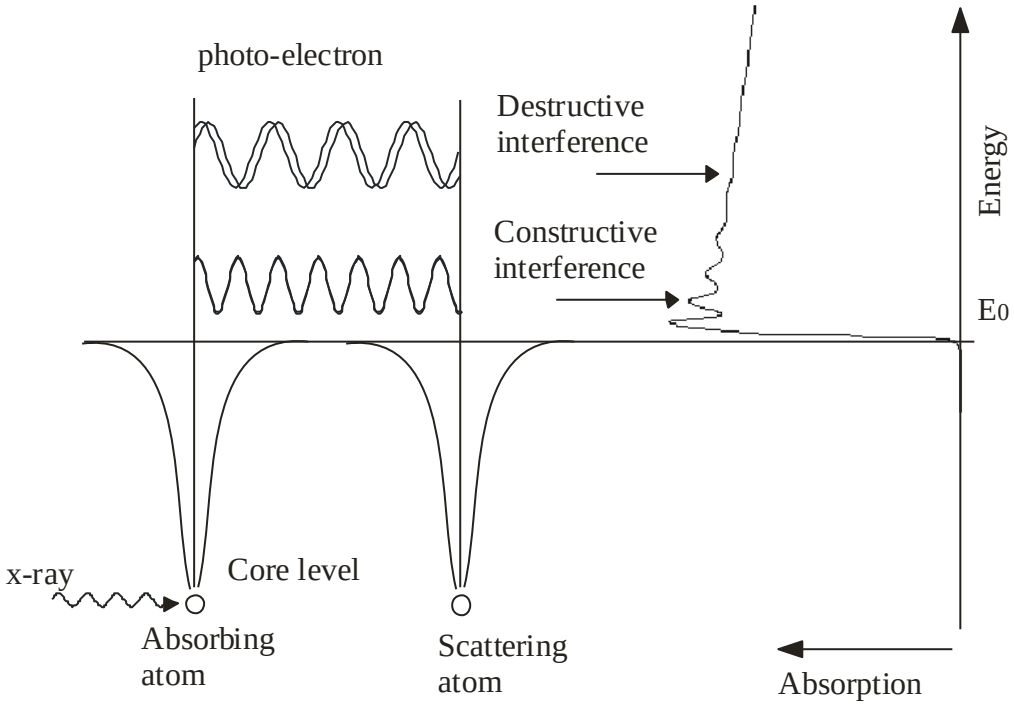

Figure 1.24 Origin of the EXAFS spectrum.

The EXAFS is determined by the structure of the studied compound. Upon analysis, it provides the type and the number of the backscatter atoms. It also provides the geometry, the coordination number of the absorber and the bond distances and bond angles between the absorber and the backscatterers. For EXAFS measurements, it is necessary to have a pure compound because the analysis of the mixtures is problematic.

The frequency of the EXAFS oscillations depends on the distance between absorber and backscatterer atoms. The amplitude of the oscillations depends on the nature of the backscatterers. The heavier the atom, the larger the amplitude. The amplitude also depends on the number of the atoms of a particular backscatterer. The more backscattering atoms of the same type, the larger the amplitude of the EXAFS oscillations for that particular backscatterer.

The EXAFS fine structure $\chi(E)$ can be described by the equation

$$\chi(E) = \frac{\mu(E)-\mu_0(E)}{\mu_0(E)} \quad 1.22$$

where $\mu(E)$ is the measured absorption coefficient and represents the probability of the transitions between quantum states, $\mu_0(E)$ is a smooth background function representing the absorption of an isolated atom.

Usually x-ray energy is given in wave-numbers, k (in $Å^{-1}$)

$$k = \sqrt{\frac{2m(E-E_0)}{\hbar^2}} \quad 1.23$$

or

$$k = \sqrt{0.262(E[eV]-E_0[eV])} \quad 1.24$$

where E_0 is the absorption edge energy and m is the electron mass, ħ is the reduced Planck's constant.

The EXAFS equation is given by

$$\chi(k) = S_0^2 \sum_i \frac{N_i S_i(k) f_i(k)}{kR_i^2} e^{-2R_i/\lambda(k)} e^{-2\sigma_i^2 k^2} \sin[2kR_i+\varphi_i(k)+\delta_c(k)] \quad 1.25$$

where N_i is the coordination number for atom type i,

R_i is the absorber-backscatterer distance for atom type i,

σ_i^2 is the mean-square deviation in R_i, the Debye-Waller factor,

S_0^2 is the total amplitude reduction factor,

$S_i(k)$ is the amplitude reduction function,

$\lambda(k)$ is the photoelectron mean free path function,

$f_i(k)$ is the EXAFS amplitude function,

$\varphi_i(k)$ is the EXAFS backscatterer phase shift function and

$\delta_c(k)$ is the EXAFS central atom (absorber) phase shift function.

These are explained in more detail below.

The EXAFS equation has two main components: amplitude, $S_0^2 \sum_i \frac{N_i S_i(k) f_i(k)}{kR_i^2} e^{-2R_i/\lambda(k)} e^{-2\sigma_i^2 k^2}$ and phase, $\sin\left[2kR_i+\varphi_i(k)+\delta_c(k)\right]$ functions. Amplitude component has an amplitude function term, $S_0^2 \sum_i \frac{N_i S_i(k) f_i(k)}{kR_i^2}$, mean free path term, $e^{-2R_i/\lambda(k)}$ and the Debye-Waller factor, $e^{-2\sigma_i^2 k^2}$.

The coordination number, N_i, of a shell can be used as a scaling factor. With increasing N_i, an increase of the amplitude for the oscillation is observed. The interatomic distance, R_i, contributes to amplitude and phase: higher R increases the frequency and decreases the amplitude. S_0^2 is the overall scale factor; its value is usually close to unity. The Debye-Waller factor, σ_i^2, is a sum of vibrational and static contributions. It acts to damp out the amplitude at higher k. Lower temperature minimizes the Debye-Waller factor (since the vibrational contribution is temperature dependent).

N_i, R_i and σ_i are structural parameters extracted from EXAFS. The accuracy in the determination of N_i is usually ± 25 %.[87-89] This can cause inaccurate determination in the coordination number. Difficulty deciding between three and four for the Mo-S coordination number in DMSO reductase has been observed.[88]

R_i and σ_i^2 parameters are correlated, where σ_i^2 is an indicator of the variation in the R_i distances. [87,88,90-92] Reasonable values for σ_i^2 are between 0.0015 to 0.0080 Å^2. R_i can usually be determined with an accuracy better than ± 0.02 Å.

1.4.5.4. Transmission vs. Fluorescence

Several measurement techniques are used to obtain an X-ray absorption spectrum. The technique chosen depends on the physical state of the sample, on the concentration of the element of interest and on the desired information.

The most commonly used mode for collecting an EXAFS spectrum is transmission mode (Figure 1.25). The x-ray beam goes through the sample and its intensity is measured before and after using the ion chamber detector (more details on detectors can be found in the literature[80,93]). The transmittance is then calculated from the ratio of the intensity of the beam transmitted through the sample (I) and the incident beam intensity (I_0).

$$T = \left(\frac{I}{I_0}\right) \qquad 1.26$$

or as absorbance

$$Abs = \mu x = \log\left(\frac{I_0}{I}\right) \qquad 1.27$$

where μ is the absorption coefficient and x is the thickness of the sample. The absorption coefficient, which is a smooth function of energy, depends on the sample density, d, the atomic number, Z, atomic mass A and the x-ray energy E:

$$\mu \approx \frac{dZ^4}{AE^3} \qquad 1.28$$

Frequently, a reference sample is placed to receive the X-rays emerging from the analytical sample, and the intensity of the beam passing through this reference sample is also measured. This reference spectrum (of a metal foil, for example) is used for calibration purposes during the experiment or during data processing.

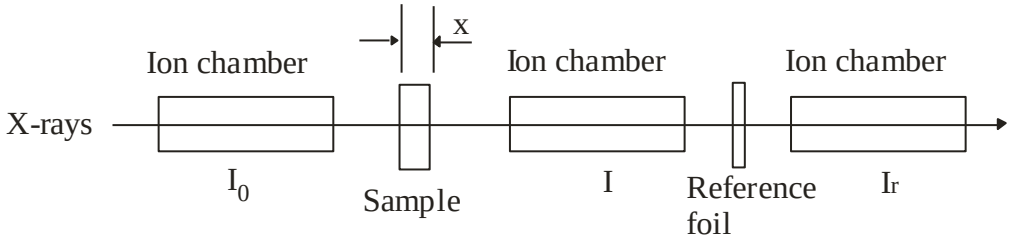

Figure 1.25 Characteristic setup of a transmission experiment.

The transmission (absorption) mode of measurement is used for thin solid samples with a high concentration of the element of interest. For transmission, the sample has to be homogeneous and free of pinholes to prevent leaking of the x-ray though holes.

For thick samples or samples with a low concentration of the element of interest (ppm levels, solutions), the fluorescence mode for collecting the spectra is used (Figure 1.26). More details on detectors can be found in the literature[80,93]. It is not suitable for concentrated samples, because the signal from the element of interest would be severely damped by self-absorption[94]. This method does not measure the background absorption due to other constituents and therefore improves the sensitivity[86]. Fluorescence yield is independent of the incident energy, but it is proportional to absorption. The absorption of an X-ray photon generates a core hole. Filling this core hole results in fluorescence radiation, the energy of which is characteristic of the absorbing element and is less than the energy of the original exciting radiation.[93] In this mode, x-rays from the sample and collected by the detector can contain the fluorescence line of interest, fluorescence lines from other elements in the sample and elastically and inelastically scattered x-rays. This complicates the analysis of the spectra. A suitable energy dispersive detector (solid state detector) is chosen to eliminate the background signal. The fluorescent signal is emitted from the sample in all directions. The detector is usually placed 90° from the incident beam (45° from the sample). This minimizes the detection of the transmitted or reflected light.

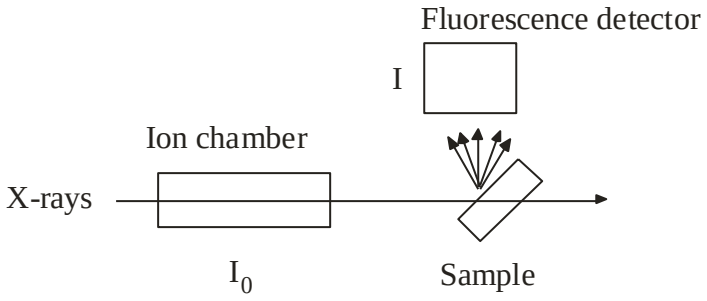

Figure 1.26 Fluorescence experiment setup. Sample is at 45° to the incident beam, detector is at 90° in the horizontal plane.

There are other more specialized EXAFS measurement methods that can be used; their specifications and descriptions can be found in the literature[86,93].

1.4.5.5. Analysis of EXAFS Data

The measured intensities are converted to μ(E). During this step, possible errors (self-absorption, detector dead-time) are corrected. A smooth pre-edge function is then subtracted from μ(E) (equation 1.22).

The threshold energy E_0 is identified. As this is hard to determine, different approaches are used. One is to set E_0 as the lowest energy inflection point. It is not an accurate number; during processing and fitting the offset of the true value from the assumed value, defined as ΔE, is refined. The other, more commonly used method is to set E_0 to an arbitrary energy above the absorption edge.

The μ(E) is normalized to go from 0 to 1. Then a smooth post-edge function (usually a spline) is removed from the data to approximate $\mu_0(E)$.

After this initial processing, the EXAFS data are then transferred into k-space (equation 1.23), then k-weighted to enhance the higher k-regions and Fourier

transformed into R-space. Although the exact bond distances cannot be read from the FT data directly, the FT gives their approximate values. Accurate values are obtained from the fitting of the data (see below).

From the fit, values of coordination numbers, N_i, interatomic distances, R_i, and Debye-Waller factors, σ_i^2 are obtained to provide structural information.

More details on the processing and fitting procedure are described in the Experimental section on EXAFS data analysis (section 2.10.3).

1.4.5.6. Copper EXAFS

The position of the Cu K-edge in Cu foil has been found to be 8979 eV[80].

The XANES of the Cu K-edge has been shown to be very important in the determination of the oxidation state, because of significant differences in both the position of the edge itself and in the pre-edge features.

An extensive study on the XANES of 40 Cu compounds was done by Kau[95]. All 19 Cu(I) compounds studied displayed a low energy maximum in the range of 8983 - 8986 eV that has been assigned to a 1s → 4p transition. The difference between the energy and the intensity of the pre-edge features is caused by the coordination number: the feature is less intense for the compounds with higher coordination number around Cu and has been shown to decrease from the 2-coordinate to 3-coordinate (8984 eV), being of the weakest intensity and highest energy (8985.5 eV) for 4-coordinate Cu(I) compounds (eg. $[Cu(py)_4]ClO_4$, $Cu(tepa)BPh_4$, $[Cu_2(XYL\text{-}O\text{-})]PF_6$). This transition within the same interval has also been observed by de Moen for the compounds of Cu_2O and $Cu(NH_4)_2^+$ at 8984 eV[96].

Sarode observed a shoulder in the near-edge spectrum at 8982.6 eV for the Cu(I) compounds which was assigned to the 1s → 4s transition as a characteristic feature for Cu(I) compounds such as $CuFeS_2$, CuCl, CuBr and CuI.[97] This feature has been observed at even lower energy: 8981.7 eV as characteristic of Cu(I) compounds by Hsiao[98]. The intensity of the characteristic peak for the 1s → 4s transition in Cu^+ compounds was observed to be dependent on the coordination number. With the increasing coordination number, the normalized intensity of this peak decreased.[95]

Since these pre-edge features characteristic of Cu(I) near-edge spectra are at lower energy than any pre-edge features characteristic of Cu(II) spectra (Table 1.19), they can be used in the determination of the presence of Cu(I). However, the absence of the pre-edge feature below 8985 eV does not necessarily mean the absence of Cu(I), as these features can appear at energy slightly higher than 8985 eV, as observed by Kau for samples with N_4 and N_3O ligation.[95]

Cu(II) compounds also have their specific pre-edge features. Berry attributed the shoulder on the main absorption edge of the Cu(II) spectra to the axial or tetragonal distortion which is characteristic for Cu(II)[99]. 21 compounds studied by Kau[95] showed the presence of a low-energy tail between 8983 - 8985 eV but no pre-edge below 8985 eV (as is characteristic for Cu(I)). The intensity of this tail was increased for compounds with S_4 or S_2N_2 ligation around Cu(II), due to increased covalency of these bonds.

Peaks characteristic for Cu(II) compounds have always been observed at energies higher than 8985 eV (characteristic for Cu(I)) and therefore can be taken as indicative of the presence of Cu(II) in the measured sample.[95-97]

The most significant difference between the near-edge spectra of Cu in oxidation states I and II is the presence of the 1s → 3d transition. The peak corresponding to this transition is not observed for the Cu(I) compounds, due to their completely filled 3d

orbitals (d^{10} configuration). This transition, when present in the near-edge spectra, is characteristic for Cu(II) compounds with $3d^9$ electronic configuration, but here has a low probability due to the almost full 3d shell with only one unpaired electron[96] and therefore might be difficult to observe in the spectra.

Except for the 1s → 3d transition observed in Cu(II) spectra at 8977.3 - 8978.3 eV, other two characteristic transitions in the near-edge spectra of the samples of X-Cu glucoronate (where X is Na, Ba or Mg) containing Cu(II) (confirmed by EPR spectra) were described by Sarode: 1s → 4s and 1s → 4p. The 1s → 4s transition was found at energies of 8985 - 8987 eV for Cu-glucoronate molecules[97]. It has been observed in other Cu(II) compounds and found to be intense for the symmetrical tetrahedral environment, especially for Cu(II) surrounded by four sulfur atoms.

The last mentioned transition in Cu(II) near-edge spectra is the 1s → 4p transition, with the average value being 8996.5 eV, as reported by Sarode for several inorganic copper salts[97]. For CuO, this transition was found at 8995.6 eV by Sarode, which is close to that found for the other previously mentioned compounds, but Nicholson reported this transition at lower energy: 8991 eV for the same compound.[100]

For the $Ba_2Cu_2O_5$ sample containing Cu^{3+}, a pre-edge transition 1s → 3d has been observed at 8985 eV and the 1s → 4s transition at 8995 eV, which is significantly higher (10 eV) than for Cu^{2+}.[97]

	Transition energies		
	1s → 3d	1s → 4s	1s → 4p
Cu^{+}	No	8982.6-8984 eV	
Cu^{2+}	8977.3-8979 eV	8985-8991 eV	8996.5 eV
Cu^{3+}	8985 eV	8995 eV	

Table 1.19. Characteristic transition energies for different oxidation states of Cu. [95-97,99]

Hsiao attributed the position of the near-edge spectra of the Cu(II) samples to the geometry. The edge at 8983.7 eV is characteristic of square planar symmetry; in octahedral symmetry, Cu(II) has an edge at 8987.8 eV[98].

Cu has been studied by EXAFS in many different compounds, mainly because of its biological importance. The main goal is to determine the bond distances and the coordination number of Cu interaction with neighboring atoms (backscatterers) where X-ray diffraction measurement cannot be used due to the physical nature of the samples (non-crystalline, solutions).

It was found that the bond distance between Cu and the neighboring atom (backscatterer) increases with the size of this atom (atomic mass); for example, Cu-S is longer than Cu-O (Table 1.18 and Table 1.19).

From several studies, typical Cu-O bond distances were found. De Moen found this distance to be 1.85 Å for the Cu_2O unit in copper(I) oxide containing a Cu(I) atom coordinated by 2 O atoms[96]. For Cu(II) coordinated by four O atoms, this distance was found by Sarode to be the same or slightly longer in several molecules, 1.85 – 2.0 Å (Table 1.18). Much larger Cu(II)-O distances were found in CuO and $Cu(OH)_2$, 2.63 and 2.78 Å, respectively, in the study by Nicholson (coordination numbers not

specified)[100]. Based on these examples, it appears that both the oxidation state of Cu and the coordination number can influence the Cu-O distance. The nature of the ligand attached to the Cu has also significant influence on the Cu-O bond lengths. This distance has a range of values for the same oxidation state of copper and the same coordination number of oxygen attached to copper (Table 1.18).

N	*Distance (Å)*	*Compound*
Cu(II)-O distance		
4.2	2.0	$CuSO_4.5H_2O$ [97]
4.1	1.96	Cu acetylacetonate[97]
4.2	1.85	Cu phthalocyanine[97]
4.1	1.99	NaCu glucoronate[97]
4.2	1.96	BaCu glucoronate[97]
4.1	1.95	MgCu glucoronate[97]
4.2	1.969	Cu acetate monohydrate[97]
4.1	1.94	Cu benzoate trihydrate[97]
3.9	1.946	Cu citrate dihydrate[97]
4.1	1.92	Cu salicylate tetrahydrate[97]
2.0	1.941	$Cu(OH)_2$ [100]
2.0	1.940	CuO [100]
Cu(I) –O distance		
2	1.85	Cu_2O [96]

Table 1.18 Characteristic distances of Cu-O bonds found from EXAFS measurements.

The uncertainty in the determination of the coordination numbers in EXAFS was discussed earlier in section 1.4.5.3. To more accurately determine the coordination number of Cu, George used Cu-S bond lengths found from EXAFS spectra. It was noticed that with increasing coordination number of the Cu-S bond the bond distance increases slightly (Table 1.19). An increase from 2.17 Å for two-coordinate Cu to 2.33 Å for four-coordinated Cu was observed. The distance found in the Cu-S-Mo complexes study was found to be between the distances characteristic for three and four coordinated structures.[101]

N	*Distance (Å)*	*Compound*
	Cu-S	
3 – 3.5	2.28	Cu-S-Mo
	Cu(I)-S	
2	2.17	Cu-S-Mo clusters
3	2.26	Cu-S-Mo clusters

Table 1.19 Characteristic distances of Cu-S bonds found from EXAFS measurements[101].

The same dependence of the bond distance on the coordination environment was also suggested by Kau for Cu-N bonding[95]. In his study, the characteristic distance for the two-coordinate structure has a bond distance of Cu(I)-N of 1.90 - 1.92 Å. In the Cu(pze)BF_4 compound with Cu(I) and N_2O ligation, the shorter Cu(I)-N bond distance of 1.87 Å suggested that the structure being closer to two-coordinate than three-coordinate (Table 1.20).[95]

N	*Distance (Å)*	*Compound*
3-coordinate	1.90-1.92	T-shaped: N_2S, N_2O, N_3 ligation[95]
3-coordinate, close to 2-coordinate	1.87	N_2O coordination [95]

Table 1.20 Characteristic distances of Cu(I)-N bonds found from EXAFS measurements.

In addition to atom directly bonded, it is possible to see other atoms which are further out (bonded or not) by EXAFS. This was the case of Cu…Mo interaction where Cu and Mo are bridged by sulfur atoms in the copper-thiomolybdate complex (Table 1.21). This distance has been determined by George to be 2.70 Å[101].

Further, distance between atoms in two separate molecules could be determined from EXAFS spectra. In the Sarode's study, the Cu…Cu interaction distance for the four studied Cu compounds was found to increase with the increasing size of the ligand bound to Cu from 2.614 Å for copper acetate to 3.728 Å for Cu salicylate (Table 1.21).[97]

N	*Distance (Å)*	*Compound*
	Cu(II)…Cu(II)	
1	2.614	Cu acetate monohydrate[97]
1	3.15	Cu benzoate trihydrate[97]
1	3.242	Cu citrate dihydrate[97]
1	3.728	Cu salicylate tetrahydrate[97]
	Cu(I)…Mo	
1	2.70	Cu-S-Mo [101]

Table 1.21 Characteristic distances of Cu…Cu and Cu…Mo interactions found from EXAFS measurements and calculations.

1.4.5.7. Molybdenum EXAFS

The Mo K-edge of Mo foil is observed at an energy of 20000 eV[80].

Similarly to the Cu K-edge (section 1.4.5.6), the exact position of the Mo K-edge depends on the oxidation state of Mo in the studied species. George observed a 2 eV increase of the position of the edge per unit of increase of the oxidation state for Mo(IV) to Mo(VI)[87]. The shift of the edge position was seen to be larger for the Mo(II) to Mo(III) than from Mo(IV) to Mo(V)[102]. Butler observed the shift in the edge spectra from 20011 to 20008 eV for nitrate reductase upon its reduction with dithionite as it was reduced from Mo(VI) to Mo(V) and to Mo(IV).[103]

It is, however, not only the oxidation state that influences the position of the absorption edge. In a study of the EXAFS spectra dependence of the xanthine oxidase on the pH of the solution, Doonan found that changes in coordination geometry and/or

the nature of the metal-ligand bonding have influence on the position of the edge[104]. In molybdenum monodithiolene complexes Jalilehvand observed that the substitution of thiolate by a more electronegative ligand resulted in the shift of the edge position by ~1.2 eV without the change of the oxidation state of Mo.[91] The effect of the electronegativity of the ligand on the edge position was also observed in bis(dithiolene)molybdenum by Musgrave.[105]

In the near-edge spectra of the compounds containing an Mo=O bond a pre-edge feature is observed. Kutzler determined this to be due to a 1s → 4d bound-state transition to antibonding orbitals directed along Mo=O bonds[106]. The presence of a Mo=O transition is not specific of the oxidation state of Mo present, as it was observed for Mo(IV), Mo(V) and Mo(VI) [87]. It was observed in DMSO reductase[88], sulfite oxidase and desulfo xanthine oxidase near-edge spectra by George (the latter two known to contain dioxo Mo active sites)[107]. Although this pre-edge feature is usually called the oxo-feature, to a lesser extent it can also be observed in the spectra of the samples containing Mo=S groups, such as samples with tetrahedral MoS_4^{2-} [90,108]. The intensity of this pre-edge feature provides information of the number of O or S substituents attached to Mo.[107]

However, in the study on molybdenum oxides catalysts, de Boer did not observe this pre-edge feature in his sample even if the EXAFS analysis showed the presence of O and S attached to Mo. He concluded that this pre-edge feature is characteristic for a tetrahedral environment[90] (rather than the presence of O or S backscatterers). But Jalilehvand observed this feature in the near-edge spectra of molybdenum monodithiolene complexes which possess several Mo=O groups, but their geometry was crystallographically determined as square pyramidal and not tetrahedral.[91]

In a study of Mo in aqueous solution, Cramer determined by EXAFS analysis the bond distances between Mo-Mo for different oxidation states (Table 1.22). This

distance increases with increasing oxidation state of Mo.[102] For every oxidation state, the Mo-Mo distance (Table 1.22) is longer than any Mo-O distance (Table 1.23).

Bond	*Coordination number*	*Distance (Å)*	*Compound*
Mo(II)-Mo(II)	1	2.12	Mo(II) aqueous [102]
Mo(III)-Mo(III)	1	2.54	Mo(III) aqueous [102]
Mo(IV)-Mo(IV)	2	2.49	Mo(IV) aqueous [102]
Mo(V)-Mo(V)	1	2.56	Mo(V) aqueous [102]

Table 1.22 Characteristic distances of Mo-Mo interactions found from EXAFS measurements.

Because Mo is a relatively heavy element (Z = 42) and therefore a good backscatterer, the Mo-Mo bond gives a very visible, and in many examples dominant, peak in the FT of the EXAFS spectra[89]. However, this might not be the case for a different type of heavy backscatterer: the Mo-As interaction has been found to be small in xanthine oxidase with As due to long distance, large Debye-Waller factor, negative interference from another component or a combination of these features[109].

The Mo-O distances for various Mo oxidation states in solution have been studied by Cramer. It was found that this distance decreases with increasing oxidation state of the Mo (Table 1.22)[102].

The Mo-O distance found by EXAFS fitting can determine the nature of the oxygen atom bound to Mo. Cramer found two different Mo-O bond distances in Mo(V) species in the solution and therefore determined the presence of both bridging and terminal oxygen atoms (Table 1.23).[102] This can be applied to other bonds as well; in

compounds with the tetrahedral unit MoS_4^{2-}, bridging S was found at the distances of 2.21 - 2.26 Å and terminal S at 2.15 - 2.17 Å from Mo[108].

Bond	*Coordination number*	*Distance (Å)*	*Compound*
Mo(II)-O	4	2.14	Mo(II) aqueous [102]
Mo(III)-O	3	2.06-2.20	Mo(III) aqueous [102]
Mo(IV)-O	2	1.88-2.04	Mo(IV) aqueous [102]
Mo(IV)=O	2	1.69[87]	monooxo Mo compounds
Mo(V)-O	2	1.68-1.93[87,102]	Mo(V) aqueous
Mo(V)-O bridging	2	1.93	Mo(V) aqueous [102]
Mo(V)-O terminal	1	1.68	Mo(V) aqueous [102]
Mo(VI)-O	1	1.69	Mo monodithiolene complexes[91]

Table 1.23 Characteristic distances of Mo-O bonds found from EXAFS measurements.

It is also evident that with increasing atomic number of the substituent, the bond distance of the bond between Mo and this substituent increases. Bond distances for Mo-S are longer than Mo-O, Mo-Mo are longer than Mo-S. George observed longer bond distances for Mo-Se than Mo-S in a study of formate dehydrogenase (Table 1.24)[107].

In the investigation of several Mo compounds, Cramer had difficulties in accurately determining Mo-N and Mo-S distances in $Mo(C_6H_4NHS)_3$ because of the overlap of their peaks. However there were other samples in which this wasn't a problem and the two peaks were clearly resolved[89].

Bond	*N*	*Distance (Å)*	*Compound*
Mo-S	4	2.24	Cu-TM4 [101]
Mo-S	4	2.41	Mo monodithiolene complexes [91]
Mo-S	3	2.349	Mo-Fe-S clusters[110]
Mo-Fe	3	2.684	Mo-Fe-S clusters[110]
Mo-Se	1	2.601-2.628	Formate dehydrogenase[107]
Mo…Cu	3	2.70	Cu-TM4[101]

Table 1.24 Characteristic distances of Mo-S, Mo-Fe bonds and Mo…Cu interaction found from EXAFS measurements.

The determination of the Mo-N and Mo-O distances present in MoO_3dien was found by Cramer to be difficult[89]. Problems in distinguishing between S and Cl ligands bound to Mo were also observed in the EXAFS spectra of molybdenum monodithiolene complexes studied by Jalilehvand.[91] This is caused not only by the similar bond distances but also by the similar atomic numbers of N and O. Their EXAFS phase and amplitude functions are also very similar[91,101,107].

1.4.5.8. Sulfur XANES

Similarly to the two previous elements discussed, the position of the S K-edge also depends on the oxidation state of the sulfur (Table 1.25). With increasing oxidation state on sulfur, the edge shifts to the higher energy, being lowest for S^{2-} and highest for S^{6+}. Near-edge spectra can also be complicated by the presence of sulfur atoms with different oxidation numbers within the same compound. Using model compounds and LCA (described in section 1.4.5.2), the amount of different sulfur compounds in mixtures can be determined.[111-114]

Compound	*Near Edge Position, eV*	*Oxidation state*
FeS	2470.2	-2
S	2472.5	0
$Na_2S_2O_3$	2472.0	-1
	2481.2	+5
$Na_2S_4O_6$	2473.4	0
	2482.1	+5
Na_2SO_4	2482.5	+6

Table 1.25 Edge position of the spectra of inorganic sulfur model compounds.[112]

1.5. Copper deficiency in ruminants and copper-thiomolybdate interaction

1.5.1. Digestion in ruminants

Ruminants have developed a sophisticated digestive system to accommodate their nutritional requirements.

The digestion of the feed starts in the oral cavity, which contains the tongue, salivary glands, pharynx and larynx and the teeth and masticatory apparatus. There are several types of salivary glands, some producing a large amount of saliva, some minor amounts. Saliva from the glands drains into the oral cavity via ducts. It can be serous (thin saliva which contains lot of protein), mucous (thick saliva rich in glycoprotein and mucin), or mixed saliva containing both types.

The exact amount of saliva produced depends on the feed type and feeding habits. Cattle on alfalfa forage can produce up to 180 L of saliva per day. Dry matter

comprises 1.0-1.4 % of saliva, ash content is 0.7-1.5 %. Major inorganic components of the saliva are Na, P, and CO_2; Cl and K are found in slightly lower amounts and small amounts of Ca and Mg can also be determined. The amounts of S and N in saliva are variable.

The main function of saliva is to help in mastication and swallowing because dry food would be hard to ingest. Buffering action is also very important, thanks to the bicarbonate and phosphate as the most prevalent anions. Mixed saliva is a weak buffer above pH 7.8 and below 5.5, thus saliva is well buffered against acid and poorly against alkali. Salivary buffers act as a first line of defense to buffer the rumen against acids (volatile fatty acids, see below).

There are other properties of saliva:

1. anti-frothing, for prevention or reduction in severity of rumen bloat;
2. helps to maintain a desirable physio-chemical environment for microbial fermentation (70 % of water entering rumen comes from saliva);
3. various ions present in saliva help to maintain a stable osmotic pressure.[7]

After digestion of the feed is initialized in the mouth, it is transported through the esophagus (the connective tube between the pharynx and the rumino-reticulum) to the stomach. The ruminant stomach contains four compartments: the reticulum, rumen, omasum and abomasum.

The main function of the forestomach (reticulum, rumen, omasum) is to store and delay the passage of ingested food. The biggest of all four compartments is the rumen, whose volume is usually 60-80 L for cattle, but which can reach up to 100 L for larger breeds. The rumen represents an open and continuous ecosystem with a constant supply of substrate (feed). Soluble material can be easily absorbed here, and larger and insoluble particles undergo fermentation and degradation to produce smaller particles.

The rumen has a large microbial population which carries out the fermentation processes. The oxygen level is very low here and most organisms are therefore anaerobic. Besides microbial organisms, the rumen also contains different types of bacteria, protozoa and other minor microorganism (anaerobic fungi, mycoplasmas, bacteriophages). The rumen temperature is usually 38 - 42 °C and the pH between 5.5 and 7.2, conditions appropriate for the actions of the microorganisms. Rumen gas typically contains 65 % CO_2, 27 % CH_4, 7 % N_2, 0.6 % O_2, 0.2 % H_2 and 0.01 % H_2S. [7]

The redox potential in the rumen is between -250 and -450 mV with the virtual absence of O_2 and an excess of reducing power. Microbes present in the rumen together with its reducing power reduce CO_2 to CH_4, sulfates to sulfide and nitrates to ammonia. Unsaturated fatty acids are saturated under anaerobic conditions.

The Volatile Fatty Acids (VFAs, acetic, propanoic, butyric and higher fatty acids) which are produced under these conditions are the main source of energy for the animal. They are produced by specific microbial pathways and absorbed continually from the rumen, most rapidly in the non-dissociated form. Some VFAs leave the rumen with digesta flowing to the gastro-intestinal tract and are absorbed from the omasum and abomasum. Their continuous removal is important in maintaining a stable ruminal pH. A large amount of ammonia is produced by the degradation of dietary protein, and the hydrolysis and turnover and degradation of microbial cells. Ammonia is a good source of nitrogen for amino acid biosynthesis by rumen microbes. Ammonia not used by microbes is absorbed directly through the rumen wall[7].

After leaving the stomach, the digesta goes thought the intestines (small and large) before being excreted. Glucose, lipids and long-chain fatty acids are digested and absorbed from the small intestine (although some minor digestion can occur in the stomach). Pancreatic and intestinal secretions containing hydrolyzing enzymes help the digestion in the small intestine. Undigested food is then excreted through feces[7].

1.5.2. Sulfur and animals

Sulfur is an essential nutrient for plants and microbes to synthesize sulfur-containing amino acids. Rather than the requirement of sulfur for animals, the molar ratio of S:N is important. This should be in the range of 0.046 – 0.067. The highest value is the same as the S:N ratio found in animal tissue and products. However, other research reported that this ratio shouldn't fall below 0.1. Mammals digest plant proteins and recombine the S-amino acids to form their tissue proteins[9].

Sulfur is available in pastures and conserved forages in amounts from 0.5 to 5.0 g S/kg DM depending on the soil sulfur, nitrogen and phosphorus and maturity of the sward. For animals, surface water and groundwater with more than 1.5 g of sulfate S/L also represent significant contributions to S intake. Water concentrations as low as 500 mg S/L have been observed to induce Cu deficiency (section 1.1.2).

Many rumen bacteria require sulfur to incorporate it into S-amino acids or to utilize these. Sulfur acts as a highly reactive element in the formation of enzymes and is also part of many proteins with vital roles (methallothionein, glutathione) and part of other molecules in connective tissue, heparin and keratin - rich appendages, hormones and vitamins.

Excess sulfur has been shown to be toxic to animals, with no other nutritional value. This can be excreted via urine or via feces (organic sulfur).[8] Sulfur poisoning is mostly related to Cu deficiency (section 1.1.2).

1.5.3. Copper deficiency

Copper deficiency can be primary, due to insufficient copper intake, or secondary, due to the action of copper antagonists. These react with copper in the animal body and produce compounds which cannot be absorbed and are not a good source of copper. Iron from soil can inhibit copper by the absorption of Cu by insoluble iron compounds. Other elements such as Ca, Zn and Cd have also been observed to have an effect on Cu absorption, but their influence is small.

The most important copper antagonists identified so far are thiomolybdates. These play a major role in ruminants; however in non-ruminants their formation is not as significant and therefore Cu – TM interaction isn't such a danger for the animal. This is caused by the rumen's ability to degrade organic and inorganic sulfur compounds to sulfide (section 1.5.1) which together with molybdenum, results in formation of thiomolybdates (section 1.2.3).

To cause secondary copper deficiency due to the TMs, the ratio of Cu and Mo (in TMs) is more important than just the absolute amount of molybdenum in food and water. The results of such studies are controversial: Alloway reported that a molar ratio of Cu:Mo = 1.5:1 caused swayback in sheep[115], Miltimore observed scouring at a ratio of 0.75:1 in cattle[116]. Gardner did not observe any effect on the growth of cows and calves for several years when the ratio of Cu:Mo was below 2:1[117], but Ward observed weight gain changes for the same ratio of Cu:Mo[118].

These inconsistencies might be due to the fact that not only molybdenum, but also the amount of sulfur is important, because increased amounts of sulfur tend to produce higher thiomolybdates (section 1.3.2). At this point, it is not clear if the sulfur amount in the studied thiomolybdate has an effect on the Cu:TM ratio. This ratio varies in the literature, however it is not always clear what conditions have been used in these

studies[15,119-121]. A study by Mattioli showed hypocupremia occurring also in a case where the ratio of Cu:Mo was higher than 2:1. However, in this study the concentration of copper in the grass was less than 8 ppm which is thought to be a critical concentration. The hypocupremia in this case was attributed to the low level of Cu rather than to Mo interference[122].

Sulfur was also shown to be important in the study of Mattioli; the combination of 9.4 ppm of Cu, 0.669 % S and less than 0.1 ppm Mo was used in a forage sample. This interfered with the effectiveness of Cu absorption in rumen because of the formation of CuS rather than the formation of TMs[122].

When a ruminant body is deprived of copper, the decrease of its concentration in the liver (below 3 mg Cu/kg DM) can be observed immediately. The decrease of copper concentration in the blood occurs later as it takes some time before erythrocytes become depleted of CuZnSOD. The deficiency of copper affects the connective tissue and skin, and aortic rupture can be observed due to insufficient formation of elastin. Bones and joints suffer due to the decreased activity of lysyl oxidase diminishing the stability and strength of bone collagen. Copper deficiency also affects the central nervous system, cardiac tissue and reproduction[8].

Severe or prolonged copper deficiency gives rise to anemia; blood Cu concentration falls to 1.5-3 μmol/l. Bone disorders occur due to uneven bone growth, connective tissue disorders due to impaired collagen and elastin. Other manifestations include neonatal ataxia (poor coordination of movements), falling disease (cardiovascular disorders), depigmentation, defective keratinization of wool and hair, scouring or diarrhea, infertility and susceptibility to infection. Diarrhea appears in early stages of Cu deficiency, before blood and liver Cu concentration reach subnormal levels and is therefore the first indicator of copper deficiency. These can result in death of the animal[8].

Prevention of the copper deficiency can be achieved by adding Cu-containing fertilizers to increase its level in plants, using salt-licks containing 0.5 – 1.9 % Cu, incorporation of Cu into mineral mixtures or concentrate or by adding Cu into either drinking water or water sprinkled over the forage to obtain 5 – 10 mg Cu/kg DM[8].

1.5.4. Structural studies of copper-thiomolybdate interaction

There are numerous examples of structures containing molybdenum, copper and sulfur in the literature, their structure being influenced by several reaction factors. Because of the large number of examples, only those produced from thiomolybdates of the formula $MoO_{4-x}S_x$ (x = 1 - 4) and Cu will be discussed here, as only those are relevant to this project.

The product structure formed when Cu reacts with a TM depends strongly on the cation of the thiomolybdate. Its nature can strongly contribute to the formation and complexity of the final product. Reaction between $(Et_4N_2)_2MoS_4$ and CuCN produced large three – dimensional cluster polymers $\{[Et_4N_2]_2[MoS_4Cu_4(CN)_4]\}_n$ (unfortunately, n was not specified). Here the Et_4N^+ cations can induce the polymeric structure and occupy the channels of the three-dimensional open frame-work. When using $(NH_4)_2MoS_4$ and CuCN as starting materials, the same clusters could not be obtained. This was attributed to the low solubility of ammonium cations and their small volumes to sustain the intersecting channels.[123]

The nature of the ligand of the reacting copper compound can also contribute to the formation of large clusters. For instance, cyanide helps in the formation of the bridges between units. However bromide[124] or pyridine[125] can act as terminal ligands clusters. The reaction between TM4 anion and Cu halide in presence of Br^- anion lead to the formation of two types of clusters (Figure 1.27 a, b). Further addition of Br^- to the structure b, produces more complicated structure (Figure 1.27c).[124] Similar structures

(as shown in Figure 1.27b) have been determined when CuCN was reacted with TM4 in the presence of pyridine (where pyridine is a terminal group).[125]

In some cases, the molar ratio of the reactants (TM:Cu) plays a major role in the development of the large structures and the polymerization of the adducts.

Reaction of $(NH_4)_2MoS_4$ and CuCl in the presence of Et_4NCl lead to addition of Cu species to the system up to ratio of 1:10, creating a structure with central MoS_4 tetrahedron encapsulated by 6 Cu across the edges of an S_4 tetrahedron[39]. TM3 reaction with 2 equivalents of CuSBu (Bu = Butyl) produced double butterfly clusters (Figure 1.28), and the addition of 3 equivalents of CuSBu and 1 equivalent of $[Cu(NCMe)_4][PF_6]$ to TM3 gives a double-incomplete cubane-like clusters (Figure 1.29) [126].

a.

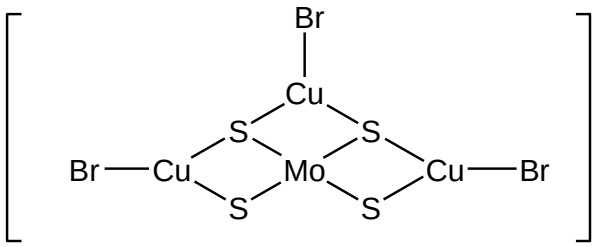

b.

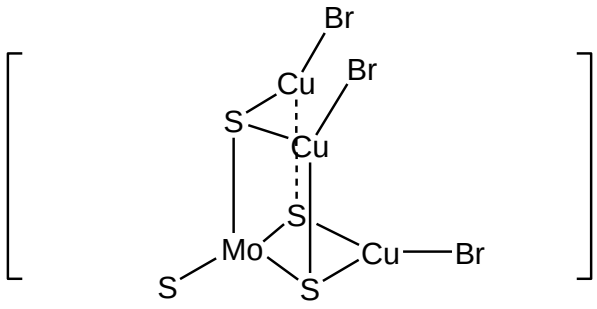

c.

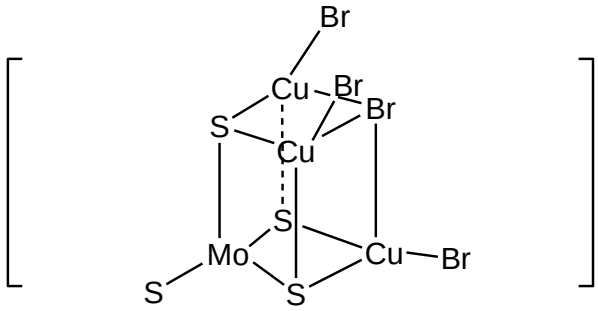

Figure 1.27 Termination of polymerization by Br atom. A. flattened structure, b. nest-shaped structure, c. cage-shaped structure. Structures have been determined from their optical property measurements.

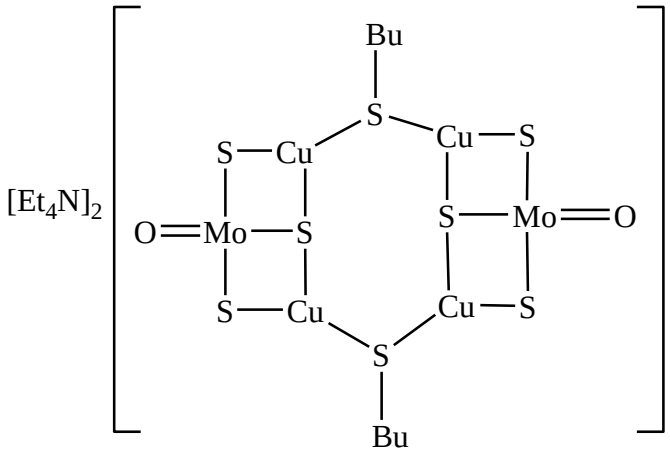

Figure 1.28 Double buttefly clusters as product of reaction between TM3 anion and two equivalents of CuSBu in Et_4NBr. Structure was determined by X-ray diffraction.[126]

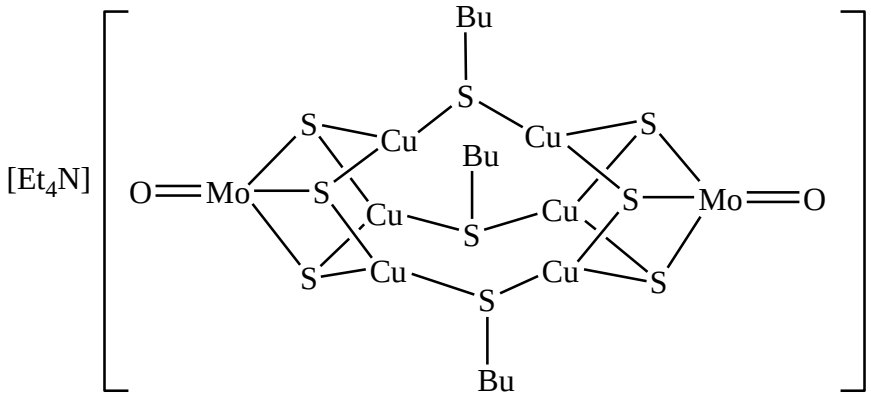

Figure 1.29 Double incomplete cubane-like clusters as a product of reaction of TM3 anion and three equivalents of CuSBu in presence of $[Cu(NCMe)_4]PF_6$ and Et_4NBr.[126]

Based on the IR, crystallographic and ^{95}Mo NMR measurements of the products of reaction between $[Et_4N]_2MoS_4$ and CuCl with increasing Cu:Mo molar ratios, a formation scheme of these cluster compounds has been proposed (Figure 1.30).[36] Similar structures were proposed by Guo for the product of the reaction between TM3 and CuBr and TM4 and CuBr where Cu:TM were mixed in molar ratio 1:2. The Cu:Mo ratio in final products was found to be 4:10[127].

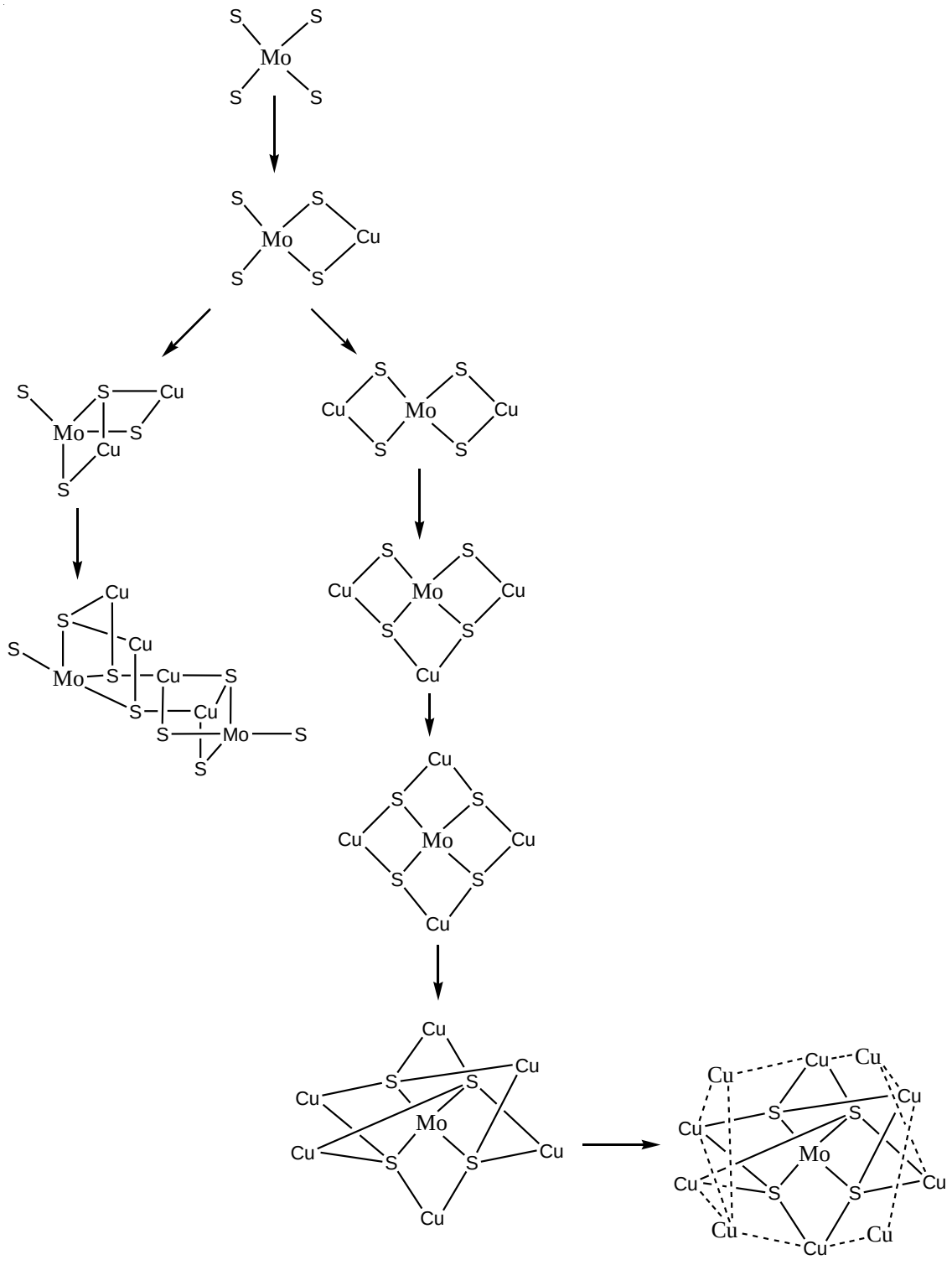

Figure 1.30 The influence of the ratio of Cu:TM on the complexity of the structure. The figure shows the change in the Cu-TM structures as more Cu is added into the reaction[36].

Not only the mixture molar ratio of reactants, but the solvent is plays a role in the final composition of the adduct as was reported by Wu[39]. Here, the reaction mixture containing molar ratio of Cu:TM4 of 10:1 in presence of Et_4NCl in acac/DMSO solvent gave a product containing Cu:Mo = 10:1. This was compared with other studies, where molar ratio of TM4:CuCl = 1:3 in CH_3CN produces $[MoS_4Cu_3Cl_3]^{2-}$ (Cu:Mo = 3:1) and $[MoS_4Cu_6Cl_9]^{5-}$ (Cu:Mo = 4:1), and the ratio of 1:4 in $(CH_3)_2CO$ or CH_2Cl_2 gives $[MoS_4Cu_4Cl_4]^{2-}$. [39] From this last study, it is not clear how important the solvent itself is in terms of its influence on the Cu:Mo ratio in the product as two different solvents using the same ratio of reactants give same results. It is therefore not confirmed that the solvent has a strong effect on the final product ratio of Cu:Mo.

Some reactions with TM3 have been observed not to proceed with a polymerization step; this was ascribed to the lower tendency of the oxygen (compared to sulfur) atom to coordinate Cu[124]. However, Hou et al. by reacting TM2 and CuCN, prepared a structure that is similar to that involving TM4 (cage-shaped)[125], so it appears that the presence of the oxygen atom plays probably just a minor role in preventing the polymerization of the Cu-TM adducts.

Similar results were obtained when comparing the reactions of TM4 vs. TM3 with CuBr, $(n\text{-}Bu)_4NBr$ in DMF. The same molar ratio of Cu:Mo was obtained in both cases in the final products (4:10). The difference was in the types of unit formed; reaction with TM3 produced butterfly and incomplete cubane-type fragments while reaction with TM4 only produced butterfly type fragments[127]. Therefore it appears that the amount of O/S in the TM used has an effect on the type of the structural unit obtained.

In the examples mentioned until this point, all the reactions were carried out using Cu in the +1 oxidation state. There are other examples in the literature of similar reactions and similar final products, as already mentioned in the previous paragraphs;

these will not be discussed here in further detail. In the addition reactions between TMs and Cu(I) compounds, the final adducts have been observed to possess an unchanged MoS_4 ($MoOS_3$) unit in which the Mo remains in tetrahedral coordination[36,123,124,126,128-132] and is present as Mo(VI)[127,131,133,134]. This was determined from the interatomic distances obtained from crystallographic data, sometimes combined with UV/Vis and IR spectrometry.

Crystal structures showed that Cu coordinated by 4 S atoms can be present in different geometries: either distorted tetrahedral[36,131,135]; or trigonal planar[124,126,129,133] as determined from crystallographic data. If multiple Cu atoms are present a combination of both is possible.[125,136,137]

Some researchers have used Cu(II) compounds rather than the Cu(I) that was used in the examples described previously. Binnie et al prepared a $Cu(NH_4)MoS_4$ adduct containing Cu(I) in the final product from the ammonium molybdate, hydrogen sulfide and cupric sulfide. The oxidation state of Cu was deduced from the fact that the final adduct produced diamagnetic species[138]. Total reduction of Cu(II) to Cu(I) upon its reaction with TM4 in formed solid species was also observed by Clarke and Laurie[119,121]. This was suggested based on the results of EPR measurements of the final adduct, where the reduction of Mo (VI) to Mo(V) was also observed. Similar products were obtained from reactions between TM (TM2, TM3 and TM4) and various Cu(II) species (bis(glycinato)copper(II), $Cu(His)_2$, $Cu(GGH)^-$, $CuEDTA^{2-}$, Cu(Albumin)) in buffered aqueous solution with the same oxidation-reduction processes[121]. The simultaneous reduction of the two metals (Mo and Cu) in these products has been suggested by the oxidation of sulfides to produced disulfides[119]. The formation of disulfides, however, was not confirmed by the spectral analysis[121].

A variety of structures have been observed to form between Cu and thiomolybdate species. Based on the reaction conditions, ratio of reactant and the

ligands or cations present in the system, formation of polymeric, nest-shaped, cage-shaped[36,123,132] and cube structures has been demonstrated. Complexation between Cu and TM species in the majority of the cases happens through coordination via sulfur. Polymerization was also observed through the formation of C=C when carbon atoms are present in species $(NH_4)_2MoS_4CuC_2(L)_n$ (L = bipy, phen with n =1, L = py, nia, tpp when n = 2)[139]. For now, it is not completely clear what the effect is of the oxidation state of Cu (+1 vs. +2) on the ratio or the structure of its product from the reaction with TM. There are also no conclusions about the individual effect of each condition itself on the reaction and final product, as many different conditions are changed in these studies.

1.5.5. The Copper-Thiomolybdate Interaction in Relation to Cu-deficiency in Ruminants

Extensive research relating to *in vitro* Cu-thiomolybdate interactions related to Cu deficiency in cattle was performed by Laurie's group in the 1980s and 1990s.

The reaction of Cu(II) and TM4 in solution led to a decrease of the UV/Vis signal of TM4 confirming an interaction between the two species. The formation of insoluble amorphous adducts was observed even at very low concentrations (10^{-5} M). The reaction of Cu and TM4 was found to be irreversible with the molar ratio of 1:1. EPR measurements determined complete reduction of Cu(II) to Cu(I). A two-step mechanism was proposed for the reaction: reduction to Cu(II) to Cu(I), followed by formation of an adduct with a final ratio of Cu:TM=1:1:

$$2Cu(II) + MoO_{4-x}S_x^{2-} + xH_2O \rightarrow 2Cu(I) + MoO_4^{2-} + S_2^{2-} + (x-2)HS^- + (x+2)H^+$$
$$2Cu(I) + MoO_{4-x}S_x^{2-} \rightarrow Cu_2^{I}MoO_{4-x}S_x \qquad 1.29$$

where x = 2,3,4. The hydrolysis to the lower thiomolybdates during this reaction was also suggested[119].

The solid adduct formed between Cu and TM was characterized as polymeric species by these and other researchers[45,120,121,140]. This conclusion was based on several spectroscopic measurements (IR), which however showed only the presence of certain groups in the adduct.

Because the Cu-TM species had not been fully spectroscopically characterized, there are several proposed structures of these polymeric species found in the literature (Figure 1.30).

Later, a more careful approach was taken to preparing Cu-TM4 adducts, by excluding any amino acids and peptides that could compete for Cu. The formation of two products was suggested from analysis of these samples. One product was obtained from the solution with reaction ratio of Cu:TM4 = 1:1. The absence of an EPR signal suggested that in this adduct Cu(I) and Mo(VI) are present. Elemental analysis confirmed this adduct to be consistent with the formula $(NH_4)CuMoS_4$ [138]. The second adduct was obtained from solution with higher reaction ratio 1.5:1. The EPR signal revealed the presence of Cu(I) and Mo(V) in the adduct. The simultaneous reduction of both, Cu(II) and Mo(VI) was suggested to be caused by disulfides.[121] However, using the published EPR parameters in a modern EPR simulation (see section 1.4.4.8) results in spectra which do not remotely resemble the measured spectra shown in the communication. It should be noted that the full-length paper mentioned in this communication has never appeared.

The formation of the later species was also confirmed by more thorough analysis, indicating the higher ratio of reactants and suggesting the formula $Cu_{1.6}MoS_4X_y$ (where $X = Cl^-$, Br^- with $y = 1.0 \pm 0.2$ or $X = SO_4^{2-}$ with $y = 0.5 \pm 0.1$). Both, EPR and EXAFS analysis indicate the presence of Cu(I) species and the rise of an EPR signal is therefore due to the presence of Mo(V) species in the adduct[120]. There is no hyperfine splitting observed in the measured EPR spectrum and therefore the

presence of Mo(V) species is not confirmed by any spectroscopic technique used in the study. The reduction of both Cu and Mo is thought to be accompanied by the oxidation of S^{2-} to S_2^{2-}, however the presence of the disulfide had not been observed in any of the IR spectra. The spectral analysis suggested the loss of sulfur on Mo resulting in the coordination of only three S atoms. The presence of both CuS_3 and CuS_4 units was proposed; the Mo and Cu structures are connected through disulfide bridges. However, the three coordinated Mo (surrounded by three atoms of S) proposed in that study is very unlikely; such a structure has never been characterized. Considering the oxidation states for the elements mentioned above, the structure proposed also cannot exist as a neutral species due to unbalanced charges.

The main problem in the results from this literature is that there is a lack of detailed procedure for preparation of these samples. As discussed previously (section 1.5.4), there are several factors influencing the final product. Without knowing the detailed conditions used in these studies, it is impossible to draw firm conclusions about their validity.

The low availability of spectroscopic techniques, such as EXAFS on Cu and Mo K-edges or XANES of the S-edge in the initial structural studies plays also a role in the ambiguous and (as will be demonstrated) probably incorrect determination of coordination and oxidation numbers of Mo, Cu and S in these adducts.

1.5.6. Spectral Characterization of Cu-TM Complexation

If soluble CuTM products are prepared at very low concentrations of reactants, the UV/Vis transition bands of CuTM species are similar to the charge transfer transitions of pure TMs.[132] Upon addition of Cu, the TM4 and TM3 charge transfer bands (section 1.4.1) are shifted to longer wavelengths[127]. Principal absorption bands have been observed for $[MoS_4(CuMe_2dtc)_2]^{2-}$: at 428 nm and 495 nm, corresponding to

the charge transfer transition of the MoS_4 moiety[135]. Other bands found for the Cu-TM compounds are summarized in Table 1.26.

Compound	*Bands (nm)*	*Solvent*
$[Et_4N]_4[Mo_4Cu_4S_{12}O_4]$ [132]	450, 420, 312, 268	DMF
$[Mo_4Cu_4S_{12}O_4(Cu(TMEN)_4]$[132] (TMEN = N,N,N',N'-tetramethylethylenediamine)	450, 320, 265	DMF
$(NEt_4)_3[MoOS_3Cu_3Br_3(\mu_2\text{-}Br)].2H_2O$[124]	501.2, 408.4, 287.4	NR
$(NEt_4)_2[MoS_4(CuBp')_2].(CH_3)_2CO$[131] ($Bp' = H_2B(3,5\text{-}Me_2Pz)_2$)	510, 323	DMF
$(NEt_4)_2[MoS_4(CuCN)_2].H_2O$[131]	492, 313	DMF
$(NEt_4)_2[MoS_4]$[131]	477, 324	DMF
$[PPh_4]_2[\eta^5\text{-}C_5Me_5)MoS_3Cu_3Br_3]_2$ [137]	550, 367, 301	CH_3CN
$\{[Et_4N_2]_2[MoS_4Cu_4(CN)_4]\}_n$[123]	521	DMF
$\{[Et_4N][S_2MoS_4Cu_2(\mu\text{-}SBu^t)]_4\}$[130]	505, red shifted with CuL attachment	NR
$[NEt_4]_2[ClCuS_2MoS_2CuCl]$[129]	266.7, 321.3, 503.6	DMF

Table 1.26 Positions of absorption bands in the UV/Vis spectra of Cu-TM compounds from.

^{95}Mo NMR shows a general decrease of the chemical shift upon reaction with Cu. Reaction of Cu^+ with TM3 in aqueous solution results in a decrease of the chemical shift of 200 - 400 ppm upon addition of each mole equivalent of Cu^+.[36,126,132] For TM4, addition of CuL (L = ligand) species also leads to a decrease of a chemical shift by 210 - 240 ppm per each CuL unit[36]. From the extent of chemical shift (characteristic to TM) decrease as Cu species are added to the TM species, the number of CuL units bound to

TM can be determined[127]. This can be used to identify the molar ratio of Cu:Mo in the adducts (Table 1.27 and Table 1.28).

Fragments	*Chemical shift (ppm)*	*Compound*
MoS_4Cu_3	1224	$[(n\text{-}Bu)_4N]_4[Mo_4Cu_{10}S_{16}O_3].H_2O$
MoS_4Cu_2	1547	$[(n\text{-}Bu)_4N]_4[Mo_4Cu_{10}S_{18}O].H_2O$
MoS_4Cu_3	1216	$[(n\text{-}Bu)_4N]_4[Mo_4Cu_{10}S_{18}O].H_2O$

Table 1.27 ^{95}Mo chemical shift of the fragment of the Cu_xTM4 structure in DMF. Small differences between the shifts of similar units are caused by the differences of the overall compound structures (S and O amount)[127].

Fragments	*Chemical shift (ppm)*	*Compound*
$MoOS_3Cu_2$	877	$[(n\text{-}Bu)_4N]_4[Mo_4Cu_{10}S_{16}O_3].H_2O$
$MoOS_3Cu_3$	481	$[(n\text{-}Bu)_4N]_4[Mo_4Cu_{10}S_{16}O_3].H_2O$
$MoOS_3Cu_2$	1152	$[(n\text{-}Bu)_4N]_4[Mo_4Cu_{10}S_{18}O].H_2O$

Table 1.28 ^{95}Mo chemical shift of the fragment of the Cu_xTM3 structure in DMF. Small differences between the shifts of similar units are caused by the differences of the overall compound structures (S and O amount)[127].

In many cases, the analysis of Cu-TM species shows the presence of the same features as in the spectra of TMs. IR spectroscopy of Cu-TM adducts shows υ(Mo - S) stetching vibrations between 400 - 500 cm^{-1} [36,38,123,125,126,128-131,133,135,136,141-143] (Table 1.29) and if TM3 is used, also the presence of an oxo-terminal ligand between 880 - 900 cm^{-1}. [36,38,123,125,126,128-131,133,135,136,141-143] In a few cases, when tetrahedral TM4 is coordinated to a metal, its symmetry is lowered and only a single band can be observed at ~ 460 cm^{-1} which is characteristic of a polymeric TM4 species bound to Cu.[44]

Characteristic IR peaks can distinguish between Mo-S bond where S is a terminal atom and bond where S is a bridging atom. The position of the peaks differs by 60 – 70 cm^{-1} where the Mo-S_b is found at lower wavenumber (Table 1.29).

The position of the peaks for Mo-S groups can be also affected by the Mo isotope that is present in the studied compound. However, this influence is very small and the position of the peak for Mo-S with ^{92}Mo vs. ^{100}Mo differs only by few cm^{-1} (Table 1.29).

Compound	*Wavenumber (cm^{-1})*	*Assignment*
[NCCu($^{92}MoS_4$)]$^{2-}$	500/486	Mo-S_t
[NCCu($^{92}MoS_4$)]$^{2-}$	447/416	Mo-S_{br}
[NCCu($^{100}MoS_4$)]$^{2-}$	493/481	Mo-S_t
[NCCu($^{100}MoS_4$)]$^{2-}$	443/415	Mo-S_{br}

Table 1.29 IR resonances in the spectra of Cu-TM compounds[144].

There are many examples of IR characteristic vibrations for Cu-TM compounds in the literature. Small differences in structure can slightly influence the exact position of the band (Table 1.30).

Cu-S can also be observed in the Cu-TM adducts; absorption at a lower wavenumber (245 cm^{-1}) is assigned to the Cu-S vibration.[44]

Compound	*Wavenumber (cm^{-1})*	*Assignment*
{[Et_4N][$S_2MoS_4Cu_2(\mu$-$SBu^t)]_4$}[130]	458	μ_3-S
[PPh_4]$_2$[(η^5-C_5Me_5)$MoS_3Cu_3Br_2$][137]	476, 458	Mo-S_{br}
[(η^5-C_5Me_5)$MoS_3Cu_3Br_2(PPh_3)_2$][137]	428, 417	Mo-S_{br}
(NEt_4)$_2$[MoS_4($CuBp')_2$].(CH_3)$_2CO$[131] *(Bp' = $H_2B(3,5$-$Me_2Pz)_2$)*	465	
{[$MoS_3Cu_3(CN)(py)_3$].0.5C_6H_6}$_n$[125]	912	Mo-O_t
	441, 412	Mo-S_b
[Et_4N][$MoS_4Cu_3(S_2COEt)_2$][141]	479	Mo(μ_2-S)
	441	Mo(μ_3-S)
{[Et_4N][$S_2MoS_4Cu_2(\mu$-$SBu^t)]_4$}[130]	~520	Symmetrical coordination around MoS_4^{2-} core
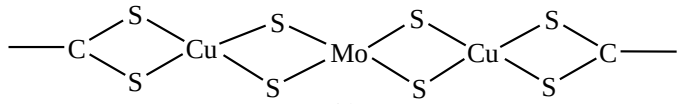 *36*	463	Mo-μ_2-S
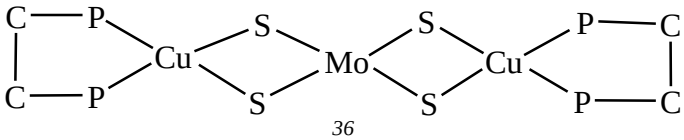 *36*	465	Mo-μ_2-S
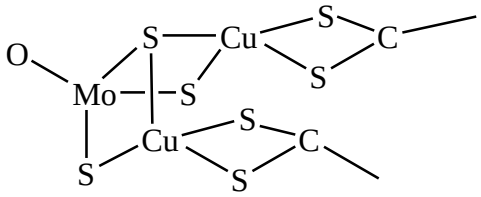 *36*	915	Mo-O_t
	460, 430	Mo-S_b
(NEt_4)$_2$[MoS_4(Cu(H_2B(pyrazolyl)$_2$)$_4$][128]	443	Mo-S
[NEt_4]$_2$[$ClCuS_2MoS_2CuCl$][129]	466	Mo-S in MoS_4 core

Table 1.30 Some IR characteristic wavenumbers for compounds formed by interaction of Cu and TMs.

…table continues

Compound	*Wavenumber (cm^{-1})*	*Assignment*
$[Et_4N][Mo(\mu\text{-}S)_3Cu_2)_2(\mu\text{-}Sn_6S_6)]$[133]	885	Mo=O
	465	Mo-S_b
	507	Mo=S
$[Et_4N]_4[(MoS_4Cu_2)_3(\mu_3\text{-}S)_2]$[133]	497	Mo=S
	451	Mo-S_b
$[(n\text{-}Bu)_4N]_4[Mo_4Cu_{10}S_{16}O_3].H_2O$[127]	894.8	Mo-O_t
	462.8, 454.5	Mo-(μ_n-S) n = 2, 3, 4
$[(n\text{-}Bu)_4N]_4[Mo_4Cu_{10}S_{18}O].H_2O$[127]	894.8	Mo-O_t
	505.3	Mo-S_t
	484.1, 462.8, 451.3	Mo-(μ_n-S) n = 2, 3, 4

Table 1.30 Some IR characteristic wavenumbers for compounds formed by interaction of Cu and TMs.

Unfortunately, all these well studied and characterized structures are not relevant to the Cu-TM interaction in biological environment. Their preparation includes the presence of large bulky organic molecules, and conditions and solvents unlikely to be found in the natural environment. So far, very little work has been done on simple Cu-TM interactions in aqueous environment similar to biological conditions with conclusive results, most likely because of the low solubility of these adducts in water. There is also limited information available from spectral studies on these adducts in the solid phase. Even simple things like molar ratio of Cu:Mo in their products, the oxidation states of metals, or their coordination environment remain in question.

1.6. Previous Work within the Reid Group

The project described in this thesis is only a part of a large study. It was started several years ago in the Reid group and has continued untill now. Here is a summary of work that was done previously by other members of the group. Only the projects highly relevant to this research will be discussed in detail. Others will be mentioned briefly.

1.6.1. ^{1}H NMR and Potentiometric Studies of Copper(II) Speciation in Ruminants

Mohammed Attaelmannan studied the interaction of the Cu(II) with some important amino acids using potentiometry and ^{1}H NMR measurements[145,146]. The NMR study of the rumen fluid sample showed the predominance of the acetic acid and the presence of other fatty volatile acids such as propanoic and butanoic. Another component of rumen fluid, ammonia, was found to be important in the speciation of Cu(II) studied by computer simulation[145].

1.6.2. X-ray crystallographic Studies of Thiomolybdates and Bovine Serum Albumin

Dean Thome developed a synthesis of thiomolybdates where their crystals can be obtained. He also crystallized all four thiomolybdates and determined their structure: bond distances, angles and unit geometry (Table 1.31).

For all of the TMs, it was found that they crystallize in tetrahedral geometry. The bond angles in all were found to be between 106-113°, corresponding to a tetrahedral environment around the Mo atom. Mo-S and Mo-O bond distances were also determined. The Mo-S bond distance was found to vary between 2.147-2.2427 Å with

the trend of having longer distances for the lower TMs. The Mo-O distance was found to be between 1.736 and 1.7814 Å.

Compound	*Bond*	*Length (Å)*	*Atoms*	*Angle (°)*
Cs_2TM1	Mo-O1	1.758 (4)	O1-Mo-O1_a	109.87 (10)
	Mo-O1_a	1.758 (4)	O1-Mo-S	109.07 (10)
	Mo-O1_b	1.758 (4)		
	Mo-S	2.2427 (18)		
$(NH_4)_2TM2$	Mo-O1	1.7789 (14)	O2-Mo-O1	112.95 (7)
	Mo-O2	1.7814 (15)	S1-Mo-O1	108.99 (5)
	Mo-S1	2.1889 (8)	S2-Mo-O1	109.09 (5)
	Mo-S2	2.1904 (9)	S1-Mo-O2	109.14 (5)
			S2-Mo-O2	109.04 (5)
			S2-Mo-S1	107.48 (3)
Cs_2TM3	Mo-O1	1.736 (15)	S2-Mo-S1	109.18 (14)
	Mo-S1	2.199 (5)	S1-Mo-O1	109.54 (53)
	Mo-S2	2.147 (5)	O1-Mo-S2	111.11 (30)
	Mo-S2_a	2.147 (5)	S2-Mo-S2_a	106.75 (24)
$(NH_4)_2TM4$	Mo-S1	2.2021 (8)	S2-Mo-S3	109.24 (3)
	Mo-S2	2.1702 (8)	S3-Mo-S3_a	108.19 (10)
	Mo-S3	2.1772 (3)	S2-Mo-S1	110.39 (3)
	Mo-S3_a	2.1772 (3)	S3-Mo-S1	109.87 (3)

Table 1.31 X-ray data on crystalline TMs. TM1 and TM3 were crystallized as Cesium salts, due to their lower solubility and water and easier separation from the solution.

The Cu-S characteristic bond distance has a value of 2.32 Å and Cu(I) prefers tetrahedral symmetry. The fact that TM4 has strictly tetrahedral symmetry (more than other lower TMs) and the actual spacing between S atoms (3.59, 3.58, 3.54 Å) being closest to the that of the sulfur atoms bound to Cu(I) (3.78 Å with the tetrahedral angle of 109.45°) are most likely the reasons of the strong complexes formed between Cu(I) and TM4. TM4 has also the highest number of S atoms to which Cu(I) can coordinate.

1.6.3. Competitive Interactions between Copper(II) ions, Thiomolybdates, and some Biological Ligands

Emmanuel Quagraine developed a simple synthesis of all four thiomolybdates using sodium molybdate and ammonium sulfide as reactants. Increasing the reaction time and decreasing the pH of the reaction mixtures favors the substitution of the oxygen by sulfur atom and therefore the formation of higher thiomolybdates. This way, the thiomolybdates can be prepared in relatively high purity (> 95 %). When better purity is needed, further purification using a Sephadex column might be necessary[16].

Thiomolybdates in the rumen are involved in Cu deficiency in ruminants. The stoichiometry of the reaction between Cu(II) and all four TMs was found to be 1:1 in aqueous solution at all the pH values studied[16,147]. The higher ratio of Cu:TM proposed in the literature was thought to be important only to drive the reaction to completion. Further increase of the Cu(II) in the solution did not produce any significant changes in the observed spectra. The ratio of Cu:Mo in the CuTM solid samples was confirmed to be close to 1.08:1 by elemental analysis.

Reaction between Cu and TMs is very rapid and leads to the formation of insoluble complexes. Precipitation of CuTM4 (1:1) was observed within an hour at pH values of 2 - 7. The precipitation of CuTM3 was somewhat slower; only at pH = 2 - 4 the precipitation occurred in one hour, for higher pH values 5 hours were needed (10^{-4}

M concentrations of TM and Cu used). This precipitation is also favored by increased ionic strength of the solution, studied by the addition of various salts into the mixture. However, these salts were not found to be a part of the formation of the precipitate (C, H, N analysis)[16].

Several other small molecules were found to have a small effect on the formation and precipitation of the CuTM species. A large excess of EDTA was found to slow down the precipitation of CuTM species, presumably by competing for Cu(II). However, it did not prevent the formation of precipitate. It was also found that once the CuTM species is formed, the EDTA cannot compete for Cu any more.

Addition of S^{2-} into a reaction mixture of Cu(II) and TM4 resulted in the formation of CuS rather than CuTM4. In the Cu(II) and TM3 mixture, the conversion of TM3 into TM4 was observed, which then reacted with present Cu. Once CuTM is formed, Cu cannot be stripped off by S^{2-}.

The presence of histidine in the solution containing Cu and TM did not produce any changes in the UV/Vis spectra of solution. In the presence of BSA, it was observed that ternary complexes (BSA-Cu(II)-TM) are formed. These were found to be soluble adducts.

The interaction between small peptide molecules containing histidine, TM and Cu(II) was investigated by ^{1}H NMR spectroscopy and elemental analysis. Elemental analysis showed that small peptide molecules are part of the CuTM species. Based on the results obtained from this study, a possible structure was proposed. The formation of the CuTM4 linear chains of Cu and TM species was terminated by the small peptide which binds to Cu through S of the histidine molecule. For the lower thiomolybdates: TM3 or TM2 the formation of CuTM-peptide polymeric species is thought to result into slightly different structure as suggested by S NEXAFS studies as well[16,147,148].

1.6.4. ^{1}H NMR and Potentiometric Studies of Mixed-Ligand Complexes of Copper(II) with some Amino Acids

Using ^{1}H NMR and potentiometric titration, Mildred Koranteng studied the interaction of the Cu(II) and some of the amino acids (glycine, lysine, methionine, histidine). The formation of several species between each amino acid and Cu(II) was observed. The formation constants of these complexes as well as mixed complexes (using two amino acids with Cu) were found in biologically relevant conditions of temperature and ionic strength[149].

1.6.5. Speciation Modelling of Copper(II) in the Thiomolybdate-contaminated Bovine Rumen

Joseph Essilfie-Dughan found that the rate of the formation and hydrolysis of thiomolybdates by replacement of O^{2-} by S^{2-} decreases with increasing S amount in the TM. TM4 is the least reactive and therefore the most stable of all four thiomolybdates. Computer simulation of the formation of TM under rumen-like conditions showed fast formation of TM1 from TM0, then degradation of TM1 and formation of TM2 (80 % of the TM at 300 s), formation of TM3 (63 % at 30 min) and eventually formation of TM4 (27 % in 3 hours)[150].

The change of $[Cu^{2+}]$ in the solution in the presence of TM4 was studied with a Cu(II) Ion-Selective Electrode. The decrease of the free Cu^{2+} concentration upon the addition of TM4 was shown to be a two-step process, starting with a fast decrease in the concentration and continuing by a slow decrease (Figure 1.31).

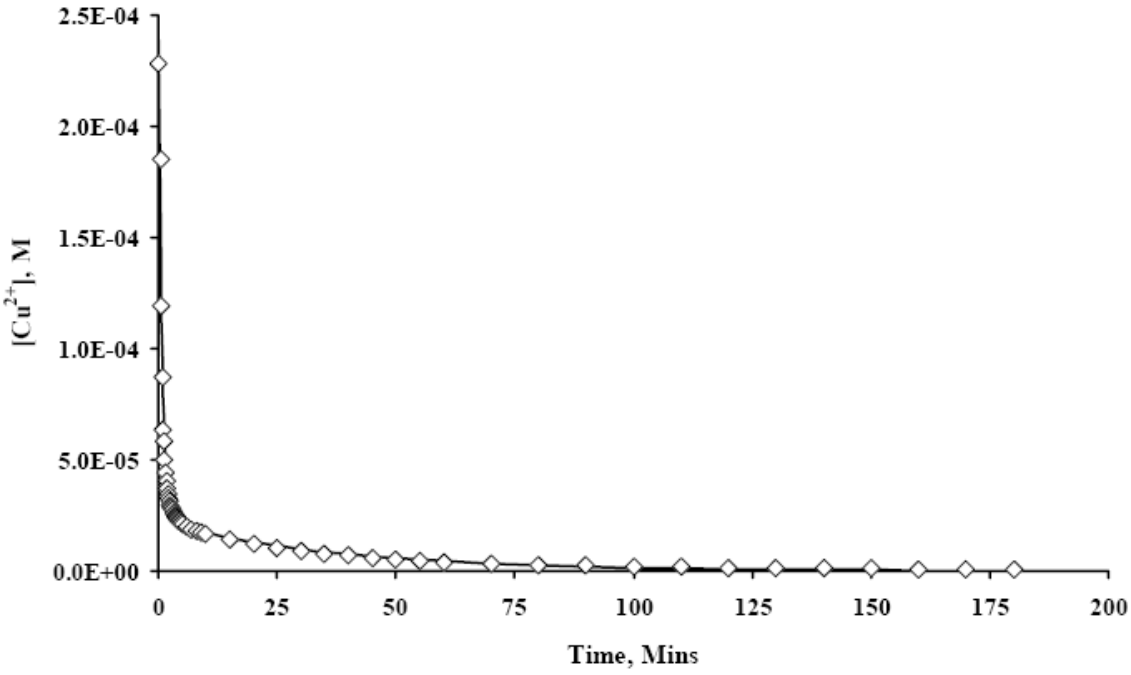

Figure 1.31 Decrease in concentration of Cu^{2+} versus time at 25 °C in an unbuffered solution as Cu^{2+} complexes with TM4. Points represent experimental data while curves represent the fit[150].

This is consistent with other results from the literature and the prediction of the redox and complexation process as the first step, followed by a slow polymerization step:

$$Cu^{2+} + TM \underset{k_{-1}}{\overset{k_1}{\rightleftharpoons}} \text{Intermediate} \xrightarrow{k_2} \text{Product} \qquad 1.30$$

where k_1 and k_2 are the kinetic constants for the forward processes and k_{-1} is the kinetic constant for the reverse process.

k_1 (min^{-1})	k_{-1} (min^{-1})	k_2 (min^{-1})
1.26 (8)	0.14 (1)	0.034 (9)

Table 1.32 Rate constants obtained from data analysis at 25°C in an unbuffered environment.

The pH and temperature dependence of the rate constants was studied. For the temperature range of 25 – 38 °C, the values of k_1 and k_{-1} were found to increase only slightly, but the increase of the k_2 value was significant with temperature. Increasing of pH for resulted in an increase of the values of forward reactions constants, k_1 and k_2 but a decrease in the value of k_{-1}. The values of rate constants at 38°C are summarized in Table 1.33.

k_1 (min^{-1})	k_{-1} (min^{-1})	k_2 (min^{-1})
11.70 (60)	0.78 (3)	1.139 (10)

Table 1.33 Rate constants obtained from data analysis at 38°C (rumen temperature) at pH = 5.00.

At the various pH values, the activation energy was for the k_1 reaction was determined as well (Table 1.34), which showed that the activation energy of the reaction is independent of pH between values of 4.0 – 5.0.

pH	*Activation energy (kJ.mol^{-1})*
4.0	11.89 (3)
4.5	11.91 (1)
5.0	11.90 (2)

Table 1.34 The activation energy values for the first step of the reaction between Cu(II) and TM4 at different pH values.

Computer modeling was used to simulate TM formation together with the Cu-TM4 interaction. It was found that the TM4 formed in the rumen is immediately consumed to produce CuTM4, and therefore it is usually not detected in rumen fluid.

In the presence of other molecules (LMM in the rumen) and at different pH values, the computer simulation showed that the rate of this reaction can be changed because of the possible competition for Cu^{2+} or the polymerization of the TM4 (pH = 4.5). This is mainly because the reaction of Cu^{2+} with LMM compounds is much faster (nanoseconds) than the Cu^{2+}-TM4 reaction (minutes, hours). In this situation also the amount of the Cu-TM4 products can be reduced by as such as 76 %.

1.6.6. Kinetics of Thiomolybdate and Copper-Thiomolybdate Interconversion Processes

Using computer software with the fitting option, Rhett Clark developed a method to quantify the composition of TM mixtures in solution. This is important because of the inability of the synthesis of TMs in their pure form without contamination from other TMs. The absorptivities of all four thiomolybdates were refined[28]. Using these results, the rate constants of forward and reverse k_{-2} processes of TM interconversions were determined in the reaction equation

$$TM0 \underset{k_{-1}}{\overset{k_1}{\rightleftharpoons}} TM1 \underset{k_{-2}}{\overset{k_2}{\rightleftharpoons}} TM2 \underset{k_{-3}}{\overset{k_3}{\rightleftharpoons}} TM3 \underset{k_{-4}}{\overset{k_4}{\rightleftharpoons}} TM4 \qquad 1.31$$

Their dependence on the temperature, pH and ionic strength was also shown. Each process in the scheme above was determined to be first-order with respect to TM, and second order overall.

Using the kinetic data a mechanism for TM interconversion was proposed:

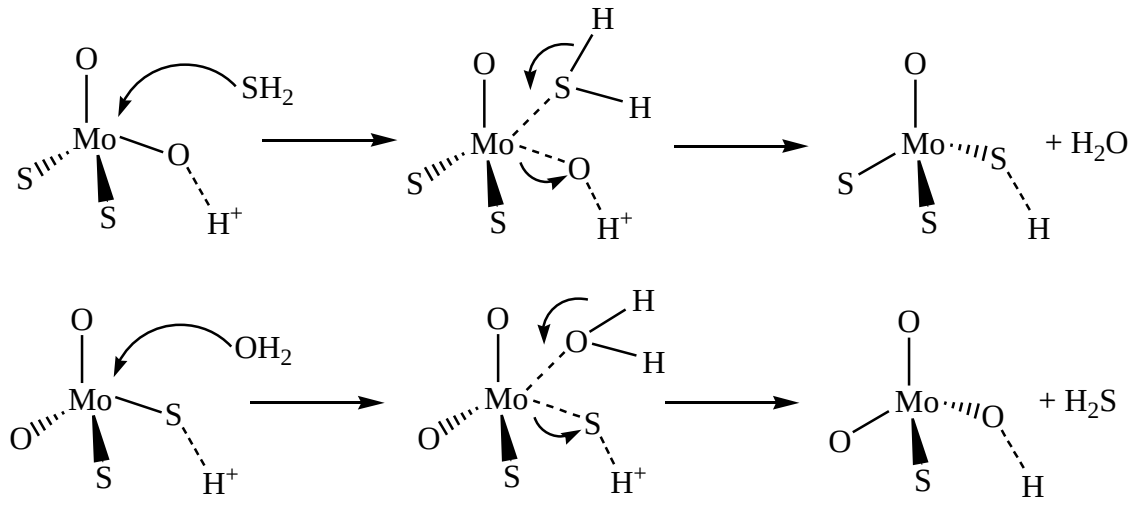

Figure 1.32 Proposed mechanism for the formation and hydrolysis of TMs.

UV/Vis spectroscopy was also used to investigate the Cu-TM interaction in solution following the scheme of the reaction for Cu-TM3 and TM4 interaction as described in equation 1.30. In this scheme, the rate constants (Table 1.35) were determined and found to be little different than the rate constants from the study using the Cu(II) ISE[150] (section 1.6.5). Differences might be caused by the slightly different conditions in the two studies. It is also important to mention that UV/Vis is sensitive to overall changes of all the species in the studied solution, while Cu(II) ISE only detects the presence (or a change in the concentration) of uncomplexed Cu(II) species. This method is also requires specific conditions to be used during measurements (such as pH or ionic strength, interference of other ions) and provides different results when these conditions are changed.

	Cu(II) + TM4	*Cu(II)+ TM3*
k_1 (min^{-1})	1.09 (3)	1.09 (3)
k_{-1} (min^{-1})	0.05 (1)	0.071 (1)
k_2 (min^{-1})	0.037 (1)	0.031 (1)

Table 1.35 The rate constants of the reactions between Cu and TMs found from UV/Vis spectra in solution at 25 °C. The reactants were mixed at a ratio of 1:1.

A UV/Vis study was performed to study the TM formation in presence of Cu(II). It was determined that a higher ratio of Cu(II):TM than the previously found 1:1 is needed to consume all the TM present. When the ratio of 2:1 was used, the prevalent species in the system are CuTM4 and to a lesser extent CuTM2. Surprisingly, CuTM3 was not present, neither were any of the TMs due to their fast reaction with the Cu(II) immediately after their formation. The presence of Cu resulted in an increase in the rate of TM formation.

Feeding habits were mimicked by adding a new portion of reactants (TM0, S^{2-} and Cu(II)) into the system in chosen intervals and the system was monitored for several hours using UV/Vis spectrophotometry. During the first few hours, TM3 was found to be the dominant species of the system; later TM4 prevailed. The presence of Cu(II) resulted in a decrease of the formed TM4.[151]

1.7. Scope of the Present Study

The main goal of the study is to gain insight into the Cu-TM interaction.

1. A considerable amount of research has been done on thiomolybdates and their interaction with metals, as described in section 1.5.4. However, none of

the mentioned structures had been prepared in conditions relevant to the biological environment. The limited research done on Cu-TM interaction related to Cu deficiency (section 1.5.5) doesn't provide sufficient information on the preparation of the samples. A method of preparation of CuTM adducts in under conditions close to the biological environment of the rumen will be developed. This includes the conditions used during the sample preparation, such as temperature, medium, pH, concentration of the reactants to be used and their molar ratio. The preparation will also focus on the characterization and possible elimination of the contaminants, side products. Solution samples as well as solid samples will be prepared as differences in structures have been shown to exist between solution and solid phase (section 1.5.5).

2. The molar ratio of Cu:TM has been shown to have several values, as discussed in section 1.5.4 depending on the conditions used in the preparation of CuTM adducts. The Cu:TM ratio in solution and solid phase for the samples related to Cu-deficiency has been a subject of controversy (section 1.5.5, section 1.6.3). Once the proper preparation of the adducts is developed at desired conditions (see above), the molar ratio of Cu:Mo in the formed complexes will be studied in solution and in the solid phase. This involves use of solution spectroscopic techniques, such as UV/Vis spectrophotometry, ^{95}Mo NMR, potentially EXAFS and solid phase spectroscopic techniques, such as elemental analysis and EXAFS.

3. As in case of the ratio of Cu:TM in their adducts, numerous different structures have been proposed to be formed by the interaction of these two reactants (section 1.5.4). For the CuTM adducts related to the Cu deficiency, unit to be formed has been proposed (section 1.5.5). However, this proposed structure is based only on the partial spectroscopic studies and contains some questionable parts. The EPR study showed presence of paramagnetic species, however, their identity has not been confirmed. The three-

coordinated Mo surrounded by sulfur atoms is very unlikely (section 1.5.5). At this point, it is also not clear in how many steps the complete reaction proceeds and how the structure formed between Cu and TM differs in solution and solid phase. Structural studies will be performed on the CuTM3 and CuTM4 complexes using various spectroscopic techniques in solution and in the solid phase. This will be related to the redox changes occurring during the reaction between Cu and TMs.

a. EPR will study the presence of paramagnetic species and their identity
b. EPR and XANES will be used to determine the oxidation states in the CuTM adducts.
c. EXAFS data will be used to determine the geometry of Cu and Mo in the prepared adducts.

2. EXPERIMENTAL

2.1. Sources of Chemicals

Sodium molybdate ($Na_2MoO_4.2H_2O$), concentrated aqueous ammonia solution (28-30 % NH_3), phosphorus pentoxide (P_2O_5) and anhydrous diethyl ether (99 %) were obtained from EMD Chemicals, Madison, WI, USA. Ammonium sulfide solution (20 % $(NH_4)_2S$), sodium dihydrogenphosphate ($NaH_2PO_4.H_2O$) were obtained from Sigma, Oakville, Ontario, Canada. Copper nitrate (99.9 % $Cu(NO_3)_2.2.5H_2O$), butyric acid (99 %), isobutyric acid (99 %) and boron nitride (BN) were obtained from Aldrich, Oakville, Ontario, Canada. Copper sulfate ($CuSO_4.5H_2O$) and propanoic acid were obtained from Fisher Scientific, Fair Lawn, NJ, USA. Acetic acid (99.7 %), sodium bicarbonate ($NaHCO_3$), potassium chloride and acetone (HPLC grade) were obtained from EM Science, Gibbstown, NJ, USA. Potassium chloride for EPR measurements (KCl, spectroscopic grade) and cesium chloride (CsCl) were purchased from Alfa Aesar, Ward Hill, MA, USA. Hydrochloric acid (HCl) and zinc nitrate were obtained from BDH, Toronto, Ontario, Canada. Copper chloride ($CuCl_2.2H_2O$) was obtained from Allied Chemicals, NY, USA. 2,2-Diphenyl-1-Picrylhydrazyl (DPPH) from Eastman Kodak, Rochester, NY, USA. Ethanol (100 %) was obtained from Commercial Alcohols Inc, Brampton, Ontario, Canada. MOPS was obtained from Avocado Research Chemicals Ltd, Heysham, Lancs, UK. Unless otherwise indicated, all water used in these studies was purified with the Milli Q system from Millipore (resistance of water was 18.2 mΩ).

2.2. Synthesis of TM4

The synthesis was performed as described by E. Quagraine[16] with a few modifications.

5 g TM0 ($Na_2MoO_4.2H_2O$) was dissolved in 10 mL of water in an Erlenmeyer flask. 75 ml of $(NH_4)_2S$ solution was added, and the mixture was allowed to sit for 7 hr at ambient temperature to increase the yield and to minimize the amount of TM3. 35 ml of 1:1 (v/v) ethanol/ether was added to the reaction mixture, which was allowed to sit for another 45 min before being filtered using suction filtration. During filtration, the solid product was washed with ~ 15 ml of cold water, ~ 35 ml of 1:1 (v/v) water/ethanol and 2 x ~ 10 ml of ether. No further purification of the obtained product was performed.

2.3. Synthesis of TM3

The synthesis was performed as described by E. Quagraine[16] with a few modifications.

2.5 g TM0 was dissolved in 5 ml water and 5 ml of ammonia was added. 25 ml of $(NH_4)_2S$ was added to the mixture. Reaction time was 8.5 min at ambient temperature. Then a solution of 7 g of CsCl dissolved in 10 ml of water was added to the mixture and the mixture was shaken and filtered. During filtration, the solid product was washed with ~ 20 ml of cold water, 2 x ~ 10 ml of ethanol and 2 x ~ 10 ml of ether. No further purification of the obtained product was performed.

2.4. Preparation of Buffer Solutions

2.4.1. Simulated Rumen Fluid (SRF)

The constituents listed in Table 2.1 were mixed in the listed amounts with water (~ 800 ml) in a large beaker. Then the appropriate amount of 36 % HCl was added to adjust the pH of the solution to 4.00. Then sufficient KCl was added to make the total concentration of Cl^- ions in the final solution 4.4×10^{-2} mol/L. Water was added to make the total volume of the solution 1 L.

Constituent	*Amount used*	*Final concentration (M)*
Acetic acid (99.7 %)	5.6 ml	9.77×10^{-2}
Butyric acid (99 %)	2.8 ml	3.06×10^{-2}
Propionic acid	3.0 ml	4.00×10^{-2}
Isobutyric acid (99 %)	186 µl	2.01×10^{-4}
$NaH_2PO_4.H_2O$	5.52 g	4.00×10^{-2}
$NaHCO_3$	1.85 g	2.20×10^{-2}

Table 2.1 Constituents of simulated rumen fluid (SRF).

2.4.2. Acetate-Ammonia Buffer

11.4 ml of acetic acid was mixed with 50 ml of ~1 M NH_3 solution. The pH of the solution was further adjusted to the value of 4.00 either with acetic acid or ammonia and its volume made up to 1.00 L with water.

2.5. Stoichiometry: UV/Vis Spectrophotometry Studies

2.5.1. Preparation of Solutions

A stock solution of TM4 was prepared by dissolving 0.0197 g of TM4 in water to a volume of 500 ml, to give a final concentration of 1.50×10^{-4} M. 0.233 g $Cu(NO_3)_2.2.5H_2O$ was dissolved in SRF to a volume of 100 ml, then 3 ml of this solution were pipetted and the flask filled up to the mark (100 ml) with SRF. The concentration of the resulting Cu(II) stock solution was 3.00×10^{-4} M.

Solutions with various ratios of Cu:TM4 were mixed, where the concentration of TM4 was kept constant and the concentration of Cu was varied, as described in Table 2.2. First, the solution of Cu(II) was pipetted into the test tube, then the appropriate amount of the buffer solution (or SRF) was added, and finally the solution of TM4 was added into the mixture. TM4 can't be mixed with the buffer solution, because at the pH 4.00, TM4 in SRF undergoes very fast hydrolysis and the measurement wouldn't give reproducible results. After the reaction time of 5.00 min (reaction is finished at this time and longer time would result in hydrolysis of unreacted TM4), UV/Vis spectrum of each solution was taken. For the blank, a solution containing 3 ml of water and 6 ml of buffer (SRF) was used.

Following the procedure described above, similar solutions were prepared for the system containing Cu and TM3.

For both systems, CuTM4 and CuTM3, solutions were also prepared as described above (Table 2.2), but in acetate-ammonia buffer instead of SRF.

Molar ratio of reactants Cu:TM4	*Volume of stock $Cu(NO_3)_2$ (mL)*	*Volume of TM4 stock solution (mL)*	*Volume of SRF (mL)*	*Total volume of the mixture (mL)*	*Final Cu(II) conc. (M)*	*Final TM conc.(M)*
3:1	4.50	3.00	1.50	9.00	1.50×10^{-4}	5.00×10^{-5}
2.5:1	3.75	3.00	2.25	9.00	1.25×10^{-4}	5.00×10^{-5}
2:1	3.00	3.00	3.00	9.00	1.00×10^{-4}	5.00×10^{-5}
1.9:1	2.85	3.00	3.15	9.00	9.50×10^{-5}	5.00×10^{-5}
1.75:1	2.63	3.00	3.37	9.00	8.77×10^{-5}	5.00×10^{-5}
1.6:1	2.40	3.00	3.60	9.00	8.00×10^{-5}	5.00×10^{-5}
1.5:1	2.25	3.00	3.75	9.00	7.50×10^{-5}	5.00×10^{-5}
1.4:1	2.10	3.00	3.90	9.00	7.00×10^{-5}	5.00×10^{-5}
1.25:1	1.88	3.00	4.12	9.00	6.27×10^{-5}	5.00×10^{-5}
1.1:1	1.65	3.00	4.35	9.00	5.50×10^{-5}	5.00×10^{-5}
1:1	1.50	3.00	4.50	9.00	5.00×10^{-5}	5.00×10^{-5}
0.8:1	1.20	3.00	4.80	9.00	4.00×10^{-5}	5.00×10^{-5}

Table 2.2 Volumes of stock solutions of 3.00×10^{-4} M Cu(II) and 1.50×10^{-4} M TM4 used to investigate ratio of Cu:TM4 in solution by UV/Vis spectrophotometry.

…table continues

Molar ratio of reactants Cu:TM4	*Volume of stock $Cu(NO_3)_2$ (mL)*	*Volume of TM4 stock solution (mL)*	*Volume of SRF (mL)*	*Total volume of the mixture (mL)*	*Final Cu(II) conc. (M)*	*Final TM conc.(M)*
0.67:1	1.00	3.00	5.00	9.00	3.33×10^{-5}	5.00×10^{-5}
0.57:1	0.86	3.00	5.14	9.00	2.86×10^{-5}	5.00×10^{-5}
0.5:1	0.75	3.00	5.25	9.00	2.50×10^{-5}	5.00×10^{-5}
0.4:1	0.60	3.00	5.40	9.00	2.00×10^{-5}	5.00×10^{-5}
0.33:1	0.50	3.00	5.50	9.00	1.67×10^{-5}	5.00×10^{-5}
0:1	0	3.00	6.00	9.00	0.00×10^{-5}	5.00×10^{-5}

Table 2.2 Volumes of stock solutions of 3.00×10^{-4} M Cu(II) and 1.50×10^{-4} M TM4 used to investigate ratio of Cu:TM4 in solution by UV/Vis spectrophotometry.

The influence of the presence of histidine on the UV/Vis spectra of TM4 and CuTM4 in solution was investigated. 0.0198 g of His was dissolved in water to the volume of 200 ml, to give a solution of concentration 6.38 x 10^{-4} M. 0.0150 g of TM4 was dissolved in water to the volume of 200 mL, giving a solution of concentration 3.00 x 10^{-4} M. To prepare a solution of TM4 and His, 1.41 mL of the His solution and 3.00 mL of TM4 solution were mixed and diluted to 9.00 mL, with the final concentration of both components being 1.00 x 10^{-4} M.

For the CuTM4His solution, 0.0218 g of $Cu(NO_3)_2.2.5H_2O$ was dissolved in water to the volume of 100 mL, giving a 9.38 x 10^{-4} M solution of Cu(II). 3.00 mL of the TM4 solution, 1.41 mL of His solution and 0.96 mL of the Cu(II) solution were mixed together. The final concentration of all three components in the mixture was 1.00 x 10^{-4} M.

2.5.2. UV/Vis Measurements

Spectra were measured on a Varian Cary 500 instrument using quartz cells with the path length of 1 cm. The spectra were measured between 200 and 800 nm. The scan rate was set to 600 nm/min.

The UV/Vis spectra of the sets of CuTM3 and CuTM4 solution samples were measured after 5 min of reaction time. Only one scan for each solution was taken.

2.6. Preparation of Solid CuTM4 and CuTM3 Samples

2.6.1. Reaction Time Studies

10 ml of a stock solution of TM4 was prepared by dissolving 0.1041 g TM4 in water. 10 ml of a stock Cu(II) solution was prepared by dissolving 0.1166 g of $Cu(NO_3)_2.2.5H_2O$ in SRF. 2.83 ml of SRF, 4.67 ml of a stock Cu(II) solution and 4.50 ml of stock TM4 solution were mixed together in a test tube. The resulting concentration of TM4 was 0.015 M and concentration of Cu(II) 0.0195 M, giving a molar reaction ratio of Cu(II):TM4 = 1.3:1. This mixture was allowed to react for 30 min, during which time the solution was mixed with slow bubbling of Ar gas. After 30 min, the solution was centrifuged for 2 min and the supernatant removed into a different test tube, which was allowed to sit for a further 30 min before being centrifuged again. This process was repeated every 30 min, up to 3 hours, giving in total 6 test tubes. The color of all solutions during and after the reaction was observed and recorded. The test tubes containing the precipitates were stored in a desiccator with P_2O_5 under vacuum until all the solid samples were dry (7-10 days). The mass of each precipitate obtained was recorded.

The same experiment was also performed for mixtures of Cu(II):TM4 = 1:1 and of Cu(II):TM3 = 1.3:1 and 1:1.

For the 1:1 Cu:TM4 and Cu:TM3 experiments, the remaining supernatant after the last (6^{th}) sample was transferred to another test tube and reacted with an additional 2 ml 0.0508 M solution of Cu(II), added dropwise, to see if further precipitation would occur.

2.6.2. Mass of Precipitate

To study the effect of varying the molar ratio of Cu:TM in the reaction mixture on the mass of the CuTM precipitate obtained an experiment was performed where several CuTM adducts were prepared. In the reaction mixture, Cu and TM were mixed at different molar ratios. The same procedure as described above (section 2.5.1) was used. The chosen molar ratios of Cu:TM were 0.5:1, 1:1, 1.2:1, 1.3:1, 1.5:1, 1.75:1, 2:1, 2.5:1, 3:1 and 4:1. These were prepared at room temperature, one set in SRF and another set in acetate-ammonia buffer.

At certain ratios (1:1, 1.3:1 and 1.5:1) a few sets were prepared under slightly different conditions. One set was prepared in SRF but at 38°C, another at room temperature in SRF but in the presence of one equivalent of histidine and the last one, in water at room temperature (no histidine).

2.7. Electron Paramagnetic Resonance (EPR) studies

2.7.1. Preparation of Solid CuTM Samples for EPR

If TM4 contained green crystals, prior to its use, it was ground with the mortar and pestle as finely as possible, in order to facilitate its dissolution. 25 ml of 0.040 M stock TM4 solution was prepared by dissolving 0.26 g of TM4 in SRF. 25 ml of 0.050 M stock Cu(II) nitrate solution was prepared by dissolving 0.29 g $Cu(NO_3)_2.2.5H_2O$ in water. A series of solid samples was prepared by keeping the concentration of TM4 in these mixtures constant and varying the concentration of Cu(II), as shown in Table 2.3.

Reaction molar ratio of reactants Cu:TM	*Volume stock TM solution (mL)*	*Volume of stock Cu(II)$(NO_3)_2$ solution (mL)*	*Volume of SRF (mL)*	*Total volume of the mixture (mL)*	*Final Cu(II) concentration (M)*	*Final TM concentration (M)*
2.00:1	4.51	7.18	0.31	12.00	0.030	0.015
1.75:1	4.51	6.30	1.19	12.00	0.026	0.015
1.60:1	4.51	5.76	1.73	12.00	0.024	0.015
1.50:1	4.51	5.40	2.09	12.00	0.023	0.015
1.25:1	4.51	4.49	3.00	12.00	0.019	0.015
1.00:1	4.51	3.59	3.90	12.00	0.015	0.015
0.80:1	4.51	2.87	4.62	12.00	0.012	0.015
0.67:1	4.51	2.41	5.08	12.00	0.010	0.015
0.50:1	4.51	1.80	5.69	12.00	0.0075	0.015

Table 2.3 Volumes of stock solution of Cu(II)$(NO_3)_2$ and TM used to prepared samples for EPR analysis. The used stock solutions were of approximate concentrations of c_{Cu} = 0.05 M and c_{TM} = 0.04 M. The Cu solution was made in SRF, the total concentration of SRF components was kept constant.

Following the same procedure, a set of solid samples of CuTM3 was also prepared. These were prepared under the same conditions and at the same molar ratios of reactants.

The appropriate amount of the Cu(II) nitrate solution was pipetted into each test tube, then the required amount of SRF. TM4 was added last to prevent any hydrolysis prior to the reaction with Cu(II)). Mixtures were allowed to react for 60 min while flushing with Ar. They were then centrifuged for 2 min in a Fisher bench centrifuge at a speed of 2700 rpm. Then the supernatant was removed with a Pasteur pipette. Another 10 ml of SRF was mixed with each precipitate to remove all unreacted starting material. Samples were again centrifuged for 2 min and the supernatant removed. The remaining solids were then stored under vacuum for several days in a dessicator containing P_2O_5.

Following the procedure described above other samples were also prepared:

- two samples contained only one equivalent of TM4 (its final concentration the same as previously mentioned) and no Cu(II). One of these samples was prepared in water and the other in SRF.

- two further samples were prepared by mixing stock TM4 solution with a stock solution containing a different Cu(II) salt ($Cu(II)SO_4$ or $Cu(II)Cl_2$) at the molar ratio of reactants 1.5:1. These were prepared in SRF.

To characterize the EPR signals, stock solutions of TM4 and of $Zn(NO_3)_2$ were mixed to prepare ZnTM4 solid sample at the molar ratios of reactants Zn(II):TM4 = 0.5:1, 1:1 and 1.5:1 in SRF. At the 1.5:1 reactant ratio, a sample was also prepared by reacting a stock solution of Na_2SO_4 and a stock solution of TM4 in SRF.

Two samples of one equivalent of TM3 without any other component were prepared as described above. One sample was prepared in water and the other in SRF. A

stock solution of $Zn(NO_3)_2$ was reacted with stock solution of TM3 at the molar ratio of 1:1 to obtain a solid sample of Zn-TM3.

In the later stages, for EPR measurements, new sets of CuTM3 and CuTM4 samples were prepared using acetate-ammonia buffer instead of SRF. This buffer was prepared as described in section 2.4.2.

The procedure used in this preparation was otherwise the same as described above with SRF. These samples were prepared with Cu:TM ratios of 0.5:1, 1:1, 1.2:1, 1.3:1, 1.5:1, 1.6:1, 1.75:1, 2:1 and 2.5:1.

2.7.2. EPR Measurements

Spectra were collected on a Bruker X-band EPR spectrometer at a frequency of 9.4 GHz, in quartz EPR tubes with 5 mm diameter. Center field was set to 3350 G with a sweep width of 1500 G or to 3400 G with a sweep width of 1000 G. Attenuation was 30 dB (power 2.01 mW), receiver gain 1×10^4, modulation frequency 100 kHz, modulation amplitude 1 G, time constant 81.92 msec and conversion time 327.68 msec. One scan was usually enough to obtain a good spectrum for each sample.

For the semi-quantitative measurements, to obtain the ratio of Cu(II):TM, DPPH diluted with NaCl or KCl was used as an external standard.

2.7.3. EPR Simulations

The spectra of solid EPR samples were simulated using Simfonia software as described in section 1.4.4.10.

2.8. Infrared (IR) Spectroscopic Studies

2.8.1. Preparation of Solid CuTM Samples for IR Measurement

Three CuTM4 samples were prepared, with the molar ratio of reactants of Cu:TM4 = 1:1, 1.5:1 and 2:1. These were prepared following the same procedure used above for the samples prepared for EPR measurements (section 2.6.1).

Three CuTM3 samples were also prepared, with the molar ratio of reactants Cu:TM3 = 1:1, 1.5 and 2:1. They were prepared following the procedure outlined in section 2.6.1.

2.8.2. IR Spectra Measurements

Prior to measurement, powdered CuTM samples were diluted with KCl with the ratio of KCl:CuTM approximately 1:1. IR spectra were measured using an FTS-40 mid IR spectrometer in the range of 400 – 1500 cm^{-1}.

2.9. Elemental Analysis of CuTM Samples

For elemental analysis, several different samples were prepared to observe the effect of various aspects of the environment in the mixture on the composition of the resulting adducts. 1:1 Cu:TM4 and Cu:TM3 mixtures were prepared containing one equivalent of histidine (His). 1:1 Cu:TM4 and one Cu:TM3 mixtures (without His) were also prepared at lower temperature. The solutions were pre-cooled to about 5 °C and the reaction mixture placed in an ice bath during the 1 hour reaction time. The procedure followed in the preparation of these samples was as described previously for EPR

samples preparation (section 2.7.1). The concentrations of the reactants in the reaction mixtures were kept at the same levels as for the samples prepared for EPR measurements. These solid samples were prepared in SRF.

To study the possible interaction between $Cu(NO_3)_2$ and SRF, a sample without TM was prepared. $Cu(NO_3)_2.2.5H_2O$ was dissolved in SRF to the same concentration as used in the sample CuTM4 with reaction ratio 1:1. The total volume of this solution mixture was 9 ml. The same procedure was followed as in the preparation of CuTM samples.

The elemental analysis on the solid samples prepared as described was performed by Geoanalytical Laboratories of the Saskatchewan Research Council, Saskatoon.

2.10. Extended X-Ray Absorption Fine Structure (EXAFS) Studies

2.10.1. Preparation of Solid CuTM Samples for EXAFS

For EXAFS measurements, solid samples of CuTM4 and CuTM3 were prepared following the same procedure as described above for EPR solid samples (section 2.7.1, table 2.2). These samples were prepared with the molar ratio of reactants Cu:TM4 being 1:1, 1.5 and 2:1 and Cu:TM3 1:1, 1.5:1 and 2:1. All these samples were prepared in SRF.

2.10.2. EXAFS Measurements

Prior to the measurement of the EXAFS spectra (transmission mode) of the powder samples, these have to be diluted. The material for dilution should be chosen so it does not react with the studied sample and does not absorb at the energy used for the study (does not contain the element of interest).

In this study, BN was chosen as a suitable dilutant. Sample dilution was determined by standard methods used at the CLS.

The mixture of CuTM solid and BN was then finely ground using mortar and pestle, mixing carefully to produce a uniform sample. The fine powder was then packed into the hole of an aluminum plate and the sample was sealed with Kapton tape.

Sometimes, the mass of the CuTM sample available was lower than the calculated needed mass. In that case, all the CuTM sample was mixed with the appropriate mass of BN to reach the total mass of 300 mg. As the absorbance doesn't have to be an exact number but has limits (between 1 and 2), this was not a problem; the mass of CuTM was found sufficient to obtain satisfactory data for all the samples.

Spectra were collected at the HXMA beamline at the CLS, Saskatoon. For all the solid samples, spectra were measured at room temperature in transmission mode. A 220 monocrystal was used and was detuned at 50 % in a mirror-mono-mirror focus mode. The ion chamber detector filled with 100 % nitrogen. For Mo K-edge measurements, a 17 µm Mo foil from EXAFS Materials, Danville, CA, USA was used for the calibration of the monochromator. For Cu K-edge measurements, a 7.5 µm Cu foil (EXAFS Materials) was used for calibration of the monochromator. Spectra were recorded from -200 eV below the edge up to 20k with a step size of 10 eV for the pre-

edge, 0.4 eV at the edge and 0.05k above the edge with a typical total scan time of about 35 min. Two or three spectra were collected and averaged for each sample.

2.10.3. EXAFS Data Processing and Fitting

The steps involved in data reduction were outlined in section 1.4.5.5. Here, more details will be provided relevant to the reduction of EXAFS data used in this study. The data processing was performed using EXAFSPAK software[152].

1. Every scan was calibrated using the spectrum of the metal foil (17 μm Mo foil or 7.5 μm Cu from EXAFS Materials, Danville, CA, USA) that was measured at the same time as the actual sample. The first inflection point for the energy calibration was computed using the first derivative of the reference spectrum. This inflection point for each scan was shifted to the same value, usually the value from X-ray energies tables[80].

2. When multiple scans were collected for the same sample, good scans (complete, no glitches) were averaged to a single spectrum. At this point, the raw data was obtained.

3. To the raw data, the pre-edge background caused by instrumental noise and absorption from other edges was fitted and subtracted from the raw data. Then the spectra were normalized from 0 to 1.

4. A spline was fitted to the data following the general trend in the data, but not the short-term oscillations. This is a function containing several intervals each having a polynomial of some order. The number of intervals and the polynomial order were adjusted so that the spline followed the data. The optimal number of intervals and the polynomial order were found to be

between 3 and 5. When only the near-edge spectrum was measured and processed, polynomial order was reduced to 2.

5. In equation 1.27, the term $\mu_0(E)$ is difficult to determine. μ_0 in the subtracted term is replaced by the spline μ_{spl} and in denominator is replaced by an idealized, calculated μ_{th}, which is a Victoreen[153]:
   $$\mu_{th}(E) = C\lambda^3 - D\lambda^4 \qquad 2.5$$
   where λ is the wavelength. This function was scaled to the data.

6. The spectrum was then plotted in k-space (section 1.4.5.2) and, using the Fast Fourier Transform, in R-space, which gives the plot of absorption intensity vs. interatomic distance R, in Å (section 1.4.5.3). If any strong peaks were observed at unrealistically low R, the spline was adjusted and the FT process repeated. Peaks at very small R (<1 Å) are artifacts.

Fitting of the processed EXAFS spectra using EXAFSPAK was done to accurately determine the coordination numbers and the interatomic distances in the studied molecules. Initial values were estimated from the Fourier transform of the spectra. These also gave an indication of the type of the backscatterer since the distance of the two atoms can be characteristic of the nature of these atoms (sections 1.4.5.6 and 1.4.5.7). The initial coordination numbers were set to one.

The goodness of fit was judged by comparison of the experimental and predicted spectra in k-space as well as the Fourier transforms. Coordination numbers were adjusted based on the difference of the peak intensity of the measured and fitted spectrum and then spectrum was refitted. This was repeated until no further improvement of the fit could be obtained and satisfactory agreement between experimental and fitted spectrum was obtained. A supporting indicator of a good fit is the thermal disorder (σ^2), (section 1.4.5.3) which should be minimal.

2.11. XANES of Solid CuTM3TM4 Samples

2.11.1. Preparation of Solid CuTM3TM4 Samples for XANES

Solid samples containing Cu, TM3 and TM4 were prepared to study the ratio of CuTM4 to CuTM3 in the system when all three components are present. 25 ml of approximately 0.10 M Cu(II) solution was prepared by dissolving 0.58 g of $Cu(NO_3)_2.2H_2O$ in acetate-ammonia buffer. 25 ml of approximately 0.040 M TM4 and 25 ml of approximately 0.040 M TM3 solutions were prepared by dissolving 0.26 g TM4 and 0.47 g of TM3, respectively, in water.

Cu(II) solution was mixed with one of the TM solutions and left to react for 15 min, while being mixed with Ar. Then the appropriate amount of the other TM solution was added into the mixture and left to react for another 45 min. Total reaction time was 60 min. The resulting concentration of TM3 added into the mixture was the same in all the samples: 0.015 M. After 1 hr of reaction time, each test-tube was centrifuged using a bench centrifuge for 2 min. The supernatant was removed and the precipitate mixed with another 10 ml of acetate-ammonia buffer. After this, each test-tube was centrifuged again for 2 min and the supernatant removed. This procedure was used to prepare solid samples with one equivalent of each TM4 and TM3 and one or two equivalents of Cu(II), as described in Table 2.4.

To study the effect of the amount of Cu(II) on both TM3 and TM4 simultaneously, another three solid samples were prepared by mixing all three reactants, TM3, TM4 and Cu(II) stock solutions at the same time (Table 2.4). In these, mixed solution containing both TM4 and TM3 was prepared and this one was added to the Cu(II) in acetate-ammonia buffer. These reaction mixtures contained one equivalent of each, TM4 and TM3 and one, one and half or two equivalents of Cu(II). Total reaction time was 60 min. The rest of the procedure was same as described above.

Molar ratio of reactants Cu:TM4:TM3	*Concentration of $Cu(II)(NO_3)_2$ (M)*	*Concentration of TM4 (M)*	*Concentration of TM3 (M)*	*Order of mixing of reactants*
1:1:1	0.015	0.015	0.015	Cu + TM4 + 15 min TM3
	0.015	0.015	0.015	Cu + TM3 + 15 min TM4
	0.015	0.015	0.015	Cu + TM4 + TM3
2:1:1	0.030	0.015	0.015	Cu + TM4 + 15 min TM3
	0.030	0.015	0.015	Cu + TM3 + 15 min TM4
	0.030	0.015	0.015	Cu + TM4 + TM3
1:0.5:1	0.015	0.0075	0.015	Cu + TM4 + 15 min TM3
	0.015	0.0075	0.015	Cu + TM3 + 15 min TM4
1.5:1:1	0.023	0.015	0.015	Cu + TM4 + TM3

Table 2.4 Preparation of CuTM3TM4 solid samples. The concentration of TM3 was kept constant, the concentration of TM4 and $Cu(NO_3)_2$ was variable. Samples Cu + TM3 + 15 min TM4 were prepared by adding the TM4 solution 15 min after mixing Cu(II) and TM3 solution. Samples Cu + TM4 + 15 min TM3 were prepared by adding TM3 solution 15 min after mixing Cu(II) and TM4 solutions. Samples Cu + TM3 + TM4 were prepared by mixing all the three components at the same time.

2.11.2. XANES Measurements

Spectra were collected on the HXMA beamline at the CLS, Saskatoon. For all the solid samples, spectra were measured at room temperature in transmission mode. A 220 monocrystal was used and was detuned at 50 % in a mirror-mono-mirror focus mode. The ion chamber detector filled with 100% nitrogen. For Cu K-edge measurements, a 7.5 μm Cu foil (EXAFS Materials) was used for calibration of the monochromator. Spectra were recorded from -20 eV below the edge up to 100 eV above the edge with a step size of 10 eV for the pre-edge, 0.5 eV at the edge and 5 above the edge with a typical total scan time of about 13 min. Three spectra (scans) were collected and averaged for each sample.

3. RESULTS AND DISCUSSION

3.1. Introduction

Various possible structures between Cu and TM have been shown to exist. Their nature depends on many reaction conditions, as was discussed in section 1.5.4. Some work has been done on the structural studies of these complexes in relation to the Cu deficiency in ruminants. However, no conclusive study has been published summarizing all the findings. The literature is also filled with controversial results not only between different researchers (eg. Laurie[120] vs. Quagraine[16,147]) but even within the same research group (eg. Laurie, Eccleston[15,120,121]).

In this chapter I present the results of a more thorough study on the Cu-TM interaction in solution as well as in the solid phase, in conditions similar to the biological environment of these species. Analyses of results from the several available techniques suitable for the study of such system will be discussed together. The combination of these results will be used in a determination of the precise nature of the interaction between Cu and the TMs.

3.2. TM Synthesis

3.2.1. TM4

The amounts of reactants used in the synthesis of TM4 were increased to 5 times the amounts of reagents used in the procedure previously developed in our lab[16]. The reaction time was also extended to 6 hours (compared to the previously used 3 hours[16]). The longer reaction time was used to maximize the amount of TM4 as this is the last possible species that could be formed in the TM formation scheme (equation 1.30, section 1.6.5) and no other species could be formed. This should also minimize the contamination of TM4 solid by lower species, such as TM3 or possibly TM2. This increased time also leads to the increased amount of TM4, approximately 2.3 g (about 44 % yield), much better than the 22 % previously obtained with the shorter reaction time[16]. Solid TM4 was obtained with a purity 98 % (as determined by UV/Vis spectroscopy[151]) or better and no further Sephadex purification was needed.

3.2.2. TM3

When starting with 2.5 grams of TM0 and corresponding amounts of other reactants, the mass of obtained TM3 was approximately 2.6 g. This corresponds to 53 % yield. This was lower than previously obtained TM3 (71 % yield[16]) which is probably due to the difference in the procedure, as no ice bath (see below) was used for the reaction mixture and therefore less solid precipitated. None of the reactants were pre-cooled as they were in the original procedure[16] because this usually results in the fast precipitation of TM2 out of the solution which was observed before addition of CsCl solution.

The purity for several trials varied slightly for unknown reasons. For TM3 synthesis when the reaction time was 5 min, the TM3 sample obtained was composed of 91.5 % of TM3, 1 % TM2 and 7.5 % of TM4. For trials with a reaction time of 6.5 min, the purity of the TM3 obtained varied from 90 - 92 % of TM3 and the rest TM4. When the reaction time was extended to 7 min, the purity of the synthesized material was improved to 93.5 – 95.3 % of TM3 and the rest TM4. Longer reaction time, 8 min, produced TM3 of purity of 91 – 92 %. This extended reaction time (8 min) was too long and the worse purity of TM3 is due to the greater conversion of TM3 to TM4. The lowest reaction time used (5 min) resulted into TM3 samples contaminated by TM2 as well (with TM4) as the decreased reaction time resulted into incomplete conversion of TM2 to TM3. In the study of the Cu-TM3 interaction, only TM3 of purity at least 94 % or better was used.

3.3. UV/Vis: stoichiometry in solution

As a TM reacts, the intensities of its characteristic UV/Vis bands decrease due to the decreasing concentration of free TM. Therefore, from the absorbances at these wavelengths, it is possible to find the concentration of unreacted TM remaining in the solution after the reaction is finished. From the spectrum with the minimum absorbance reached at the chosen wavelength, the concentration of Cu(II) needed to react with the maximum possible amount of TM is found.

Similarly, if new peaks corresponding to the formed adduct between Cu and TM appear, these can be used to find the amount of Cu(II) needed to form the maximum amount of adduct at the constant concentration of TM (section 1.4.1.2).

3.3.1. Cu-TM4

Wavelengths of 468, 317 and 242 nm represent peaks characteristic for TM4.

Several solutions were prepared with a constant initial concentration of TM4 and variable concentration of Cu(II) and their UV/Vis spectra measured, as described in section 2.5. Results are shown in Figure 3.1.

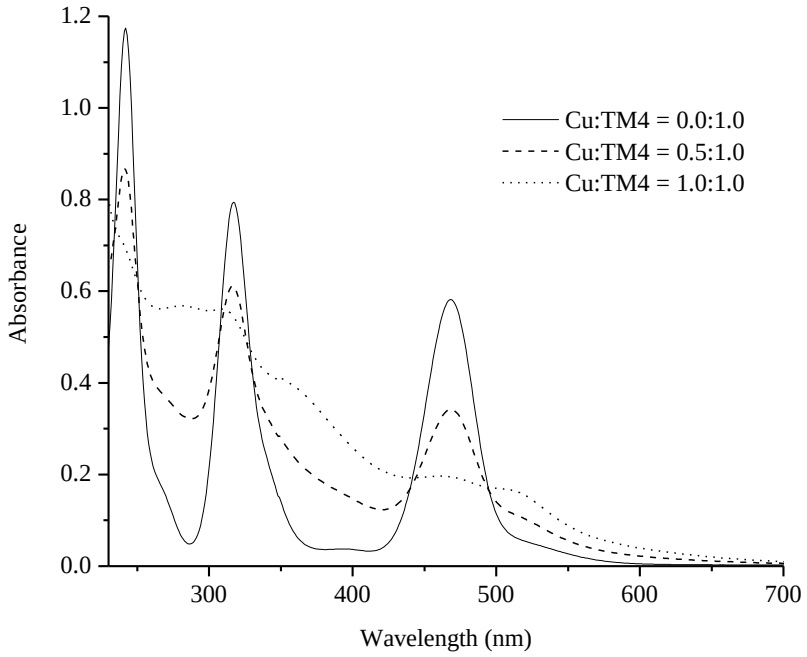

Figure 3.1 Change in the UV/Vis spectra of TM4 with different amounts of Cu(II) added in acetate-ammonia buffer.

The decline in absorbance at the three peaks characteristic for TM4 peaks with increasing Cu:TM4 ratio is shown in Figure 3.2.

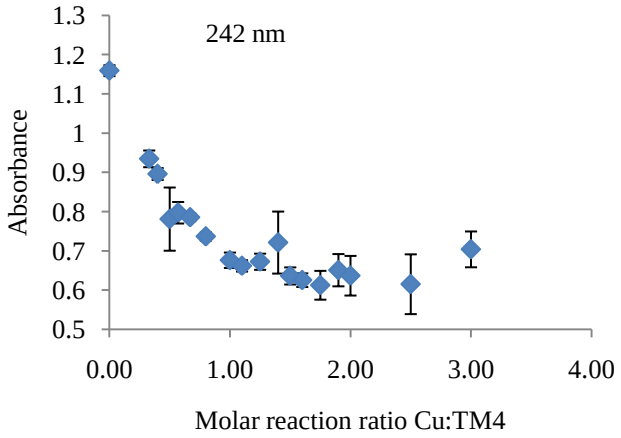

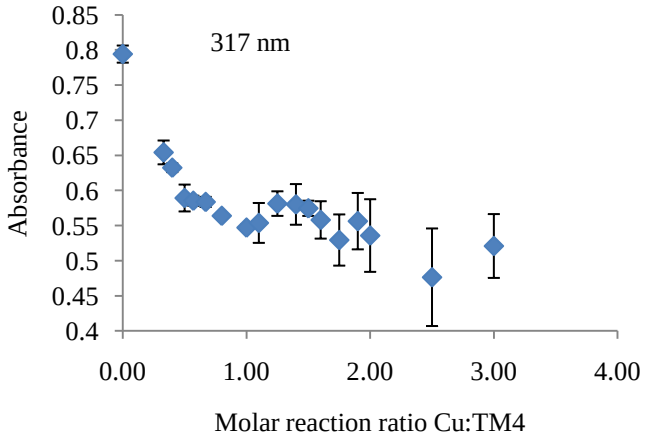

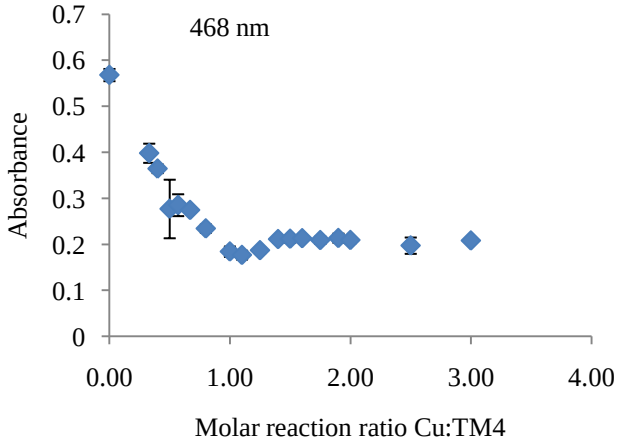

Figure 3.2 Influence of the increasing amount of Cu(II) added to the solution (acetate-ammonia buffer) of TM4 on the UV/Vis spectra.

For the absorbance measured at these wavelengths, a decrease was observed up to a certain ratio of reacting Cu(II):TM4. After this point, an increase of the absorbance was observed followed by the part where the absorbance levels off (no significant change observed) with increasing ratio of Cu(II):TM4. The data are shown with error bars representing standard deviations (based on three measurements). The errors bars for later data were similar.

The decreasing absorbance shows the increasing amount of TM4 being reacted with the increasing amount of Cu(II) added into the solution. The slight increase of the absorbance for the ratio of Cu:TM4 higher than 1:1 could be potentially caused by a minor redissolution of the Cu-TM4 species. These are formed in the equilibrium reaction from Cu and TM4 and which further proceeds into a formation of insoluble polymeric CuTM4 species as proposed by Essilfie-Dughan (section 1.6.5, equation 1.30). Fluctuations in the absorbance readings at higher Cu(II):TM4 ratios is most likely caused by the poor quality of collected data as this fluctuation is of different magnitude for different data sets (larger for 242 and 317 nm, lower at 468 nm). This might be due to the possible overlap of absorptions for several species at certain wavelengths, in this case of TM4 and CuTM4 (see below).

To determine the point of the minimum absorbance reached for TM4 species (the ideal ratio of Cu:TM4) more accurately, the two parts of each data set were fitted with a straight line. This is calculated from the regression analysis of the measured data. The point of intersection of the two lines represents the ideal ratio of Cu:TM4. This is necessary to find the ratio from this intersection, as from the data plot alone, it is not always possible to determine accurately, especially in case of equilibrium reaction, where the curvature of the plot occurs (section 1.4.1.2, Figure 1.7).

For the points close to the intersection of the two lines, it is difficult to determine if these belong to the first (change in absorbance) or second (stable absorbance) line, several scenarios were used in the regression analysis. The point

closest to the two imaginary lines is either included or excluded in the regression analysis of the two parts of the curve.

For the data set at 242 nm, the point corresponding to the ratio of Cu:TM4 of 1.1 was excluded. The resulting fits are shown in Figure 3.3A. The intersection of the two lines was found to be at the ratio of Cu:TM4 = 1.01:1.

Since (see above) data collected at a ratio of 3.0 may be suspect, another regression analysis was performed on the second part of the data, where this point was excluded. Results are shown in Figure 3.3B. In this case, the intersection of the two lines was found at the ratio of Cu:TM4 = 0.87:1.

Next, the regression analysis was performed with the point of 1.1 (Cu:TM4 ratio) being included in the both parts. The result of this fit is in Figure 3.3C. The intersection of the two lines was found to be at the ratio of Cu:TM4 = 1.04.

If the point of Cu:TM4 = 3:1 is excluded from this regression analysis, the fit of Figure 3.3D is observed. The intersection of the two lines was found at the ratio of Cu:TM4 of 0.95:1.

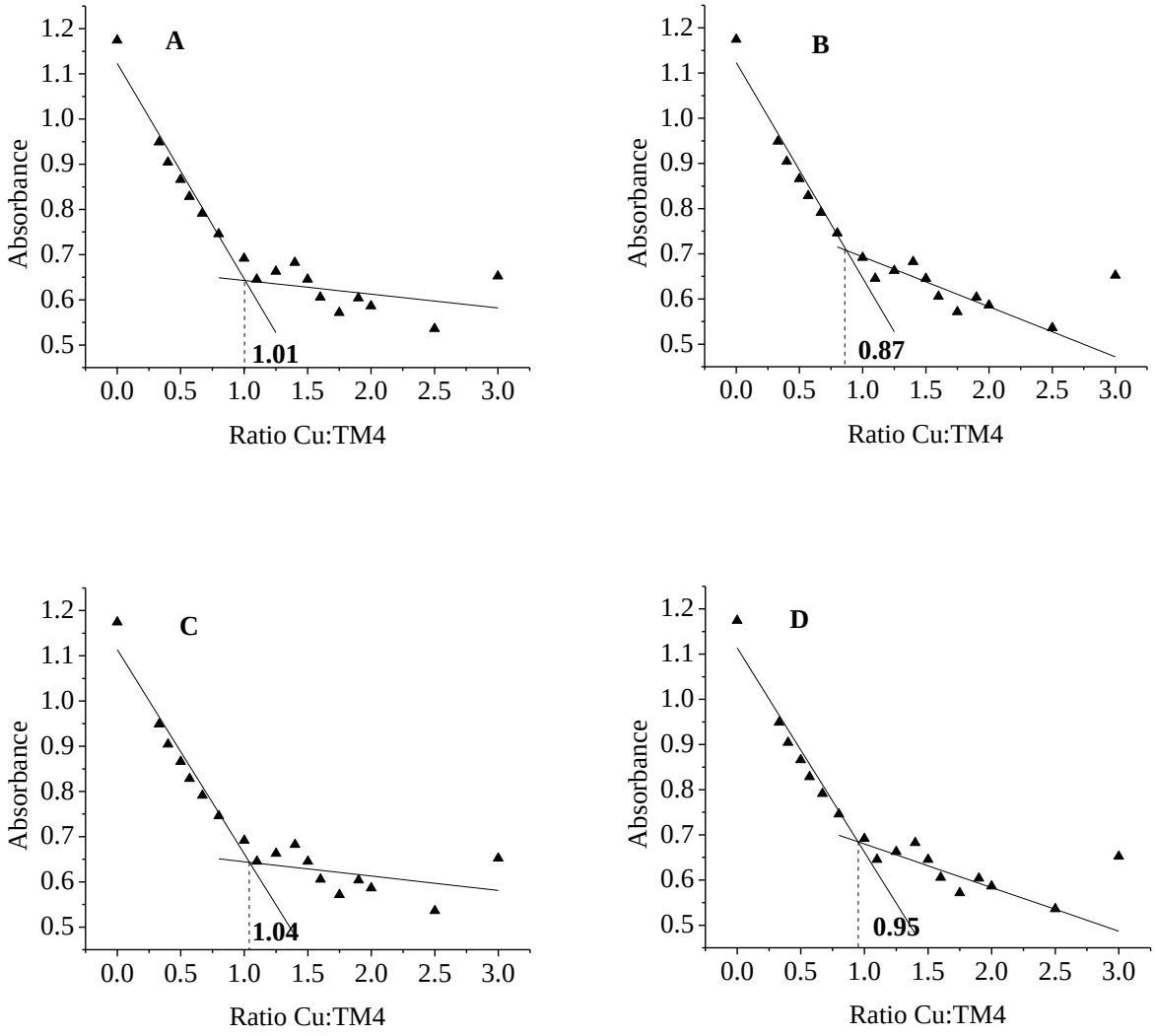

Figure 3.3 The intersection of the lines of theoretical absorbance change with increasing Cu:TM4 ratio in acetate-ammonia buffer at 242 nm. The graphs correspond to different fitting scenarios (points chosen) as described above.

The data set of 317 nm provided very poor data for regression analysis and fitting as the change in the absorbance of the spectra with increasing Cu:TM4 ratio is not as significant as for the other wavelengths. This data set was therefore not fitted.

For data at 468 nm, the point corresponding to the Cu:TM4 ratio of 1.1:1 was excluded from the regression analysis of the two part of the curve. The fit using this regression analysis is in Figure 3.4A. The point of intersection was found at a Cu:TM ratio of 0.90:1.

Next, the regression analysis was performed on the two parts of the data set with point of Cu:TM4 = 1.1:1 being included in the both lines. The fit using this regression analysis is shown in Figure 3.4B. The point of intersection was found at a Cu:TM4 ratio of 0.96:1.

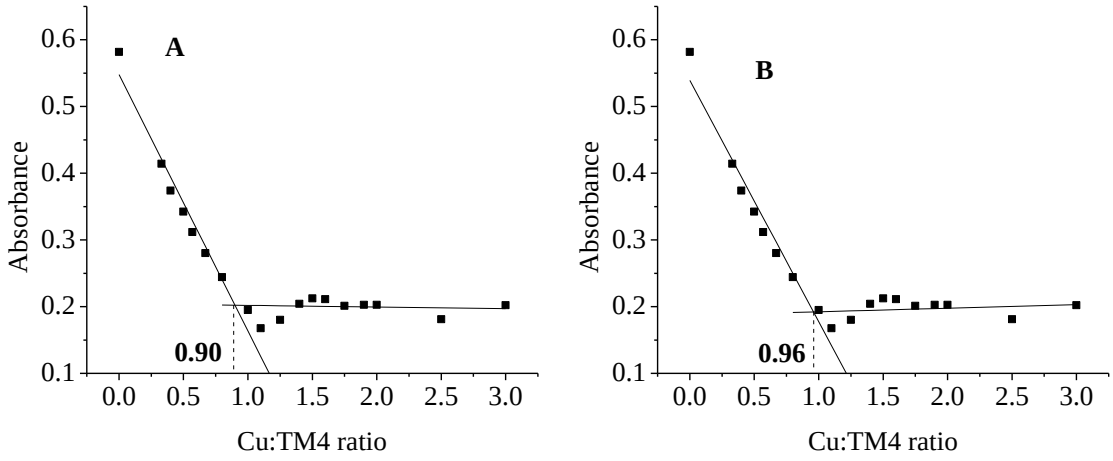

Figure 3.4 The intersection of the lines of theoretical absorbance change with increasing Cu:TM4 ratio in acetate-ammonia buffer at 468 nm.

For the set of solution samples of Cu and TM4 mixtures with variable Cu:TM4 ratio, at wavelengths of 279 and 362 nm (Figure 3.5), an increase of absorbance was observed with increasing Cu:TM4 ratio. At these two wavelength, the absorbance of TM4 is negligible and therefore these peaks represents the formation of CuTM4 adduct species. The data are shown with error bars representing standard deviations (based on three measurements). The errors bars for later data were similar.

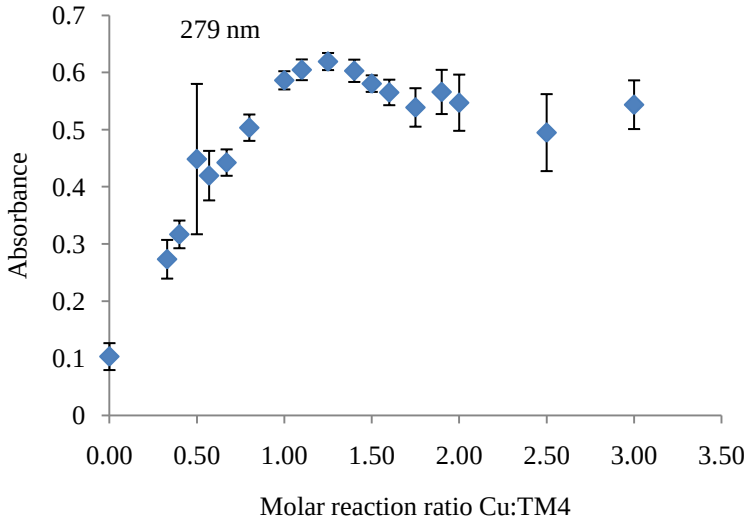

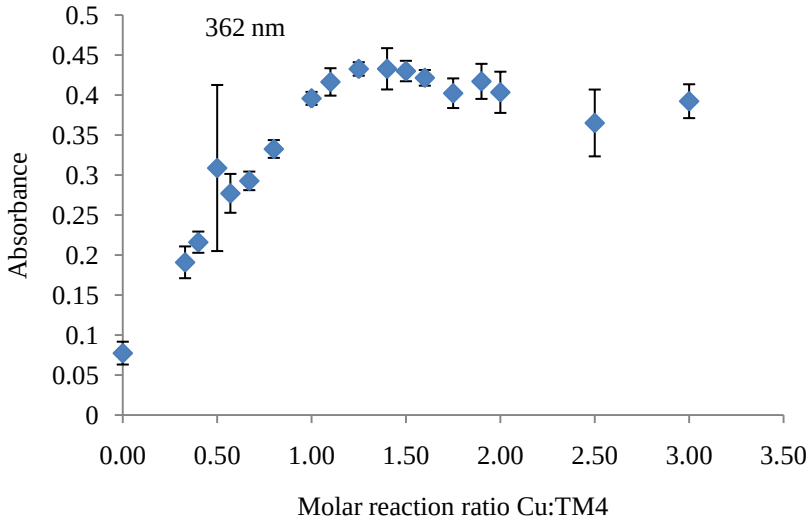

Figure 3.5 Increase in absorbance of the CuTM4 characteristic peaks of the UV/Vis spectra with increasing Cu:TM4 ratio in acetate-ammonia buffer solution.

For these two wavelengths, an increase of absorbance is observed up to a certain ratio of Cu:TM4 reactants. After that a slight decrease in absorbance is observed with further increase of Cu:TM4 ratio. This might be caused by a poor quality of data or by a possible precipitation or formation of some other species of the formed CuTM4 adduct and therefore its lower concentration.

To more accurately determine ratio of Cu:TM4 where the maximum amount of TM4 is reacted, regression analysis and fitting was performed, as described above for the decline in TM4 absorbance.

For the 279 nm data, two regression analyses were performed. In the first, the point corresponding to the ratio of Cu:TM4 = 1.4:1 was excluded and in the second, this point was included in the regression analysis of both lines. Results are shown in Figure 3.6 A and B, respectively.

When the 1.4 point was excluded from the regression analysis, the intersection of the two lines was observed at the ratio of Cu:TM4 = 1.06:1. When this point was included, the intersection was found at Cu:TM4 = 1.15:1.

The second scenario of the regression analysis was further modified. Due to the poor quality of the measured data, the point corresponding to the ratio of Cu:TM4 = 2.5:1 was excluded from the regression analysis (1.4:1 included). This had no significant influence on the intersection of the two lines, as it was found at the ratio of 1.14:1.

For the wavelength of 362 nm, the two regression analyses were performed: one with the point corresponding to the ratio of Cu:TM4 = 1.4:1 excluded from both parts of the data set (Figure 3.6C), and another, with this point included in both lines (Figure 3.6D). The intersection of the two lines was observed at the ratio of Cu:TM4 = 1.18:1 (Figure 3.6C) for the first fit and Cu:TM4 = 1.24:1 for the second fit (Figure 3.6D).

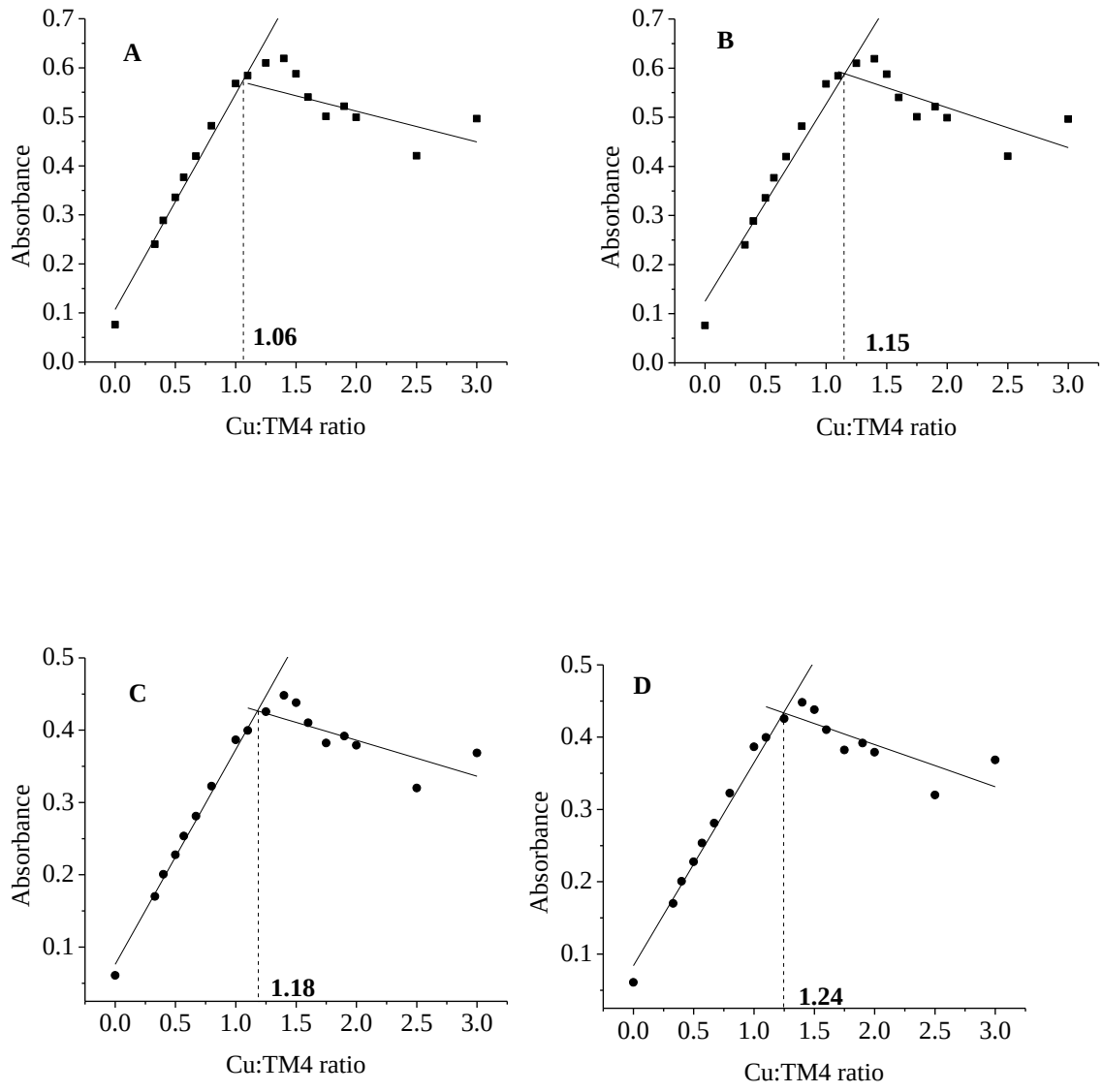

Figure 3.6 The intersection of the lines of theoretical absorbance change with increasing Cu:TM4 ratio in acetate-ammonia buffer at 279 nm (A, B) and at 362 nm (C, D).

From the regression analysis and fit results, the average ratio of Cu:TM4 in the solution was calculated (Table 3.1). This was found to be not statistically different from that previously found by E. Quagraine in solution (1:1)[16,121]. Although several different scenarios were used with some points being included or excluded from the fit and

analysis, there is no significant difference between two trials used on the same set of data.

Wavelength (nm)	*Ratio of Cu:TM4 where the intersection of the two lines was found*	
	Fit one	Fit two
242	1.01	1.04
317	-	
468	0.90	0.96
279	1.06	1.15
362	1.18	1.24
Average Cu:TM4 ratio of intersection point	1.1 ± 0.1	

Table 3.1 Ratio of Cu:TM4 in the Acetate-Ammonia buffer solution found at various wavelengths.

In the earlier stages of the research, the same experiment was performed in SRF to find the ratio of Cu:TM4 in solution (Figure 3.7). The experiment was performed following the same procedure as described for experiment performed in acetate-ammonia buffer. The results of the SRF experiment are summarized in Table 3.2. For most of the data sets, a point corresponding to Cu:TM4 = 0.5 was removed from the analysis because it was found far from the linear trend of the part of data.

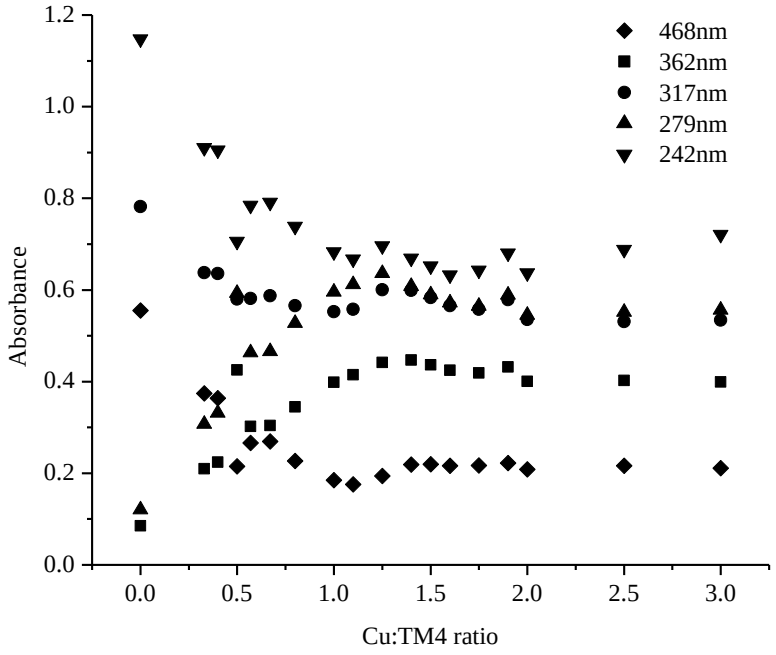

Figure 3.7 Change of absorbance vs. Cu:TM4 ratio in SRF at several wavelengths.

The ratio of Cu:TM4 found at 317 nm is significantly lower than those found at other wavelengths. This is caused by fairly poor quality of data obtained at this wavelength. Therefore this result wasn't included in the calculation of the average Cu:TM4 ratio in SRF solution. The average ratio of Cu:TM4 was calculated from the results obtained at wavelengths of 468, 362, 279 and 242 nm using only results obtained by regression analysis of data where the bad data point was excluded. This calculation provided the average Cu:TM4 ratio in SRF solution of 1.0 ± 0.1:1.0, which is not significantly different than the ratio found in acetate-ammonia buffer (Table 3.1). Excluding a point from the fit and analysis of the data didn't have a significant effect on the Cu:TM ratio (when compared with the analysis including all the measured point), as is observed from Table 3.2.

Wavelength (nm)	*Ratio Cu:TM4 for regression when all the points of the range are included*	*Ratio Cu:TM4 for regression when the 0.5 point excluded*	*Range of regression*
468	0.80	0.83	0-1 and 1.25-3
	0.88	0.91	full range
362	1.09	1.12	0-1.1 and 1.4-3
	1.15	1.17	full range
317	0.54		0-0.8 and 1-3
	0.65		full range
279	0.95	0.99	0-1.1 and 1.4-3
	1.04	1.06	full range
242	0.96	0.99	0-1 and 1.25-3
	1.01	1.03	full range

Table 3.2 Ratio of Cu:TM4 in the SRF solution found at various wavelengths by regression analysis.

The wavelengths of TM4 and CuTM4 peak maxima are slightly shifted in SRF compared to acetate-ammonia buffer. This could be due to some reaction between the reactants and the medium. The discrepancy in the ratios obtained in different media might be due to partial hydrolysis of TM in SRF which is not observed in the buffer solution during the time of the experiment. The other major problem is the possible reaction of Cu(II) with the components of SRF, mainly carbonate and phosphate that results in the formation of precipitate and therefore decreased availability of free Cu(II) for the reaction with TM4 (section 3.6). This precipitation is not visible to the naked eye at the concentration used in here but was proved by the elemental analysis (section 3.6) and was also observed during the preparation of the solid samples, with much higher

concentration of the reactants. In general, these experimental problems resulted in fairly poor quality data (Figure 3.7) compared to data obtained in acetate-ammonia buffer.

3.3.2. Cu-TM3

The UV/Vis spectra of the CuTM3 system are somewhat more complicated than the CuTM4 system. This is because the peaks characteristic of TM3 have significantly different absorptivities in different media. The position of the peaks is also different in water, buffer or SRF (Figure 3.8).

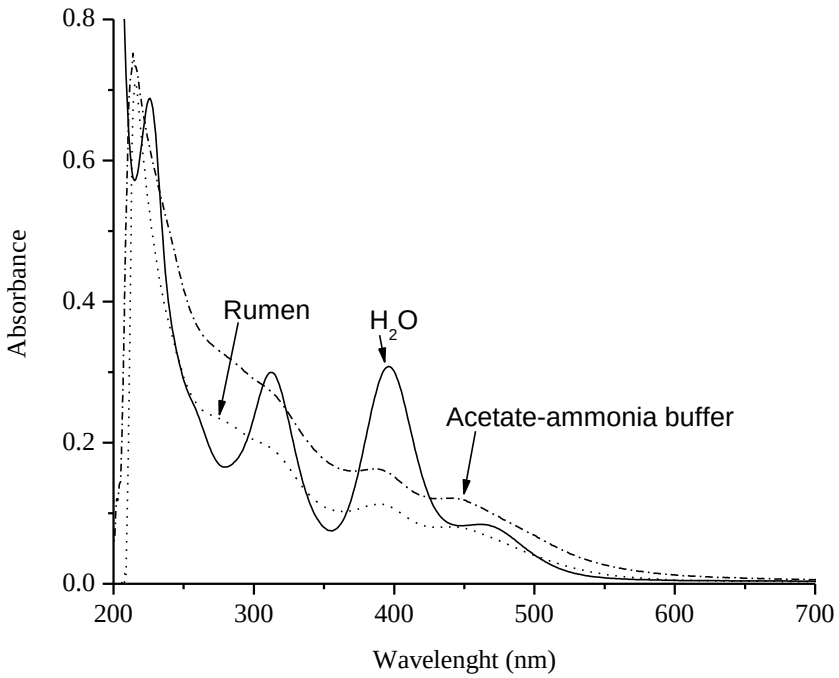

Figure 3.8 UV/Vis spectra of TM3 in three different solution media.

For the CuTM3 UV/Vis spectra, shown in Figure 3.9, the maximum absorbancies of the TM3 in acetate-ammonia buffer are found at 388, 446 and 462 nm.

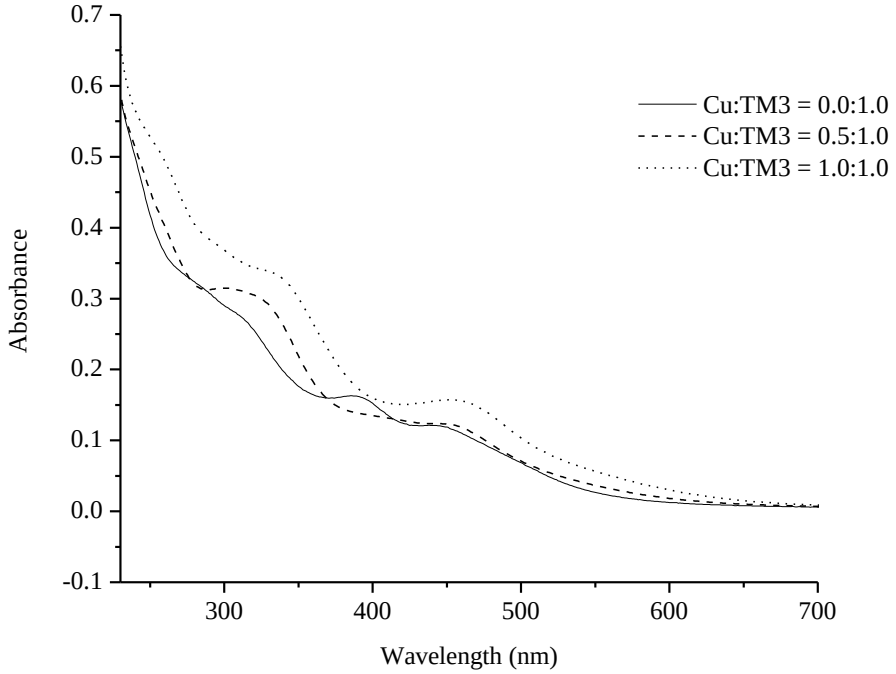

Figure 3.9 UV/Vis spectra of CuTM3 with variable Cu:TM3 ratio in acetate-ammonia buffer.

At these wavelengths, at very low Cu:TM3, the expected decrease of absorbance is observed with increasing ratio of Cu:TM3 reactants (Figure 3.10). At slightly higher ratios, the absorbance rapidly increases at both wavelengths. This most likely corresponds to the formation of new CuTM3 species which have strong absorptivities at these wavelengths. Close to the ratio of Cu:TM3 = 1:1, a maximum in the absorbance is reached, and further increase of Cu:TM3 yields no further changes in the spectra.

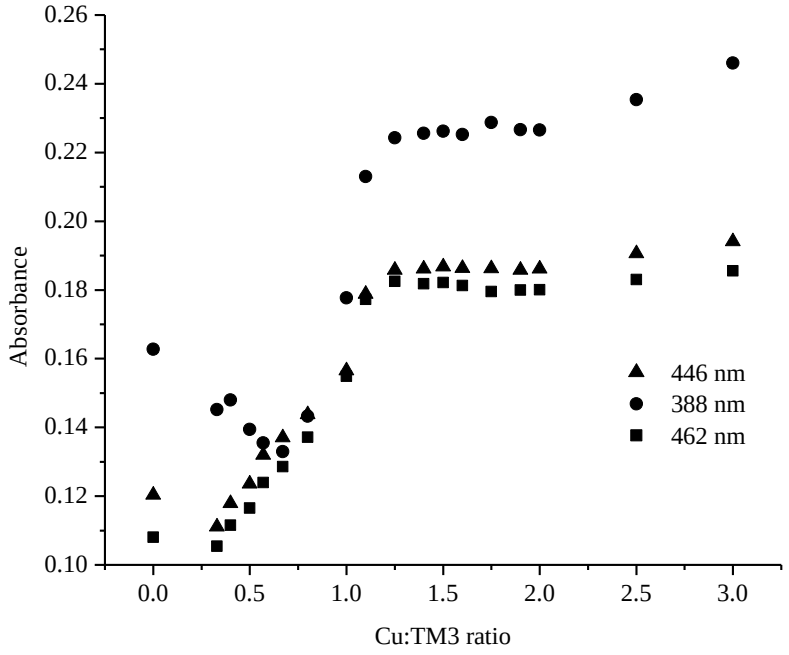

Figure 3.10 Change in the UV/Vis absorbance of the characteristic TM3 peaks.

The data sets measured at wavelengths of 388 and 446 were treated as the peaks characteristic of CuTM3 species. The regression analysis and fitting of the spectra, performed the same way as previously described for the CuTM4 system, provided a more accurate determination of the Cu:TM3 reaction ratio in the solution phase. The first part of the data was eliminated from the analysis for the three chosen wavelengths as this did not represent the formation of the new product, but rather disappearance of a reactant. The last point (Cu:TM3 = 3:1) was also eliminated from the analysis, as it did not follow the general trend of the curve. This might be caused by the concentration issue (not being the same as the rest of the solutions) or might be caused by the formation of some other product as the one studied for lower Cu:TM3 ratio.

The result of the analysis for the data set of 388 nm (Figure 3.11A) was performed on the data corresponding to the data points of Cu:TM3 ratio from 0.67:1 – 2:1 due to the poor quality of data. In the first scenario, the point of Cu:TM3 = 1.25:1

was excluded. The intersection of the two lines was observed for a Cu:TM3 ratio of 1.24.

When the Cu:TM3 = 1.25:1 data point was included in the regression analysis (Figure 3.11B) of both parts, the intersection of the two lines was observed at the ratio of Cu:TM3 = 1.22:1.

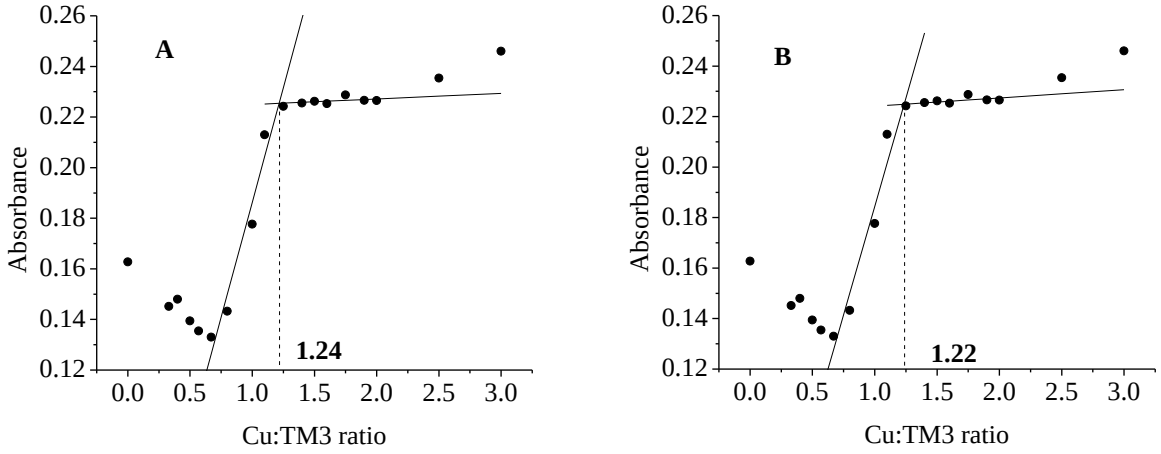

Figure 3.11 The intersection of the lines of theoretical absorbance change with increasing Cu:TM3 ratio in acetate-ammonia buffer at 388 nm.

For the data set of 446 nm, some of the data points were removed from the regression analysis due to the poor quality of data. The analysis was performed on the data corresponding the ratio of Cu:TM3 = 0.33:1 – 2:1.

In the first scenario (Figure 3.12A), data point corresponding to the Cu:TM3 ratio of 1.25 was excluded from both parts of data. The intersection of the two lines was obtained at the ratio of Cu:TM3 = 1.30:1.

When the data point of Cu:TM3 = 1.25:1 was included in the regression analysis of both parts of data (Figure 3.12B), the intersection was observed at Cu:TM3 ratio of 1.28:1.

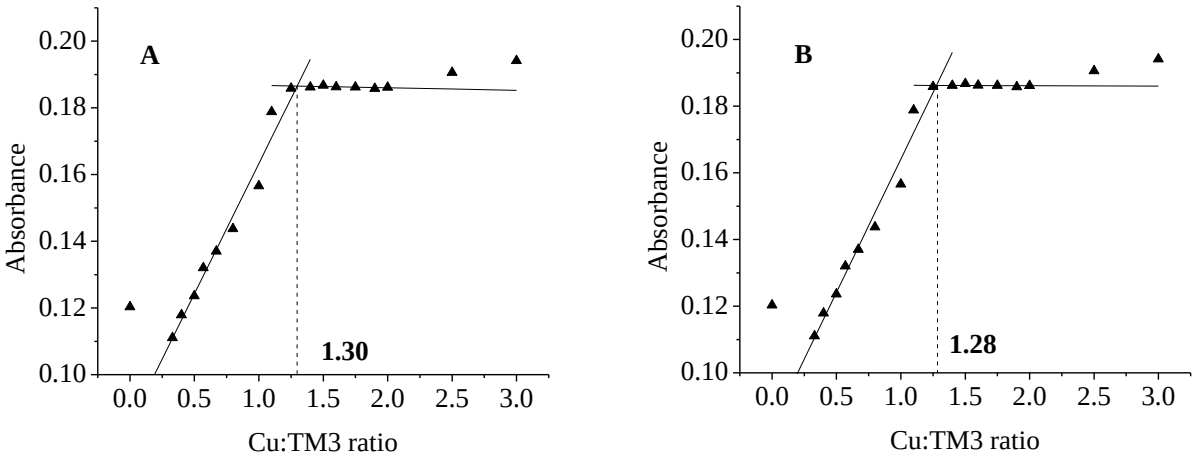

Figure 3.12 The intersection of the lines of theoretical absorbance change with increasing Cu:TM3 ratio in acetate-ammonia buffer at 446 nm.

For the data set of wavelength of 462 nm (Figure 3.13A), the first scenario of the regression analysis was performed on the points of the ratio of Cu:TM3 = 0.33 – 2:1, excluding data point corresponding to 1.25:1. The intersection of the two lines was observed at the Cu:TM3 = 1.27:1.

When the data point of Cu:TM3 = 1.25:1 was included in the regression analysis (Figure 3.13B) of the both parts of the data set, the intersection of the two lines occurred at Cu:TM3 = 1.26:1.

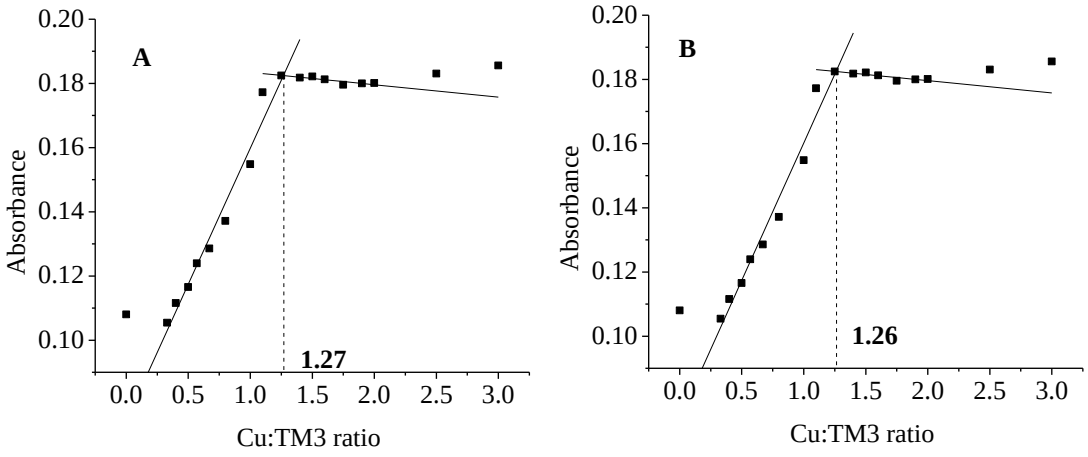

Figure 3.13 The intersection of the lines of theoretical absorbance change with increasing Cu:TM3 ratio in acetate-ammonia buffer at 462 nm.

At a wavelength of 338 nm (Figure 3.14A), no decrease of the absorbance with increasing Cu:TM3 reaction ratio was observed. The first addition of Cu(II) into TM3 solution resulted in an increase of the absorbance of the spectra. The linear increase was observed up to Cu:TM3 ratios close to 1.25:1. Further increase of the Cu:TM3 ratio didn't result in any significant changes in the absorbance. The wavelength of 338 nm is therefore characteristic of a newly formed CuTM3 adduct species.

To more accurately determine the ratio of Cu:TM3 species in the solution phase, regression analysis was performed on the whole set of measured data (from Cu:TM3 = 0:1 – 3:1). In the first scenario, the point of Cu:TM3 = 1.25:1 was excluded from both parts. The intersection of the two lines was observed at the Cu:TM3 ratio of 1.18.

When the point of Cu:TM3 = 1.25:1 was included in the regression analysis (Figure 3.14B) of both parts of data, the intersection of the two lines was observed at the ratio of Cu:TM3 = 1.14:1.

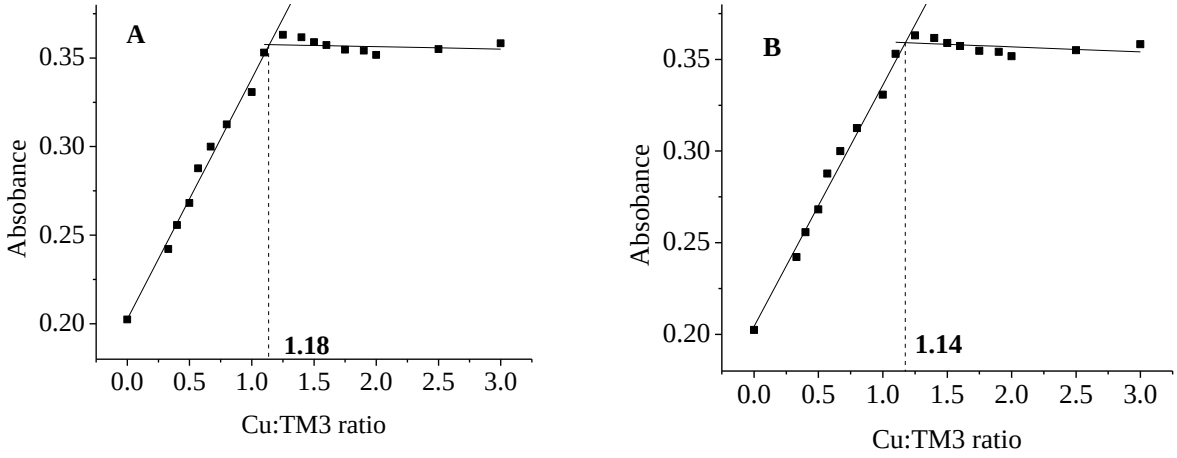

Figure 3.14 The intersection of the lines of theoretical absorbance change with increasing Cu:TM3 ratio in acetate-ammonia buffer at 338 nm.

From the results obtained at different wavelengths, the average ratio of Cu:TM3 in the solution phase was calculated (Table 3.3). This is slightly higher than the ratio of (1.0 ± 0.1:1.0) found for Cu:TM4 in the solution phase (section 3.3.1) and also higher than the ratio Cu:TM3 = 1:1 previously found by E. Quagraine[16].

Wavelength (nm)	*Ratio of Cu:TM3 where the intersection of the two lines was found*	
388	1.22	1.24
446	1.30	1.28
462	1.27	1.26
338	1.18	1.14
Average Cu:TM3 ratio of intersection point	1.23 ± 0.05	

Table 3.3 Ratio of Cu:TM3 in the acetate-ammonia buffer found at various wavelengths by regression analysis.

A similar analysis of earlier UV/Vis data collected in SRF gave an average ratio of Cu:TM3 in solution of 1.44 ± 0.07 which is slightly higher than in acetate-ammonia buffer.

The ratio of Cu:TM3 in solution was found to be higher than Cu:TM4. The ratio of Cu:TM4 was statistically the same as that previously found 1:1[16,119], although a higher ratio has been reported as well[121]. The ratio of Cu:TM3 was found to be significantly higher than previously published (1:1)[16] (Table 3.4).

System	*Ratio Cu:TM found in solution*		
	In this work: acetate-ammonia buffer	In this work: SRF	In literature
CuTM4	1.1 ± 0.1	1.0 ± 0.1	1:1[16,119], 1.5:1[121]
CuTM3	1.23 ± 0.05	1.44 ± 0.07	1:1[16]

Table 3.4 Comparison of the results of Cu:TM ratio found in solution.

Later, these results will be compared with data obtained for Cu:TM3 and Cu:TM4 in the solid phase (section 3.6 and 3.11.2).

The UV/Vis spectra of CuTM4His and CuTM3His did not show any differences compared to the spectra of CuTM4 and CuTM3 without His. Therefore it is concluded that the presence of His does not have any significant effect on Cu-TM interaction under these conditions used in this study.

3.4. TM4 and TM3 in Solution: Stability with Respect to Precipitation

When TM4 or TM3 are in aqueous solution at a concentration of 0.015 M and no Cu(II) is added, no precipitation is observed within an hour. However, when the same experiment is performed in SRF, MOPS or acetate-ammonia buffer, a precipitate can be obtained in one hour. This is most likely the formation of polymeric TM species which precipitate due to increased ionic strength (section 1.6.3). The addition of inert salts into the solution where the reaction between ions of the same charge occurs results in an increase of the rate constant of this reaction. Higher ionic strength favors the formation of a single, highly charged ionic complex from two less highly charged ions because the new ion has a denser ionic atmosphere and interacts with that atmosphere more strongly.[154]

3.5. Preparation of Solid Cu-TM Samples

3.5.1. Reaction Time

To obtain the highest possible amount of the solid CuTM sample, a study was performed to optimize conditions. The mixture of Cu and TM was allowed to react for 30 min, then the solid and solution were separated. The solution was allowed to sit for another 30 min, after which another portion of solid was removed. The six amounts of solid were removed in total from the same mixture, each after 30 min (see section 2.5 for complete experimental details). The interaction of Cu and TM is fast; reaction can be observed to happen instantaneously. 30 min was chosen to allow sufficient time to produce the solid. Results are given in Table 3.5 and Table 3.6.

Most of the solid was precipitated the in first 30 min of the reaction time. The remaining samples of longer reaction time contained very little or no black (Cu-TM4) or brown (Cu-TM3) solid. The second and every subsequent sample have an insignificantly low mass and the samples of the longest reaction times (120-180 min)

contained also low amounts of white solid. This is probably due to precipitation of the buffer solution components. This was confirmed using carbon analysis, which showed 29 % by mass of carbon in the CuTM4 sample prepared in MOPS. It is evident that 30 min reaction time is sufficient to obtain the adequate amount of precipitate out of the solution, while avoiding possible contamination which becomes significant at longer reaction times.

Time periods (min from mixing)	*Mass of the product (g) for Cu:TM4 mixed in molar ratio of:*	
Cu:TM4 mixed	1.3:1	1:1
30	0.0683	0.0593
60	0.0006	0.0004
90	0.0004	0.0001
120	0.0012	0.0003
150	0.0003	0.0004
180	0.0015	0.0004

Table 3.5 Mass of CuTM4 solid samples obtained over different time intervals.

The amount of CuTM solid obtained (Table 3.7 and Table 3.8) is less than the mass of reactants mixed for both systems, CuTM3 and CuTM4. This indicates that the reactants were not consumed completely during the reaction and unreacted species stay dissolved in the solution. This was also confirmed by the observation of the color of the supernatant solution. If the reactants were consumed completely, the solution would become colorless. However, the solutions were of red-brown color, indicating the presence of unreacted TM.

Time periods (min from mixing)	*Mass of the product (g) for Cu:TM3 mixed in molar ratio of:*	
Cu:TM3 mixed	1.3:1	1:1
30	0.0653	0.0617
60	0.0012	0.0007
90	0.0006	0.0004
120	0.0005	0.0004
150	0.0006	0.0005
180	0.0009	0.0004

Table 3.6 Mass of CuTM3 solid samples obtained over different time intervals.

The weight of the obtained solid for the CuTM4 system is different for the two ratios studied. This suggests that if more $Cu(NO_3)_2$ is added into the reaction mixture, more will react and a higher mass of precipitate will be obtained. This, and the fact that a lower mass of solid than expected is obtained, suggest that the ratio of Cu:TM in the formed adduct might be different than the previously reported 1:1[16]. The same was true for the CuTM3 complex as well. This suggests that if more Cu is added, it might react with other components of the solution and these species coprecipitate together with CuTM species.

This mass dependence of the amount of solid on the ratio of reactants was investigated further and will be discussed later (section 3.5.5) together with the results from the elemental analysis (section 3.6) and results of EXAFS study (section 3.11.2).

Mixed at ratio Cu:TM4	*$c(NH_4)_2TM4$ (mol/l)*	*$V(NH_4)_2TM4$ (ml)*	*Mass of $(NH_4)_2TM4$ (g)*	*$cCu(NO_3)_2$ (mol/l)*	*$VCu(NO_3)_2$ (ml)*	*Mass of $Cu(NO_3)_2$ (g)*	*Total mass of reactants (g)*	*Mass of precipitate obtained (g)*
1:1	0.0401	3.58	0.0374	0.0503	4.49	0.0424	0.0797	0.0609
1.3:1	0.0400	4.50	0.0468	0.0501	4.67	0.0439	0.0907	0.0723

Table 3.7 Comparison between total and obtained mass of CuTM4 solid samples. The molar masses used in the calculations are: for $(NH_4)_2TM4$ 260.28 g/mol and for $Cu(NO_3)_2$ 187.57 g/mol.

Mixed at ratio Cu:TM3	*$c(Cs_2TM3)$ (mol/l)*	*$V(Cs_2TM3)$ (ml)*	*Mass of Cs_2TM3 (g)*	*$c(Cu(NO_3)_2)$ (mol/l)*	*$V(Cu(NO_3)_2)$ (ml)*	*Mass of $Cu(NO_3)_2$ (g)*	*Total mass of reactants (g)*	*Mass of precipitate obtained (g)*
1:1	0.0408	4.49	0.0868	0.0501	3.59	0.0337	0.121	0.0641
1.3:1	0.0400	4.50	0.0853	0.0503	4.65	0.0439	0.129	0.0691

Table 3.8 Comparison between total and obtained mass of CuTM3 solid samples. The molar masses used in the calculations are: for $(NH_4)_2TM4$ 473.95 g/mol and for $Cu(NO_3)_2$ 187.57 g/mol.

3.5.2. Observations of the Reaction of Cu and TM during Preparation of CuTM Adducts

When the solid CuTM samples (for EPR, section 2.7.1) were prepared in pH 7.00 MOPS buffer solution to mimic the rumen pH environment, there was an interference from the precipitation of $Cu(OH)_2$. Shortly after Cu solid was dissolved in buffer, cloudiness of the solution was observed. The solubility constant, K_{sp}, of copper hydroxide has a value of 4.8×10^{-20}, and is governed by the expression

$$K_{sp}=\left[Cu^{2+}\right]\left[OH^{-}\right]^{2} \qquad 3.1$$

The stock solution of Cu has concentration 0.05 mol/l. The concentration of OH^- ions at pH 7.00 buffer is 1.0×10^{-7} mol/l. The product of the concentration of ions

$$\left[Cu^{2+}\right]\left[OH^{-}\right]^{2} = 0.05\left(10^{-7}\right)^{2} = 5.00 \times 10^{-16} \qquad 3.2$$

is larger than the K_{sp} of $Cu(OH)_2$ at 25 °C (4.8×10^{-20})[155] and therefore suggests that precipitation at this pH will occur.

The mass of the solid obtained for the sample prepared using the same procedure varied, and amounts of desired adducts insufficient for any measurement were commonly observed. This might be caused by the interference of Cu and buffer where precipitation of $Cu(OH)_2$ results into insufficient amount of Cu to react with TM. As mentioned previously, it is likely that MOPS was part of the formed solid adduct as carbon was found to be present in these samples.

It was discussed previously that at pH 7, Cu will precipitate in the form of $Cu(OH)_2$. The precipitation was also observed for pH 6 and 5. The tabulated value of Ksp for $Cu(OH)_2$ suggests that pH should be below 5 (concentration of OH^- below 9.8×10^{-10} M) to avoid precipitation of Cu. This agrees with our observations, where at a pH

of 5 precipitation was observed, but at a pH of 4 it was not. Therefore, pH of the solution had to be lowered to a value of 4 to eliminate this interference.

As the MOPS is not a good buffer for lower pH values (pH 4), other buffers were used to prepare solid CuTM samples for spectral analysis (EPR, EXAFS, IR, elemental analysis). To mimic the conditions close to the biological environment of the ruminants, simulated rumen fluid was used (section 2.4.1).

In the 0.05 M Cu(II) stock solution prepared for the preparation of solid CuTM samples for EPR (section 2.7.1), interaction of Cu(II) with components of SRF solution could be observed because of the cloudiness that appears in few minutes. However, this did not seem to cause problems as in the case of MOPS buffer (pH 7) discussed above for the preparation of Cu-TM adducts. Solid CuTM samples were obtained in quantities sufficient for spectral measurements (EPR, EXAFS, elemental analysis). The masses of the adducts obtained, given in section 3.5.5, were more consistent in SRF than MOPS for several trials using the same amounts of reactants. This was true for trials when TM was added to the Cu solution fast enough before the cloudiness and precipitation of Cu in SRF was observed. When the interaction between Cu and TM4 was previously studied[16], it was found that the adduct formed is very strong and none of the studied reagents (EDTA or S^{2-}) could strip off the Cu from TM4. This was also observed for samples containing TM3[16]. Therefore the Cu-TM interaction is much stronger than the Cu-SRF interaction. The reaction between Cu and TM is most likely much faster than the reaction between Cu and components of SRF; for Cu-TM, precipitation is observed immediately upon mixing reactants together, but for Cu-SRF, it takes a few minutes for the cloudiness to be observed.

As the interaction of the Cu-SRF solution might still cause problems (section 3.5.3) during the preparation of solid CuTM samples for further analysis (EPR, EXAFS), the buffer solution was changed again. An acetate-ammonia buffer (section

2.4.2) was used instead of SRF. In a stock solution of Cu prepared for the reaction with TM to form adducts for spectral measurements, no interaction (cloudiness, precipitation) was observed at pH 4 between Cu and acetic acid and ammonia. Copper reacts with both of these components; however, in both cases, soluble products are formed, copper acetate and copper ammonium ion.

Most of the studies were done in SRF but great effort was made to minimize the reaction between copper and components of SRF. In later stages of the study, acetate-ammonia was used in the preparation of solid CuTM samples. The results of spectral analyses using both buffer solutions will be presented where available and the differences will be discussed in this chapter (section 3.11).

3.5.3. Investigation of the Cu-SRF Interaction

When Cu(II) is dissolved in SRF, formation of a precipitate is observed in about 5 min at room temperature. Most likely this is either Cu phosphate or Cu carbonate because the other components (acids) of SRF do not form precipitates with Cu(II). To confirm this, two other experiments were performed. A sample of Cu(II) in carbonate solution produced a precipitate a few minutes after $Cu(NO_3)_2$ was added into the test-tube, under comparable conditions to the SRF experiments. In a similar experiment with Cu(II) and phosphate, the formation of a precipitate was also observed.

To further confirm this, a solid sample prepared by the reaction of Cu(II) and SRF was submitted to for elemental analysis. The results confirmed the presence of phosphate; the amount of phosphorus was found to be 14.1 % by mass and the amount of Cu 36.0 % by mass. Unfortunately, the amount of carbon was not determined. It is not known if the remaining 50 % is carbonate or other species. However, given that precipitation was observed for the Cu(II) in carbonate solution (absence of phosphate), it is most likely that both phosphate and carbonate form a precipitate with Cu(II).

The precipitation of these compounds might interfere with the formation of Cu-TM adducts in two ways. Due to the formation of copper phosphate and copper carbonate the amount of Cu(II) available to react with TM added later to the solution is lowered. This could lead to faulty results for the true stoichiometry of the CuTM adducts. The other possibility is that added TM could also react with already formed Cu(II)-phosphate and/or Cu(II)-carbonate, which could contaminate the CuTM adducts.

When $Cu(NO_3)_2$ was dissolved in the acetate-ammonia, no precipitation was observed before the reaction with TMs which also confirms the phosphate and carbonate species reacting with Cu.

3.5.4. Color of the Reaction Solutions of CuTM Mixtures

During the preparation of the solid CuTM adducts for spectral analyses (EPR, EXAFS, elemental analysis), the sample in the test-tube was centrifuged after one hour of reaction time and the solution was separated from the solid (sections 2.7.1 and 2.10.1). To remove the unreacted (soluble) species, solid samples were washed with another portion of acetate-ammonia buffer. Samples of higher ratios (2:1 and 3:1) were also prepared following the same procedure for these observations. The color of the supernatant and washing solution was observed.

3.5.4.1. Color of the Supernatant for Different Ratios

For the CuTM4 samples, after the centrifuging step the supernatant was observed to be orange-brown in color for the samples mixed at ratios up to 1.2:1. This color can be attributed to the presence of unreacted TM4 species.

For higher ratios, 1.3 - 2.5:1, the supernatant was colorless. This suggests that all the TM4 was consumed completely during the preparation of the samples. However, solutions of low concentrations of $Cu(NO_3)_2$ (approximately 1 x 10^{-4} M) also result in colorless solutions. It is, therefore, not clear at this stage, if in this range complete consumption of Cu occurs for all the ratios or if some Cu is left unreacted in the solution for some ratios.

For higher ratios, the color of the supernatant was observed to be light blue, clearly indicating the presence of unreacted Cu species.

For CuTM3 adducts, orange colored supernatant was observed up to the reaction ratio of 1.6:1. A colorless supernatant was observed for reaction ratios of 1.75 – 2.5:1 and a blue supernatant for higher ratios.

This study therefore suggests that the ratio of Cu:TM in the formed adducts might be higher for TM3 than TM4. It also suggests that for both systems, the ratio of Cu:TM in adducts is higher than that previously reported 1:1.[16]

3.5.4.2. Washing solutions

For the samples of CuTM4 mixed at ratios up to 1.2:1 for Cu:TM4, the washing solution was of red-brown color. This could suggest the presence of the unreacted TM4 species in the solid that dissolved with a new portion of buffer. Or it could be due to the dissolution of the CuTM4 precipitate. This is however not likely the case, as attempts to dissolve solid CuTM4 were not successful.

For mixed ratios of 1.3 - 2.5:1, the supernatant was colorless. Therefore, it is very unlikely that solid CuTM4 would dissolve (above). The TM4 was completely consumed during the reaction. Cu might be completely consumed as well in this range

of used mixing ratios or a small amount might be still present which does not show any color.

For ratios higher than 2.5:1, the supernatant was colorless. Therefore, it is likely that no unreacted species were present in the system and the unreacted Cu was dissolved and removed with the original supernatant.

These results were obtained for the CuTM samples prepared by the same method in the SRF and acetate-ammonia buffer. It is concluded from this study that, when careful preparation is performed, there is no difference in the ratio of Cu:TM in the prepared samples between these two environments.

A conclusion on the true stoichiometries cannot be made at this point. The results indicated only a range of possible stoichiometries. This is investigated further in other studies in the solid phase (section 3.6 and 3.8) and in solution (section 3.3).

3.5.5. Mass of the Cu-TM Precipitate

Several CuTM4 solid adducts were prepared to study the effect of the variable Cu:TM reaction molar ratio on the mass of the obtained precipitate (section 2.6.2). During their preparation, the amount of the TM4 was kept constant and the amount of Cu(II) was varied to achieve the desired molar reaction ratio of reactants. Previous studies suggested that the ideal ratio of reactants of Cu:TM4 was somewhat higher than 1:1, that in fact it was at least 1.2:1 (section 3.5.4).

The mass of the prepared adducts was studied to see if the amount of the solid would be the same for different amounts of Cu or if it would vary. As concluded from the supernatant color observation (section 3.5.4.1), it wasn't clear if the ratio of

reactants is exactly 1.2:1 or if it can be in fact higher when more Cu is added. The study was performed on the samples prepared in SRF.

Three samples were also prepared in water (not buffered, room temperature) to observe possible effects of the buffer components on the mass of the solid. Three samples were prepared at higher temperature of 38°C (buffer), which is close to the biological temperature. Another three samples were prepared in the presence of histidine (His) (room temperature, buffer), to observe its effect on the sample masses. Histidine was chosen because it is thought that the interaction of the CuTM4 and peptides happens through the nitrogen atoms of the histidine molecule[16]. Results are given in Table 3.9 and Figure 1.15.

With increasing amount of Cu(II) added to the mixtures, an increasing mass of the precipitate obtained was observed for CuTM4 and CuTM3 samples. This was expected for the samples mixed at ratio lower than 1:1; as previously reported[15,119] this ratio was found to be at least 1:1 in the formed solid. An increase of the mass of adduct was observed up to the reactant ratio Cu(II):TM4 of 2.5:1. This could mean that this high ratio is the actual true ratio of Cu:TM4 in the adduct. This agrees with previous observations of the supernatant color where above 2.5:1 ratio, unreacted Cu(II) was present in the solution. Therefore, if more Cu is available for the reaction with TM4 more Cu(II) will be consumed during this reaction up to the 2.5 times the amount of TM4. The true ratio of the components in the adduct will be investigated further by elemental analysis (section 3.6).

Cu:TM4	*Moles Cu(II)*	*Mass product in SRF (g)*	*Mass of product at 38°C (g)*	*Mass of product with His (g)*	*Mass of product in water (g)*
0.497:1	8.95×10^{-5}	0.0592			
1.00:1	1.80×10^{-4}	0.0718	0.0588	0.0765	0.0551
1.20:1	2.16×10^{-4}	0.0696			
1.30:1	2.34×10^{-4}	0.0707	0.0702	0.0807	0.0603
1.50:1	2.70×10^{-4}	0.0754	0.0743	0.0844	0.0606
1.75:1	3.15×10^{-4}	0.0785			
1.87:1	3.36×10^{-4}	0.0781			
2.50:1	4.50×10^{-4}	0.0804			
3.00:1	5.40×10^{-4}	0.0814			
4.00:1	7.20×10^{-4}	0.0835			

Table 3.9 Mass of Cu-TM4 adducts obtained at different amounts of Cu(II) added into the reaction mixture and constant TM concentration. Total concentration of TM4 was 0.015 M and total volume of the mixture was 12 mL.

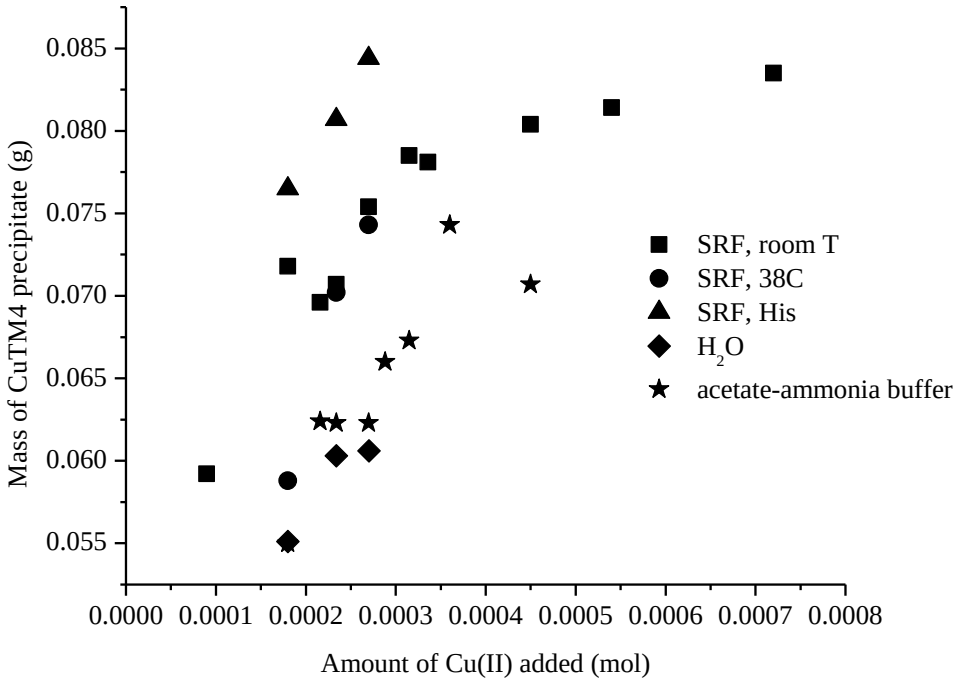

Figure 3.15 Mass of precipitate of the CuTM samples influenced by the amount of Cu(II) mixed with TM and by environment.

When the reaction mixture contained His in buffer solution, the mass of the precipitate increased. This indicates possibility of His being the part of the complex or might be caused by increased ionic strength pushing the equilibrium to the product side and therefore resulting into the formation of a larger amount of product[16]. This will be investigated further by elemental analysis (section 3.6).

Solid CuTM4 samples were of lower mass when prepared in SRF at 38 °C compared to room temperature. This could be due to faster formation of Cu(II)-phosphate and Cu(II)-carbonate precipitation which would lower the amount of Cu(II) available for the reaction with added TM. The fact that a formation of cloudy precipitate including Cu(II) in SRF was observed sooner (1-2 min) than at room temperature (5-7 min) supports this hypothesis.

When the preparation of the samples was carried out in water (non-buffered environment), lower amounts of solid were obtained than in acetate-ammonia buffer. Each component added to the reaction mixture (acetate-ammonia buffer, SRF) can potentially interfere with the formation of the adducts in such a way that they become part of the Cu-TM adducts. This would result in a higher amount of product obtained. However, if this is an equilibrium system, the precipitation could also be enhanced by the presence of other molecules in the solution (buffer components). This would result in higher amount of precipitate than in their absence (water, non-buffered).

The amount of solid obtained in SRF and acetate-ammonia was also compared (Table 3.10, Figure 3.16) to see if the environment has an effect on the precipitation.

Cu:TM4	*Moles Cu(II)*	*Mass product in SRF (g)*	*Mass product in acetate-ammonia buffer (g)*
0.497:1	8.95×10^{-5}	0.0592	0.0489
1.00:1	1.80×10^{-4}	0.0718	0.0550
1.20:1	2.16×10^{-4}	0.0696	0.0624
1.30:1	2.34×10^{-4}	0.0707	0.0623
1.50:1	2.70×10^{-4}	0.0754	0.0623
1.75:1	3.15×10^{-4}	0.0785	0.0660
1.87:1	3.36×10^{-4}	0.0781	0.0673
2.50:1	4.50×10^{-4}	0.0804	0.0743
3.00:1	5.40×10^{-4}	0.0814	0.0707
4.00:1	7.20×10^{-4}	0.0835	

Table 3.10 Comparison of mass of CuTM4 precipitate obtained in SRF and acetate-ammonia buffer.

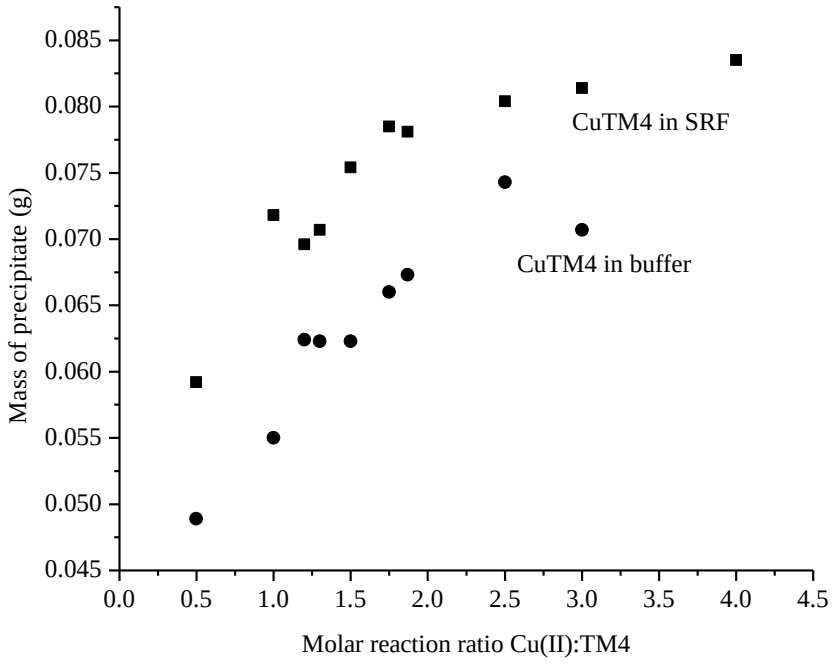

Figure 3.16. Amount of solid CuTM4 obtained in SRF and acetate-ammonia buffer.

Below (Table 3.11) are results of the mass dependence of precipitate on the amount of Cu(II) added for the CuTM3 solid samples.

For CuTM3 samples, it is again observed that with increasing amounts of Cu(II) in the reaction with TM3, increased amounts of precipitate are observed.

Cu:TM3	*Moles Cu(II)*	*Mass product in SRF (g)*	*Mass product in acetate-ammonia buffer (g)*
0.501	9.02×10^{-5}	0.0449	0.0441
1.00	1.80×10^{-4}	0.0605	0.0521
1.20	2.16×10^{-4}	0.0606	0.0566
1.30	2.34×10^{-4}		0.0568
1.50	2.70×10^{-4}	0.0634	0.0566
1.60	2.88×10^{-4}	0.0618	0.0621
1.76	3.16×10^{-4}	0.0637	0.0607
2.01	3.61×10^{-4}	0.0651	0.0634

Table 3.11 Mass of CuTM3 precipitate obtained for different amounts of Cu(II) added to the TM3 solution.

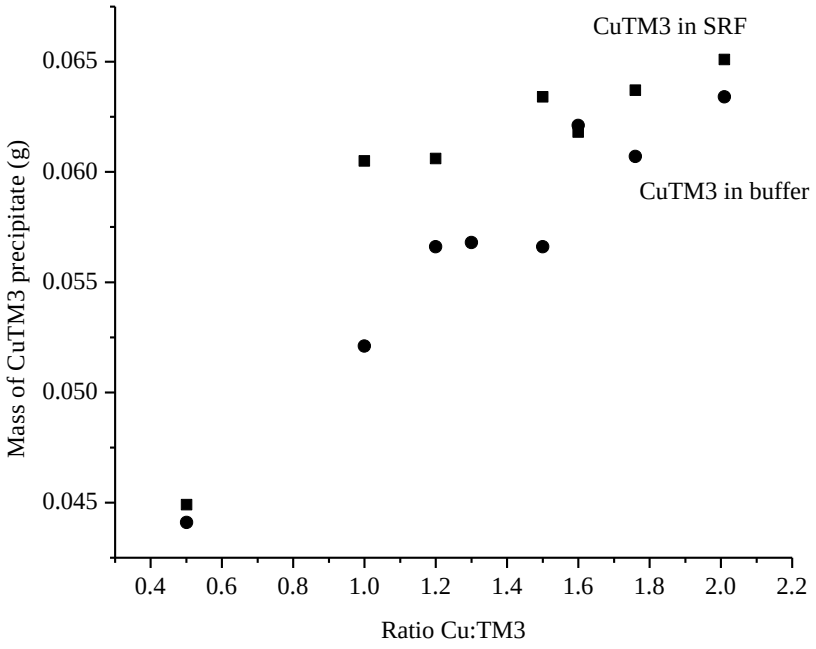

Figure 3.17 Dependence of the mass of CuTM3 solids obtained on the molar ratio of Cu:TM3 in reaction in SRF and acetate-ammonia buffer.

From the data, the same trend is observed for the samples prepared in the two environments: increase in the mass of adduct when the amount of Cu(II) is increased. However, a higher amount of precipitate was observed when samples were prepared in SRF rather than acetate-ammonia buffer. The likely reason is that the interaction of Cu with SRF results in formation of insoluble species, and therefore a higher mass of solid is obtained. This hypothesis will be investigated later (section 3.6). Another possibility is that if the system is in equilibrium (equation 1.30, first step of reaction), then higher concentrations of species in the solution (buffer components) would result in lower solubility of CuTM3 species and therefore more precipitate.

3.6. Elemental Analysis of Solid CuTM Samples

Solid CuTM samples were prepared at three different ratios in SRF at room temperature. At a molar reaction ratio of Cu:TM 1:1, samples of CuTM4 and CuTM3 were prepared in buffer at low temperature to study the effect of the temperature on the stoichiometry. Another two samples were also prepared, one of CuTM4 and one of CuTM3 at room temperature in the presence of histidine. These samples were submitted to elemental analysis for Mo, Cu and S. Results are shown in Table 3.12.

From the results the ratios of these elements in the adducts were calculated (Table 3.13).

The ratio of Cu:Mo in the sample is not constant as the amount of Cu(II) introduced into the mixture increases. The true ratio of elements Cu:Mo is increasing with the increasing ratio of reactants introduced into the system. The variable ratios of these elements in their adducts were observed previously in the literature in many cases (section 1.5.4), depending on several factors, such as solvent and ligand, but are strongly dependent on the ratio of Cu:TM available.

Reactant ratio	*Conditions*	*% Mo*	*% Cu*	*% S*	*Total %*
Cu:TM4 = 1:1	Room T	19.3	16.9	36.7	72.9
Cu:TM4 = 1:1	Room T, His	17.1	14.7	32.3	64.1
Cu:TM4 = 1:1	Ice bath	19.2	16.8	35.5	71.5
Cu:TM4 = 1.5:1	Room T	16.9	21.8	29.9	68.6
Cu:TM4 = 2:1	Room T	14.5	24.2	32.9	71.6
Cu:TM3 = 1.:1	Room T	19.6	17.1	28.1	64.8
Cu:TM3 = 1.:1	Room T, His	16.9	14.4	26.0	57.3
Cu:TM3 = 1:1	Ice bath	19.5	19.5	28.9	67.9
Cu:TM3 = 1.5:1	Room T	14.7	24.6	27.4	66.7
Cu:TM3 = 2:1	Room T	12.5	32.5	27.0	72.0

Table 3.12 Results of elemental analysis: mass percentage found in CuTM powders for Mo, Cu and S. The samples were prepared in SRF, at room temperature (room T), at lower temperature (ice bath, ~0-5 °C) and at room temperature in the presence of histidine. Results are expressed as % by mass.

This dependence of the true (Cu:Mo molar ratio found by elemental analysis) on the reaction (mixed Cu:TM) ratio agrees with previously mentioned studies (section 3.5.4), where observation of the supernatant solution suggested complete consumption of reactants in the range of mixing ratios of 1.2 – 2.5:1 and not only at one exact value.

Ratio	*Cu:TM4*		*Conditions*	*Cu:TM3*	
Mixed	Found				
	Cu:Mo	S:Mo		Cu:Mo	S:Mo
1:1	1.32	5.69	Room T	1.32	4.29
	1.30	5.65	Histidine	1.29	4.60
	1.32	5.53	Low T	1.51	4.44
1.5:1	1.95	5.30		2.53	5.58
2:1	2.52	6.79		3.92	6.46

Table 3.13 Mass ratios for the CuTM3 and CuTM4 samples prepared in SRF, as determined by elemental analysis.

From the results, it is also observed that presence of histidine does not have a significant effect on the ratio of Cu:Mo (Table 3.13); however, given the literature results, it is possible that His affects the structure. This will be studied and discussed later (section 3.11.2).

For CuTM4 adduct, no significant effect was observed when the sample was prepared at a lower temperature. For CuTM3 sample, the sample prepared at lower temperature has a higher ratio of Cu:Mo. This however might be caused by the difficulty of dissolving TM3 at lower temperature. The TM3 that precipitated before Cu(II) was added would be removed during the washing step as at this time it might redissolve again.

Later, new samples were submitted for elemental analysis (Table 3.14). These were prepared by the same method as before, but acetate-ammonia was used as the buffer. As it had been determined that including His or lowering the temperature does not have a significant effect on the stoichiometry, these samples were not studied again.

Sample mixed	*% Mo*	*% Cu*	*% S*	*Total %*
Cu:TM4 = 1:1	18.5	18.0	37.1	73.6
Cu:TM4 = 1.2:1	18.6	22.3	3.4	79.3
Cu:TM4 = 1.5:1	16.2	24.3	33.7	74.2
Cu:TM4 = 2:1	16.4	29.2	33.0	78.6
Cu:TM3 = 1:1	18.0	19.6	25.1	62.7
Cu:TM3 = 1.2:1	16.5	22.0	22.2	60.7
Cu:TM3 = 1.5:1	15.9	27.4	21.4	64.7
Cu:TM3 = 2:1	15.3	27.6	19.7	62.6

Table 3.14 Results of elemental analysis: weight percentage found in CuTM powders for Mo, Cu and S. Samples were prepared in acetate-ammonia buffer.

Again, the ratios of elements were calculated and are presented in Table 3.15.

Ratio	*Cu:TM4*		*Cu:TM3*	
Mixed	Found			
	Cu:Mo	S:Mo	Cu:Mo	S:Mo
1:1	1.47	6.00	1.65	4.17
1.2:1	1.81	6.18	2.01	4.03
1.5:1	2.27	6.22	2.60	4.03
1.75:1	2.69	6.02	2.72	3.85

Table 3.15 The molar ratio of elements in samples prepared in acetate-ammonia buffer as found by elemental analysis.

In these samples, the ratio of Cu:Mo was found again to increase with the increasing amount of Cu available in the reaction mixture. However for these samples, a slightly higher ratio of Cu:Mo was found for the prepared adducts than in the previous samples prepared in SRF. This might be caused by avoiding interferences that were observed previously in the SRF environment (section 3.5.3).

It is also observed that the Cu:Mo ratio found by elemental analysis is somewhat higher than the reaction ratio used in the solution mixture. Therefore each molybdenum entity most likely reacts with more than one Cu entity. In this case, some TM would be left unreacted and all the Cu would be consumed in the reaction. The unreacted TM, which is soluble, is then left in the solution and does not precipitate as solid. Another possibility is that TM in solution undergoes hydrolysis (loss of sulfur atoms) before it reacts with Cu. The hydrolysis might be partial (lower TM than dissolved reactant) or complete (formation of TM0). Sulfide species then react with Cu which decreases Cu availability for reaction with TM4. Soluble species (lower unreacted TMs, including possibly TM0) are then left in the solution phase, do not contribute to the total mass of the solid product and are left out of the measurements of elemental analysis.

It is also interesting that the amount of Cu in the adducts is higher for the samples prepared with TM3 than TM4, although it was reported previously that Cu would preferentially bind to TM4 because of its high S content. Previous studies in our group by Quagraine showed the ratio of Cu:Mo to be same (1:1) for both systems in solution (section 1.6). This will be studied further by other spectroscopic techniques (EPR, EXAFS), see sections 3.8 and 3.11.

For both sets of samples, in acetate-ammonia buffer and in SRF, the ratio of S:Mo is higher than expected in all the studied samples. The original TMs have S:Mo ratios of 4:1 (TM4) and 3:1 (TM3) and the higher sulfur amount found by the elemental

analysis is therefore unexpected. The only source of sulfur in these systems is the TM used.

There is a possibility of TM3 disproportionation into TM2 and TM4; however, there is no such possibility for TM4. If we assume that all the Cu(II) introduced into the mixture reacts and is used up, then from the composition results it is evident that some of the TM is unreacted after an hour of reaction time. This would either stay dissolved in the solution or would precipitate as TM polymeric species. The unreacted TM molecules most likely undergo hydrolysis which is significant in an hour of the reaction time and at the concentration used in the experiment.

This would be the source of sulfur which can now react with the Cu-TM complex or any unreacted Cu to form Cu-S species which are insoluble and would also precipitate.

The most likely option is the first one, sulfur interaction with the Cu-TM complex, because Cu-TM formation is much faster than the hydrolysis of the TM. To chose between these possibilities, we have to look at structural studies (section 3.11).

If the ratio of Cu:TM increases with an increasing availability of Cu(II), then there might be not enough TM to reduce all the Cu(II) to Cu(I) even if all the Cu is bound to TM. In that case the final adduct, insoluble polymeric precipitate, would contain both, Cu(I) and Cu(II) at higher amounts of Cu available in the system. More insight into this will be provided by EPR (section 3.8) and XANES (section 3.11.1) analyses on the solid CuTM samples.

Based on the results of the elemental analysis, the true stoichiometry of the reactants Cu:TM can be calculated for all the prepared adducts that were studied by

other spectroscopic techniques (mainly EPR used more samples at different ratios). Regression analysis provided linear equation of the dependence of stoichiometry on the mixed ratio. For CuTM4 dependence is

$y = (1.61 \pm 0.02)x + 0.14 (\pm 0.03)$ with $R^2 = 0.9996$

and for CuTM3 it is

$y = (1.5 \pm 0.2)x + 0.22 (\pm 0.3)$ with $R^2 = 0.9526$

where x = mixed molar Cu:TM ratio and y = found Cu:TM ratio. The interpolated stoichiometries of the other CuTM solid adducts are below (Table 3.16).

Mixed molar ratio Cu:Mo	*Ratio Cu:Mo obtained from elemental analysis*	*Interpolated Cu:Mo ratio*
0.50		0.68
1.00	1.47	
1.20	1.81	
1.30		1.96
1.50	2.27	
1.60		2.44
1.75	2.69	
2.00		3.09
2.50		3.90

Table 3.16 Interpolated stoichiometries of the solid CuTM4 adducts based on the results (second column) obtained from the elemental analysis.

Mixed molar ratio Cu:Mo	*Ratio Cu:Mo obtained from elemental analysis*	*Interpolated Cu:Mo ratio*
0.50		0.96
1.00	1.65	
1.20	2.01	
1.30		2.15
1.50	2.60	
1.60		2.60
1.75	2.72	
2.00		3.19
2.50		3.94

Table 3.17 Interpolated stoichiometries of the solid CuTM3 adducts based on the results (second column) obtained from the elemental analysis.

3.7. CuTM3TM4

Several mixtures were prepared that contained three reaction components: Cu(II), TM3 and TM4. Samples were prepared at different molar ratios of the three components and different mixing order as well. Details on their preparation can be found in section 2.11.1. These solid samples were prepared to study the interaction of Cu(II) with both TMs together and investigate its potential preference to bind TM4 rather than to TM3 because of the difference in sulfur content. This could be studied by analysis of the XANES spectra of the solid samples. The oxidation state of the copper in the resulting adducts will also be studied by XANES. Results of the XANES analysis will be discussed later (section 3.11.1), here the observation of the masses of adducts obtained will be presented (Table 3.18).

Composition of the sample and molar ratio of reactants	*Mass of the precipitate obtained (g)*	*Theoretical mass of the precipitate ($mCu(NO_3)_2$+mTM4+mTM3) (g)*
Cu+TM3+TM4		
1:1:1	0.1054	0.166
2:1:1	0.1142	0.200
1.5:1:1	0.1152	0.183
Cu+TM4+15 min TM3		
1:1:1	0.1068	0.166
2:1:1	0.1085	0.200
1:0.5:1	0.0794	0.143
Cu+TM3+15 min TM4		
1:1:1	0.1023	0.166
2:1:1	0.1195	0.200
1:1:0.5	0.0819	0.143

Table 3.18 Mass of the Cu-TM3-TM4 solid samples obtained. In the first set, TM3 and TM4 were added to the Cu(II) solution at the same time. In second, TM3 was added 15 min later than TM4 and third, TM4 was added 15 min later than TM3.

When the TM3 and TM4 reactants were mixed together with Cu at the same time (the first three samples in a Table 3.18), no significant difference in the mass of the CuTM3TM4 precipitate was observed for different amounts of Cu(II) in the mixture. The mass of the final adduct obtained was only slightly lower with 1 equivalent of Cu(II) compared to 1.5 and 2 equivalents. This confirms the hypothesis that if the larger amount of Cu(II) is added into the solution, more Cu(II) will react with the TM present. At lower amounts of Cu(II), formation of polymeric TM species is more significant.

The actual amount of the CuTM3TM4 precipitate obtained is lower than the sum of the masses of the reactants (last column in the Table 3.18). Therefore, not all of the reactants were completely consumed in the reaction and the unreacted part stayed dissolved in the solution.

For both ratios, 1:1:1 and 2:1:1, the order in which TMs are added doesn't seem to influence the amounts of adduct produced (Table 3.18). This is probably because very similar products are formed for the same ratio of reactants. This could be caused by the interconversion between present TMs (TM3 ⇆ TM4) which would then lead into formation of the same product without effect of the order of mixing. Or it could be caused simply by unreacted Cu reacting with the second added TM; therefore for both orders of mixing, the same products will be formed in the end.

The mass of the CuTM3TM4 solid adducts was compared to the mass of CuTM3 and CuTM4 adducts. Results are summarized in Table 3.19.

The amount of the solid obtained when Cu and two TMs are present is larger compared to when only one equivalent of one of the TMs is present. This suggests that upon the addition of TM at later stage to the reaction mixture, this TM reacts with the already formed CuTM adduct and produces an adduct of a larger mass (Table 3.19), or that unreacted Cu reacts with the second TM added and therefore more precipitate is obtained. This agrees with previous findings which showed that if more Cu is present (in ratio with TM), more will react (Table 3.10). It also agrees with the results of elemental analysis, where it was observed that the ratio of Cu:TM in the solid can be variable and depends on the reaction ratio of Cu:TM (section 3.6).

Mass (g) for the sample mixed at ratio		*Sum of mass of CuTM4 + CuTM3*	*Mass of CuTM4TM3 mixed at ratio*
Cu:TM4 = 1:1	CuTM3 = 1:1		2:1:1
0.0550	0.0521	0.1071	0.1142[a]
			0.1085[b]
			0.1195[c]
CuTM4 = 0.5:1	CuTM3 = 0.5:1		1:1:1
0.0489	0.0441	0.0930	0.1054[a]
			0.1068[b]
			0.1023[c]
Cu:TM4 = 0.5:0.5	CuTM3 = 0.5:1		Cu+TM4+15 min TM3 = 1:0.5:1
0.0275	0.0441	0.0716	0.0794
CuTM4 = 0:1	CuTM3 = 1:1		Cu+TM3+15 min TM4 =1:1:0.5
0[d]	0.0521	0.0521	0.0819
Cu:TM4 = 1:1	CuTM3 = 0.5:1		Cu+TM3+TM4=1.5:1:1
0.0550	0.0441	0.0991	0.1152

Table 3.19 Mass of CuTM3TM4 adducts compared to the masses of CuTM3 and CuTM4 adducts. [a]mixed at the same time, [b]TM3 added 15 min later, [c]TM4 added 15 min later, [d]assumes all the Cu(II) reacted with TM3 and TM4 added 15 min later is assumed not to react because there is no more free Cu(II) available.

The mass of the final adduct formed is a little larger than the sum of the masses of CuTM3 = 1:1 and CuTM4 = 1:1 when formed separately in two different solutions (Table 3.19). The interaction of the three components, Cu, TM3 and TM4 therefore leads to the greater consumption of the reactants than a reaction of only two components, Cu and TM.

In the experiment where Cu was mixed with TM3 and lower amount (half equivalent) of TM4 was added 15 min later to the mixture, the amount of solid obtained was larger than for mixture of only two components, Cu and TM3 (Table 3.19). Therefore, TM4 can still react with already formed CuTM3 precipitate, even if it is added at later stage.

If Cu was reacted with TM4 first and TM3 was added to the reaction mixture later, the mass of the obtained precipitate was larger than mass of precipitate of the reaction between only two components, Cu and TM4 (Table 3.19). Therefore, added TM3 at later stage to the reaction mixture still reacts with already formed CuTM4 precipitate. This agrees with previous findings, where an increase in the reaction ratio of Cu:TM resulted in an increased mass of formed product (Table 3.7).

3.8. EPR of Solid CuTM Samples

3.8.1. EPR Spectra of Starting Materials

Solid samples of TM3 and TM4 as prepared (sections 2.2 and 2.3) had no features in their EPR spectra. All the elements are in a diamagnetic state; Mo^{6+} and S^{2-} possess no unpaired electrons.

$Cu(NO_3)_2$ contains copper in the oxidation state +2, which has one unpaired electron and is therefore paramagnetic (Figure 3.18).

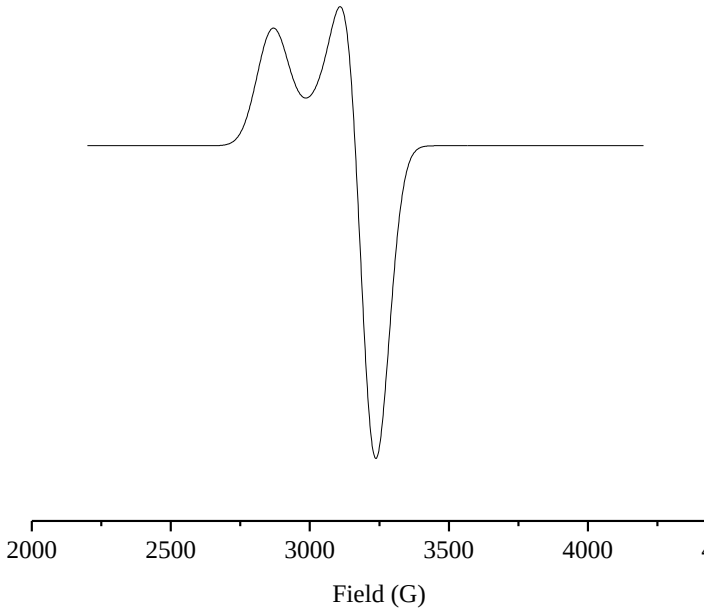

Figure 3.18 EPR spectrum of solid $Cu(NO_3)_2$. $2.5H_2O$ (used as the reactant in the reaction with TMs). More information can be found in section 1.4.4.10.

If upon the reaction of TM with Cu any peaks are observed in the EPR spectrum of the adduct, these peaks are due to reduced Mo, oxidized S or Cu(II) species. Mo has two paramagnetic oxidation states, Mo(V) and Mo (III). S(-I) is paramagnetic. Cu(I) and Cu(III) are both diamagnetic and therefore EPR inactive. Details of the EPR characteristics of these elements can be found in the sections 1.4.4.9, 1.4.4.10 and 1.4.4.11.

Several peaks are observed in the spectra of CuTM4 and CuTM3 adducts. The same peaks (same field values) are observed in all measured samples, however their intensity and the resolution changes as TM used in the sample and the amount of Cu(II) changes.

3.8.2. CuTM4 adducts

3.8.2.1. Identity of the EPR Peaks

The EPR spectrum of a CuTM4 adduct is shown in Figure 3.19.

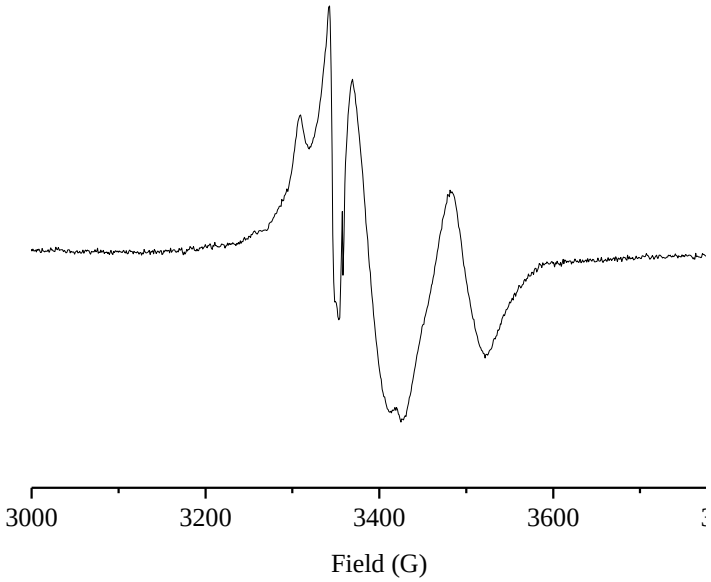

Figure 3.19 EPR spectrum of a CuTM4 solid sample (the molar reaction ratio Cu:TM4 = 1:1 prepared in SRF) taken at room temperature.

A set of three peaks is observed at B = 3275-3400 G for CuTM4 samples and another peak at approximately 3475 G. The g-factor values of all these peaks are between 1.9 - 2.1; it is difficult to decide the nature of the element in which the unpaired electron resides. Based on literature g-factor values, it could be any of the three studied elements, Mo, Cu or S (sections 1.4.4.9, 1.4.4.10 and 1.4.4.11).

When we look at the spectrum, the three peaks situated at the lower field and the peak situated at higher field value have different linewidths. Again, the range of linewidths are characteristic for all three of the elements studied here (sections 1.4.4.9, 1.4.4.10 and 1.4.4.11), so it is difficult to determine based on this the nature of the element. However, due to the differences in linewidths, it is most likely that the spectrum is composed from signals due to more than one element.

Several experiments were done to determine the nature of the peaks in the EPR spectra of CuTM samples. These include a precipitate of Zn-TM4 (no Cu used), Na-TM4 and precipitate of TM4 in absence of any other metal in buffer solution (section 2.7.1). To study the effect of the Cu compound anion on the EPR spectrum, several Cu-TM4 precipitates were also prepared using different salts of Cu(II): $CuCl_2$, $CuSO_4$ instead of $Cu(NO_3)_2$ (section 2.7.1).

A similar spectral feature to the first set of three peaks was observed in the EPR spectra of the samples Zn-TM4 and Na-TM4. It is unlikely that TM4 would have any redox effect on sodium, yet an EPR spectrum is obtained of this solid sample to produce paramagnetic species. Therefore these peaks are most likely due to an unpaired electron on or in the proximity of Mo or S. This agrees with previously reported simulations in the literature[121].

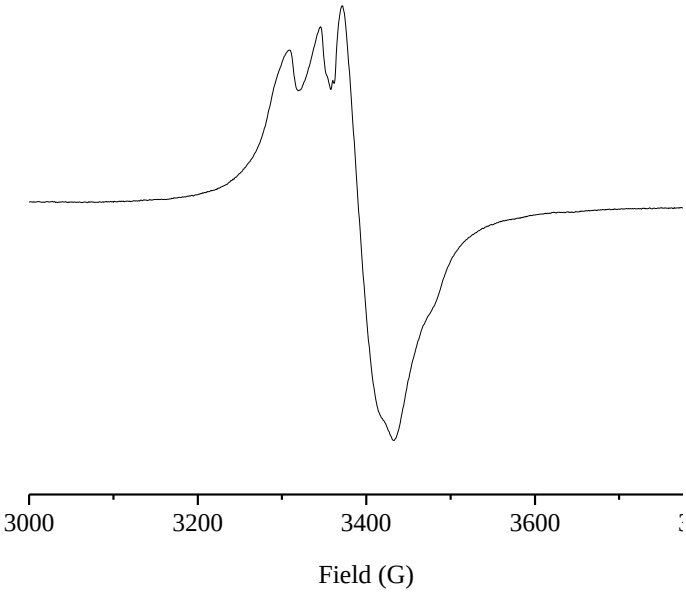

Figure 3.20 EPR spectrum of Zn-TM4 mixed at a ratio of 2:1 of Zn:TM4.

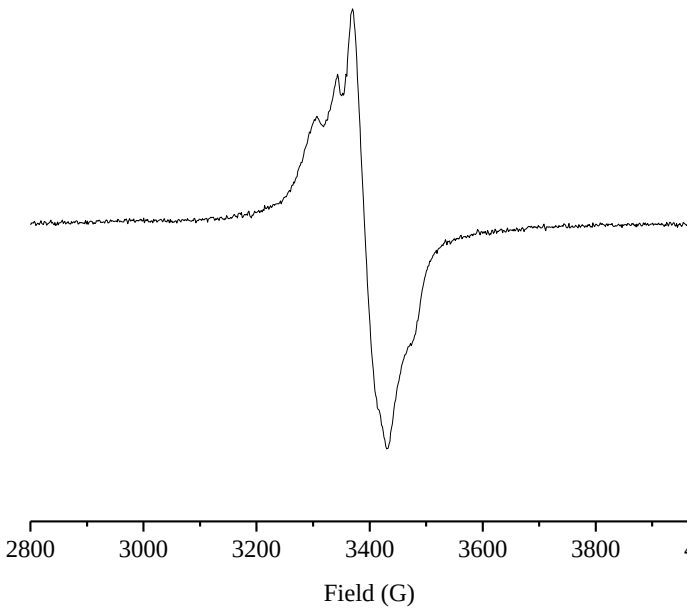

Figure 3.21 EPR spectrum of Na-TM4 precipitate.

To confirm the presence of an Mo or S paramagnetic signal rather than a signal due to any other added metal, a spectrum of TM4 precipitate in the absence of any other metal (other than Na^+) in the buffer solution was measured (Figure 3.22).

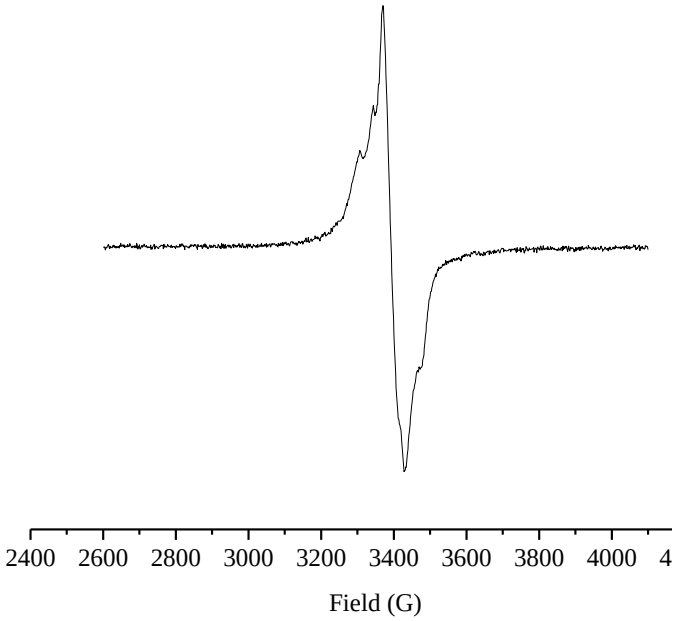

Figure 3.22 EPR spectrum of TM4 precipitate in SRF in absence of Cu.

Part of the Zn-TM4 spectrum is similar to the CuTM4 spectrum. The indication of the set of three peaks is observed at about 3300 – 3400 G, as in the EPR spectra of CuTM4. They are, however, less resolved in the TM4 sample spectrum although present at the same field value. Due to the fact that the signal-to-noise ratio is fairly small (high noise observed) in the measured spectra, it is suspected that the concentration of these paramagnetic species is low and they are present as minority species in the sample (section 4.4).

The peak at 3475 G in Figure 3.19 is only present for the samples prepared with $Cu(II)(NO_3)_2$. It is probably due to an unpaired electron in proximity to Cu, either unreacted Cu(II) species or Cu(II) species present in the complex with TM4. However,

the EPR spectrum of the reactant $Cu(NO_3)_2$ (Figure 3.18) has different features and for the CuTM4 samples, the same peak is observed regardless of the Cu(II) salt used ($Cu(NO_3)_2$, $CuCl_2$, $CuSO_4$) (Figure 3.23).

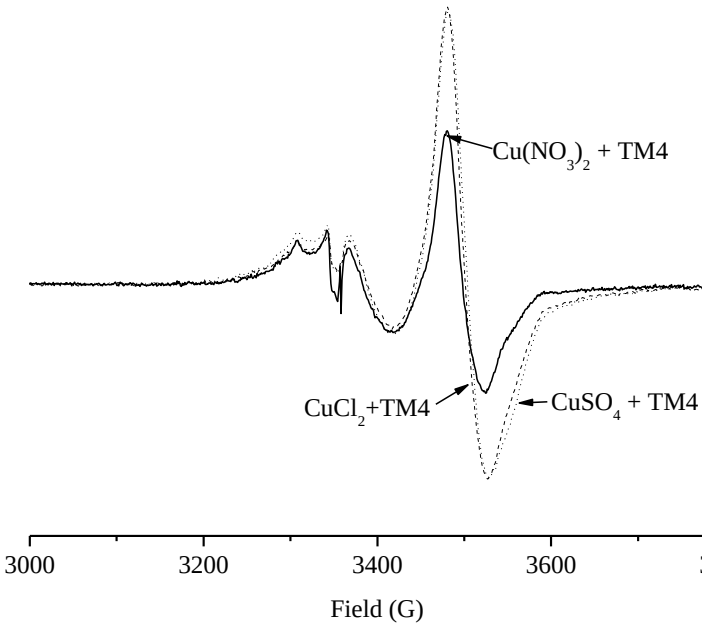

Figure 3.23 Comparison of the EPR spectra of CuTM4 samples mixed with Cu(II) from three different salts. Reactants were mixed at ratio of Cu:TM4 = 1.5:1 for all three samples studied.

The sample of precipitated Cu(II) in SRF, in absence of any TM, also shows different features (Figure 3.24).

It is noticeable that in the EPR spectrum of the Cu(II) precipitated in SRF, the level of noise is significantly higher compared to the other CuTM4 samples. This means that this signal in Cu(II) precipitate is very low. On top of it, the signal is very broad and is therefore significantly different than a peak of 3475 G in the EPR spectra of CuTM4 samples. Therefore the peak at 3475 G in the CuTM4 samples is most likely some paramagnetic Cu species present in the adduct.

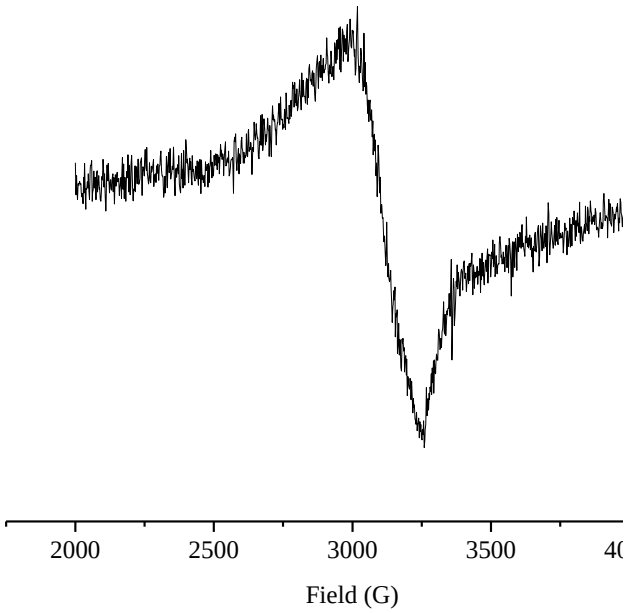

Figure 3.24 EPR spectrum of a sample of Cu(II) precipitated in SRF.

3.8.2.2. Intensity of the EPR Peaks

Several CuTM4 solid samples were prepared with a constant amount of TM4 and variable amounts of Cu(II) as reactants (section 2.7.1). The assignments of the EPR peaks of their spectra were described above. All the CuTM4 samples show peaks at the same positions. The intensity of the peaks is, however, changing with increasing Cu(II) input into the reaction mixture (Figure 3.25 and Figure 3.26). This dependence will be discussed here.

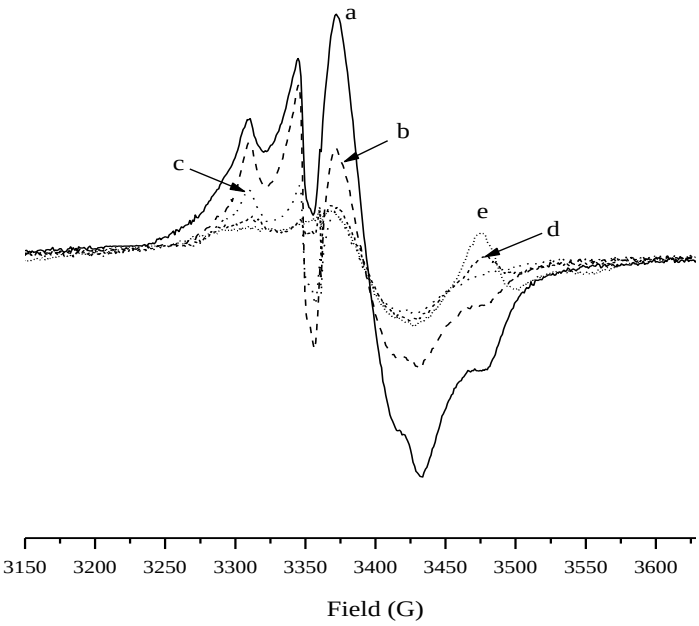

Figure 3.25 The effect of increasing amount of Cu(II) in reaction with TM4 on the EPR spectra of solid Cu-TM4 samples prepared in acetate-ammonia buffer. a. Cu:TM4 = 0.68:1 (0.5:1), b. Cu:TM4 = 1.48:1 (1:1), c. Cu:TM4 = 1.96:1 (1.3:1), d. Cu:TM4 = 2.44:1 (1.6:1), e. Cu:TM4 = 2.69:1 (1.75:1). The ratios are interpolated (Table 3.16) molar ratios for the mixed Cu(II):TM4, the ratios in the brackets are mixed molar ratios. For clarity, several spectra are omitted from the figure.

As the amount of Cu(II) mixed with TM4 is increased, the intensity of the peak at 3475 G which was attributed to Cu species is expected to increase. The intensity of this peak, however, increases in practice only up to the molar reaction ratio of Cu:TM4 = 1.75:1 (a 2.69:1 composition ratio) for the samples prepared in acetate-ammonia buffer. Beyond that point, the intensity of the peak decreases slightly.

For CuTM4 samples prepared in SRF, the maximum intensity of the Cu peak is reached at the mixed molar ratio of Cu:TM4 = 2.5:1 (composition ratio = 3.9:1). With further increase of Cu(II) in the reaction mixture, the intensity of the copper peak again decreases, and unreacted Cu(II) is also observed in the spectra.

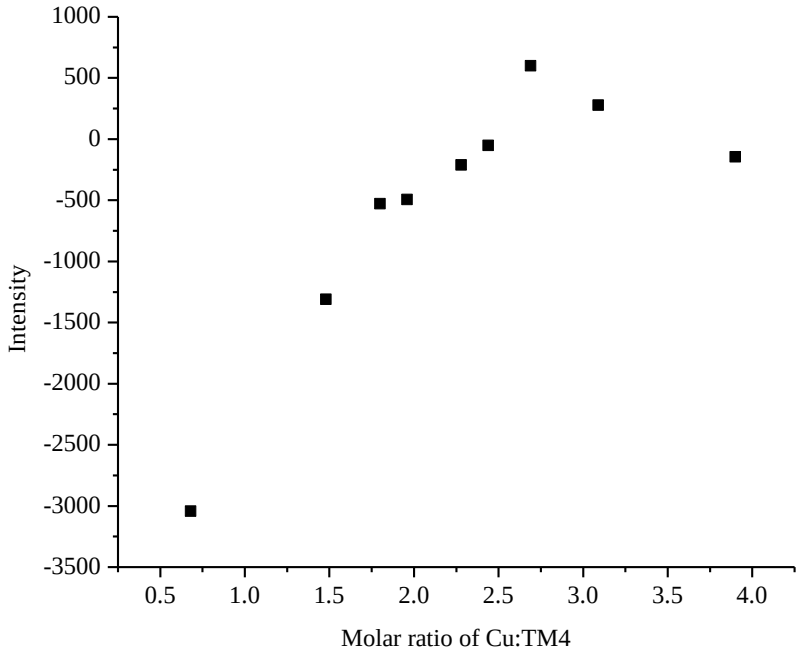

Figure 3.26 The intensity of the Cu(II) peak at 3475 G as a function of the interpolated Cu:TM4 ratio (from the results of elemental analysis).

This difference in the ratio of Cu:TM4 at which the maximum peak is obtained in two different solution media demonstrates the potential influence of the medium (environment) on the solid sample formation. In SRF, carbon and phosphate species are present, their interaction with Cu(II) was proved by elemental analysis results (section 3.5.3). These can interfere with the formation of adducts between Cu(II) and TM4 and the reduction of Cu(II) to Cu(I) to some extent, which results in the lower intensity of the paramagnetic Cu species. Partial reduction of Cu(II) to Cu(I) will be studied later by XANES of the CuTM solid samples (section 3.11.1).

The Cu peak (at 3475 G) is not observed when Cu-TM samples are prepared in pure water (unbuffered), which confirms a strong influence of the environment on the redox processes in the system. In the absence of the buffering material in solution, there is no competition for Cu(II). Therefore all the Cu can react with TM, during which

reaction this Cu(II) is completely reduced to Cu(I), and the solid sample does not have a peak at 3475 G.

Addition of His or change in temperature (38 °C) don't have any effect on the EPR spectra of CuTM in terms of new features. However, the intensity of the Cu peak changes (Figure 3.27 and Figure 3.28).

For the three studied reaction ratios (Cu:TM4 = 1:1, 1.3:1 and 1.5:1), the highest intensity of the Cu feature is observed for samples prepared at 38 °C. At this temperature, the precipitation of Cu with components of SRF is much faster, which prevents the reaction of Cu(II) with TM. Therefore, there is less reduction of Cu(II) to Cu(I). For samples prepared in the presence of His, the intensity of this peak is either the same or lower than for samples in SRF without His (Figure 3.27 and Figure 3.28). The presence of His in the reaction mixture increases the ionic strength of the solution and enhances the precipitation of polymeric TM (section 3.3). His reacts strongly with Cu(II), which then would compete with the carbonate and phosphate. This soluble Cu-His species could then react with TM, which would contribute to the reduction of Cu(II) to Cu(I) and therefore lower the Cu(II) signal. This is also supported by the previously presented results (section 3.5.5), when addition of His into the reaction mixture of Cu and TM resulted in the production of a higher mass of solid than in the absence of His.

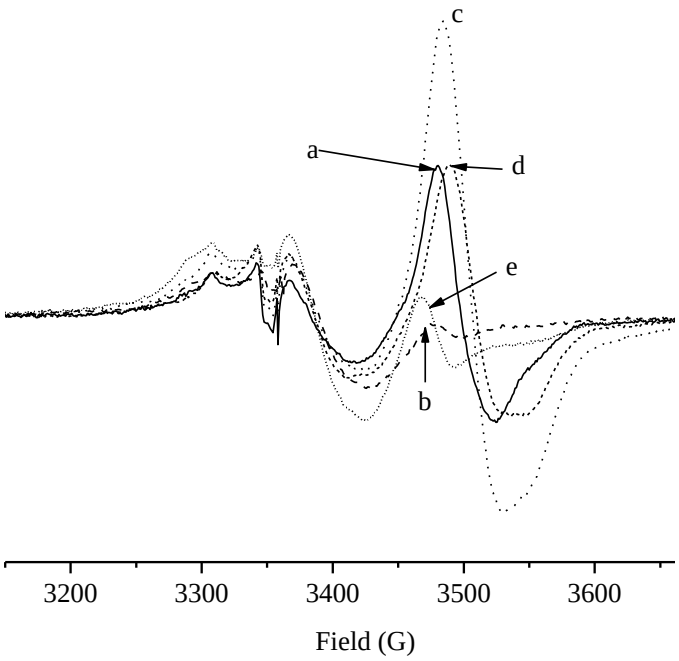

Figure 3.27 Influence of the medium on the EPR spectra of CuTM4 complex mixed at the ratio Cu:TM4 = 1.5:1. Prepared a. in SRF, at room temperature, b. in acetate-ammonia buffer at room temperature, c. in SRF at 38 °C, d. in SRF, with His, at room temperature, e. in H_2O, room temperature.

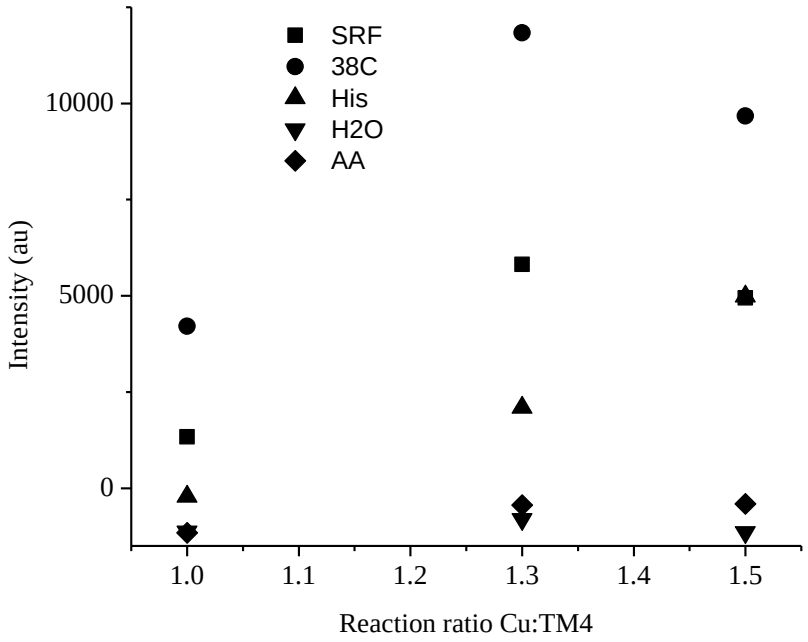

Figure 3.28 The intensity of the Cu peak of the EPR spectra of solid CuTM4 samples prepared in various media: SRF = SRF at room temperature, 38C = SRF at 38°C, His = SRF with His, room temperature, H2O = H_2O at room temperature, AA = acetate-ammonia buffer, at room temperature.

3.8.3. CuTM3 Adducts

In the EPR spectra of solid CuTM3 samples (Figure 3.29), similar peaks to those previously observed for CuTM4 are again observed, with only small differences. The three peaks corresponding to Mo or S species are resolved less and have lower intensity than in the CuTM4 species. As previously established for the TM4 case (section 3.8.2), these features belong to TM3 polymeric species as they are also present in the precipitate prepared from TM3 in buffer medium (SRF and acetate-ammonia) in the absence of any other components (Figure 3.30). The Cu peak is also present at the same field value and displays similar behavior (an increase up to a certain Cu:TM ratio, then a decrease with further increases of the Cu:TM ratio) as in the case of CuTM4.

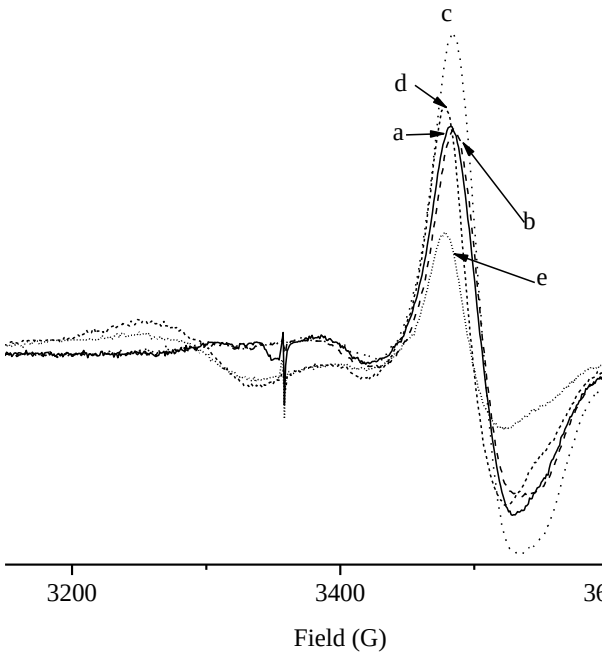

Figure 3.29 The effect of increasing amount of Cu(II) in reaction with TM3 on the EPR spectra of solid Cu-TM3 samples prepared in acetate-ammonia buffer. a. Cu:TM3 = 0.96:1 (0.5:1), b. Cu:TM3 = 1.65:1 (1:1), c. Cu:TM3 = 2.01:1 (1.2:1), d. Cu:TM3 = 2.72:1 (1.75:1), e. Cu:TM3 = 3.19:1 (2:1). The ratios are interpolated (Table 3.17) molar ratios for the mixed Cu(II):TM4, the ratios in the brackets are mixed molar ratios. For clarity, several spectra are omitted from the figure.

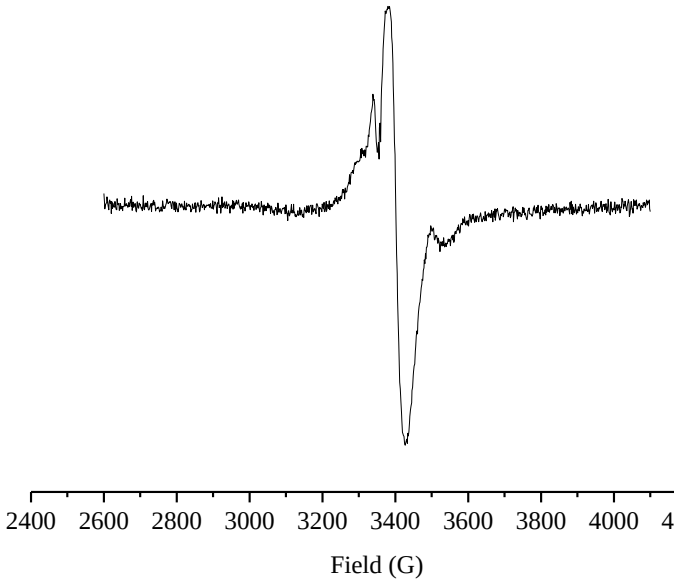

Figure 3.30 EPR spectrum of the TM3 precipitate formed in SRF.

The Cu peak reaches its maximum intensity at the molar ratio of reactants Cu:TM3 = 1.75:1 (Figure 3.29 and Figure 3.31) for the solid samples prepared in the acetate-ammonia buffer. For samples prepared in SRF, the maximum intensity was observed at Cu:TM3 = 1.2:1.

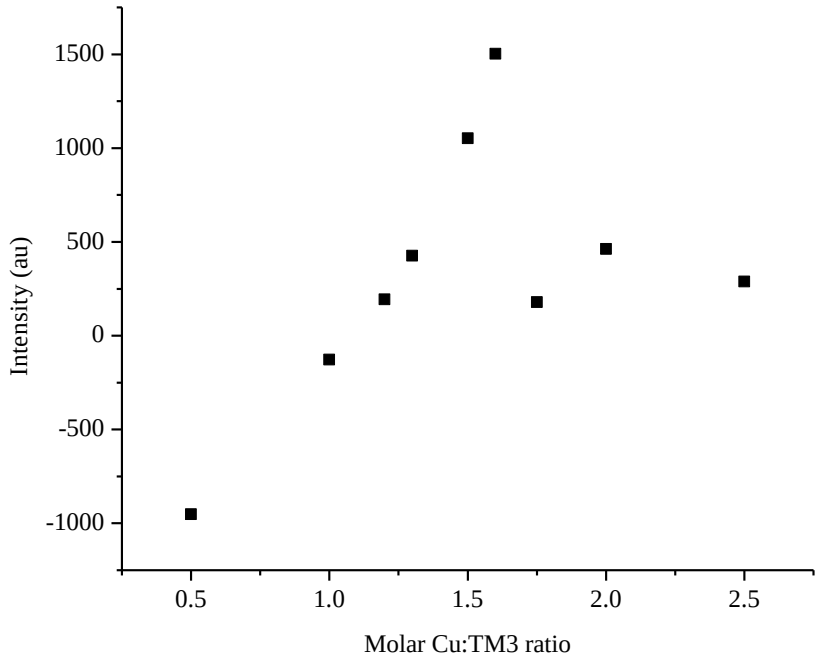

Figure 3.31 The change of the intensity of the Cu peak (~ 3478 G) of the EPR spectra of solid CuTM3 samples with the change of the Cu:TM3 reaction ratio in acetate-ammonia buffer.

The EPR spectra of CuTM3 samples prepared in various environments (Figure 3.32) show Cu features, even in water, which were not observed for CuTM4 samples. It has been suggested that sulfur atoms could be the reducing agent in the reaction of TMs with Cu.[120] TM3 has only three sulfur atoms (compared to four in TM4) available to reduce Cu(II). This could cause less Cu(II) to be reduced to Cu(I); therefore there will more Cu(II) observed in the EPR spectra of CuTM3 samples than of CuTM4 samples. This hypothesis will be further investigated by analysis of the Cu K-edge XANES spectra (section 3.11.1.2).

There are no new features observed in the samples prepared in buffer solution, in presence of His or at higher temperature (38 °C). However, the intensities of the

spectral features change, especially those characteristic of Cu. For mixed ratios of Cu:TM3 = 1:1 and 1.2:1, the highest intensity of the Cu feature is observed when the sample is prepared in SRF at room temperature, then in SRF at 38 °C, then in presence of His and in water, and the lowest for the sample prepared in acetate-ammonia buffer. For the higher ratio of reactants, Cu:TM3 = 1.6:1, the highest intensity of Cu signal is surprisingly observed for sample prepared in water, then SRF, acetate-ammonia buffer, at 38 °C in SRF and last in presence of His. This shows how complicated the Cu-TM3 system is. The reaction ratio together with the environment plays an important role in the redox processes in the system. The presence of other species can lead to formation of other Cu(II) precipitates which prevents Cu(II) reduction upon its reaction with TM (high intensity of Cu peak). The presence of Cu(II) and other oxidation state will be further studied from XANES analysis of the CuTM3 samples (section 3.11.1).

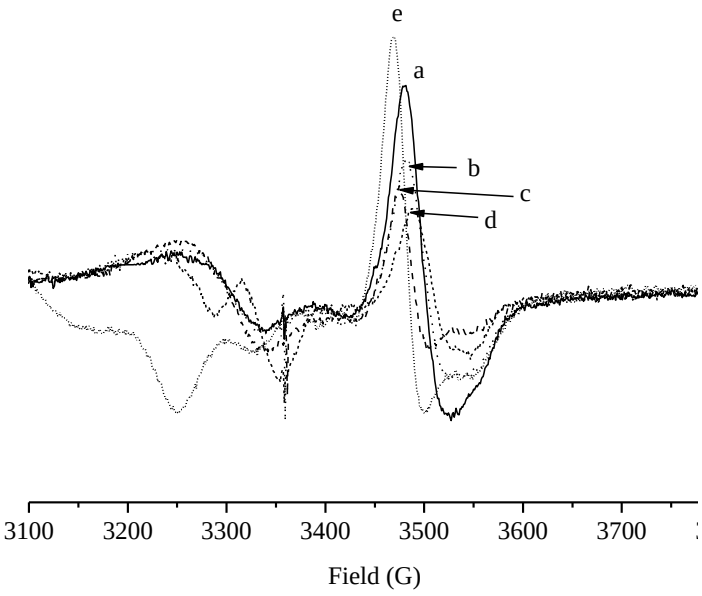

Figure 3.32 Influence of the medium on the EPR spectra of CuTM3 complex mixed at the ratio Cu:TM3 = 1.6:1. Prepared a. in SRF, at room temperature, b. in acetate-ammonia buffer at room temperature, c. in SRF at 38 °C, d. in SRF, with His, at room temperature, e. in H_2O, room temperature

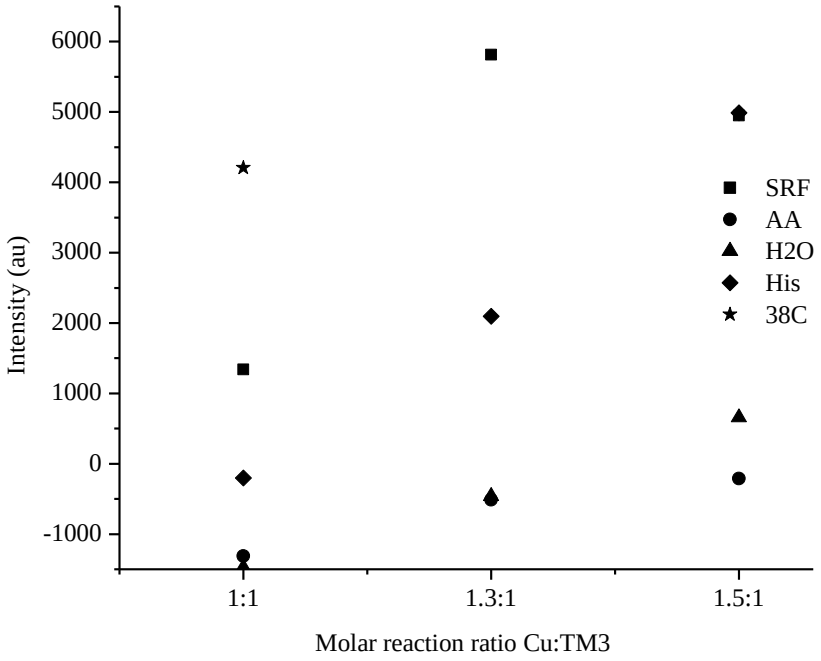

Figure 3.33 The effect of the environment on the intensity of the Cu peak (~ 3475 G) of the EPR spectra of solid CuTM3 samples in various environments: SRF = SRF at room temperature, 38C = SRF at 38°C, His = SRF with His, room temperature, H2O = H_2O at room temperature, AA = acetate-ammonia buffer, at room temperature.

The peaks in the EPR spectra of solid CuTM samples are found at g values close to 2 (2.07 – 1.85). This value can be characteristic for the EPR active species of all the three possible elements: Mo, Cu or S (section 1.4.4). Therefore based on the value of the g-factor itself, it is impossible to specify the EPR active element in the CuTM samples. Unfortunately, clear hyperfine splitting that might help specify the element was also not observed.

Several attempts to simulate the EPR spectra of solid CuTM samples were made but were not successful. The simulation parameters determined previously[120] could not be fitted to the presented spectra from this literature source nor to spectra measured in this study. Therefore, it appears that there may be errors in the reported values. The

results from the literature suggested the presence of diamagnetic Cu(I) and paramagnetic Mo(V) and S(I) species. In this research, the EPR spectra suggested the possibility of the presence of Cu(II) species in addition to other paramagnetic centers. The difficulties in simulating the EPR spectra also suggest that more than one paramagnetic center is present in solid CuTM samples, which causes the presence of overlapping signals.

3.8.4. EPR of Solutions of CuTM samples

Several attempts to measure the EPR spectra of solutions containing CuTM samples were made. However, no EPR spectra were observed for these systems in solution, either at room temperature or frozen at the temperature of liquid nitrogen. This could be caused by the fact that the solution can contain different species in terms of redox processes than the solid adduct. In solution, the first step of the reaction for CuTM system occurs which than proceeds into second step in solid phase. Therefore, the absence of paramagnetic species in solution may be the reason of absence of an EPR signal. The second step (solid phase) than produces paramagnetic species which could be detected by EPR (sections 3.8.2 and 3.8.3).

3.9. IR Spectra of Solid CuTM Samples

To determine the presence of certain groups in the solid CuTM samples, IR spectra were measured on the same samples that were prepared for EPR measurements (section 2.7.1). The spectra are presented in Figure 3.34. The IR spectra of another two samples with higher reaction ratios of Cu:TM (= 1.5:1 and 2:1) gave the same results and therefore are not shown here.

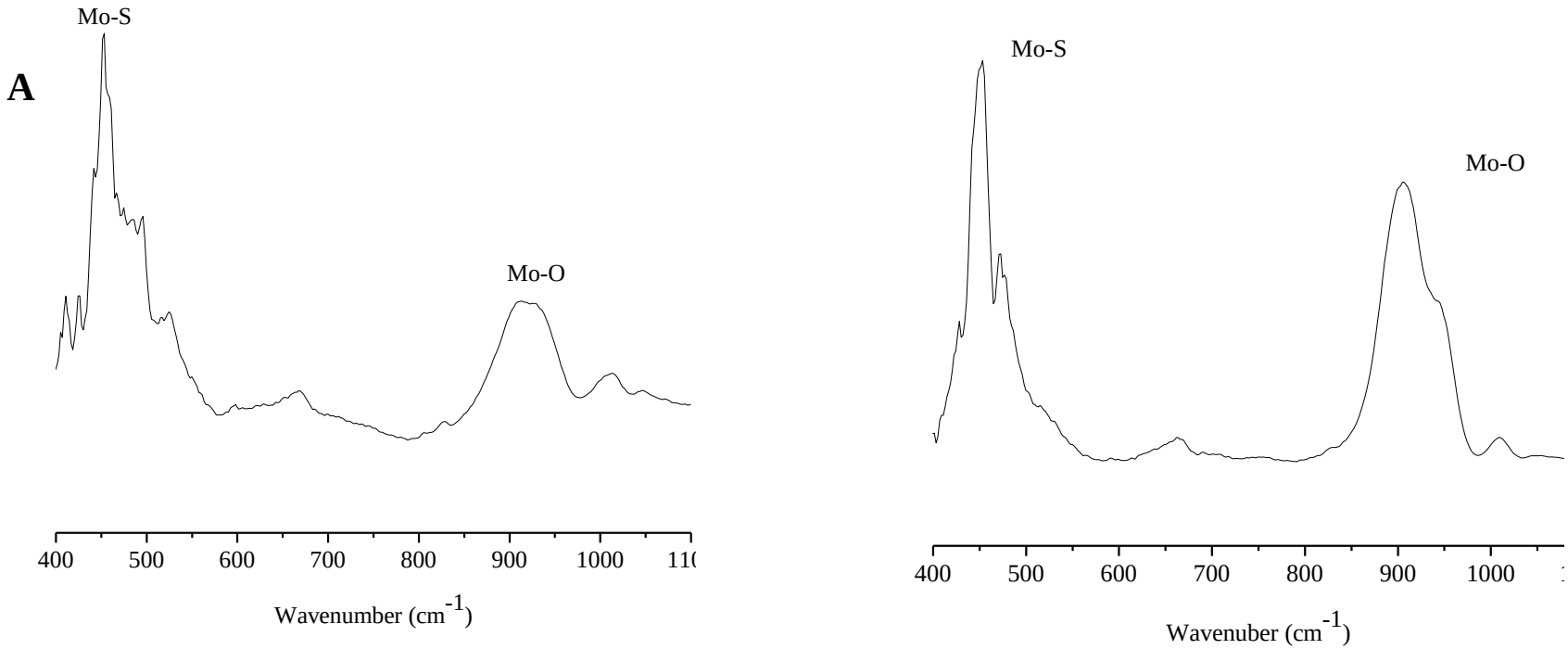

Figure 3.34 IR spectra of the solid CuTM4 (A) and CuTM3 (B) samples mixed at ratio of Cu:TM =1:1.

The IR spectra of solid CuTM samples show the presence of Mo-S groups with an intense peak at ~ 440 cm^{-1}. A lower intensity signal at ~ 900 cm^{-1} is caused by the presence of the Mo-O groups in the samples. This isn't surprising for the CuTM3 sample, since TM3 as a starting material already contained Mo-O. However, in the CuTM4 sample, the presence of this feature in its IR spectrum could mean possible hydrolysis of the TM4 during its reaction with Cu.

Because the intensity of this feature is lower in CuTM4 than CuTM3 it is most likely that TM3 also undergoes hydrolysis during its reaction with Cu. In the CuTM3 sample, the fact that the intensities of Mo-O and Mo-S peaks are comparable supports the hypothesis of the TM3 hydrolysis, which would result in Mo being surrounded by two sulfur atoms and two oxygen atoms in the CuTM3 solid. In the IR spectrum of the CuTM4 sample (Figure 3.34A), the ratio of peak intensities of Mo-O vs. Mo-S is approximately 3:1. This suggests that Mo is surrounded by three S atoms and one O atom which is the same as TM3 environment. In the IR spectrum of CuTM3 sample (Figure 3.34B), it is observed that the relative ratio of the two peaks is different than in spectrum of CuTM4. Here, this ratio is approximately 1:1. Therefore, the number of S and O atoms around Mo is the same, where CuTM3 contains TM2-like entities. These findings will be further studied by EXAFS (section 3.11.2).

The presence of Mo-O groups and their coordination number will be studied further by EXAFS of the solid CuTM samples (section 3.11.2).

3.10. XAS of TM samples

3.10.1. XANES

All four TMs (TM1-TM4) were measured at the Mo K-edge. Observation of the near-edge spectra (Figure 3.35) provided the geometry and the nearest neighbor identity of the Mo central atom. The similarities in the spectra, mainly the characteristic pre-edge feature at about 20008 eV, confirm the tetrahedral environment around the Mo in all four TMs. This was previously attributed to the 1s → 4d transition (section 1.4.5.7). The intensity of this transition for the four studied TMs is the highest for TM1 and decreases with the increasing amount of S. This agrees with previous observation of this pre-edge feature being more intense for Mo=O groups than Mo=S groups.[87,88,90,104,156]

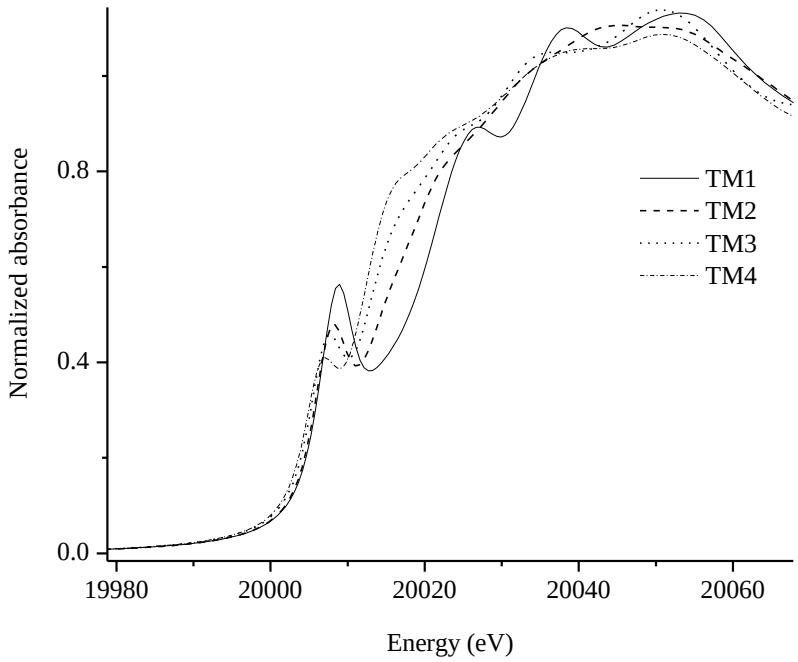

Figure 3.35 Near-edge spectra of the thiomolybdate samples.

3.10.2. EXAFS

Fitting of the EXAFS data (section 2.10.3) using EXAFSPAK software for all the measured TM samples provided the bond lengths and the identity of the neighboring atoms.

The EXAFS spectrum and the Fourier Transform of the TM1 sample are shown in Figure 3.36. Several peaks corresponding to various groups are noticeable in the Fourier transform. The strongest peak is found at the distance of around 1.5 Å. Another of much weaker intensity is observed at slightly longer interatomic distance of around 2 Å. In the sample of solid TM1, there are 3 atoms of oxygen and one atom of sulfur surrounding central atom of molybdenum. Because these are bonding groups, the strongest peaks are most likely due to Mo-O and Mo-S groups.

There are also other peaks of lower intensity found in the Fourier transform spectra. These are observed at longer distances than the previous ones. There are peaks observed at around 3 - 4 Å and another weak one at around 5 Å. These peaks correspond to atoms situated further from the Mo atom (compared to three oxygens and one sulfur); the furthest peak might represent a either multiple scattering effect of a backscatterer or long-range scattering.

A satisfactory fit (Figure 3.36) of the EXAFS spectrum of TM1 was obtained including single scattering along three Mo-O of 1.747 Å and one Mo-S groups at 2.257 Å.

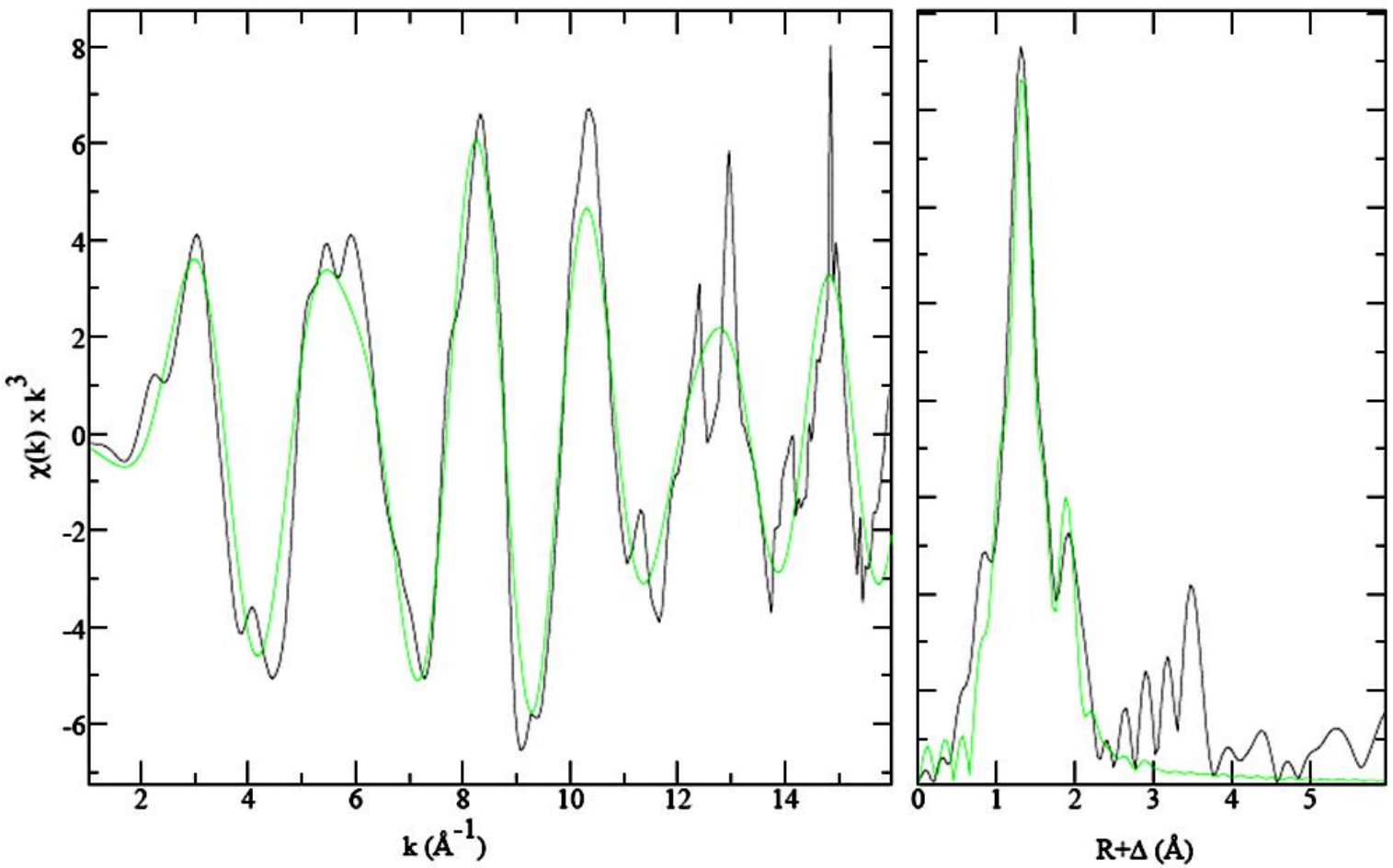

Figure 3.36 EXAFS spectrum of TM1. Darker trace is the measured spectrum, lighter is the fit.

The EXAFS spectrum and its Fourier transform of the solid TM2 sample reveals two peaks of strong intensity at about 1.2 and around 2 Å, the latter being the strongest one of the spectrum. These two peaks most likely correspond to two oxygen and two sulfur atoms, as these are surrounding the central atom of molybdenum. The intensities of these peaks are different than in the spectrum of TM1 sample. The relative intensity of the first peak is lower than second peak in the sample of TM2 (opposite for sample of TM1) which means than there are more sulfur atoms than in TM1. This agrees with the structure of TM2 which contains one more sulfur and one less oxygen atom than TM1.

There are other peaks in the Fourier Transform of TM2 observed at around 3 Å and around 4.5 Å which are of much lower intensity than the first ones (S and O). These peaks correspond to the backscatterers situated at longer distances from the central Mo (absorber) or to the multiple scattering effect, similarly to the peaks in FT of TM1.

A satisfactory fit of the EXAFS of TM2 (Figure 3.37) was obtained with single scattering along two Mo-O groups at 1.769 Å and two Mo-S groups at 2.195 Å.

In the spectra and Fourier Transform of the TM3 sample, there is a very strong peak found at about 2 Å and a weak one at shorter distance of about 1 Å. As in the two previous samples (TM1 and TM2), these are most likely due to the S and O atoms neighboring the central Mo atom. The relative intensity of the first peak (1 Å) compared to the intense peak is lower than in previous two samples and therefore this peak is attributed to the oxygen atom as backscatterer. This agrees with the structure of TM3 which contains less oxygen atoms (only one compared to two in TM2 and three in TM1) and therefore more sulfur atoms (three compared to two in TM2 and one in TM1). The strong peak around 2 Å is therefore most likely the sulfur backscatterer.

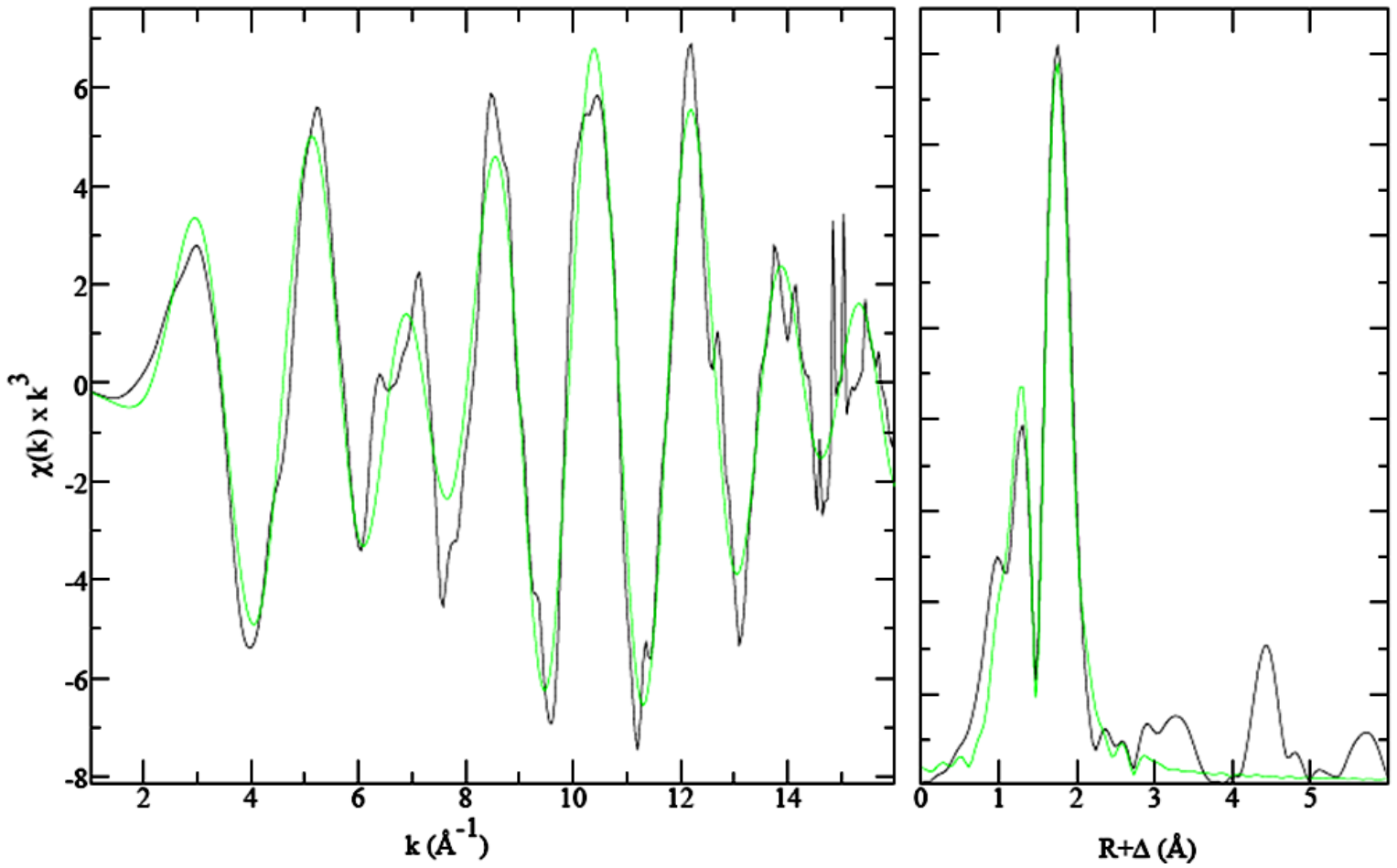

Figure 3.37 EXAFS spectrum of TM2. Darker trace is the measured spectrum, lighter is the fit.

There are two other peaks of lower intensity in the Fourier transform of TM3 below 4 Å and above 4 Å. These correspond to the backscatterers at longer distance from central Mo atom (absorber) or also could represent the multiple scattering effect in the TM3 solid.

The EXAFS spectrum was satisfactorily fitted with single scattering contribution along one Mo-O group of the distance of 1.740 Å and three Mo-S groups at distance of 2.204 Å.

The Fourier transformation of the EXAFS spectrum of the solid TM4 sample shows one peak of a very strong intensity at about 2 Å. If we compare this to the three previous samples this would correspond to the sulfur backscatterer in the proximity of central Mo atom. This agrees with the structure of the TM4 which has four sulfur atoms in the first coordination shell. There are no other peaks of significant intensity found in the TM4 spectrum.

The EXAFS spectrum of the TM4 solid sample was fitted with single scattering of only one component, Mo-S group. A satisfactory fit of the spectrum was obtained with four Mo-S components of the same distance of 2.190 Å.

All four TMs were closely fitted including only single scattering components and only the closest neighbors to the central absorbing Mo atom. The results of the fitting of all four TMs are summarized in Table 3.20. The values are comparable to those from literature (last column of the Table 3.20).

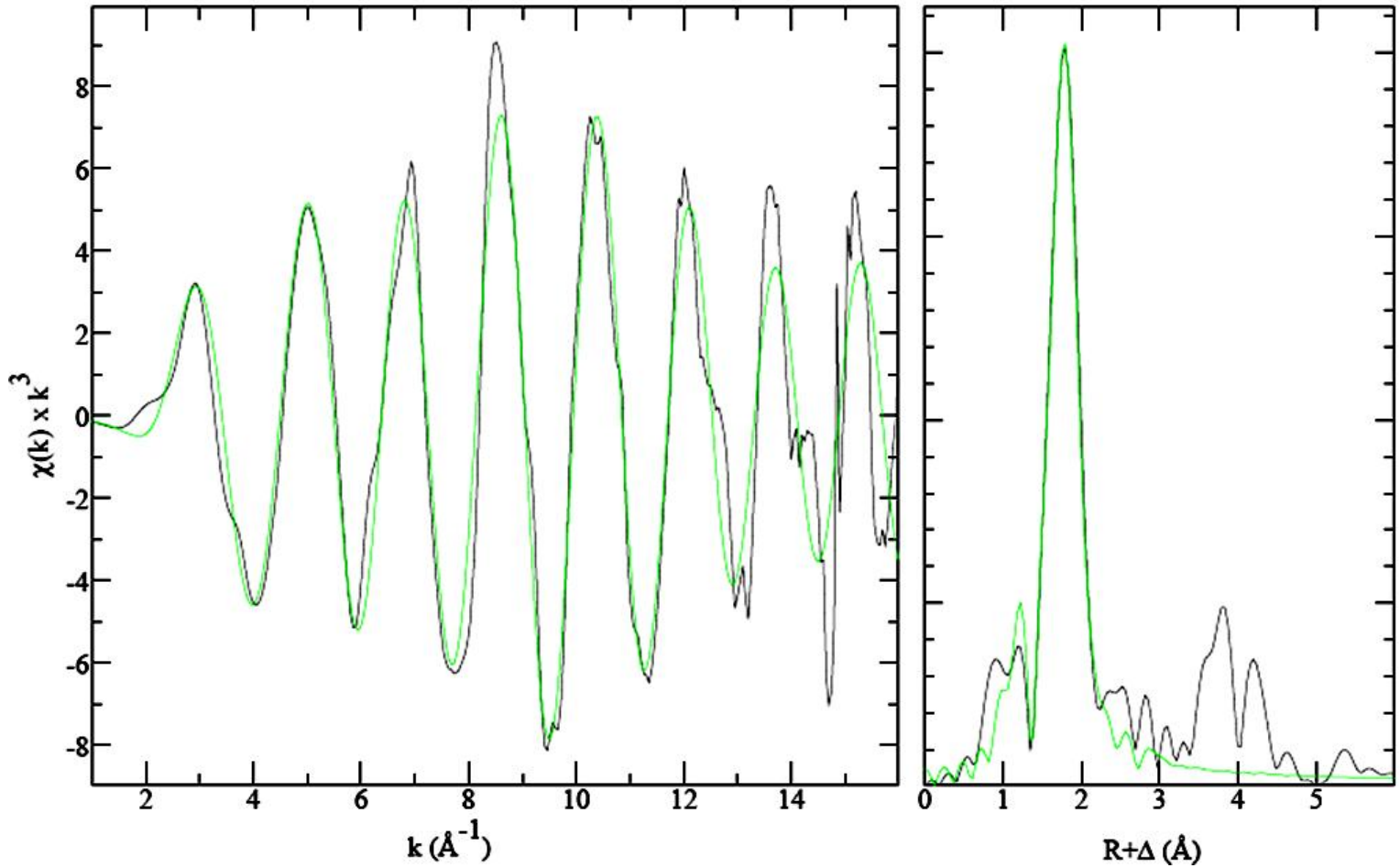

Figure 3.38 EXAFS spectrum of TM3. Darker trace is the measured spectrum, lighter is the fit.

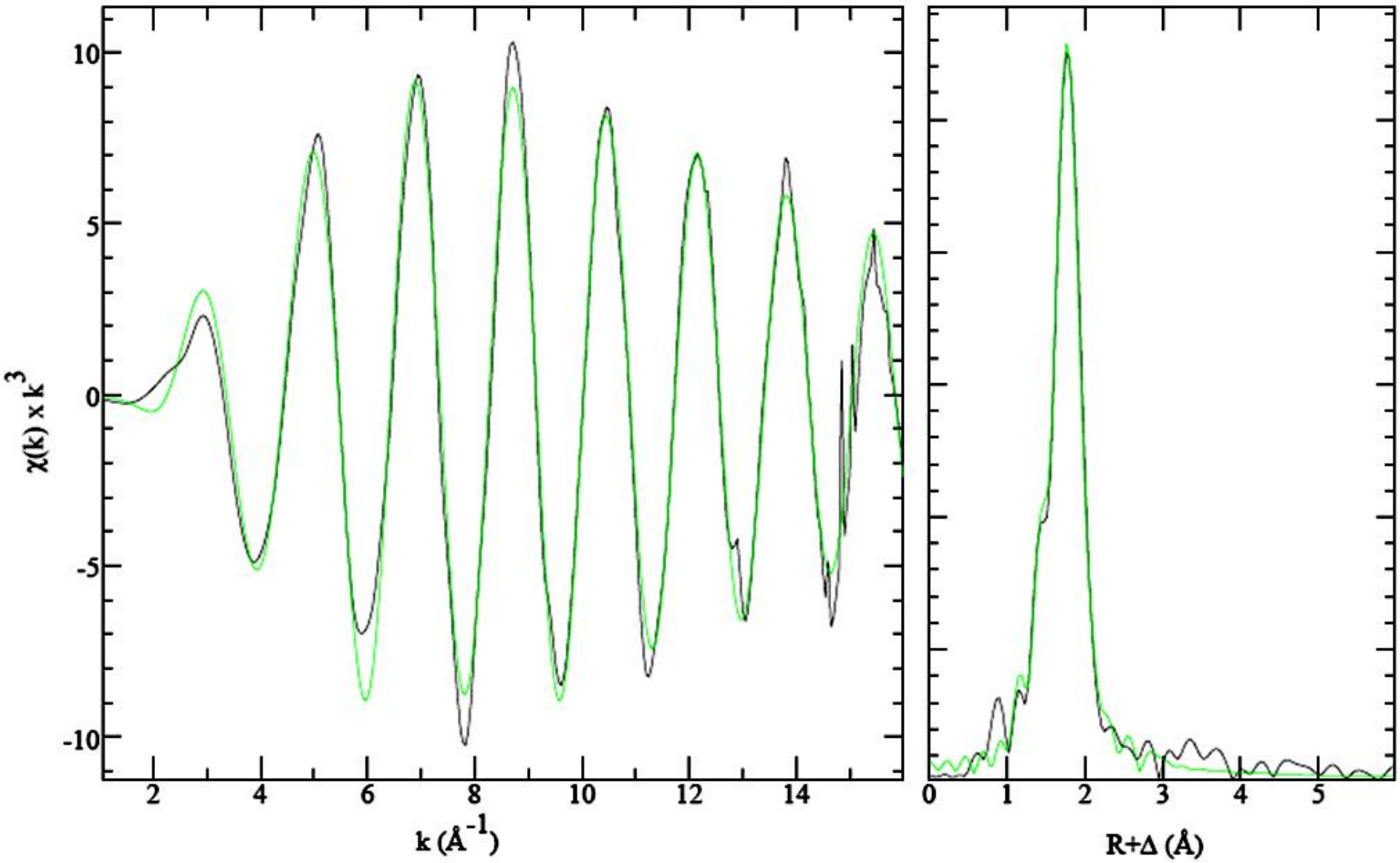

Figure 3.39 EXAFS spectrum of TM4. Darker trace is the measured spectrum, lighter is the fit.

Sample	*Bond*	*CN*	*Bond length (Å)*	σ^2	*Average bond length (Å)*
TM1	Mo-O	3	1.747 (2)	0.0020 (1)	1.758[157]
	Mo-S	1	2.255 (4)	0.0026 (3)	2.2427[157]
TM2	Mo-O	2	1.769 (2)	0.0020 (2)	1.7802[157], 1.758[106]
	Mo-S	2	2.194 (2)	0.00148 (9)	2.1897[157], 2.188[106]
TM3	Mo-O	1	1.739 (5)	0.0022 (5)	1.736[157]
	Mo-S	3	2.204 (2)	0.0020 (1)	2.164[157]
TM4	Mo-S	4	2.190 (1)	0.00191 (4)	2.1816[157], 2.18[108]

Table 3.20 Distances found by the fitting of the measured powder spectra of TMs. The last column contains average bond lengths found previously. (CN = coordination number)

3.11. EXAFS and XANES of CuTM solid samples

3.11.1. XANES: CuTM4 and CuTM3

3.11.1.1. Mo K-edge

The edge position of the CuTM4 sample mixed at a ratio of Cu:TM4 = 1:1 (Figure 3.40), when comparing to the TM4 spectrum, doesn't change. The difference in the position of the edge between different oxidation states is, however, so small that this doesn't mean that there is no change in the oxidation state of Mo. The EPR results on these samples showed the possibility of the Mo being reduced for Mo^{6+} to Mo^{5+} and this would only provide a shift of the edge of about 1-3 eV[103] which might not be easily

seen on an EXAFS spectrum. As the pre-edge feature at about 20008 eV visible in the pre-edge of TM4 is not observed in the pre-edge spectra of CuTM sample, there is most likely no Mo=O or Mo=S double bond (section 1.4.4.9).

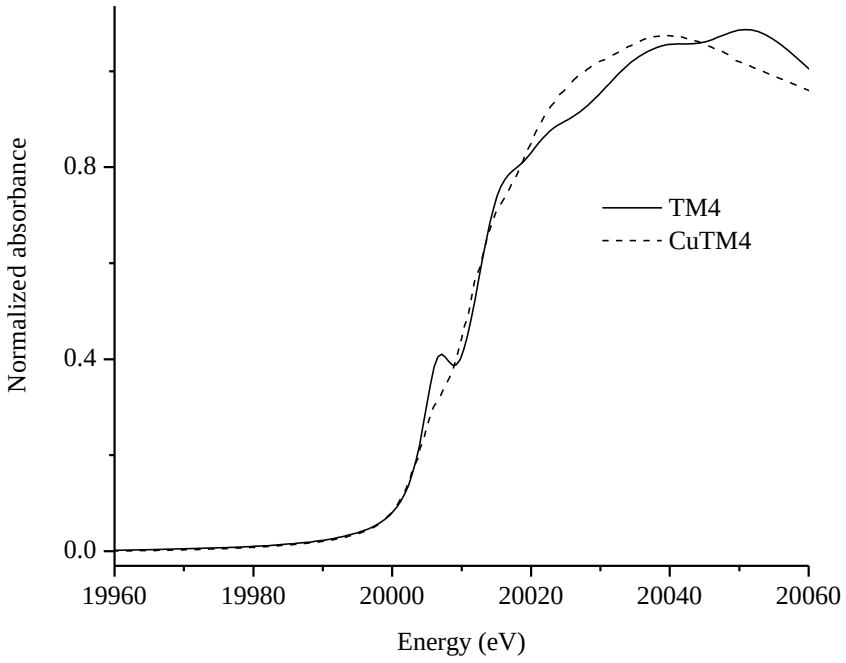

Figure 3.40 Comparison of the near edge spectra of TM4 and CuTM4 (mixed at ratio Cu:TM4 = 1:1)

For the CuTM3 sample (Figure 3.41), similar observations were made. The near-edge region of the CuTM3 spectrum is very similar to that of TM3 and the intensity of the pre-edge feature decreases.

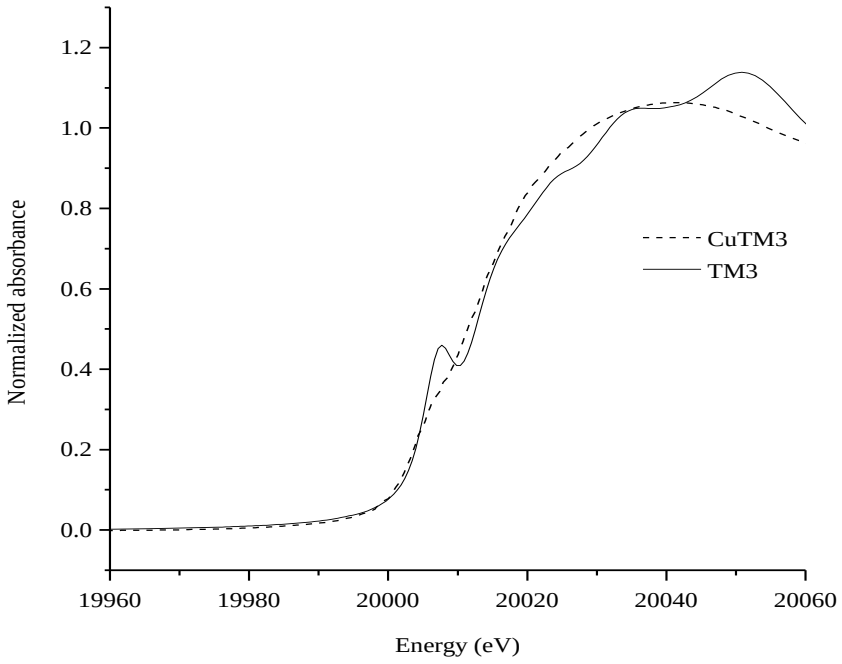

Figure 3.41 Comparison of the near edge spectra of TM3 and CuTM3 (mixed at ratio Cu:TM3 = 1:1)

In both cases, CuTM4 and CuTM3 lack the pre-edge peak in their spectra which is visible in the near-edge spectra of pure TM4 and TM3, respectively. This peak is caused by the presence of Mo=O or Mo=S groups. The absence of this peak means the absence of the double bond between these elements in the final CuTM adducts.

There is a negligible difference of the near edge position between the spectra of the samples of CuTM4 and CuTM3 (Figure 3.42) when the ratio (mixed) of Cu:TM = 1:1. The great similarity of the near edge is due to the formation of very similar adducts with Cu for both studied TMs. The small difference could be only caused by slightly different S and O amounts in these samples. The similar intensities of the pre-edge feature suggest very similar oxidation state and geometry around the Mo atom.

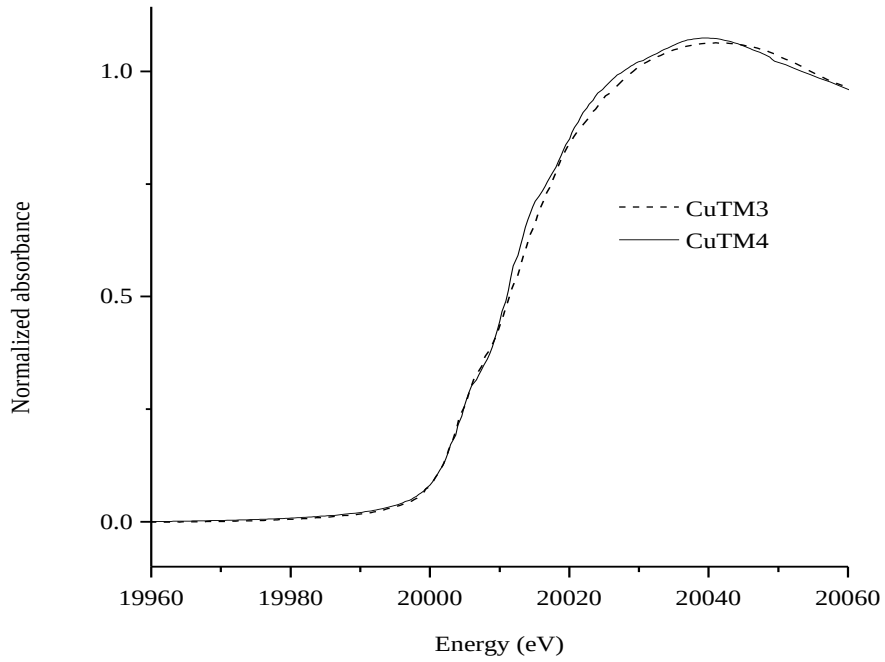

Figure 3.42 Near-edge spectra (Mo edge) of the samples of CuTM4 and CuTM3, both prepared with the reaction ratio of Cu:TM = 1:1.

3.11.1.2. Cu K-edge

Figure 3.43 shows the near-edge spectra of two Cu samples: CuCl containing Cu(I) and $CuSO_4$ containing Cu(II) to illustrate the strong dependence of the position of the Cu K-edge on the oxidation state of Cu.

The exact edge position was found from the first derivative of the spectrum: 8982 eV for CuCl and 8987eV for $CuSO_4$. The difference between oxidation states 1+ and 2+ can be more than 8 eV[95-97,99], with the higher oxidation state being at higher energy.

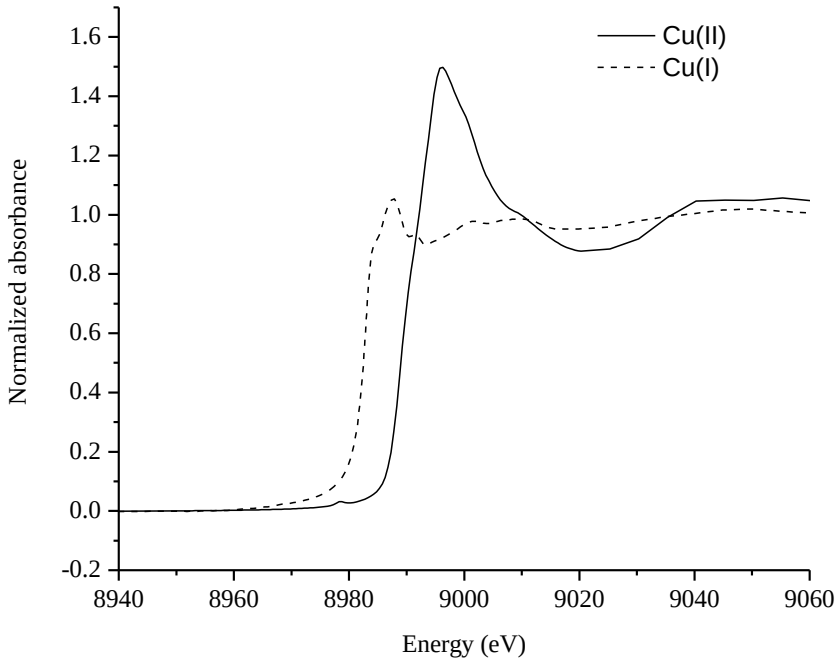

Figure 3.43 Characteristic near-edge spectra of Cu(I) (CuCl) and Cu(II) ($CuSO_4$).

Figure 3.44 shows the position of the Cu edge of the CuTM4 sample with respect to the Cu(I) and Cu(II) edges discussed above. The figure shows that the edge of the CuTM4 sample is situated in between the two edges of the reference samples. This indicates a possibility of the presence of the two oxidation states in the prepared CuTM4 sample. Eccleston[120] reported that Cu(II) is completely reduced to Cu(I) upon its reaction with TMs to form solid CuTM4 but the EPR results already presented above (section 3.8) showed the possible presence of Cu(II).

To confirm the hypotheses of coexistence of Cu in two different oxidation states in the same sample of CuTM, the near –edge spectra of the six studied CuTM compounds were fitted with the two near-edge spectra of the standard samples (CuCl, $CuSO_4$) (Figure 3.44).

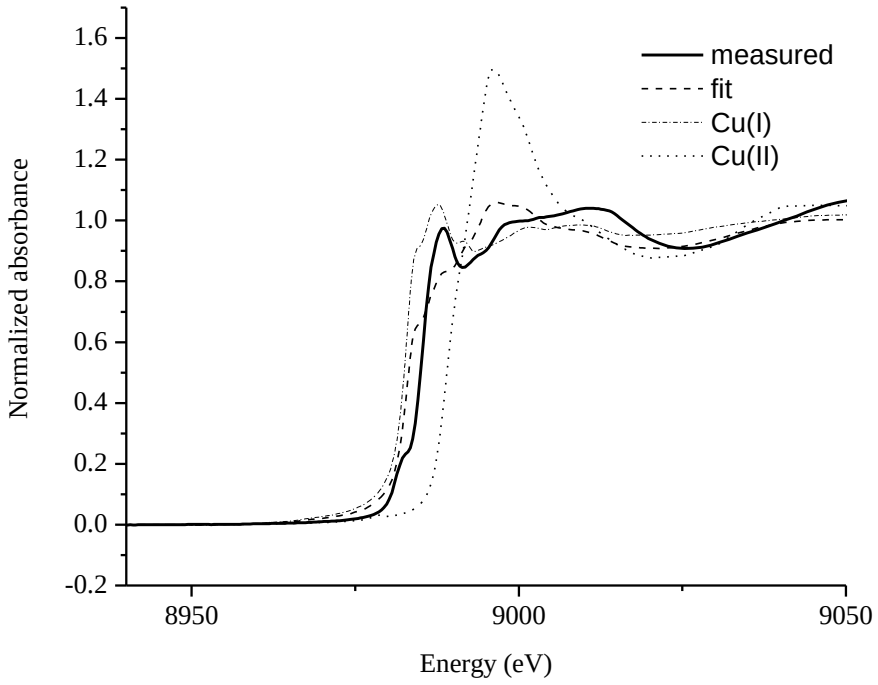

Figure 3.44 Fitting of near-edge spectrum of the CuTM4 sample mixed at ratio Cu:TM4=1:1 with near-edge spectra of Cu(I) and Cu(II).

The linear combination fitting with spectra of two reference samples, Cu(II) and Cu(I) provided the fractions of the copper in two oxidation states present in the CuTM samples (Table 3.21).

The fit of Cu(I) and Cu(II) compounds into the XANES spectra of CuTM samples is not perfect mainly because CuCl and $CuSO_4$ were used as the reference samples. The surrounding atoms, as well as the geometry, in these standards are obviously different.

Mixed	*Cu(I)*	*99 % CL*	*Cu(II)*	*99 % CL*	*Total*	*Residual*
Cu:TM4 =1:1 in SRF	0.70	0.02	0.27	0.02	0.98	0.004
In acetate-ammonia buffer	0.70	0.02	0.27	0.02	0.98	0.004
Cu:TM4 =1.5:1 in SRF	0.73	0.01	0.25	0.01	0.98	0.003
Cu:TM4 = 2:1 in SRF	0.75	0.01	0.23	0.01	0.98	0.002
In acetate-ammonia buffer	0.73	0.01	0.25	0.01	0.98	0.002
Cu:TM3 = 1:1 in SRF	0.76	0.01	0.22	0.01	0.98	0.002
Cu:TM3=1.5:1 in SRF	0.778	0.009	0.206	0.008	0.984	0.001
Cu:TM3 = 1.6:1 in SRF	0.773	0.008	0.208	0.008	0.982	0.001
Cu:TM3 = 2:1 in SRF	0.781	0.008	0.203	0.009	0.984	0.001
In acetate-ammonia buffer	0.765	0.007	0.219	0.007	0.984	0.001

Table 3.21 Fractions of Cu(I) and Cu(II) present in the CuTM4 and CuTM3 samples as obtained by LCA in EXAFSPAK.

LCA (section 1.4.5.2) using the EXAFSPAK program showed the presence of both main oxidation states of Cu: Cu(I) and Cu(II). The exact fractions are reported in Table 3.21, together with the 99 % confidence limits as calculated by the software. The total fraction (sum of the fractions of all the components) should be 1 since there are only two components present and both are fitted into the measured spectrum. The deviation of the total fraction from unity is most likely because the standard samples used in the fitting are somewhat different in terms of the geometry and the closest neighbors compared to the measured spectrum of CuTM. The minor deviation from a total fraction of unity can be observed in cases when all the spectra are not normalized the same way. The residual represents the mean sum of squares of the differences between the observed and calculated intensities and the smaller this number is, the better fit is obtained. This is only measure of precision, but not accuracy and therefore can’t be used to estimate the goodness of data.

For samples prepared at a reaction ratio of Cu:TM4 = 1:1, the ratio of Cu(I)/Cu(II) is the same whether the sample was prepared in SRF or in acetate-ammonia buffer (Table 3.21). However, when the reaction ratio of Cu:TM is increased (for CuTM4 and CuTM3), the ratio of Cu(I)/Cu(II) in the final adduct is larger when samples are prepared in SRF than when samples are prepared in acetate-ammonia buffer. This might be due to the interaction of the reactants with the components of the buffer media, as was shown in section 3.5.3. This also agrees with the results of the EPR analysis, where the Cu peaks was of higher intensity for samples prepared in SRF compared to those prepared in acetate-ammonia buffer (section 3.8). Without the presence of carbonate and phosphate (acetate – ammonia buffer), more Cu is available to react with TM as it doesn't precipitate as Cu(II) – carbonate or Cu(II) – phosphate, and therefore more Cu(II) is reduced to Cu(I) in acetate-ammonia buffer than in SRF.

3.11.1.3. S K-edge XANES

A sample of CuTM4 mixed at a ratio of 1:1 (Cu:TM4) was measured at the S K-edge by Dr. Graham George at SSRL (Figure 3.45).

The position of the edge was found to be 2473 eV which by comparison with data from the literature is characteristic of the oxidation state of – I (section 1.4.5.8).

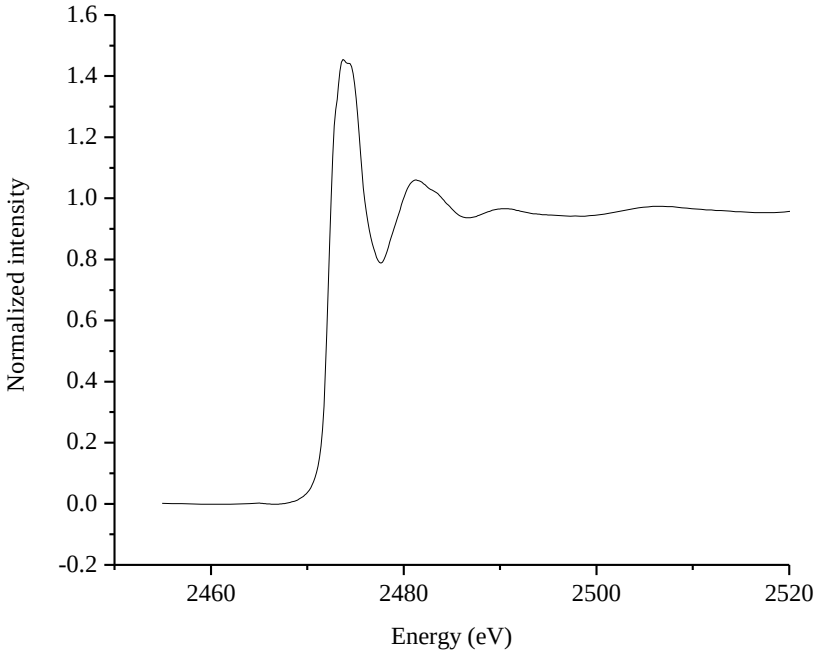

Figure 3.45 S K-edge spectrum of the CuTM4 sample prepared at ratio of Cu:TM4 = 1:1.

3.11.2. EXAFS: CuTM4 and CuTM3

3.11.2.1. Mo K-edge EXAFS spectra fitting

The EXAFS spectra of the solid CuTM samples (preparation outlined in section 2.10.1) were collected to a high k-value, usually to k = 20 $Å^{-1}$. As measuring the spectra to such high k value gives a better resolution of the peaks, more peaks are present in the Fourier Transform. An attempt was made to fit these spectra (Figure 3.46). However, EXAFSPAK wouldn't fit the spectra in such detail. In the measured spectra there is an indication of two sulfur atoms at slightly different distances from central Mo atom, as observed by the two peaks around value of approximately 1.8 Å (Figure 3.46). The EXAFSPAK wasn't able to fit these separately as two peaks most likely due to their proximity.

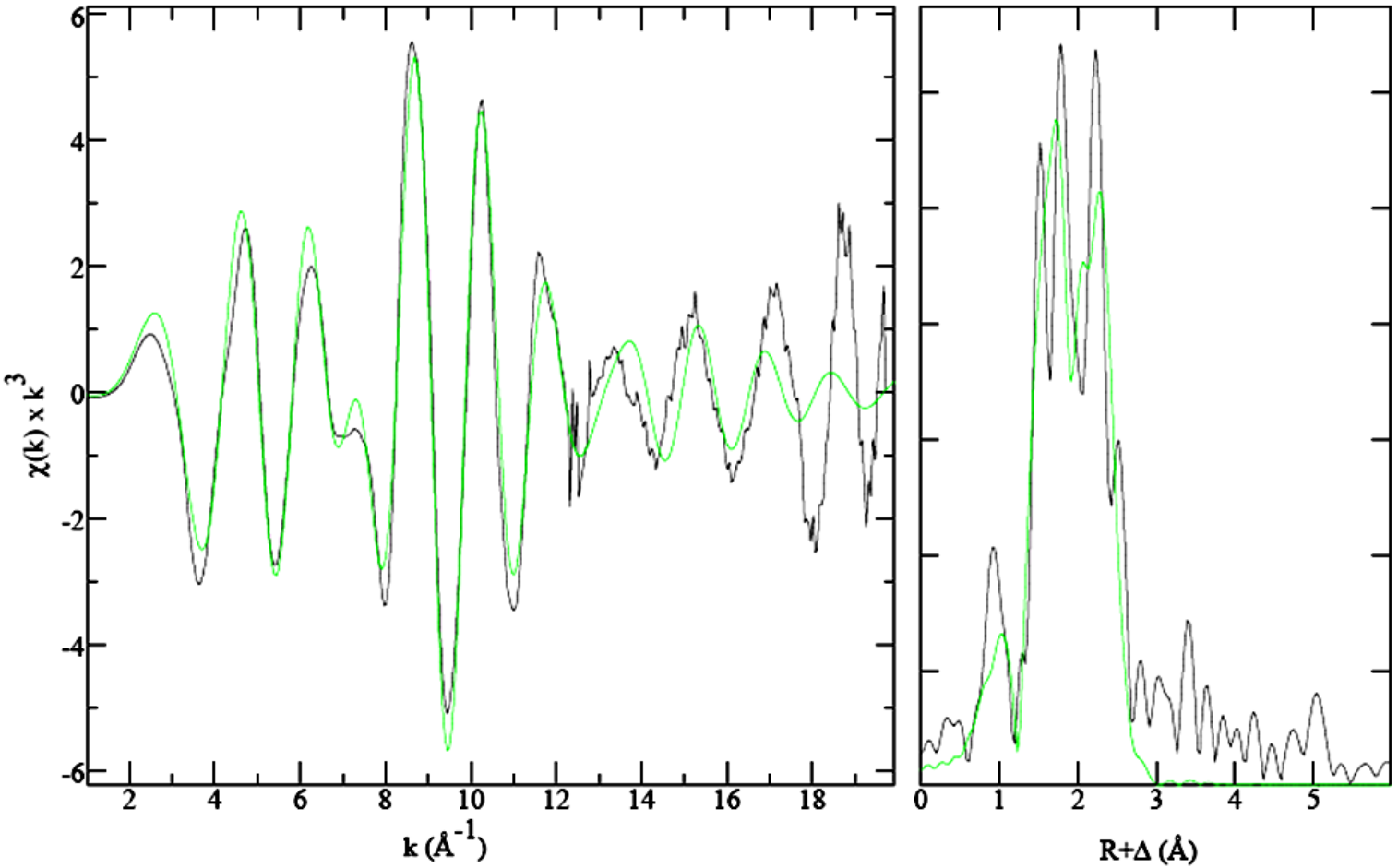

Figure 3.46 Best fit of the EXAFS spectrum of CuTM4 sample with reaction ratio of Cu:TM4 = 1:1. The spectrum was measured up to k = 20 $Å^{-1}$. The darker line is measured spectrum, the lighter line is fitted spectrum.

Therefore, the measured spectra of the solid CuTM samples, were only handled up to k = 16 to simplify the fitting process (Figure 3.47). The fitting of these spectra provided the same results as the original full range spectra for the best obtained fit.

For the sample of CuTM4 prepared at the reaction ratio of Cu:TM4 = 1:1, the best fit of its EXAFS spectrum was obtained with Mo being 3-coordinated surrounded by an atom of oxygen and two atoms of sulfur (Table 3.22).

Bond	*Coordination number*	*Bond length (Å)*	σ^2
Mo-S	2	2.203 (2)	0.0044 (1)
Mo-O	1	1.670 (5)	0.0069 (6)
Mo-Cu	3	2.673 (3)	0.0085 (2)

Table 3.22 The results of the best fit of the CuTM4 (Cu:TM4 reaction ratio = 1:1) sample at Mo K-edge fitted up to k = 16 $Å^{-1}$.

Although Eccleston suggested 3-coordinated Mo in the CuTM samples previously[120], there is no well characterized compound containing such Mo environment in the literature. Addition of a second oxygen atom into the fit of the EXAFS spectrum didn't have any significant influence on the apparent quality of this fit (Figure 3.48) However, this addition of second oxygen increased the value of σ^2 to quite a high value (Table 3.23).

The spectrum was also fitted by considering the Mo atom surrounded by one oxygen atom and three sulfur atoms (Figure 3.49, Table 3.24). This fit was not significantly worse than the previous two fits.

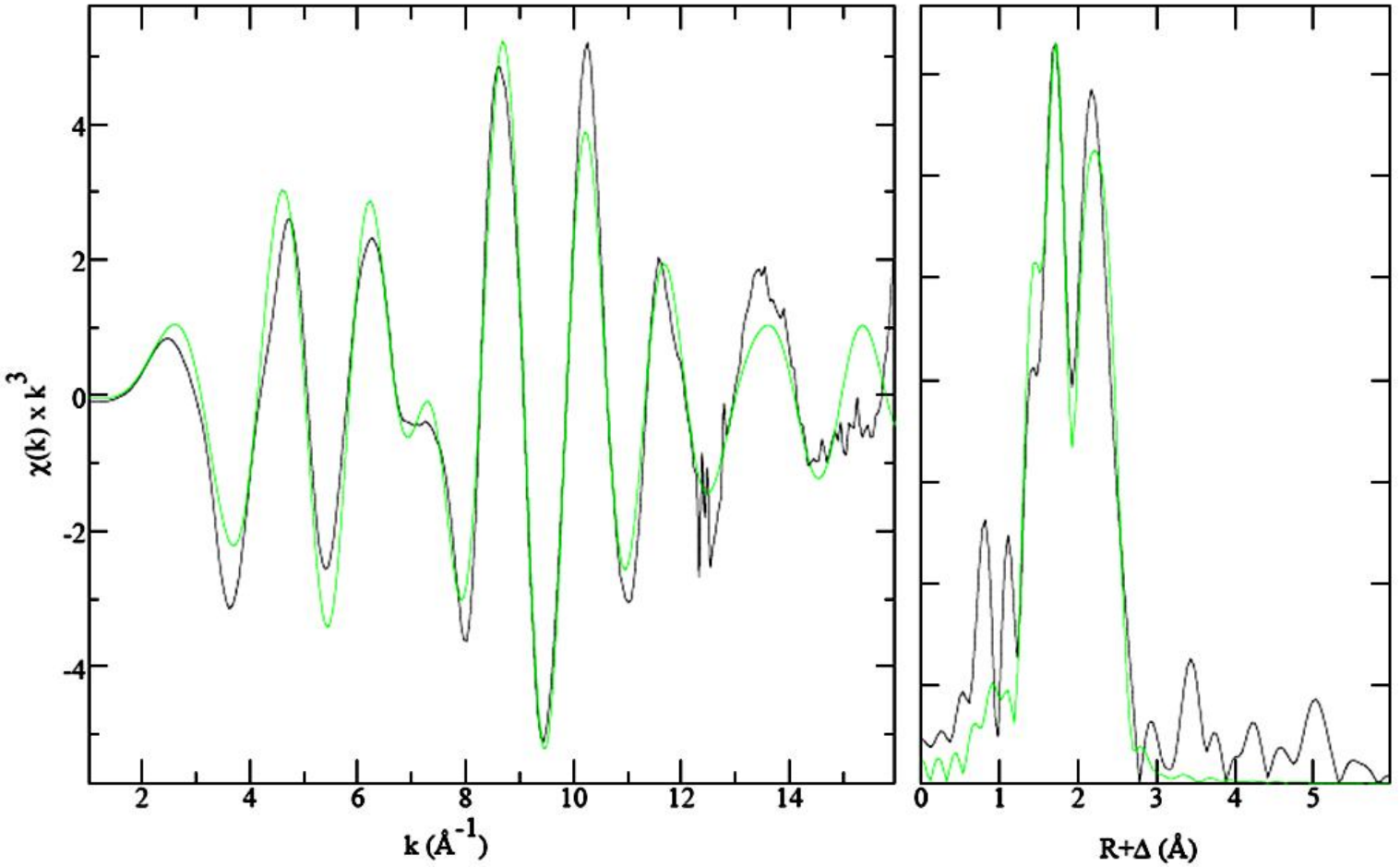

Figure 3.47 Best fit of the EXAFS spectrum of CuTM4 sample with reaction ratio of Cu:TM4 = 1:1. The spectrum was fitted up to k = 16 $Å^{-1}$. The darker line is measured spectrum, the lighter line is fitted spectrum (values found from fit are presented in Table 3.22).

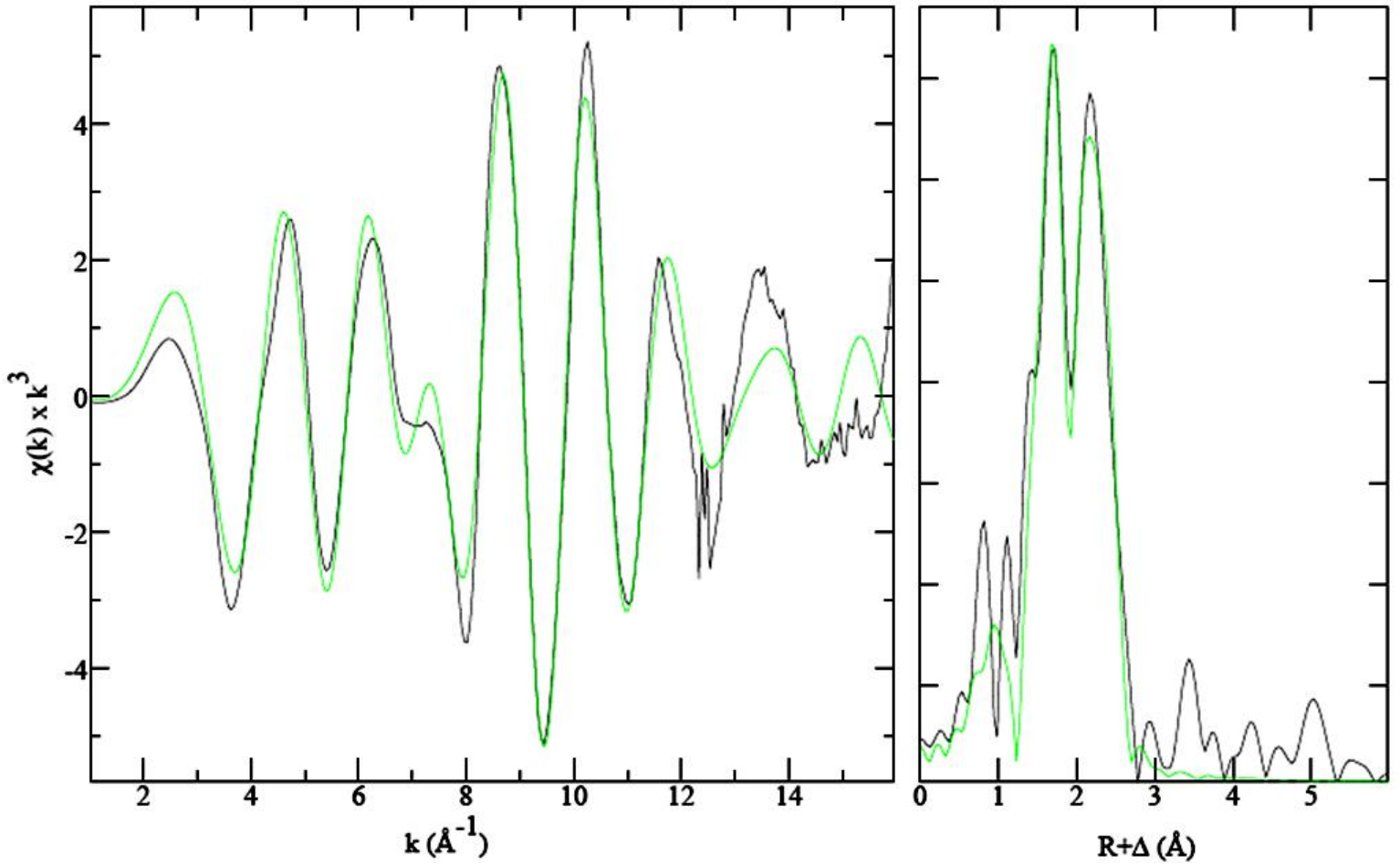

Figure 3.48 Fit of the EXAFS spectrum of CuTM4 sample with reaction ratio of Cu:TM4 = 1:1. The spectrum was fitted with Mo atom surrounded by two oxygen and two sulfur atoms. The darker line is measured spectrum, the lighter line is fitted spectrum.

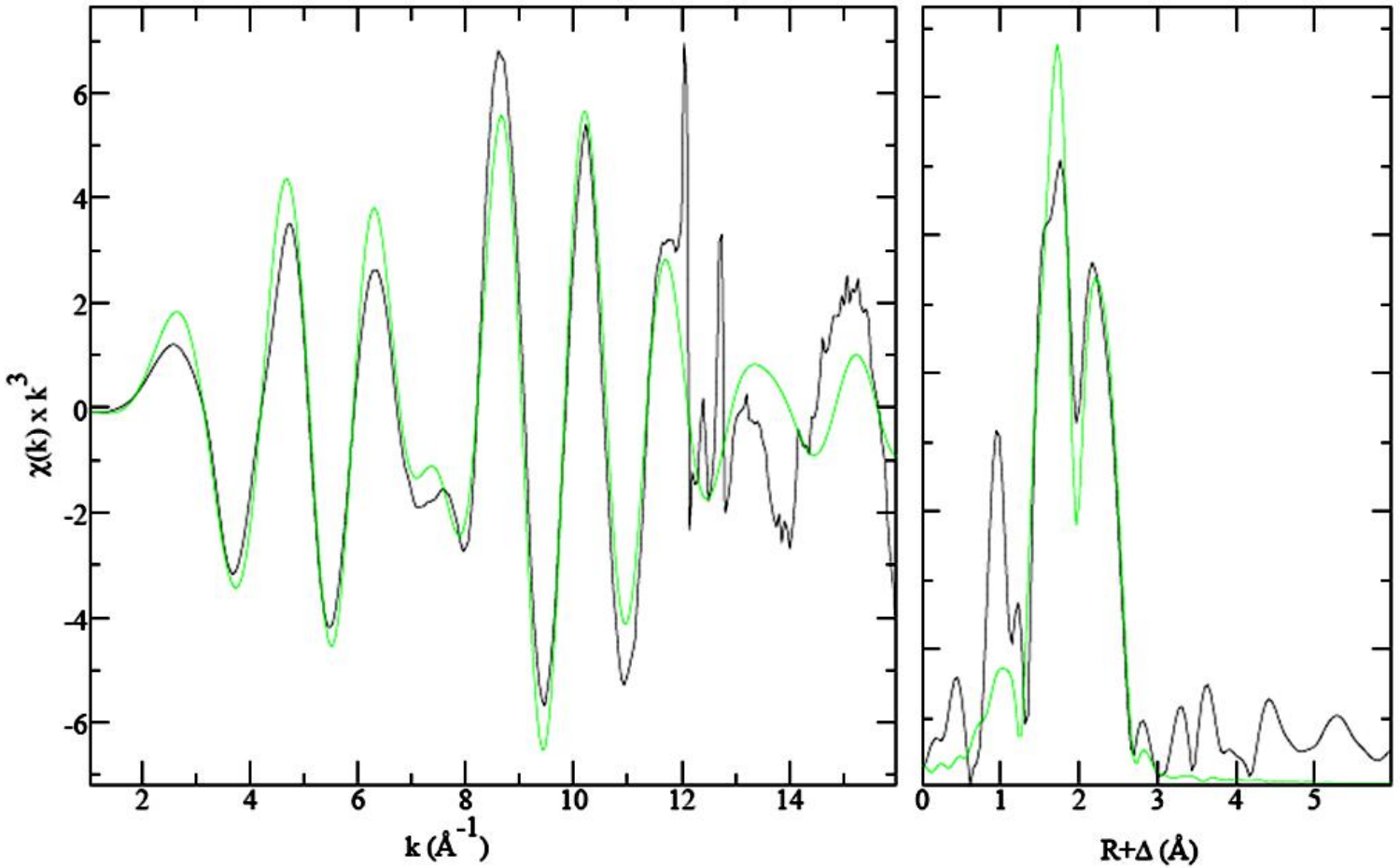

Figure 3.49 Fit of the EXAFS spectrum of CuTM4 sample with reaction ratio of Cu:TM4 = 1:1. The spectrum was fitted with Mo atom surrounded by one oxygen and three sulfur atoms. The darker line is measured spectrum, the lighter line is fitted spectrum.

Bond	*Coordination number*	*Bond length (Å)*	σ^2
Mo-S	2	2.200	0.0043
Mo-O	2	1.685	0.0163
Mo-Cu	3	2.667	0.0084

Table 3.23 Results of the fit of CuTM4 solid sample (Mo K-edge) prepared at reaction ratio of Cu:TM4 = 1:1 (Figure 3.48).

Bond	*Coordination number*	*Bond length (Å)*	σ^2
Mo-S	3	2.22	0.00484
Mo-O	1	1.699	0.00747
Mo-Cu	3	2.678	0.00767

Table 3.24 Results of the fit of CuTM4 solid sample (Mo K-edge) prepared at reaction ratio of Cu:TM4 = 1:1 (Figure 3.49).

Although the best obtained fit was the one with three-coordinated Mo, the other two, with a four-coordinated Mo atom, were not significantly worse and these results are structurally more reasonable. All the CuTM solid samples were fitted to obtain reasonably good fits but also structurally plausible results in terms of Mo environment (sections 3.11.2.2 and 3.11.2.3).

3.11.2.2. CuTM4

The fit of the EXAFS spectra of the solid CuTM4 sample (for a reaction ratio of Cu:TM4 = 1:1) provided the identity of the Mo and Cu neighbors, and their coordination numbers as well as their interatomic distances (Table 3.25).

For the sample of CuTM4 solid prepared at a reaction ratio of Cu:TM4 = 1:1, a reasonable fit (Figure 3.48) at Mo K-edge revealed the presence of two oxygen and two sulfur atoms around the central Mo atom. The presence of a Mo-O bond was also observed in the IR spectra of this sample (section 3.9) as a peak at 900 cm^{-1}. This suggests that the TM4 undergoes hydrolysis in solution during its reaction with copper.

Bond	*Coordination number*	*Bond length (Å)*	σ^2
Mo-O	2	1.685 (7)	0.016 (1)
Mo-S	2	2.200 (2)	0.0043 (1)
Mo…Cu	3	2.667 (3)	0.008 (2)
Cu-N	1	1.900 (3)	0.00010 (3)
Cu-S	3	2.276 (3)	0.0055 (2)
Cu…Mo	1	2.709 (5)	0.0054 (3)

Table 3.25 Results of the analysis of the EXAFS spectra of the CuTM4 sample mixed at a ratio of Cu:TM4 = 1:1 in SRF.

The Mo-O has most likely only a single bond because of the absence of the characteristic pre-edge feature for Mo=O in the near-edge spectrum of the solid CuTM4 sample. The Mo-O with the distance of 1.69 Å was previously observed for Mo(IV)-O, terminal Mo(V)-O and Mo(VI)-O (section 1.4.5.7). The EPR spectra of the solid CuTM4 samples (section 3.11.2.1) suggested the possible existence of a paramagnetic Mo species, which would only be Mo(V) out of these three oxidation states. Therefore, CuTM4 (1:1 reaction ratio) most likely contains Mo(V)-O groups.

The Mo-S bond in the CuTM4 sample was found to be slightly shorter than previously observed in the same type of sample (section 1.4.5.7), but comparable to the Mo-S distance in TM4 (2.19 Å, section 3.10.2) which contains 4 Mo-S bonds.

The best fit of the EXAFS spectrum of CuTM4 solid (reaction ratio Cu:TM4 = 1:1) at the Cu K-edge (Figure 3.50) showed that copper is surrounded by three sulfur atoms and a light atom. This light atom could be either oxygen or nitrogen as both of these are present in the reaction mixture. EXAFS fitting cannot clearly distinguish between these two because their atomic masses are very close to each other. Therefore an assumption was made and this atom was chosen as being nitrogen due to the greater affinity of copper towards nitrogen than oxygen. The Cu-N bond distance is comparable to the one previously observed in the literature (section 1.4.5.6).

The distance of Cu-S bond (Table 3.25) is found to be in between the distances of the four-coordinate and three-coordinated Cu-S (section 1.4.5.6).

The Mo…Cu interaction (non-bonding) was also observed in the EXAFS spectra measured at both, Cu and Mo K-edges. The distance found in the two spectra is slightly different but this is not a significant difference. The non-bonding Cu…Mo distance found by the best fit is comparable to the one found previously for the similar CuTM4 compounds (sections 1.4.5.6 and 1.4.5.7).

The best fit of the Mo K-edge EXAFS spectrum (Figure 3.51) of CuTM4 solid where Cu:TM4 were mixed at ratio of 1.5:1 shows the Mo surrounded by one oxygen and three sulfur atoms (Table 3.26). As in the previous sample, the presence of oxygen (also observed by the IR spectra (section 3.9) reveals that hydrolysis of TM4 during its reaction with Cu occurs. The distances found between Mo and its backscatterers are comparable to those found in the fit of the EXAFS spectra of the previous sample (Table 3.25).

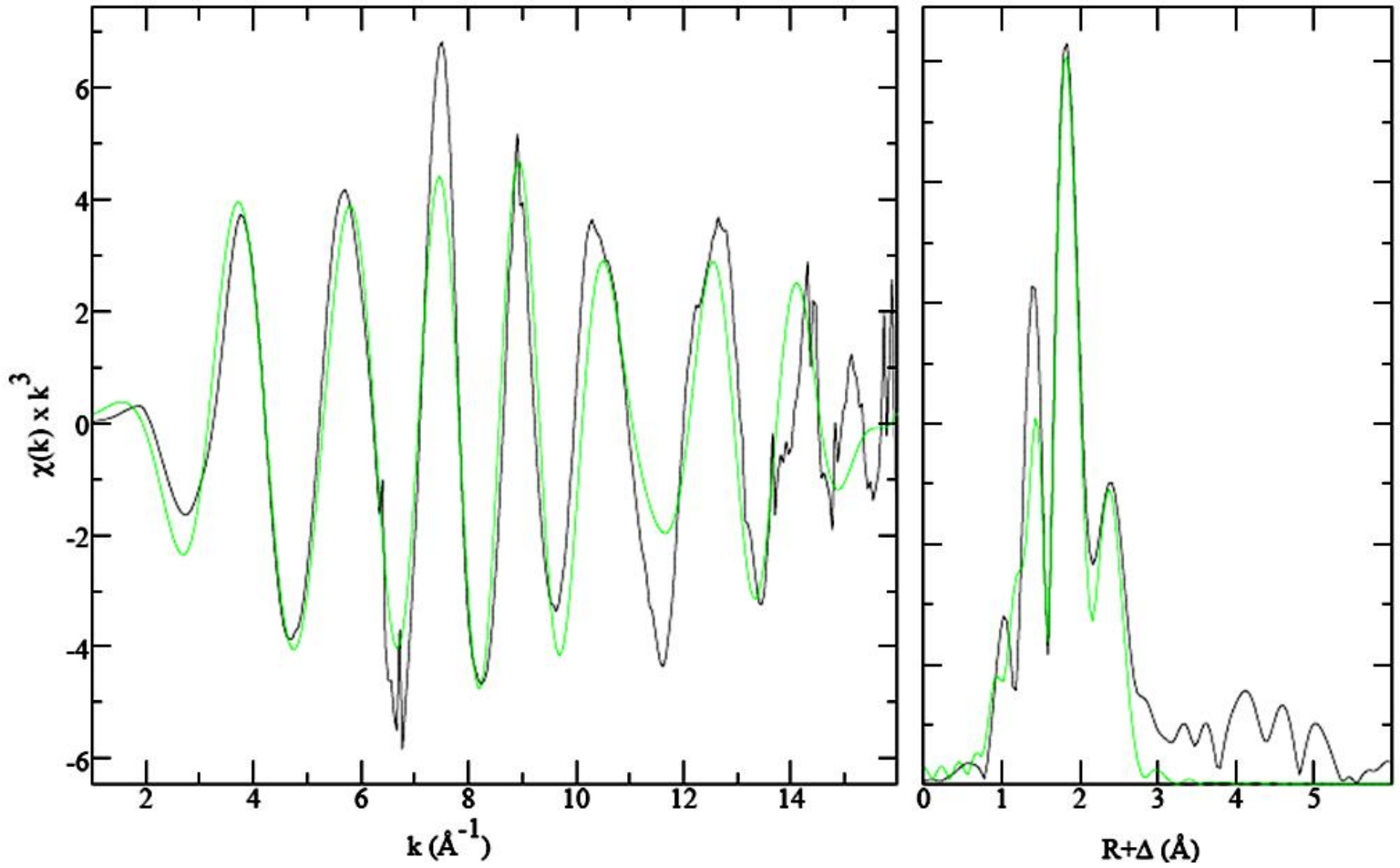

Figure 3.50 Best fit of the Cu K-edge EXAFS spectrum of CuTM4 sample with reaction ratio of Cu:TM4 = 1:1. The darker line is measured spectrum, the lighter line is fitted spectrum.

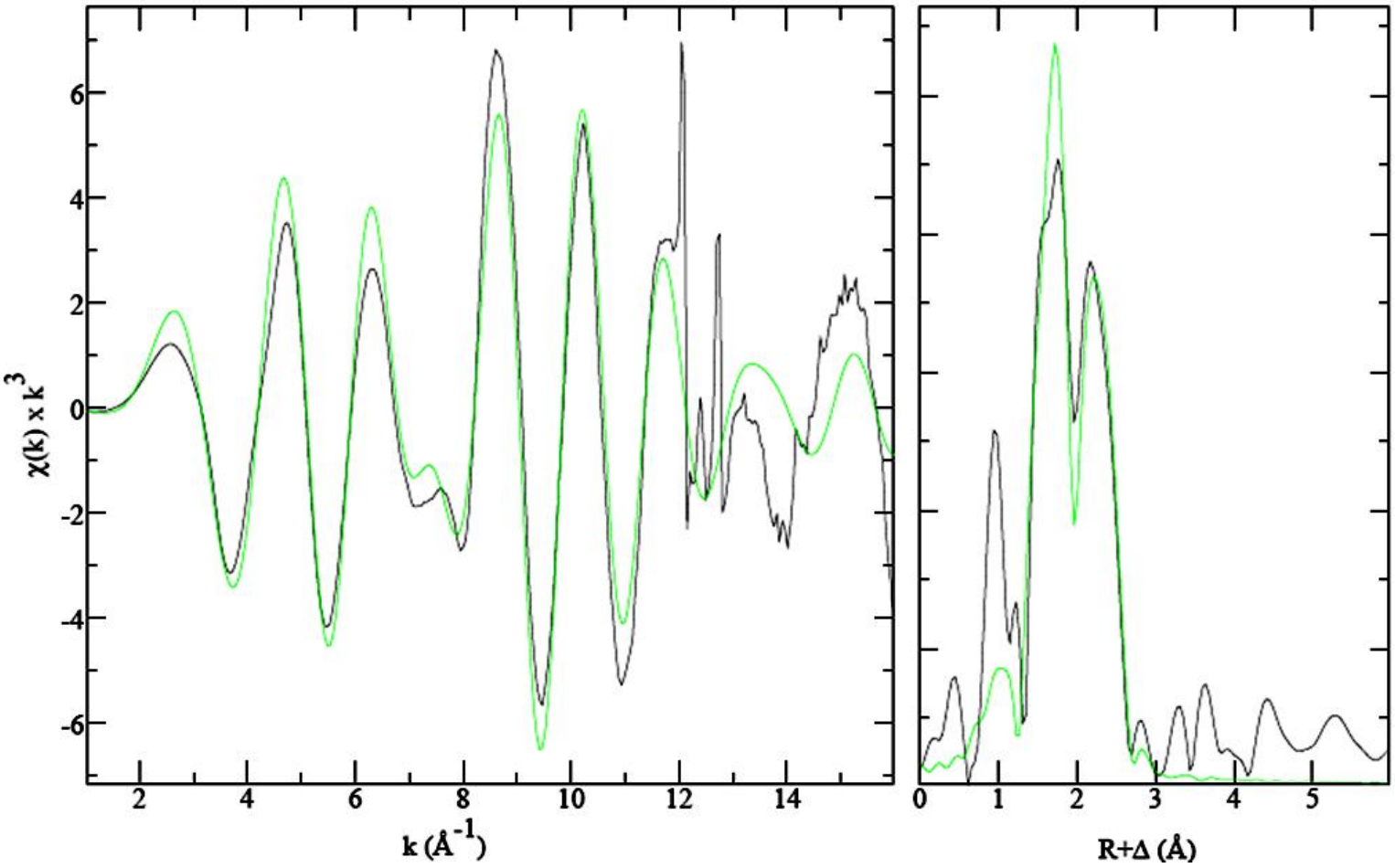

Figure 3.51 Fit of the EXAFS spectrum of Mo K-edge CuTM4 sample with reaction ratio of Cu:TM4 = 1.5:1. The darker line is measured spectrum, the lighter line is fitted spectrum.

Bond	*Coordination number*	*Bond length (Å)*	σ^2
Mo-O	1	1.70 (1)	0.007 (1)
Mo-S	3	2.220 (3)	0.0048 (2)
Mo…Cu	3	2.678 (4)	0.0077 (3)
Cu-N	1	1.683 (2)	-0.0016 (1)
Cu-N	2	1.958 (8)	0.007 (1)
Cu-S	1.5	2.287 (3)	0.0015 (2)
Cu…Mo	1	2.705 (4)	0.0046 (3)
Cu…S	1	3.96 (2)	0.003 (1)

Table 3.26 Results of the analysis of the EXAFS spectra of the CuTM4 sample mixed at the ratio of Cu:TM4 = 1.5:1 in SRF.

Several components were needed to obtain a satisfactory fit of the Cu K-edge EXAFS spectrum of the sample prepared at Cu:TM4 = 1.5:1 (Figure 3.52). Three atoms of nitrogen surround the central Cu atom at two different distances. The coordination number of S atom was found to be between one and two, which makes the total coordination of Cu atom between four and five.

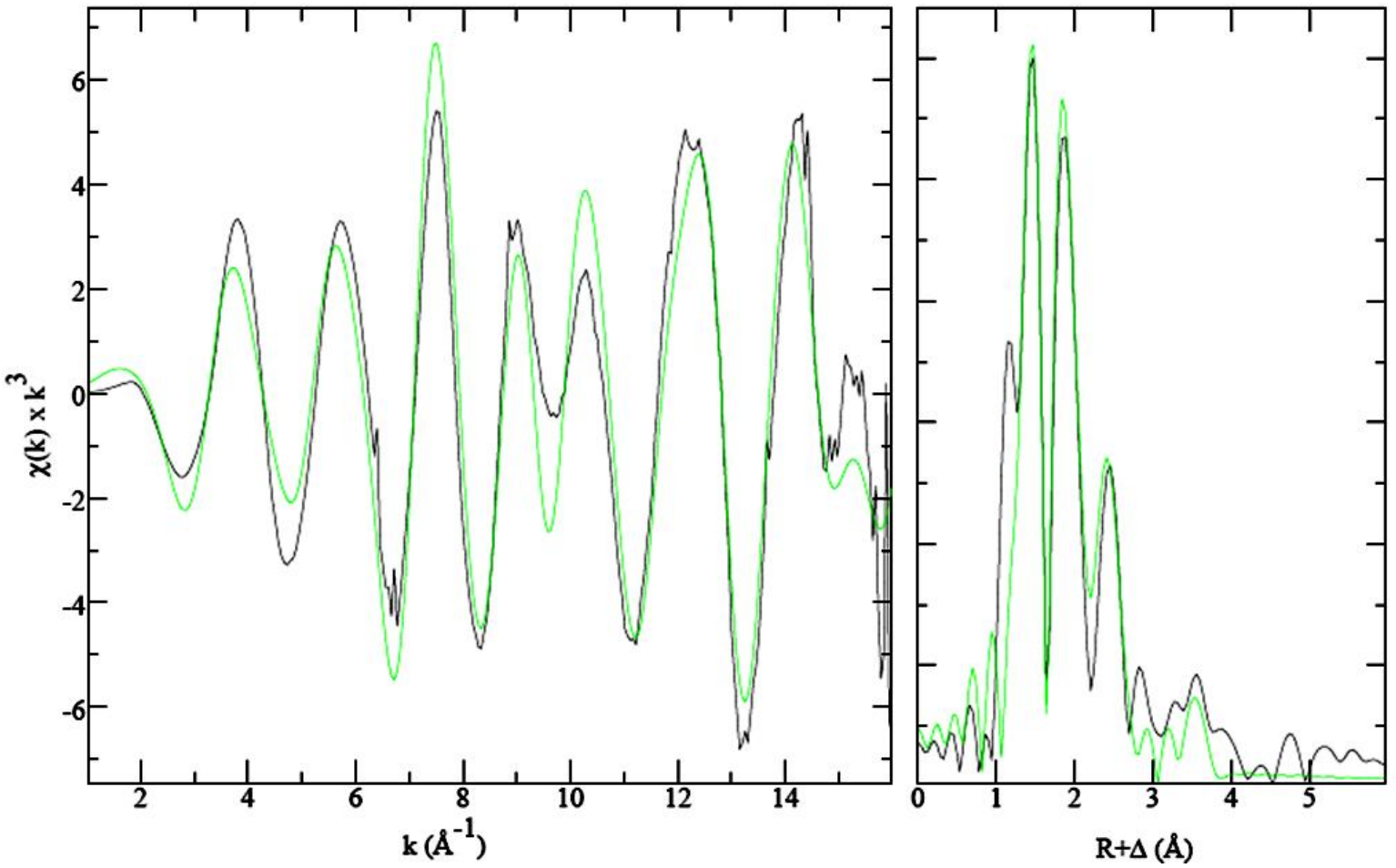

Figure 3.52 Best fit of the Cu K-edge EXAFS spectrum of CuTM4 sample with reaction ratio of Cu:TM4 = 1.5:1. The darker line is measured spectrum, the lighter line is fitted spectrum.

The Cu…Mo distance and coordination number are comparable to those observed previously (Table 3.25). The longer range interaction used in the previous fit was also needed here to improve the fit. This component was found at almost 4 Å from the central Cu and it is most likely a sulfur atom bound to the molybdenum atom (Table 3.26).

The satisfactory fit (Figure 3.53) of the Mo K-edge EXAFS spectrum of the solid CuTM4 mixed at a reaction ratio of Cu:TM4 = 2:1 revealed that the central Mo atom is surrounded by both, oxygen and sulfur atoms (Table 3.27). The distance of Mo-O is comparable to the one found in two previous samples (Table 3.25 and Table 3.26) where Mo and O are single bonded. The average Mo-S distance is slightly longer than the one found for the CuTM4 sample mixed at ratio of Cu:TM4 = 1:1 (Table 3.25) and also has higher coordination number (three) when Cu:TM is increased.

Bond	*Coordination number*	*Bond length (Å)*	σ^2
Mo-O	1	1.672 (9)	0.008 (1)
Mo-S	3	2.236 (2)	0.0049 (2)
Mo…Cu	3	2.671 (3)	0.0078 (2)
Cu-N	1	2.007 (4)	-0.0015 (3)
Cu-S	1	2. 237 (4)	0.0064 (3)
Cu…Mo	1	2.706 (4)	0.00511 (4)

Table 3.27 Results of the analysis of the EXAFS spectra of the CuTM4 sample mixed at the ratio of Cu:TM4 = 2:1 in SRF

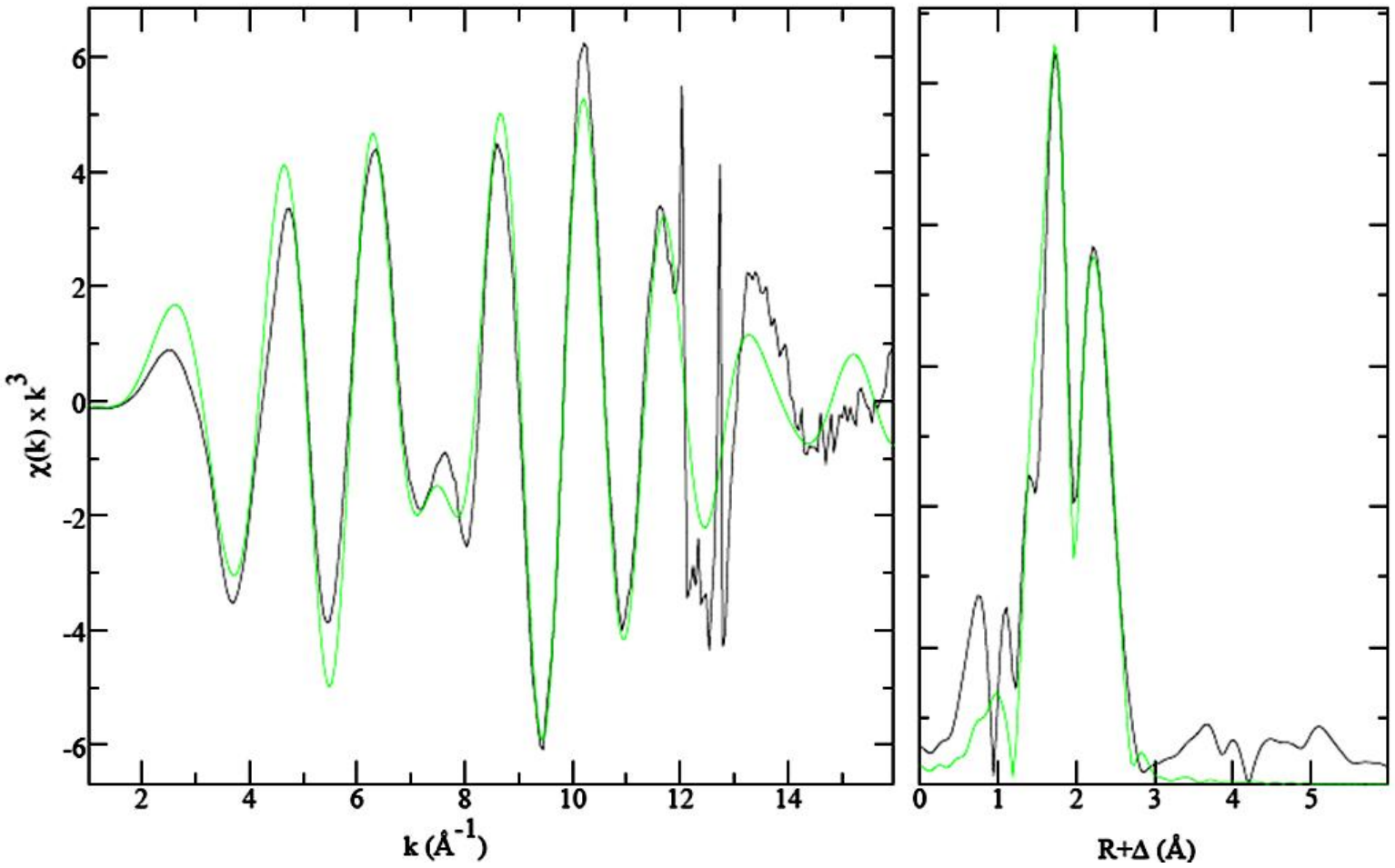

Figure 3.53 Fit of the EXAFS spectrum of Mo K-edge CuTM4 sample with reaction ratio of Cu:TM4 = 2:1. The darker line is measured spectrum, the lighter line is fitted spectrum.

The best fit of the Cu K-edge EXAFS spectrum (Figure 3.54) of the CuTM4 sample mixed at ratio of Cu:TM4 = 2:1 showed the central Cu atom surrounded by nitrogen and sulfur. The coordination number of Cu-S is lower and this distance is also shorter than in the previous sample prepared at lower Cu:TM4 (Table 3.25). The Cu…Mo distance is comparable to the one found in the previously described sample (Table 3.25). This distance is slightly but not significantly different than is found from the Mo K-edge spectrum (Table 3.27).

From the EXAFS spectra of all three CuTM4 prepared at different Cu:TM4 reaction ratios similar results were obtained. The presence of O in the coordination sphere of Mo showed the hydrolysis of the TM4 during its reaction with Cu. The spectra of the CuTM4 with the lowest ratio of Cu:TM4 (1:1) showed the presence of two oxygen and two sulfur atoms; however, two samples with higher Cu:TM4 ratio showed only one oxygen atom and three sulfur atoms around Mo. These results were obtained as the compromise between the best possible fit and reasonableness in the results (the three-coordinate Mo provided a slightly better fit than four-coordinate, but this didn't agree with previous spectral analysis and is structurally very unlikely). The IR spectra of all three CuTM4 solid samples (three different Cu:TM4 ratios) were very similar in terms of the relative intensity of Mo-S and Mo-O peaks. Therefore Mo is most likely surrounded by one oxygen and three sulfur atoms in all three studied CuTM4 samples.

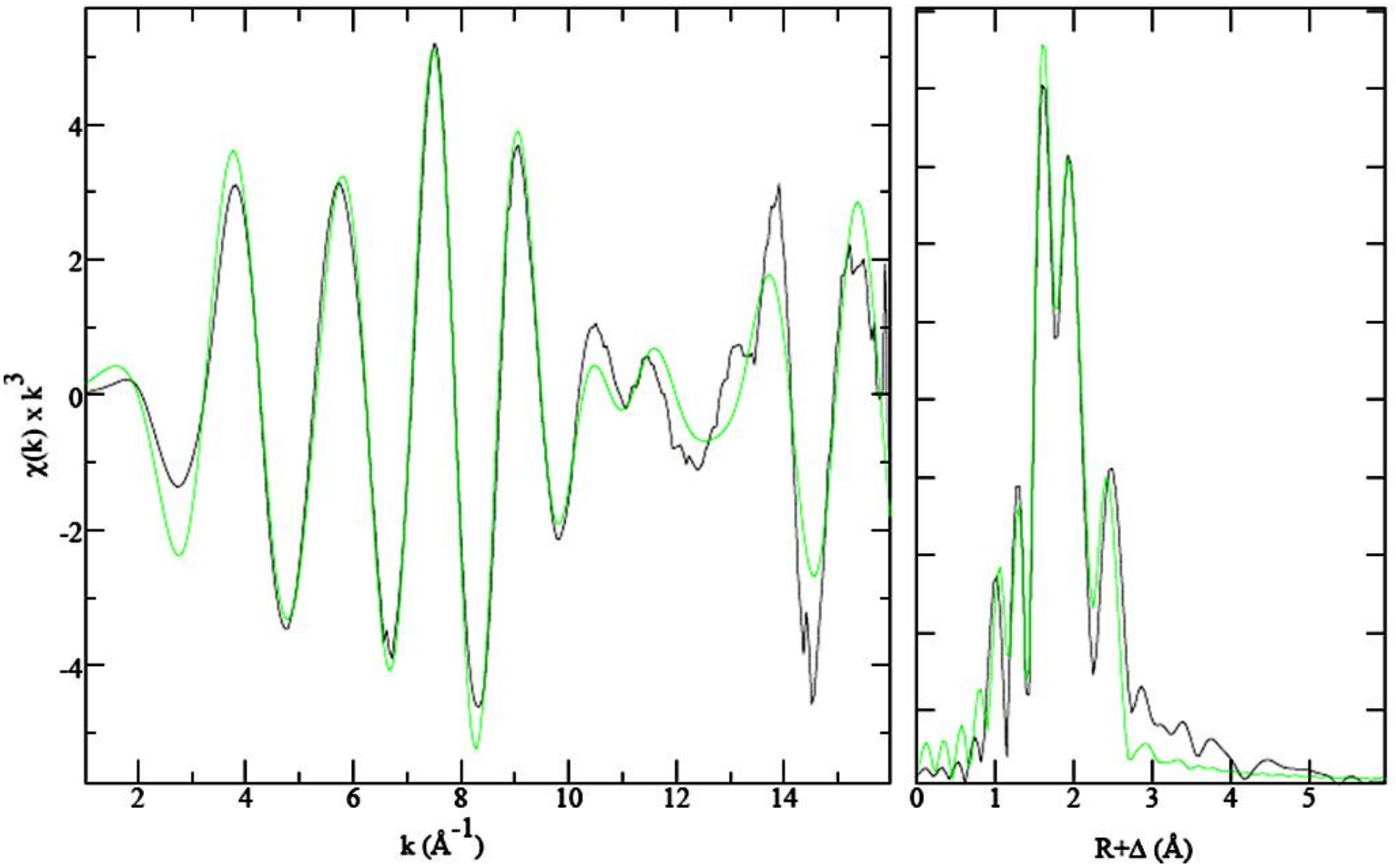

Figure 3.54 Best fit of the Cu K-edge EXAFS spectrum of CuTM4 sample with reaction ratio of Cu:TM4 = 2:1. The darker line is measured spectrum, the lighter line is fitted spectrum.

The Mo-O distance in studied CuTM4 samples is characteristic for the Mo in oxidation state +5. The reduction of Mo(VI) to Mo(V) was also suggested by the presence of the paramagnetism of the CuTM4 samples (section 3.8.2). This oxidation state was also observed previously by Eccleston[120].

The interaction of the TM4 with Cu resulted into a slight elongation of the Cu-S distance compared to the TM4 reactant which agrees with the previous findings of D. Thome[157] (section 1.6.2).

The copper atom has been found to be coordinated by both, nitrogen and sulfur atoms in all the three samples. The coordination numbers, however, vary between these samples. It might be true difference in the coordination of Cu. But during the fitting of the Cu K-edge spectra it was noticed that the slight change in the nitrogen coordination number doesn't have a strong influence on the fit. This atom is very light and therefore the number of coordinating N atoms is difficult to determine accurately.

Based on the results of the analysis of the EXAFS spectra of three CuTM4 solid samples, a structure that is formed between Cu and TM4 can be proposed (Figure 3.55).

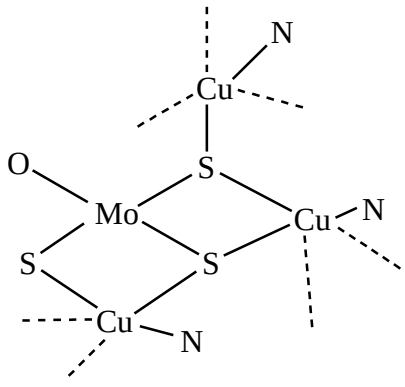

Figure 3.55 Proposed structure formed between Cu and TM4. The dotted lines represent possible coordination of nitrogen and sulfur atoms (found by EXAFS fit in some of the CuTM4 samples).

A similar structure was proposed by George[101], having the same ratio of Cu:TM 4 in the unit but with slightly different Mo environment: tetrahedral coordination with 4 S and no O present. In the George's study, the Cu is trigonal planar and in oxidation state +1. However, Eccleston found, that it is more likely CuS_3 and CuS_4 environment, so the combination of trigonal planar and tetrahedral coordination[120].

The atoms of oxygen and nitrogen are not very likely to be further coordinated to other atoms of Mo. The motive of the CuTM4 unit (Figure 3.55) with only one sulfur and one nitrogen coordinated to Cu atom doesn't suggest the formation of larger, possibly polymeric species. However, if another sulfur atom is attached to S, this may be a possible site of further coordination of another CuTM4 unit. There are several possibilities for the type of atom attached to this sulfur atom.

1. Terminal S is attached to another Cu

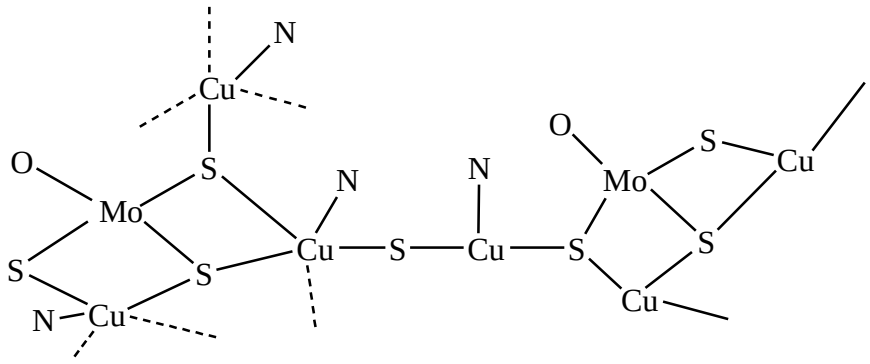

2. Terminal sulfur is attached to another molybdenum

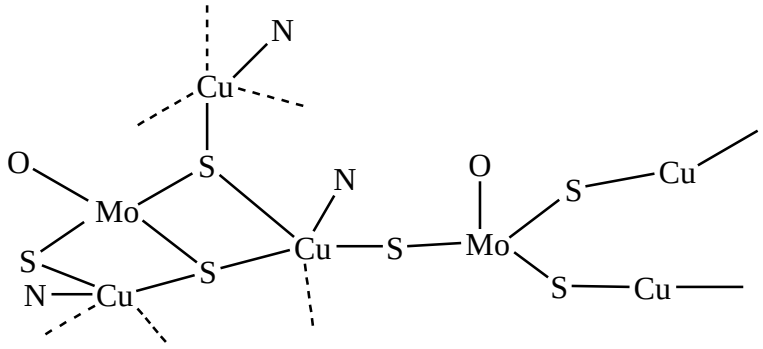

3. Terminal sulfur is attached to another S, forming S-S bridges

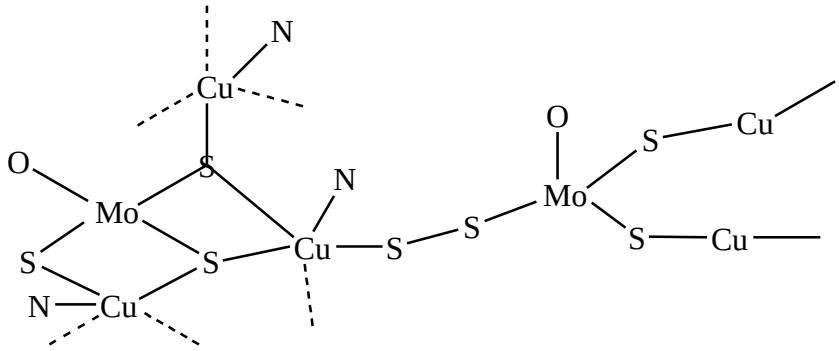

Since there is no detailed analysis of the CuTM4 solid from the point of view of the sulfur atom, it is not possible to definitely determine which of these three option is most likely to occur and contribute to the formation of large (possibly polymeric) species.

If the first suggested structure was to be the correct one here, there would a Cu…Cu interaction observed in the Cu K-edge spectrum. The single scattering of the fit of this spectrum didn't show this interaction to be present.

If the second structure was the probable one, the Cu…Mo interaction would have a coordination number of two. However, the fit of the Cu K-edge spectra showed the presence of only one Mo in the proximity of Cu.

Therefore, the last proposed interaction of the CuTM4 units is the most likely one based on the results of EXAFS spectra fitting. This formation of disulfide bonds was also previously suggested by Eccleston's investigation of Cu-TM4 interaction[120]. However, the formation of disulfide bond wasn't observed in the IR spectra of the CuTM4 solids at all. However, if a disulfide bond was present in the studied sample, its non-polar or only slightly polar character might mean that this bond would not be observable by IR spectroscopy. Instead, its presence would have to be determined from other spectroscopic techniques (section 4.4).

To conclude the discussion of the results of the analysis of the EXAFS data, the formation of CuTM4 species is very similar for the three ratios of Cu:TM4 studied. The units are most likely linked through the disulfide bonds. Other possibilities of the polymerization bonding between these units cannot be determined from the EXAFS spectra.

3.11.2.3. CuTM3

Similarly to the CuTM4 solid samples, CuTM3 solid samples at different Cu:TM3 ratios were prepared (section 2.10.1) and their EXAFS spectra measured and analyzed. The best fit of the Mo K-edge EXAFS spectrum of the solid CuTM3 sample (Figure 3.56) mixed at ratio of Cu:TM3 = 1:1 showed the Mo central atom surrounded by oxygen and sulfur atoms (Table 3.28), similar to the CuTM4 samples (section 3.11.2.2). The presence of the oxygen upon the reaction of TM3 with Cu was also observed in the IR spectra of this sample as a peak at 900 cm^{-1} (section 3.9). The Mo-O bond distance is comparable to the one observed in CuTM4 samples (section 3.11.2.2).

Mo and O are singly bonded, as the pre-edge feature characteristic of Mo=O or Mo=S is missing in the edge spectra of this sample (section 3.11.1.1). The Mo-O distance is characteristic of Mo(V)-O bond where the oxidation state of Mo is concluded from the EPR results of this solid sample (section 3.8).

The Mo-S bond distance is slightly longer than in CuTM4 samples (section 3.11.2.2). It is also longer in CuTM3 than in unreacted TM3, without indication of the double bond (absence of the pre-edge feature in the CuTM3 near-edge spectrum).

The main difference from the CuTM4 samples is that each central Mo has only one Cu atom at the distance of 2.68 Å, compared to the three which were observed for CuTM4 samples (section 3.11.2.2). Because the coordination numbers of oxygen and sulfur are the same as in the unreacted TM3, the results of the analysis of the Mo K-edge spectrum doesn't suggest the hydrolysis of the TM3 upon its reaction with Cu in solution for this sample.

The best fit of the Cu K-edge EXAFS spectrum of the CuTM3 solid sample (Figure 3.57) mixed at ratio of Cu:TM3 = 1:1 showed the central Cu atom coordinated by nitrogen and sulfur atoms. The Cu-N distance is comparable to the one in CuTM4 samples, the Cu-S distance is shorter which is most likely related to the lower coordination number of S than in CuTM4 sample mixed at the same ratio (section 3.11.2.2).

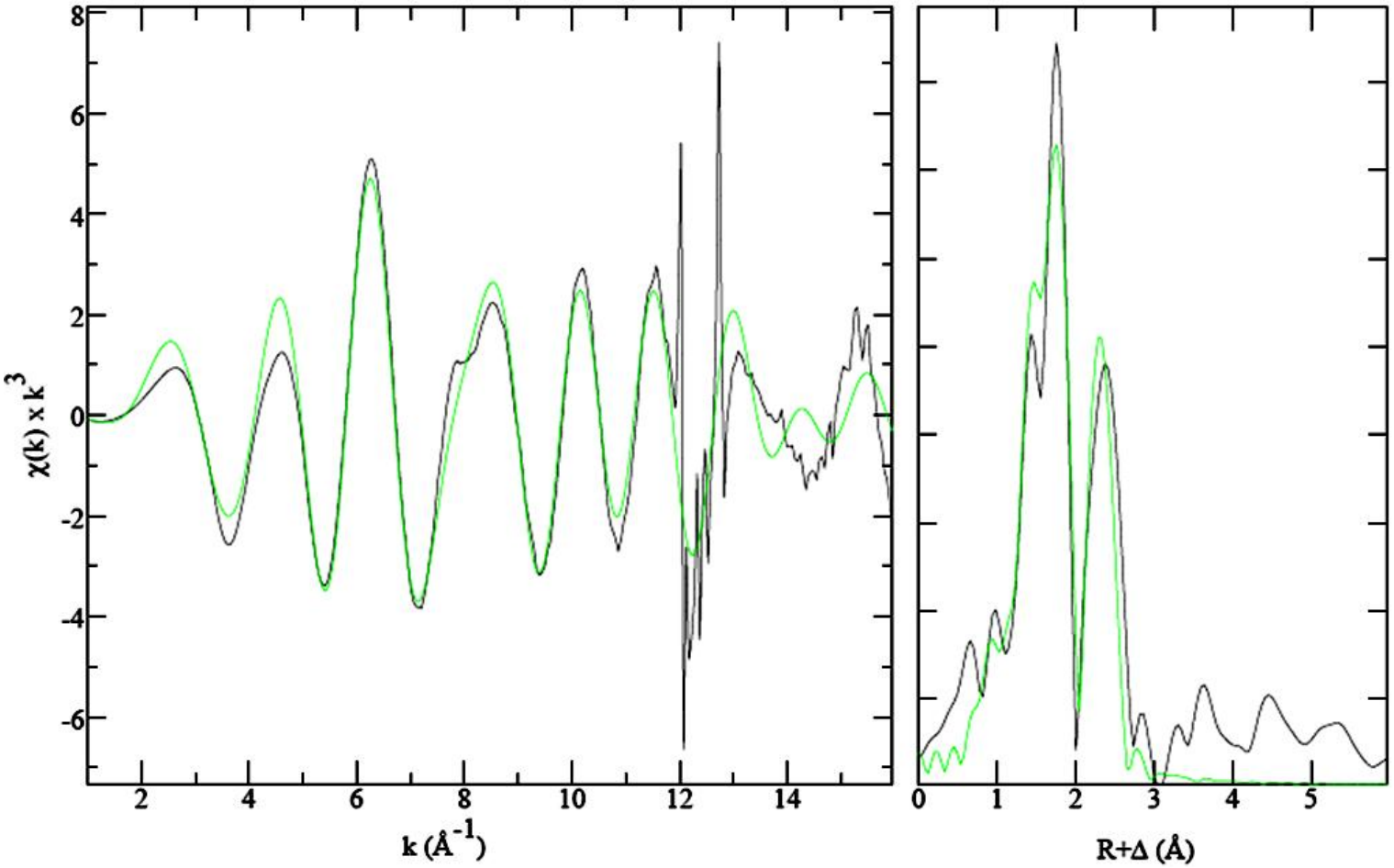

Figure 3.56 Best fit of the Mo K-edge EXAFS spectrum of CuTM3 sample with reaction ratio of Cu:TM3 = 1:1. The darker line is measured spectrum, the lighter line is fitted spectrum.

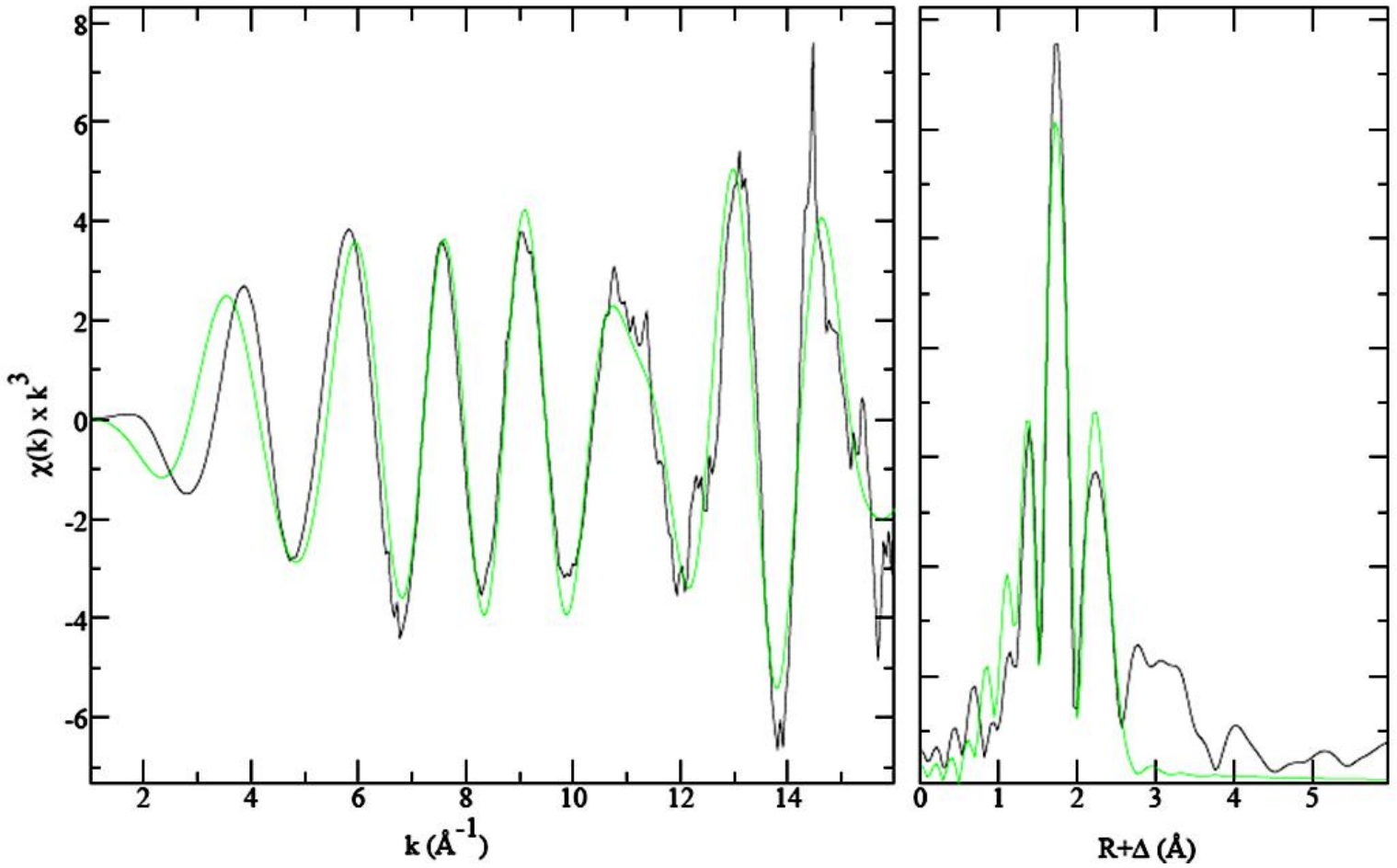

Figure 3.57 Best fit of the Cu K-edge EXAFS spectrum of CuTM3 sample with reaction ratio of Cu:TM3 = 1:1. The darker line is measured spectrum, the lighter line is fitted spectrum.

Bond	*Coordination number*	*Bond length (Å)*	σ^2
Mo-O	1	1.678 (5)	0.0035 (4)
Mo-S	3	2.266 (4)	0.0075 (3)
Mo…Cu	1	2.677 (4)	0.0040 (3)
Cu-N	1	1.832 (2)	-0.0015 (1)
Cu-S	2	2.182 (4)	0.0040 (2)
Cu…Mo	1	2.623 (4)	0.0043 (2)

Table 3.28 Results of the analysis of the EXAFS spectra of the CuTM3 sample mixed at the ratio of Cu:TM3 = 1:1 in SRF

For the solid sample of CuTM3 mixed at ratio of Cu:TM3 = 1.5:1, the best fit of the Mo K-edge EXAFS spectrum (Figure 3.58) shows the presence of oxygen and sulfur atoms around the central Mo (Table 3.29). The total coordination number is four, composed of two oxygens and two sulfurs. Because the number of coordinated sulfurs is decreased and of oxygen increased compared to the unreacted TM3, these results suggest that hydrolysis of TM3 is occurring during its reaction with Cu.

The Mo-O distance is comparable to the one found in the previous CuTM3 sample (above). The Mo-S distance is slightly longer than in the previous CuTM3 sample which is most likely related to the lower coordination number of Mo-S. It is also longer than in the unreacted TM3, most likely because of the decreased coordination number and the absence of a double bond in CuTM3.

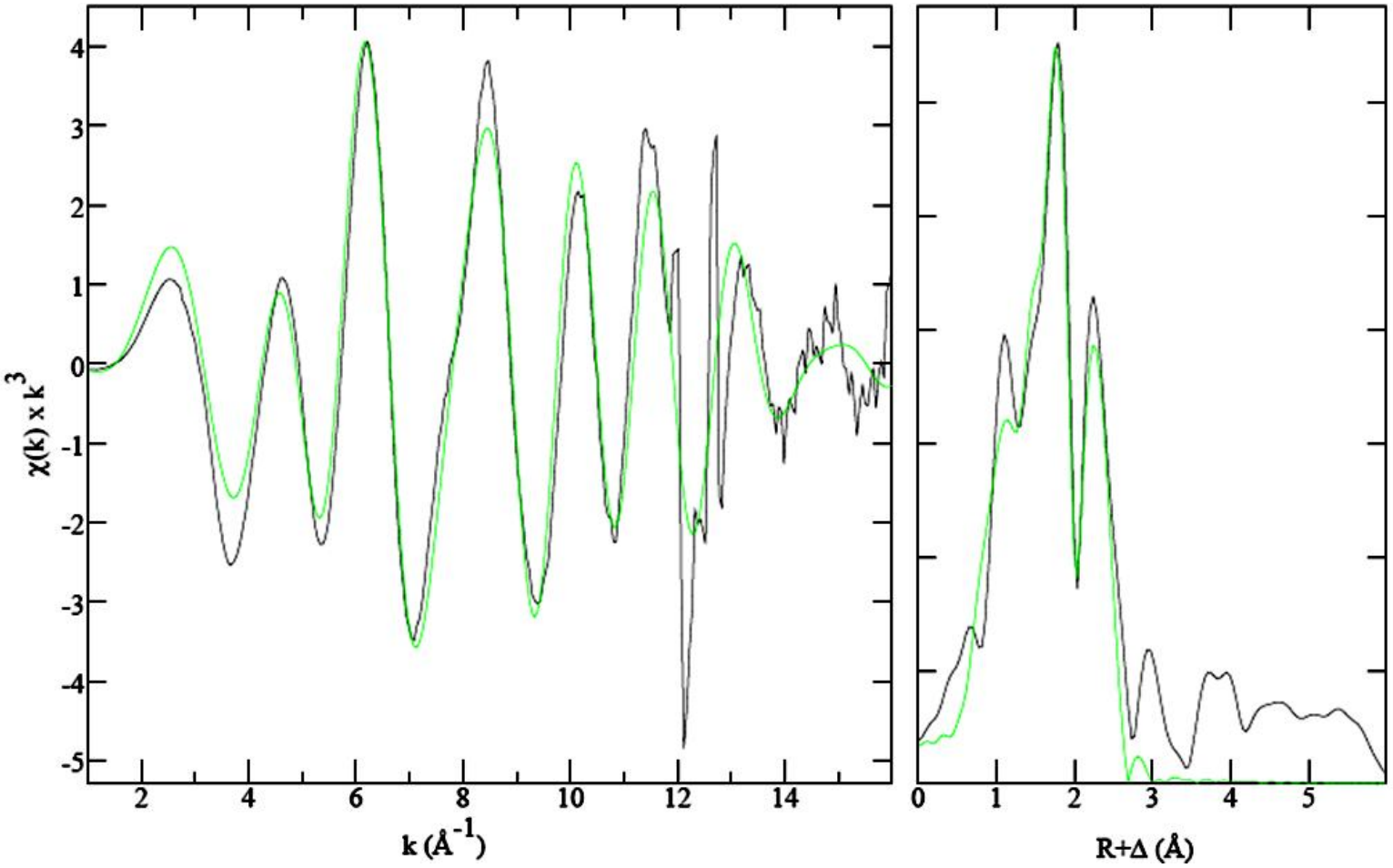

Figure 3.58 Best fit of the Mo K-edge EXAFS spectrum of CuTM3 sample with reaction ratio of Cu:TM3 = 1.5:1. The darker line is measured spectrum, the lighter line is fitted spectrum.

As in the first CuTM3 sample, there is only one atom of Cu at a distance of 2.67 Å from Mo.

The results of the analysis of the Cu K-edge EXAFS of the sample of CuTM3 prepared at reaction ratio of Cu:TM3 = 1.5:1 (Table 3.29) provided similar results for the Cu coordination as the sample at lower ratio (Table 3.28). The coordination of Cu-S is of partial order, between one and two, which is slightly lower than the previous sample (Table 3.28). This means that there is most likely a combination of Cu coordinated by two sulfur atoms and by three sulfur atoms.

Bond	*Coordination number*	*Bond length (Å)*	σ^2
Mo-O	2	1.681 (4)	0.0074 (4)
Mo-S	2	2.254 (3)	0.0051 (2)
Mo…Cu	1	2.673 (4)	0.0054 (4)
Cu-S	1.5	2.279 (3)	0.0040 (2)
Cu-N	1	2.051 (7)	0.0039 (6)
Cu…Mo	1	2.708 (5)	0.0092 (4)

Table 3.29 Results of the analysis of the EXAFS spectra of the CuTM3 sample mixed at the ratio of Cu:TM3 = 1.5:1 in SRF

The EXAFS spectrum of the Mo K-edge of the solid sample of CuTM3 mixed at ratio of Cu:TM3 = 2:1 and its best fit (Figure 3.60) showed the same results as for the previous sample (Cu:TM3 = 1.5:1). The coordination numbers of the components of the spectrum are the same and their found distances from Mo are comparable to the ones found previously (above).

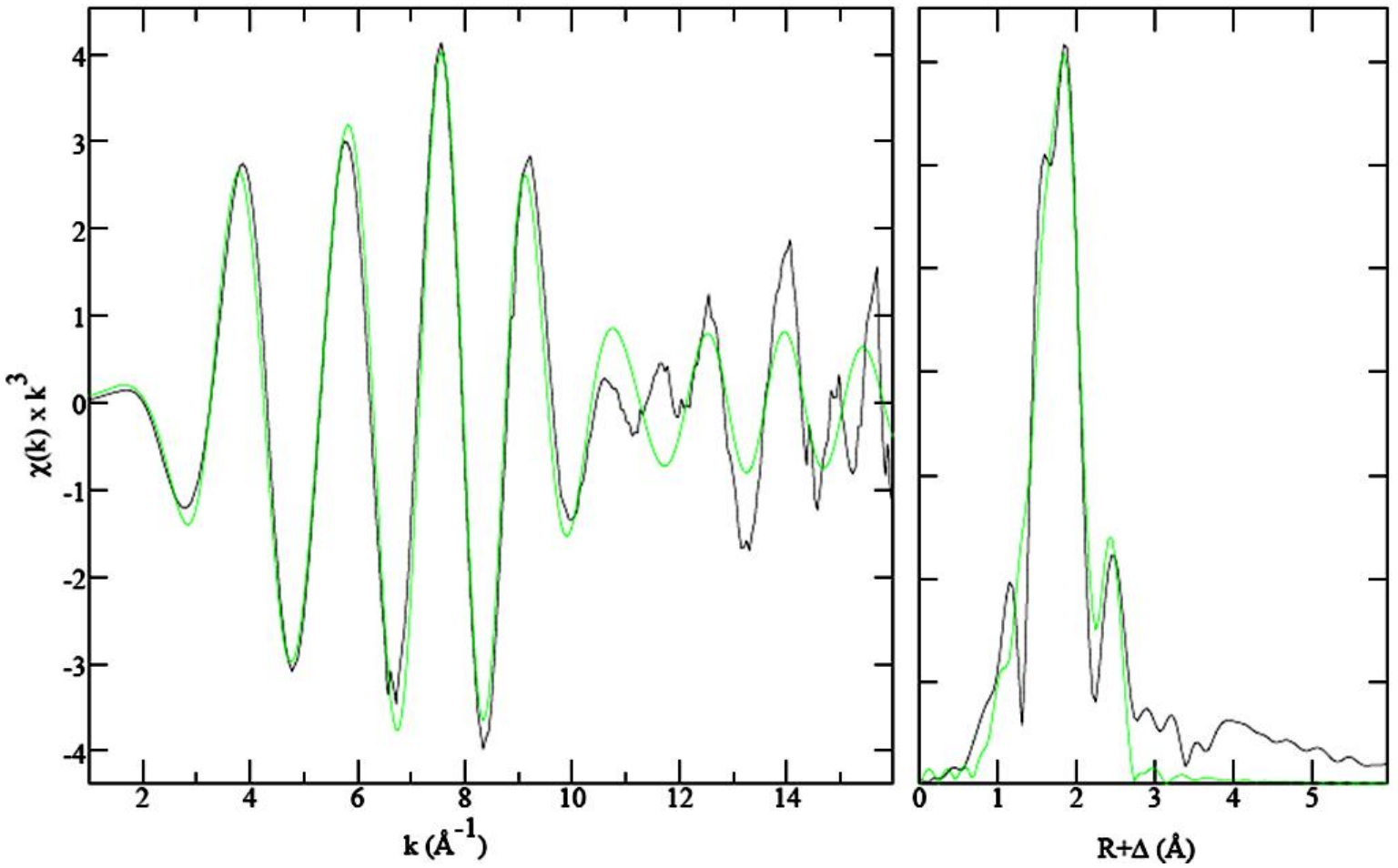

Figure 3.59 Best fit of the Cu K-edge EXAFS spectrum of CuTM3 sample with reaction ratio of Cu:TM3 = 1.5:1. The darker line is measured spectrum, the lighter line is fitted spectrum.

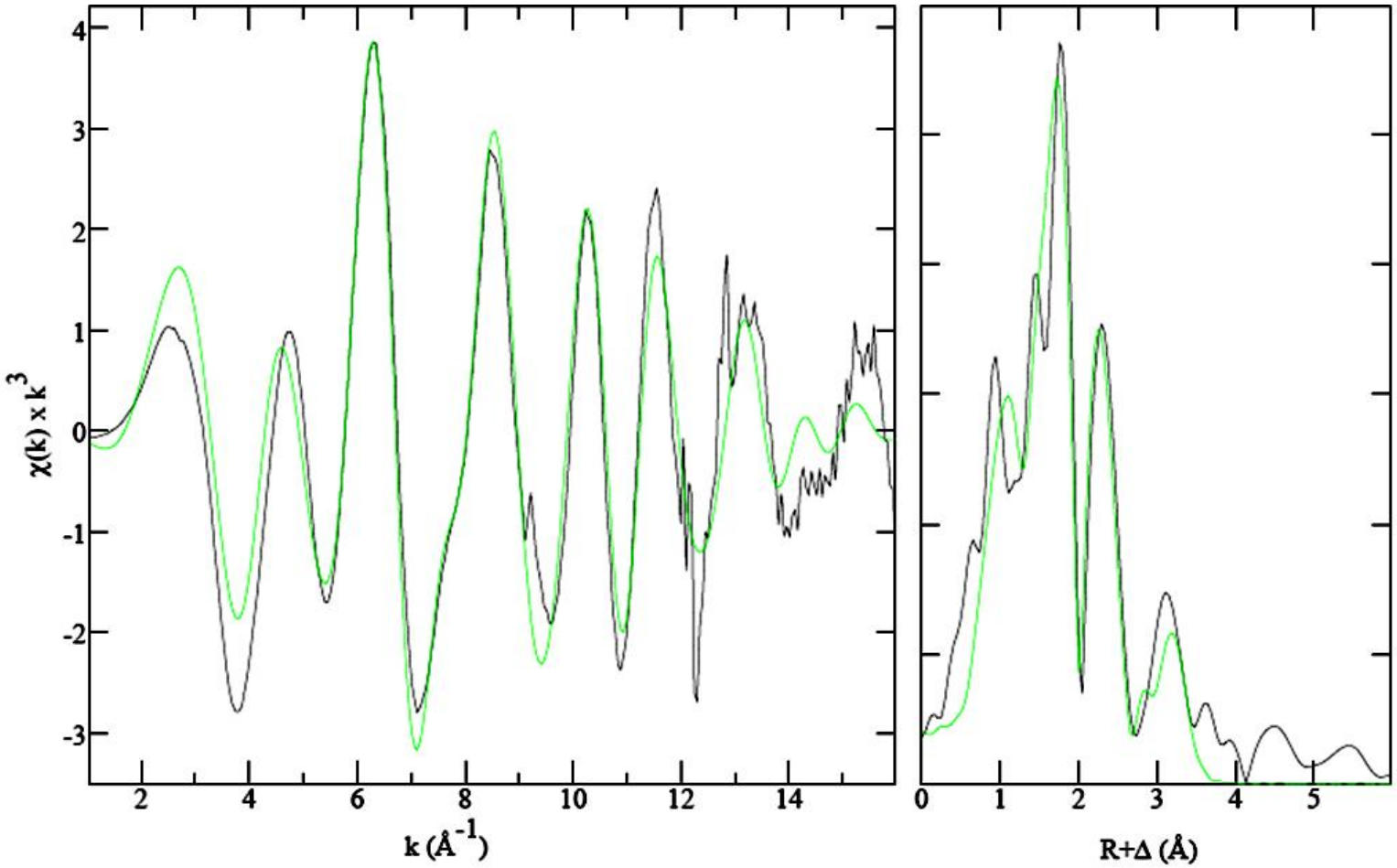

Figure 3.60 Best fit of the Mo K-edge EXAFS spectrum of CuTM3 sample with reaction ratio of Cu:TM3 = 2:1. The darker line is measured spectrum, the lighter line is fitted spectrum.

The best fit (Figure 3.61) of the Cu K-edge EXAFS spectrum of the CuTM3 (Cu:TM3 reaction ratio = 2:1) showed the Cu atom surrounded by nitrogen and sulfur atoms (Table 3.30).

Each Cu atom has only one Mo atom at the distance of about 2.7 Å, which is slightly longer than was found from the Mo EXAFS spectrum.

Bond	*Coordination number*	*Bond length (Å)*	σ^2
Mo-O	2	1.673 (3)	0.0087 (3)
Mo-S	2	2.241 (3)	0.0066 (2)
Mo…Cu	1	2.663 (3)	0.0057 (3)
Cu-N	2	2.158 (2)	0.0024 (2)
Cu-S	3	2.231 (5)	0.0131 (5)
Cu…Mo	1	2.719 (7)	0.0135 (7)

Table 3.30 Results of the analysis of the EXAFS spectra of the CuTM3 sample mixed at the ratio of Cu:TM3 = 2:1 in SRF.

In the CuTM3 samples, Mo has only one Cu atom close to be seen in the EXAFS spectra. This is a little surprising, taking into account the results provided by elemental analysis, where the Cu:Mo molar ratio was found to be higher in the CuTM3 samples than in the CuTM4 samples. Because of the lower amount of sulfur in the system, it is possible that there is a lower probability of the formation of large branched molecules than in the CuTM4 samples. CuTM3 would therefore favor the formation of smaller molecules and/or more simple chain polymeric species.

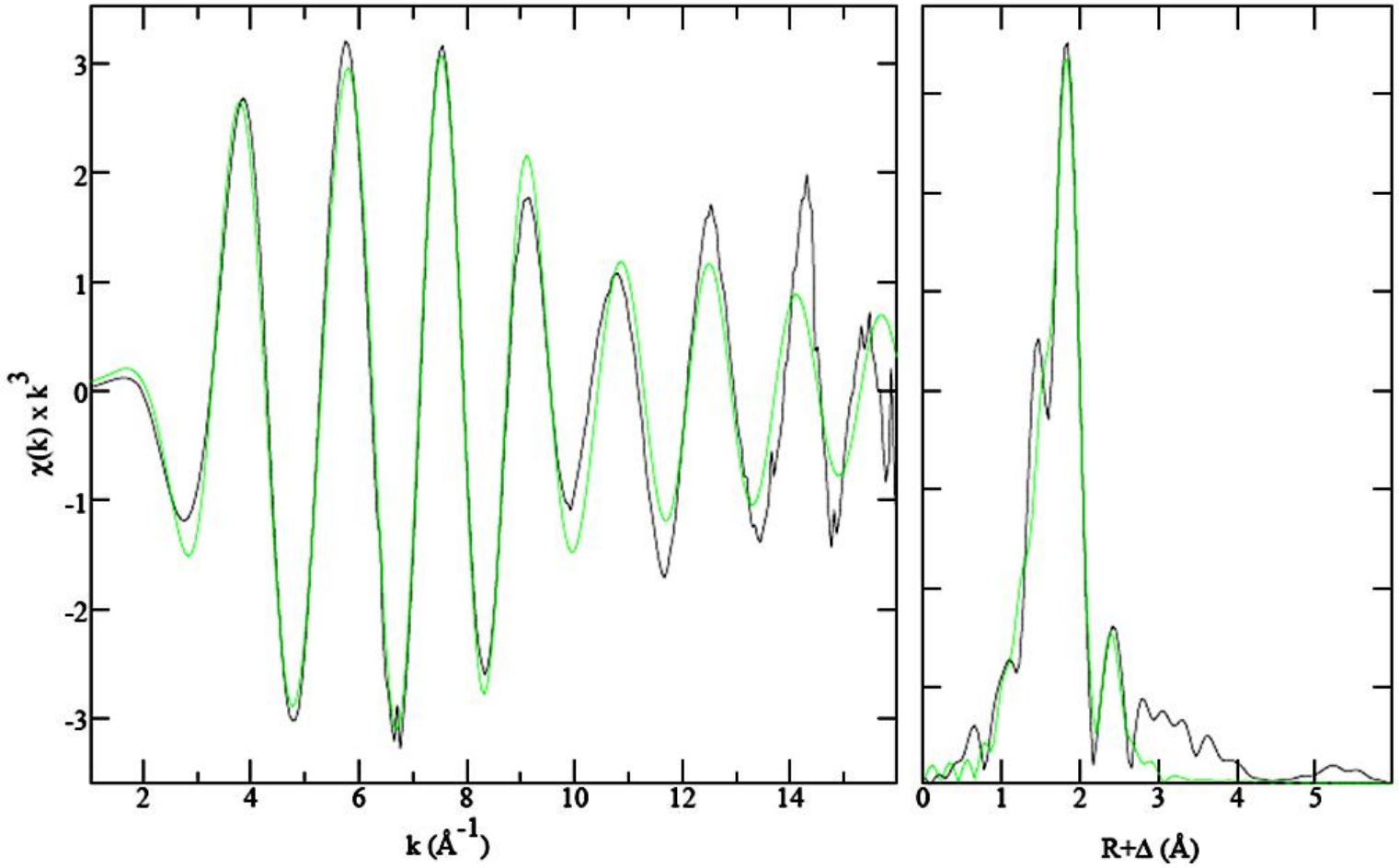

Figure 3.61 Best fit of the Cu K-edge EXAFS spectrum of CuTM3 sample with reaction ratio of Cu:TM3 = 2:1. The darker line is measured spectrum, the lighter line is fitted spectrum.

The CuTM3 samples of lowest studied ratio didn't show the sign of hydrolysis of TM3 but the EXAFS analysis of the two samples prepared at higher Cu:TM3 ratios showed that TM3 undergoes hydrolysis during its reaction with Cu. This discrepancy could be caused by the imperfection of the EXAFS fit, as the two options don't provide significantly different results in the fit, but here, the best fit was chosen from the analysis. The IR spectra of the three CuTM3 samples provided similar results in terms of the intensity of Mo-S and Mo-O peaks and therefore the hydrolysis of TM3 is most likely present.

The coordination numbers of the Cu-S and Cu-N are slightly different for the three CuTM3 samples which is also reflected in their distances. This will be further considered when the structures are proposed as these will be slightly different.

Based on the results of the analysis of three CuTM3 samples, the structure unit of CuTM3 species can be proposed:

Cu:TM3 = 1:1 (molar ratio of reactants during the preparation of the samples):

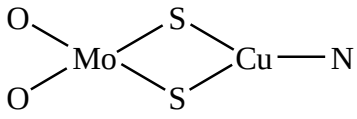

The Cu atom is attached to two sulfur atoms from Mo because the Mo-S distances are the same and the Cu-S distances are also the same. There are no terminal S atoms in the structure and therefore there is a lower probability of the polymerization than in CuTM4 structural unit. However, if three coordinate, these S atoms can provide further sites of bonding. There are three options for the atom coordinated to sulfur, Mo, Cu or S but it is most likely S as no Cu…Cu interaction is observed in the EXAFS

spectrum and there is only one Cu… Mo and also one Mo…Cu interaction in the Cu K edge and Mo K edge spectra, respectively.

Cu:TM3 = 1.5:1

Due to the partial integral of the Cu-S coordination number, there are two possibilities. The sample is most likely a combination of two structural units. One of the unit is of the same structure as the previous one proposed for the reaction ratio of Cu:TM3 = 1:1. The other one is:

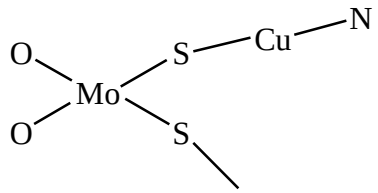

The terminal sulfur provides site for further coordination. The coordinated atom would be most likely another S, as the results of the EXAFS analysis didn't show the presence of another Cu at either Mo or Cu K-edge.

The analysis of the EXAFS spectra shows that both S atoms are at the same distance from Mo and at the same distance from Cu. This does not agree with this proposed structure which has two different S atoms. But in reality, these S atoms could be different and the distances found by the fit of the Mo K-edge and Cu K-edge spectra are just the average of the two slightly different Mo-S or Cu-S distances, respectively, which is not resolved well in the EXAFS spectra.

Cu:TM3 = 2:1

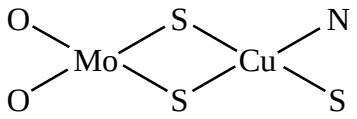

This structure has a terminal S atom on the sulfur atom which provides a site of further coordination of another unit. This one is most likely, as in two previous samples, bonded through another sulfur atom because there is only one Mo in the Cu coordination sphere as observed from the EXAFS analysis (Table 3.30).

The EXAFS spectra presented here were measured for CuTM4 and CuTM3 samples prepared in SRF. Some of these samples were prepared in acetate-ammonia buffer and measured again. These results suggested the same structures as described above and therefore will not be discussed here in details.

3.11.3. XANES: Cu-TM3-TM4

Several samples were prepared containing three components: Cu, TM4 and TM3.These were prepared using different order of mixing and different molar ratios, as described in section (section 2.11.1).

The LCA of the samples containing all three Cu, TM3 and TM4 by linear combination fit showed the presence of both Cu(I) and Cu(II). The results are summarized in Table 3.31.

Ratio of reactants	*Order of mixing of reactants*	*Cu(I)*	*Cu(II)*
1:1:1	Cu + TM3 + TM4	0.69 ± 0.02	0.27 ± 0.02
	Cu + TM3 + 15 min TM4	0.69 ± 0.02	0.27 ± 0.02
	Cu + TM4 + 15 min TM3	0.69 ± 0.02	0.27 ± 0.02
2:1:1	Cu + TM3 + 15 min TM4	0.71 ± 0.02	0.25 ± 0.02
	Cu + TM4 + 15 min TM3	0.72 ± 0.02	0.25 ± 0.02
	Cu + TM3 + TM4	0.72 ± 0.02	0.24 ± 0.02
1:1:0.5	Cu + TM3 + 15 min TM4	0.71 ± 0.02	0.26 ± 0.02
1:0.5:1	Cu + TM4 + 15 min TM3	0.70 ± 0.02	0.27 ± 0.02
1.5:1:1	Cu + TM3 + TM4	0.69 ± 0.02	0.27 ± 0.02

Table 3.31 The fractions of Cu(I) and Cu(II) in the CuTM3 and CuTM4 samples as determined by LCA by EXAFSPAK.

For the system containing the same amount of TM3 and TM4 but increasing amount of Cu(II) where both TMs were mixed with Cu at the same time, a very small increase of Cu(I)/Cu(II) is observed as Cu is increasing. The same trend was observed for samples where TM4 was added 15 min after TM3 was mixed with Cu and also for samples where TM3 was added 15 min after TM4 was mixed with Cu. These results agree with previous analysis of CuTM4 and CuTM3 samples (section 3.11.1.2).

For the samples prepared at the same ratio of all three reactants, the ratio of Cu(I)/Cu(II) is the same for any order of mixing the reactants. Therefore the order of reactants doesn't have an effect on the reduction of the Cu(II). Previously, the LCA of the near-edge spectra of CuTM4 and CuTM3 samples showed more reduction of Cu for CuTM3 samples than for CuTM4 samples. This means that in the CuTM3TM4 system, both, TM3 and TM4 have an effect on the reduction of Cu(II) to Cu(I) and therefore

both TMs react with available Cu even if one of them is added later into the reaction mixture.

Unfortunately, there was no success in the determination of the ratio of CuTM3:CuTM4 in these samples. The XANES spectra of both, Cu and Mo K-edges (Figure 3.62) of the samples showed great similarities with the spectra of the sample of CuTM4. The reason of the unsuccessful determination of the CuTM3 is probably because both, TM3 and TM4 react with Cu very similar way and produce the compounds containing Cu in the same oxidation state and environment.

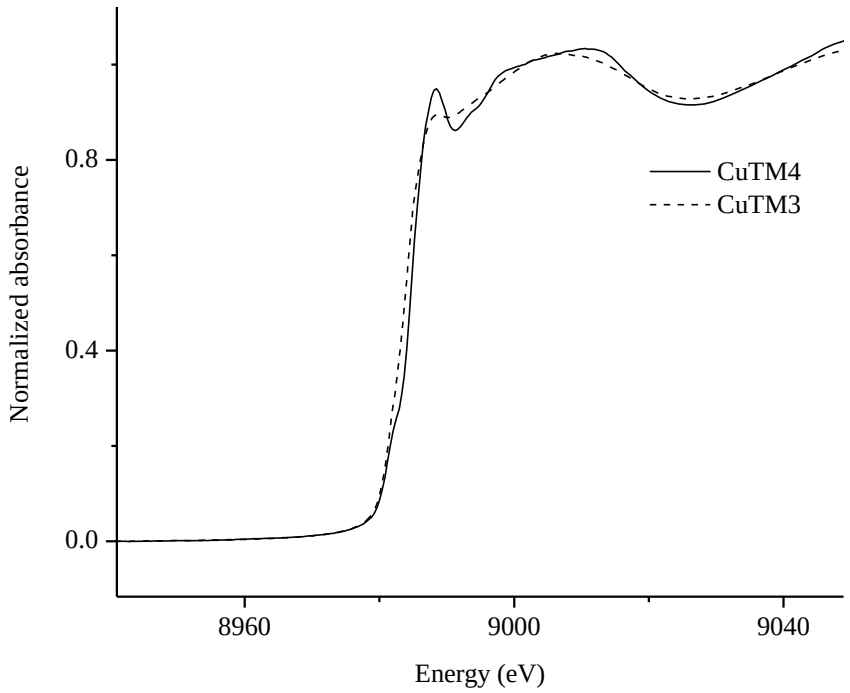

Figure 3.62 Near-edge spectra (Cu edge) of CuTM4 and CuTM3. Both samples were prepared with the reaction ratio Cu:TM = 1:1.

4. CONCLUSIONS AND FUTURE WORK

4.1. CuTM4

Based on the results of the measurements using various techniques described in Chapter 3, a reaction scheme for a CuTM4 adduct formation can be proposed (Figure 4.1).

The complete reaction of formation of a CuTM4 adducts proceeds in two steps, the first step in solution, and the second, the formation of a solid adduct. These two steps will be described here, based on the results of the spectral analysis of reactions between Cu and TM4, and other results.

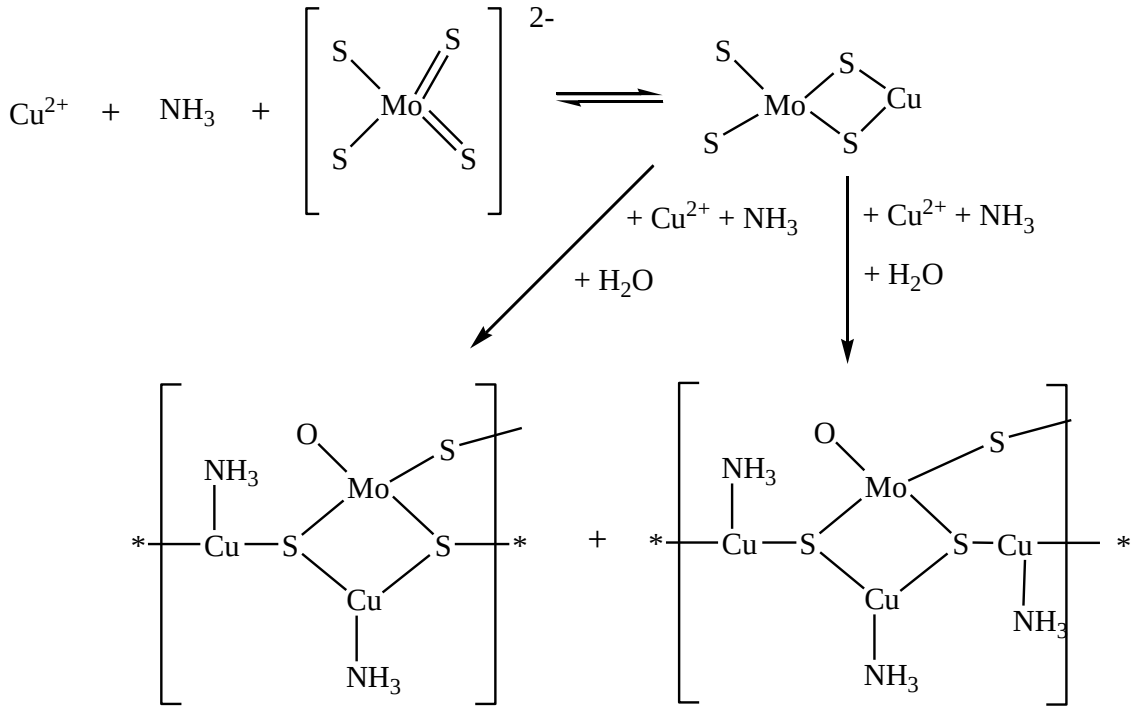

Figure 4.1 A proposed reaction scheme for the formation of a CuTM4 adduct.

4.1.1. CuTM4 in solution

When Cu(II) and TM come into contact in the solution, they react together. UV/Vis spectra of solution samples showed a decrease in absorbance of TM4 as the amount of Cu was increasing (Figure 3.1 and Figure 3.2). Simultaneously, an increase in absorbance at two other wavelengths was also observed; these new peaks were attributed to the newly formed CuTM4 species in solution (Figure 3.1 and Figure 3.5).

The Cu:TM4 ratio in solution was determined by observing and analyzing increases and decreases in the absorbance of TM4 and CuTM4 species, respectively, up to the Cu:TM4 ratio, after which no significant change was observed with further increase of Cu. Analysis at several wavelengths provided ratios close to 1:1, with the average calculated as 1.1:1. The values were similar for different scenarios used in

fitting data at the same wavelengths, but varied slightly for different wavelengths (Table 3.1).

In solution, the type of medium (acetate-ammonia buffer vs. SRF) affected the quality of data. However, the found ratio of Cu:TM4 was not significantly different (Table 3.1 and Table 3.2) in these two media. The fact that data have poor quality in SRF is most likely due to the presence of carbonate and phosphate, both of which complete for Cu and form insoluble species.

This is the first step of the complete reaction between Cu and TM, during which the interaction between the two reactants, and to some extent redox processes occur. This step represents most likely an addition reaction. The species formed in the solution are diamagnetic as no EPR signal was observed (section 3.8.4). Therefore, this suggests Mo(VI) and S^{2-} as both of these are diamagnetic.

The complete absence of the EPR signal in solution suggests the presence of Cu either in the diamagnetic state Cu(I) state, or in a paramagnetic silent state: two Cu(II) interacting and therefore acting as paramagnetic species.

4.1.2. CuTM4 solid

When the concentration of Cu and TM is higher, precipitation of the adducts occurs in the solution. Increased amount of Cu (increased ratio of Cu:TM4) results in the formation of a slightly larger mass of precipitate (Table 3.7). This suggests that in the solid phase, the ratio of Cu:TM4 could be somewhat higher than in solution (1:1). The same result was obtained based on elemental analysis, where the ratio of Cu:Mo in the product increased with increasing Cu:TM4 reaction ratio (Table 3.13). The observation of the supernatant color during the preparation of the solid samples also

showed that a ratio of Cu:TM4 = 1.3:1 is needed to remove all the TM4 from the solution (section 3.5.4).

However, this does not agree with the results of EXAFS analysis, where for three samples prepared at different ratios of Cu:TM4, similar species were obtained. In these, each Mo is surrounded by three Cu, but each Cu is surrounded by only one Mo (Table 3.25, Table 3.26, Table 3.27).

Considering all the results mentioned above, the formed CuTM4 adduct is most likely a combination of units containing different ratios of Cu:TM4. This also explains the difficulty in choosing the best fit of the EXAFS data of the studied samples.

The structure proposed to form between Cu and TM4 contains Mo surrounded by three sulfur atoms and an oxygen atom (TM3-like species), for all three studied ratios. This was concluded based on the results of the IR spectrum of a solid CuTM4 sample (Figure 3.34 A). This showed the ratio of Mo-S:Mo-O groups to be approximately 3:1. The presence of oxygen was also confirmed by the results of the fit of EXAFS spectrum of these samples (Table 3.25 and Table 3.26 and Table 3.27). The results of elemental analysis on the CuTM4 samples showed an unusually high S:Mo ratio in the products formed (Table 3.13). As the only source of sulfur is TM4 reactant, the loss of sulfur from TM4 suggests hydrolysis, which explains the presence of oxygen in the product. For part of the TM4 reactant, the hydrolysis most likely proceeds further: to the formation to TM0, which is soluble in water. This would explain the high Cu:Mo and high S:Mo ratio in solid adducts.

The H_2S from the hydrolysis of the TM4 is very likely to react with Cu(II) species and produce CuS species. CuS is characterized by the insoluble black colloidal precipitate and mixed oxidation states of the atoms: $Cu_2^{I}Cu^{II}S_2S$ (sulfide, S^{2-} and

disulfide, S_2^{2-})[3]. Both adducts: CuS and CuTM4 are of the same appearance and it is therefore not possible to distinguish between them based on visual observations.

The final product proposed to be formed between Cu and TM4 is of a polymeric nature. This is based on the fact that the formed species are insoluble in any commonly known solvent even at low concentration. The fact that each Mo is surrounded by three Cu atoms despite the fact that the ratio of Cu:TM4 is 1:1 found by analysis of EXAFS spectra (Table 3.25 and Table 3.26 and Table 3.27) also supports this hypothesis. Another indication of the polymeric nature of the product is the fact that the double bond between Mo and S present in TM4 is not present in CuTM4. This was observed by the disappearance of the pre-edge feature (characteristic of Mo=S and Mo=O) in the near-edge spectra of TM4 and CuTM4 collected at Mo K-edge (Figure 3.40). The formation of single bonds, rather than double bonds suggests the formation of more bonds and therefore larger, polymeric molecules.

The EPR analysis showed the presence of paramagnetic species in the powders. The intensity of the peaks at ~3475 G which were assigned to paramagnetic copper species, increases with the increasing amount of Cu added into the system (section 3.8.2.2). Therefore after the first addition step, the second step of the reaction includes redox processes, which lead to the reduction of Mo(VI) to Mo(V), and therefore the observed EPR spectrum. It is likely that the oxidation of S^{-II} is also involved, as there has to be some oxidant species present in the system (see below). Due to the fairly strong noise level in the EPR spectra, it is suspected that the reduction of Mo(VI) to Mo(V) is incomplete and the two oxidation states coexist in the final adduct.

XANES analysis showed that the Cu(I):Cu(II) ratio changes very little with an increase in Cu added (Table 3.21). Therefore, the absolute amounts of both Cu(II) and Cu(I) must both be increasing. Cu(I) is not EPR active but Cu(II) is, and therefore an increase of the Cu(II) peak is observed in the EPR spectra (Figure 3.25).

The partial reduction of Cu(II) to Cu(I) is caused by the electron from S. Therefore S^{-II} is oxidized to S^{-I}. In the meantime, the transfer of electron from S to Mo also occurs, resulting in the reduction of Mo(VI) to Mo(V). This gives rise to the observed EPR spectra of the CuTM adducts. The presence of Cu(II) was determined from the analysis of the near-edge spectra (Table 3.21) as well as EPR (section 3.8.2.1). The near-edge analysis also determined the coexistence of copper in two oxidation states: Cu(I) and Cu(II) (Table 1.21). The absolute amount of Cu(I) increases but the relative amount of Cu(I) in comparison with Cu(II) does not change significantly.

The nature of the reaction media used in this project showed no significant influence on the ratio of Cu:TM4 in the formed adduct. The EXAFS analysis of the samples suggested the formation of the same species in acetate-ammonia buffer and SRF buffer. The investigation on the mass of adduct formed in different media showed some differences between the two media, but these can be attributed to the coprecipitation of Cu with other components of reaction media (Table 3.9).

The ratio of Cu:TM4 in solid adduct proposed in this work is somewhat different than that proposed by Eccleston[120]. However, from the available published information, it is not clear what conditions were used in their work. Missing information includes the ratio of the reactants, reaction medium, time, temperature and other species present, all of which have been demonstrated in this and other similar projects to be of importance. Therefore, a meaningful comparison of the two studies, or an evaluation of the validity of their results, is not possible.

4.2. CuTM3

A proposed reaction scheme for the formation of a CuTM3 adduct is given in Figure 4.2.

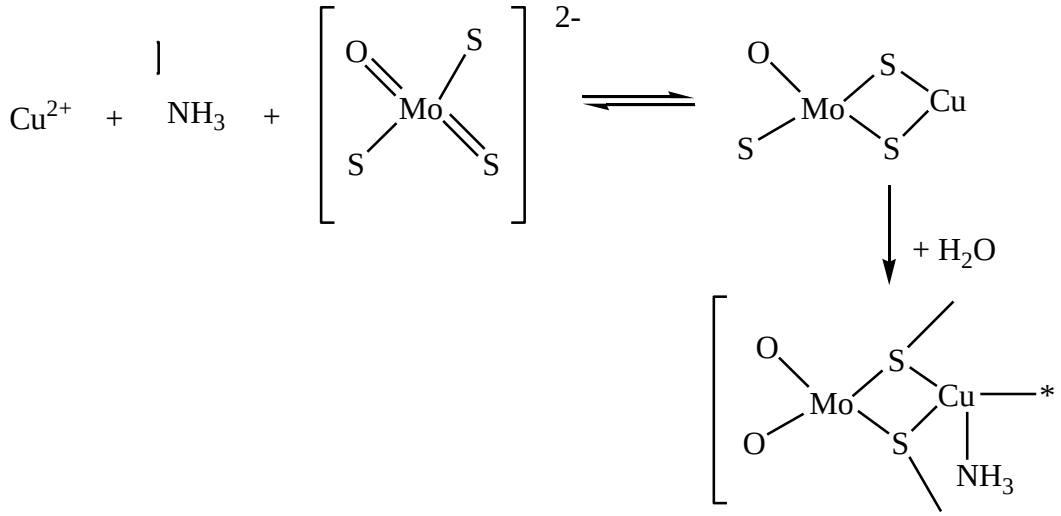

Figure 4.2 A proposed reaction scheme for the formation of a CuTM3 adduct.

4.2.1. CuTM3 in solution

The nature of the solution media had some effect on the TM3 UV/Vis spectrum (Figure 3.8). The changes of the UV/Vis spectra of CuTM3 species as the Cu:TM3 ratio was increasing were therefore not as obvious and their analysis was more complicated than in the CuTM4 system. The newly formed peaks were observed at the same wavelengths as TM3 peaks. The limited available data however still provided some results. The investigation on the ratio of Cu:TM3 in solution suggested that the two reactants form a complex of 1.23:1 stoichiometry in acetate-ammonia buffer and 1.44:1 in SRF. This difference is larger than for Cu:TM4 in solution in the two media. This is also slightly higher than has been previously suggested by other researchers[16]. It is possible that these results are caused only by the poor quality of available data and the real ratio of Cu:TM3 might be similar to Cu:TM4, 1:1.

4.2.2. CuTM3 solid

For Cu and TM3 concentrations higher than used in UV/Vis experiments (5 x 10^{-5} M), the precipitation of CuTM3 species can be observed to form quickly after the two reactants come in contact.

The ratio of Cu:TM3 in solid was found from the elemental analysis to be same as in case of CuTM4 for the reaction ratio of reactants Cu:TM3 = 1:1. But when the two reactants were mixed at a higher ratio, the resulting Cu:TM3 ratio in the solid formed was much higher (Table 3.13). The fact that the resulting ratio is higher than the mixing ratio suggests that either the ratio of Cu:TM3 is variable in solids or that an excess of Cu coprecipitates with other components of medium. The latter is most likely, as the ratio of Cu:TM3 found from the EXAFS fit analysis was found to be 1:1 (Table 3.28 and Table 3.29 and Table 3.30). The same ratio was also concluded for the CuTM4 system (section 4.1.2). The mass of CuTM3 precipitate increases with increasing reaction ratio of Cu:TM3 for the few samples prepared at lowest ratio. But when Cu:TM3 increases to above 1:1, the increase in the mass of CuTM3 precipitate is not that obvious (Table 3.11). This is another indication, that the probable ratio of Cu:TM3 in the product is close to 1:1.

The structure proposed to be formed as the final product contains two oxygen and two sulfur atoms surrounding central Mo atom. However, for the sample prepared at a reaction ratio of 1:1 the analysis of EXAFS spectrum showed that there is only one Mo-O and three Mo-S bonds (Table 3.28). For the other two samples, the EXAFS analysis revealed that Mo is surrounded two oxygen and two sulfur atoms (Table 3.29 and Table 3.30) which was used in the proposed structure. The reason for this decision is supported by the results of IR spectra of CuTM3 samples, where for all the three samples, the peaks characteristic of Mo-O and Mo-S are of the similar intensity (Figure 3.34B). Therefore structure proposed in the Figure 4.2 is most likely to be formed here.

For the EXAFS spectrum of the sample prepared at lowest Cu:TM3 ratio, the best fit was chosen to characterize the final product. However, it was shown, that in some cases, replacement of sulfur by an oxygen atom does not give a significantly worse result for the fit (section 3.10.2), and it is therefore difficult to decide which fit is structurally correct purely on the EXAFS spectra.

Another indication of the hydrolysis of the TM3 during its reaction with Cu is also the results of elemental analysis performed on solid CuTM3 samples. The S:Mo ratio found in the final product is higher than the ratio in the TM3 reactant (Table 3.13). This means that some S is lost from TM3, and replaced by O in the adduct which contains TM2-like moieties.

Similar to the CuTM4 samples, CuTM3 samples are also of polymeric nature. These are not soluble in any common solvent. The near-edge analysis of the Mo K edge in CuTM3 reveals the disappearance of the double bond originally present in the TM3 reactant (Figure 3.41).

The EPR spectra of the CuTM3 solid samples show features similar to those found in the spectra of CuTM4 samples (Figure 3.30). The diamagnetic species are therefore assumed to be similar to those proposed for CuTM4 samples (section 4.1.2). The presence of Cu(II) suspected to be responsible for part of the EPR spectrum of CuTM3 was also confirmed by the analysis of the near-edge spectra of all three CuTM3 studied solid samples (Table 3.21), which showed the coexistence of Cu in two oxidation states. Due to the complicated EPR spectrum, it is suggested that other paramagnetic species are also present, probably Mo(V), similar to those in the CuTM4. Because both, Cu and Mo are being partially reduced during their interaction, S is assumed to be oxidized (from S^{2-} to S^{-}), as was described above for the CuTM4 case.

4.3. Comparison of the Structure of Synthetic Sample and Real Sample

The pH in the rumen environment can vary from 5.5 - 7.2 depending on the feeding habits of the animal. The pH used in this study was chosen to be 4.0. The main reason for this was to avoid precipitation of the $Cu(OH)_2$. This is caused by relatively high concentration of Cu and buffer components in the study compared to the rumen. At higher pH values and lower concentration of the species present in the rumen the precipitation of $Cu(OH)_2$ might not be significant as this process strongly depends on the concentration of Cu (section 3.5.2).

The pH has a significant effect on the hydrolysis of the TM in the solution which is faster at lower pH (section 1.3.3). However, the reaction time for CuTM formation was chosen so be fairly short to minimize the hydrolysis as at higher pH value and lower concentration of TM it would proceed at a slower rate in the rumen.

Relatively high concentrations of Cu and TM had to be used in the preparation of CuTM adducts compared to those found in the rumen. This is expected to have an effect on the rate of precipitation and on the amount of the adducts, but not on the structure of the formed species. As reported elsewhere (section 3.11.2) considerable variation in the ratio of reactants resulted in no significant difference in the structure found in the EXAFS study.

4.4. Future work

To confirm the structures proposed to be formed between Cu and TMs, as shown in Figure 4.1 and Figure 4.2, additional studies are needed. These are described below.

No evidence has been obtained to prove the existence of disulfide bond in CuTM solid adducts. The IR spectra of CuTM samples didn’t show absorption for this

bond either. However, this doesn't mean that the bond is absent, since IR generally detects only asymmetric vibrations, not symmetric ones. An S-S bond might be very nearly symmetrical. Possibly this transition could be seen using Raman spectroscopy, which can often detect symmetric vibrations.

Near-edge spectra of the sulfur edge would provide more information on the sulfur atom neighbors. This would also indicate if in fact the disulfide bond is present. If several different sulfur atoms (in terms of environment) exist, this could also be determined from near-edge spectra using their analysis.

The structures to be formed between Cu and TM in solution were proposed based on the results that only provided ratio of Cu:TM. The validity of the proposed structure should be studied by measuring and analyzing the EXAFS spectra collected on all 3 edges (Mo K, Cu K and S K-edge). This would provide more information not only on the structure (intermediate), but also on the oxidation processes occurring at this stage. This would require the preparation of the samples in a short time frame (seconds), at a low concentration (10^{-5}M or lower), and fast freezing of samples in liquid He to prevent further reaction.

The reaction media used to prepare samples in this work were carefully chosen to mimic the biological environment. However, it would of great interest to compare results presented in this thesis with real biological sample of CuTMs prepared in real rumen fluid. This would prove that the structures proposed in this work are relevant to Cu deficiency in cattle.

In the solution study using UV/Vis spectroscopy, it was assumed that only one type of product is formed. The more thorough analysis, using PCA could determine the exact number of species present in the solution.

It was mentioned previously (section 3.8.2.1) that the reduction of Mo(VI) to Mo(V) is only partial. The paramagnetic species are therefore only minority species of the whole prepared adduct. The integration of the EPR spectra would provide the more accurate amount of the paramagnetic species and therefore indicate if the signal represent the bulk of sample or only trace.

Although some more measurements are needed to prove the structures proposed based on the measurements described in this work, this project has given us considerable insight into the structure of CuTM adducts related to Cu deficiency in cattle. For the first time, not only the CuTM4 but also the CuTM3 interaction was studied from the structural point of view, which should be of considerable help in understanding Cu speciation in the bovine rumen environment.

REFERENCES

(1) Cotton, F. A.; Wilkinson, G.; Murillo, C. A.; Bochmann, M. *Advanced Inorganic Chemistry*; 6th ed.; John Wiley & Sons, Inc. : New York, 1999.

(2) Cotton, F. A.; Wilkinson, G.; Gauss, P. L. *Basic Inorganic Chemistry*; 3rd ed.; John Wiley & Sons, 1995.

(3) Greenwood, N. N.; Earnshaw, A. *Chemistry of the Elements*; 2nd ed.; Elsevier, 2003.

(4) Solomon, E. I. *Copper Coordination Chemistry: Biochemical and Inorganic Perspectives*; Adenine Press: New York, 1983.

(5) Hathaway, B. *Orbital* **1971**, 14-18.

(6) House, J. E.; House, K. A. *Descriptive Inorganic Chemistry*; Harcourt/Academic Press, 2001.

(7) Church, D. C. *The Ruminant Animal, Digestive Physiology and Nutrition*; Prentice-Hall, New Jersey, 1988.

(8) Underwood, E. J.; Suttle, N. F. *The Mineral Nutrition of Livestock*; 3rd ed.; CABI Publishing: Oxon, 1999.

(9) McDowell, L. R. *Minerals in Animal and Human Nutrition*; Academic Press, Inc: San Diego, 1992.

(10) Kaim, W.; Schwederski, B. *Bioinorganic Chemistry: Inorganic Elements in the Chemistry of Life*; John Wiley & Sons, Ltd.: West Sussex, 1994.

(11) NRC *Nutrient Requirements of Domestic Animals, Nutrient Requirements of Beef Cattle*, National Research Council, Washington, D. C., 1984.

(12) Berzelius, J. J. *Poggendorffs Ann. Phys. Chem.* **1826**, *7*, 262-272.

(13) Muller, A.; Diemann, E.; Krebs, B.; Leroy, M. J. F. *Angew. Chem. Internat. Edit.* **1968**, *7*, 817.

(14) Muller, A.; Diemann, E.; Jostes, R.; Bogge, H. *Angew. Chem. Int. Ed. Engl.* **1981**, *20*, 934-955.

(15) Clarke, N. J.; Laurie, S. H. *J. Inorg. Biochem.* **1980**, *12*, 37-43.

(16) Quagraine, E. K. P., *Competitive Interactions between Copper(II) ions, Thiomolybdates, and some Biological Ligands*, University of Saskatchewan, 2002.

(17) Lorentz, B.; Orgzall, I.; Dorhout, P. K.; Raymond, C. C.; Brister, K.; Weishaupt, K.; D'Adamo, R.; Hochmeimer, H. D. *Phys. review B* **1997**, *55*, 2800-2807.

(18) McDonald, J. W.; Friesen, G. D.; Rosenhein, L. D.; Newton, W. E. *Inorg. Chim. Acta-Articles* **1983**, *72*, 205-210.

(19) Saxena, R. S.; Jain, M. C.; Mittal, M. L. *Monatshefte Fur Chemie* **1968**, *99*, 530-538.

(20) Srinivasan, B. R.; Vernekar, B. K.; Nagarajan, K. *Indian J. Chem. Sec. A* **2001**, *40*, 563-567.

(21) Alonso, G.; Aguirre, G.; Rivero, I. A.; Fuentes, S. *Inorg. Chim. Acta* **1998**, *274*, 108-110.

(22) Kanatzidis, M. G.; Coucouvanis, D. *Acta Cryst. C* **1983**, *39*, 835-838.

(23) Poisot, M.; Bensch, W.; Fuentes, S.; Alonso, G. *Thermochimica Acta* **2006**, *444*, 35-45.

(24) Saxena, R. S.; Jain, M. C.; Mittal, M. L. *Austr. J. Chem.* **1968**, *21*, 91-96.

(25) Jostes, R.; Muller, A.; Diemann, E. *J. Mol. Struc.* **1986**, *30*, 311-328.
(26) Pohkrel, S.; Nagaraja, K. S.; Varghese, B. *J. Chem. Cryst.* **2003**, *33*, 903-908.
(27) Beheshti, A.; Clegg, W.; Brooks, N. R.; Sharafi, F. *Polyhedron* **2005**, *24*, 435-441.
(28) Reid, R. S.; Clark, R. J.; Quagraine, E. K. *Can. J. Chem.* **2007**, *85*, 1083-1089.
(29) Harmer, M. A.; Sykes, A. G. *Inorg. Chem.* **1980**, *19*, 2881-2885.
(30) Aymonino, P. J.; Ranade, A. C.; Diemann, E.; Muller, A. *Z. Anorg. Allg. Chem.* **1969**, *371*, 300-305.
(31) Bernard, J. C.; Tridot, G. *Bull. Soc. Chim. France* **1961**, 818-822.
(32) Minelli, M.; Enemark, J. H.; Brownlee, R. T. C.; O'Connor, M. J.; Wedd, A. G. *Coord. Chem. Rev.* **1985**, *68*, 169-278.
(33) Mason, J. *Multinuclear NMR*; New York : Plenum Press, 1987.
(34) Brule, J.; Hayden, Y. T.; Callahan, K. P.; Edwards, J. O. *Gazetta Chimica Italiana* **1988**, *118*, 93-99.
(35) Young, C. G.; Minelli, M.; Enemark, J. H. *Polyhedron* **1986**, *5*, 407-413.
(36) Hong, M. C.; Wu, D. X.; Cao, R.; Lei, X. J.; Liu, H. Q.; Lu, J. X. *Inorg. Chim. Acta* **1997**, *258*, 25-32.
(37) Malito, J. *Annual Reports on NMR Spectr.* **1997**, *33*, 151-204.
(38) Gheller, S. F.; Hambley, T. W.; Rodgers, J. R.; Brownlee, R. T. C.; Oconnor, M. J.; Snow, M. R.; Wedd, A. G. *Inorg. Chem.* **1984**, *23*, 2519-2528.
(39) Wu, D. X.; Hong, M. C.; Cao, R.; Liu, H. Q. *Inorg. Chem.* **1996**, *35*, 1080-1082.
(40) Rittner, W.; Muller, A.; Neumann, A.; Bather, W.; Sharma, R. C. *Angew. Chem. Int. Ed. Engl.* **1979**, *18*, 530-531.
(41) Xin, X.; Morris, N. L.; Jameson, G. B.; Pope, M. T. *Inorg. Chem.* **1985**, *24*, 3482-3485.
(42) Laurie, S. H. *Eur. J. Inorg. Chem.* **2000**, 2443-2450.
(43) Alonso, G.; Yang, J.; Siadati, M. H.; Chianelli, R. R. *Inorg. Chim. Acta* **2001**, *325*, 193-197.
(44) Lakshmanan, V.; Nagaraja, K. S.; Udupa, M. R. *Indian J. Chem.* **1994**, *33A*, 772-774.
(45) Sarkar, S.; Mishra, S. B. S. *Coord. Chem. Rev.* **1984**, *59*, 239-264.
(46) Abragam, A.; Bleaney, B. *Electron Paramagnetic Resonance of Transition Ions*; Clarendon Press: Oxford, 1970.
(47) Atherton, N. M. *Principles of Electron Spin Resonance*; Ellis Horwood: Chichester, 1993.
(48) Symons, M. *Chemical and Biochemical Aspects of Electron-Spin Resonance Spectroscopy*; John Wiley & sons: New York, 1978.
(49) Alger, R. S. *Electron Paramagnetic Resonance: Techniques and Applications*; Interscience Publishers, 1968.
(50) Geschwind, S. *Electron Paramagnetic Resonance*; Plenum Press, 1972.
(51) Wertz, J. E.; Bolton, J. R. *Electron Spin Resonance: Elementary Theory and Practical Applications*; McGraw-Hill, 1972.

(52) Pilbrow, J. R. *Transition ion electron paramagnetic resonance*; Oxford University Press: Nw York, 1990.
(53) Poole, C. P. *Electron Spin Resonance: A Comprehensive Treatise on Experimental Techniques* 2nd ed.; John Wiley & Sons, 1983.
(54) Mabbs, F. E.; Collison, D. *Electron Paramagnetic Resonance of d Transition Metal Compounds*; Elsevier: Amsterdam, 1992; Vol. 16.
(55) Hathaway, B. J.; Billing, D. E. *Coord. Chem. Rev.* **1970**, *5*, 143-207.
(56) Peisach, J.; Blumberg, W. E. *Arch. Biochem. Biophys.* **1974**, *165*, 691-708.
(57) Granwehr, J., *EPR Instrumentation*, 2001, http://www.esr.ethz.ch/education/pcp2/esr/en/EPR/Instrumentation.htm
(58) Xie, G.; Jiang, Z. *Chinese Science Bulletin* **2000**, *45*, 1562-1564.
(59) Andreev, V. N.; Nikitin, S. E.; Klimov, V. A.; Kozyrev, S. V.; Leschev, D. V.; Shtel'makh, K. F. *Physics of the Solid State* **2001**, *43*, 788-791.
(60) Miyamoto, R.; Kawata, S.; Iwaizumi, M.; Akashi, H.; Shibahara, T. *Inorg. Chem.* **1995**, *36*, 542-546.
(61) Eccleston, T.; Laurie, S. H.; Symons, M. C. R.; Taiwo, F. A. *Polyhedron* **1998**, *17*, 1435-1438.
(62) George, G. N.; Garrett, R. M.; Prince, R. C.; Rajagopalan, K. V. *Inorg. Chem.* **2004**, *43*, 8456-8460.
(63) Nikolova, D.; Edreva-Karjieva, R.; Gouliev, G.; Grozeva, T.; P.Tzvetkov *Applied Catalysis A* **2006**, *297*, 135-144.
(64) Chenah, N.; Sid, S. D.; Benali-Baitich, O.; Deroide, B.; Zanchetta, J. V. *J. Soc. Alger. Chim.* **1996**, *6*, 277-290.
(65) Dhawan, I. K.; Enemark, J. H. *Inorg. Chem.* **1996**, *35*, 4873-4882.
(66) Mader, M. L.; Carducci, M. D.; Enemark, J. H. *Inorg. Chem.* **2000**, *39*, 525-531.
(67) Berger, R.; Haddad, M. *Phys. Stat. Solidi B: Basic Research* **1991**, *163*, 463-471.
(68) Dowerah, D.; Spence, J. T.; R.Singh; Wedd, A. G.; Wilson, G. L.; Farchione, F.; Enemark, J. H.; J.Kristofzski; Bruck, M. *JACS* **1987**, *109*, 5655-5665.
(69) Zhang, J.; Kamdem, D. P. *Holzforschung* **2000**, *54*, 343-348.
(70) Ehsan, M. Q.; Orba, Y.; Yamauchi, S.; Iwazumi, M. *J. Bangladesh Chem. Soc.* **1998**, *11*, 1-8.
(71) Voronkova, V. K.; Zaripov, M. M.; Kogan, V. A.; Yablonkov, Y. V. *Phys. Stat. Sol. B* **1973**, *55*, 747-754.
(72) Durny, R. *Acta Physica Slovaca* **1979**, *29*, 78-80.
(73) A.Parobets, M.; Krivonosov, V. V.; P.Strakhov, L. *Vestnik Sankt-Peterburgskogo Universiteta, Seriya 4: Fizika, Khimiya* **1997**, 101-108.
(74) Mkami, H. E.; Smith, G. M. *Nuclear Instruments and Methods in Physics Research B* **2005**, *229*, 392-396.
(75) Levillain, E.; Leghie, P.; Gobeltz, N.; Lelieur, J. P. *New J. Chem* **1997**, *21*, 335-341.
(76) Gobeltz, N.; Demortier, A.; Lelieur, J.-P. *New J. Chem* **1997**, *21*, 423-428.

(77) Schneider, J.; Dischler, B.; Rauber, A. *Phys. Stat. Solidi B* **1966**, *13*, 141-157.

(78) Zdravkova, M.; Gochev, G.; Yordanov, N. D. *Phosphorus, Sulfur and Silicon* **1998**, *141*, 71-77.

(79) Engstrom, M.; Vahtras, O.; Agren, H. *Chemical Physics Letters* **2000**, *328*, 483-491.

(80) Lawrence Berkeley National Laboratory, *X-ray Data Booklet*, 2001

(81) Vairavamurthy, M. A.; Maletic, D.; Wang, S.; Manowitz, B.; Eglinton, T.; Lyons, T. *Energy & Fuels* **1997**, *11*, 546-553.

(82) Malinowski, E. R.; Howery, D. G. *Factor Analysis in Chemistry*; 1st ed.; John Wiley & Sons, 1980.

(83) Beauchemin, S.; Hesterberg, D.; Beauchemin, M. *Soil Sci. Soc. Am. J.* **2002**, *66*, 83–91.

(84) Alcacio, T. E.; Hesterberg, D.; Chou, J. W.; Martin, J. D.; Beauchemin, S.; Sayers, D. E. *Geochim. Cosmochim. Acta* **2001**, *65*, 1355–1366.

(85) Scheinhost, A. C.; Kretchmar, R.; Pfister, S. *Environ. Sci. Technol.* **2002**, *36*, 5021-5028.

(86) Teo, B. K. *EXAFS : basic principles and data analysis* Springer-Verlag, 1986.

(87) George, G. N.; Kipke, C. A.; Prince, R. C.; Sunde, R. A.; Enemark, J. H.; Cramer, S. P. *Biochemistry* **1989**, *28*, 5075-5080.

(88) George, G. N.; Hilton, J.; Temple, C.; Prince, R. C.; Rajagopalan, K. V. *JACS* **1999**, *121*, 1256-1266.

(89) Cramer, S. P.; Hodgson, K. O.; Stiefel, E. I.; Newton, W. E. *JACS* **1978**, *100*, 2748-2761.

(90) deBoer, M.; Dillen, A. J. v.; Koningsberger, D. C.; Geus, J. W. *J. Phys. Chem.* **1994**, *98*, 7862-7870.

(91) Jalilehvand, F.; Lim, B. S.; Holm, R. H.; Hedman, B.; Hodgson, K. O. *Inorg. Chem.* **2003**, *42*, 5531-5536.

(92) Teo, B.-K.; Antonio, M. R.; Averill, B. A. *JACS* **1983**, *105*, 3751-3762.

(93) Koningsberger, D. C.; Prins, P. R. *X-Ray Absorption: Principles, Applications, techniques of EXAFS, SEXAFS and XANES*; John Wiley & Sons, 1988; Vol. 92.

(94) Newville, M., *Fundamentals of XAFS*, 2004, http://cars9.uchicago.edu/xafs/xas_fun/xas_fundamentals.pdf

(95) Kau, L.-S.; Spira-Solomon, D. J.; Penner-Hahn, J. E.; Hodgson, K. O.; Solomon, E. I. *JACS* **1987**, *109*, 6433-6442.

(96) deMoen, A.; Nicholson, D. G.; Ronning, M. *J. Chem. Soc. Faraday Trans.* **1995**, *91*, 3189-3194.

(97) Sarode, P.; Sankar, G.; Rao, C. N. R. *Proc. of Indian Academy of Sciences: Chem. Science* **1983**, *92*, 527-542.

(98) Hsiao, M. C.; Wang, H. P.; Huang, Y.-J.; Yang, Y. W. *J. Synch. Rad.* **2001**, *8*, 931-933.

(99) Berry, A. J.; Hack, A. C.; Mavrogenes, J. A.; Newville, M.; Sutton, S. R. *American Mineralogist* **2006**, *91*, 1773-1782.

(100) Nicholson, D. G.; Nilsen, M. H. *J. of Material Chemistry* **2000**, *10*, 1965-1971.

(101) George, G. N.; Pickering, I. J.; Harris, H. H.; Gailer, J.; Klein, D.; Lichtmannegger, J.; Summer, K.-H. *JACS* **2003**, *125*, 1704-1705.

(102) Cramer, S. P.; Eidem, P. K.; Paffett, M. T.; Winkler, J. R.; Dori, Z.; Gray, H. B. *JACS* **1983**, *105*, 799-805.

(103) Butler, C. S.; Charnock, J. M.; Bennett, B.; Sears, H. J.; Reilly, A. J.; Ferguson, S. J.; Garner, C. D.; Lowe, S. J.; Thomson, A. J.; Berks, B. C.; Richardson, D. J. *Biochemistry* **1999**, *38*, 9000-9012.

(104) Doonan, C. J.; Stockert, A.; Hille, R.; George, G. N. *JACS* **2005**, *127*, 4518-4522.

(105) Musgrave, K. B.; Lim, B. S.; Sung, K.-M.; Holm, R. H.; Hedman, B.; Hodgson, K. O. *Inorg. Chem.* **2000**, *39*, 5238-5247.

(106) Kutzler, F. W.; Scott, R. A.; Berg, J. M.; Hodgson, K. O.; Doniach, S.; Cramer, S. P.; Chang, C. H. *JACS* **1981**, *103*, 6083-6088.

(107) George, G. N.; Colangelo, C. M.; Dung, J.; Scott, R. A.; Khangulov, S. V.; Gladyshev, V. N.; Stadtman, T. C. *JACS* **1998**, *120*, 1267-1273.

(108) Conradson, S. D.; Burgees, B. K.; Newton, W. E.; Hodgson, K. O.; McDonald, J. W.; Rubinson, J. F.; Gheller, S. F.; Mortenson, L. E.; Adams, M. W. W.; Mascharak, P. K.; Armstrong, W. A.; Holm, R. H. *JACS* **1985**, *107*, 7935-7940.

(109) Cramer, S. P.; Hille, R. *JACS* **1985**, *107*, 8164-8169.

(110) George, S. J.; Igarashi, R. Y.; Piamonteze, C.; Soboh, B.; Cramer, S. P.; Rubio, L. M. *JACS* **2007**, *129*, 3060-3061.

(111) Takahashi, Y.; Kanai, Y.; Kamioka, H.; Ohta, A.; Maruyama, H.; Song, Z.; Shimizu, H. *Environ. Sci. Technol.* **2006**, *40*, 5052-5057.

(112) Morra, M. J.; Fendorf, S. E.; Brown, P. D. *Geochim. Cosmochim. Acta* **1997**, *61*, 683-688.

(113) Bostick, B. C.; Theissen, K. M.; Dunbar, R. B.; Vairavamurthu, M. A. *Chemical Geology* **2005**, *219*, 163-174.

(114) Akabayov, B.; Doonan, C.; Pickering, I. J.; George, G. N.; Sagi, I. *J. Synchrotron Rad.* **2005**, *12*, 392-401.

(115) Alloway, B. J. *J. Agric. Sci.* **1973**, *80*, 521-524.

(116) Miltimore, J. E.; Mason, J. L. *Can. J. Anim. Sci.* **1971**, *51*, 193-200.

(117) Gardner, W. C.; Broersma, K.; Popp, J. D.; Mir, Z.; Mir, P. S.; Buckley, W. T. *Can. J. Anim. Sci.* **2003.**, *83*, 479-485.

(118) Ward, G. M. *J. Anim. Sci.* **1978**, *46*, 1078-1089.

(119) Clarke, N. J.; Laurie, S. H. *Inorg. Chim. Acta* **1982**, *66*, L35-L38.

(120) Eccleston, T.; Laurie, S. H.; Symons, M. C. R.; Taiwo, F. A. *Inorg. Chem. Comm.* **1998**, *1*, 460-462.

(121) Laurie, S. H.; Pratt, D. E.; Raynor, J. B. *Inorg. Chim. Acta* **1986**, *123*, 193-196.

(122) Mattioli, G. A.; Ramirez, C. E.; Giuliodori, M. J.; Tittarelli, C. M.; Yano, H.; Matsui, T. *Livestock Prod. Sci.* **1996**, *47*, 7-10.

(123) Zhang, C.; Song, Y. L.; Xu, Y.; Fun, H.; Fang, G. Y.; Wang, Y. X.; Xin, X. Q. *J. Chem. Soc. - Dalton Trans.* **2000**, 2823-2829.

(124) Shi, S.; Chen, Z. R.; Hou, H. W.; Xin, X. Q.; Yu, K. B. *Chem. Mater.* **1995**, *7*, 1519-1524.

(125) Hou, H. W.; Zheng, H. G.; Ang, H. G.; Fan, Y. T.; Low, M. K. M.; Zhu, Y.; Wang, W. L.; Xin, X. Q.; Ji, W.; Wong, W. T. *J. Chem. Soc.-Dalton Trans.* **1999**, 2953-2957.

(126) Li, Z. H.; Du, S. W.; Wu, X. T. *Dalton Trans.* **2004**, 2438-2443.

(127) Guo, J.; Sheng, T.; Zhang, W.; Wu, X.; Lin, P.; Wang, Q.; Lu, J. *Inorg. Chem.* **1998**, *37*, 3689-3697.

(128) Sadr, M. H.; Clegg, W.; Bijhanzade, H. R. *Polyhedron* **2004**, *23*, 637-641.

(129) Sadr, M. H.; Razmi, H.; Brooks, N. R.; Clegg, W. *Acta Cryst.* **2003**, *E59*, M1134-M1136.

(130) Li, Z. H.; Du, S. W.; Wu, X. T. *Polyhedron* **2005**, *24*, 2988-2993.

(131) Beheshti, A.; Clegg, W.; Sadr, M. H. *Inorg. Chim. Acta* **2002**, *335*, 21-26.

(132) Huang, Q.; Wu, X. T.; Wang, Q. M.; Sheng, T. L.; Lu, J. X. *Inorg. Chem.* **1996**, *35*, 893-897.

(133) Zhang, W. J.; Wu, X. T.; Ebel, M.; Wang, D. R.; Rehder, D. *Inorg. Chem. Comm.* **2002**, *5*, 768-770.

(134) Bursakov, S. A.; Gavel, O. Y.; DiRocco, G.; Lampreia, J.; Calvete, J.; Pereira, A. S.; Moura, J. J.; Moura, I. *J. Inorg. Chem.* **2004**, *98*, 833-840.

(135) Zhu, H.; Huang, X.; Deng, Y.; Wu, D.; Chen, C.; Liu, Q. *Inorg. Chim. Acta* **1997**, *256*, 29-34.

(136) Bernes, S.; Secheresse, F.; Jeannin, Y. *Inorg. Chim. Acta* **1992**, *191*, 11-13.

(137) Lang, J. P.; Kawaguchi, H.; Ohnishi, S.; Tatsumi, K. *Inorg. Chim. Acta* **1998**, *283*, 136-144.

(138) Binnie, W. P.; Redman, M. J.; Mallio, W. J. *Inorg. Chem.* **1970**, *9*, 1449-1452.

(139) Sharma, S. B.; Tewari, I. N. *Synth. Inorg. Met.-Org. Chem* **1992**, *22*, 217-225.

(140) Muller, A.; Hellmann, W.; Schneider, J.; Schimanski, U.; Demmer, U.; Trautwein, A.; Bender, U. *Inorg. Chim. Acta* **1982**, *65*, L41-L42.

(141) Li, J. R.; Du, S. S.; Wu, X. T. *J. Cluster Sci.* **2005**, *16*, 489-500.

(142) Potvin, C.; Manoli, J. M.; Secheresse, F.; Marzak, S. *Inorg. Chem.* **1987**, *26*, 4370-4374.

(143) Lei, X.; Huang, Z.; Liu, Q.; Hong, M.; Liu, H. *Inorg. Chem.* **1989**, *28*.

(144) Muller, A.; Diemann, E. *Comp. Coord. Chem.* **1987**, *2*, 559-576.

(145) Attaelmannan, M. A., *^{1}H NMR and Potentiometric Studies of Copper(II) Speciation in Ruminants*, University of Saskatchewan, 1998.

(146) Attaelmannan, M. A.; Reid, R. S. *Journal of Inorganic Biochemistry* **1996**, *64*, 215-224.

(147) Quagraine, E. K.; Reid, R. S. *J. Inorg. Biochem.* **2001**, *85*, 53-60.

(148) Quagraine, E. K.; Kraatz, H. B.; Reid, R. S. *J. Inorg. Biochem.* **2001**, *85*, 23-32.

(149) Koranteng, M. A., *^{1}H NMR and Potentiometric Studies of Mixed-Ligand Complexes of Copper(II) with some Amino Acids*, University of Saskatchewan 2004.
(150) Essilfie-Dughan, J., *Speciation Modelling of Copper(II) in the Thiomolybdate-contaminated Bovine Rumen*, University of Saskatchewan, 2007.
(151) Clark, R. J., *Kinetics of Thiomolybdate and Copper-Thiomolybdate Interconversion Processes*, University of Saskatchewan, 2008.
(152) George, G. N.; Pickering, I. J., *EXAFSPAK*, 2000
(153) George, G. N.; Pickering, I. J., *EXAFSPAK manual*, 2000, http://ssrl.slac.stanford.edu/~george/exafspak/manual.pdf
(154) Atkins, P.; dePaula, J. *Physical Chemistry*; 7th ed.; W. H. Freeman and Company: New York, 2002.
(155) Harris, D. C. *Quantitative Chemical Analysis*; Fourth ed.; W. H. Freeman and Company: New York, 1995.
(156) Clausen, B. S.; Topoe, H.; Candia, R.; Villadsen, J.; Lengeler, B.; Als-Nielsen, J.; Christensen, F. *J. Phys. Chem.* **1981**, *85*, 3868-3872.
(157) Thome, D. M., *X-ray crystallographic Studies of Thiomolybdates and Bovine Serum Albumin*, University of Saskatchewan, 2001.